PNNL-24412 Rev. 1

Pacific Northwest
NATIONAL LABORATORY
Proudly Operated by Battelle Since 1965

Nondestructive Examination Guidance for Dry Storage Casks

September 2016

RM Meyer
EH Hirt
JP Lareau
A Qiao
P Ramuhalli
S Suffield
JD Suter
JW Zhuge
TL Moran

Prepared for the U.S. Nuclear Regulatory Commission
under a Related Services Agreement with the U.S. Department of Energy
CONTRACT DE-AC05-76RL01830

U.S. DEPARTMENT OF ENERGY

DISCLAIMER

PACIFIC NORTHWEST NATIONAL LABORATORY
operated by
BATTELLE
for the
UNITED STATES DEPARTMENT OF ENERGY
under Contract DE-AC05-76RL01830

Printed in the United States of America

Available to DOE and DOE contractors from the
Office of Scientific and Technical Information,
P.O. Box 62, Oak Ridge, TN 37831-0062;
ph: (865) 576-8401
fax: (865) 576-5728
email: reports@adonis.osti.gov

Available to the public from the National Technical Information Service,
U.S. Department of Commerce, 5285 Port Royal Rd., Springfield, VA 22161
ph: (800) 553-6847
fax: (703) 605-6900
email: orders@ntis.fedworld.gov
online ordering: http://www.ntis.gov/ordering.htm


This document was printed on recycled paper.
(9/2003)

Nondestructive Examination Guidance for Dry Storage Casks

RM Meyer
EH Hirt
JP Lareau
A Qiao
P Ramuhalli
S Suffield
JD Suter
JW Zhuge
TL Moran

September 2016

Prepared for
the U.S. Nuclear Regulatory Commission
under a Related Services Agreement
with the U.S. Department of Energy
Contract DE-AC05-76RL01830

Pacific Northwest National Laboratory
Richland, Washington 99352

Abstract

This report reviews nondestructive examination (NDE) methods and their applicability to aging effects in concrete overpack and metal canister components to support U.S. Nuclear Regulatory Commission staff with review of renewal applications for welded canister-type dry storage systems (DSSs). In the United States, several DSSs for commercial spent nuclear fuel are approaching the end of their initial licensed or certified term. Many of these systems have originally been licensed or certified for 20 years, after which they may be renewed for periods up to 40 years, according to Title 10 of the *Code of Federal Regulations* (10 CFR), Part 72, "Licensing Requirements for the Independent Storage of Spent Nuclear Fuel, High-Level Radioactive Waste, and Reactor-Related Greater than Class C Waste." An analysis of implementation of NDE methods to concrete horizontal storage modules (HSMs) in Transnuclear NUHOMS 80 and 102 DSSs is provided as an example to illustrate factors that should be considered when reviewing NDE methods proposed by applicants for welded canister-type DSSs in general. The analysis for concrete HSM components is performed by literature review of documents by the American Concrete Institute (ACI), Transportation Research Board (TRB), International Atomic Energy Agency (IAEA), U.S. Department of Energy (DOE), the BAM Federal Institute for Materials Research and Testing in Germany, and others. For the metal canister, the American Society for Mechanical Engineers Boiler & Pressure Vessel Code is used primarily as the basis for NDE methods considered, along with currently funded efforts through industry (Electric Power Research Institute) and the DOE to develop inspection technologies for canisters.

Summary

In the United States, several dry storage systems (DSSs) for commercial spent nuclear fuel are approaching the end of their initial licensed or certified term. Many of these systems have originally been licensed or certified for 20 years, after which the licensing or certification may be renewed for periods up to 40 years, according to Title 10 of the *Code of Federal Regulations* (10 CFR), Part 72, "Licensing Requirements for the Independent Storage of Spent Nuclear Fuel, High-Level Radioactive Waste, and Reactor-Related Greater than Class C Waste." Guidance for review of license renewal applications is provided in NUREG-1927, *Standard Review Plan for Renewal of Spent Fuel Dry Cask Storage System Licenses and Certificates of Compliance*. A review of aging effects that could affect important to safety (ITS) structures, systems, and components (SSCs) is required in renewal applications and applicants are required to address aging effects using either a time-limited aging analysis or an aging management program. The U.S. Nuclear Regulatory Commission (NRC) has recently prepared a revision to NUREG-1927 (Rev. 1) to clarify guidance on aging management expectations for renewal applications.

This report is intended to support NRC staff in the reviews of renewal applications for welded canister DSSs. It provides a review of nondestructive examination (NDE) techniques applicable to concrete structures and metal welded canisters in DSSs. For each of the NDE techniques, the report provides a summary of the operating principles, a narrative of laboratory and field experience, a discussion of the important factors that influence the quality of the data, and a listing of the limitations. Although the NUHOMS 80 and 102 system designs are specifically considered in this report, the information on NDE methods and their applicability to aging effects in ITS SSCs included in Sections 2.0 and 3.0 are generally applicable to all welded canister DSSs that employ similar materials. The application to NUHOMS 80 and 102 system designs provides an example to highlight factors NRC staff should consider in reviewing proposed applications of NDE methods to welded canister DSS designs, in general. Several documents provide the basis for the NDE methods considered in this report for inspection of horizontal storage module (HSM) concrete components including documents by the American Concrete Institute (ACI): ACI 349.3R, *Evaluation of Existing Nuclear Safety-Related Concrete Structures* and ACI 228.2R-13, *Report on Nondestructive Test Methods for Evaluation of Concrete in Structures*. In addition, documents by the Transportation Research Board (TRB), International Atomic Energy Agency (IAEA), U.S. Department of Energy (DOE), and the BAM Federal Institute for Materials Research and Testing in Germany have informed the consideration of NDE methods for concrete structures in this report. Applicability of NDE methods is analyzed for several aging effects in concrete including delaminations and voids, vertically oriented cracks, continuously distributed degradation, corrosion of embedded steel, and changes in dimensions. Implementation capability for NDE methods is also analyzed for HSM components by considering relevant factors such as the specimen thickness, size and density of reinforcing steel, accessibility to the surface, and specimen geometry.

For the metal canister, the American Society for Mechanical Engineers (ASME) Boiler & Pressure Vessel Code (B&PV Code) is used primarily as the basis for NDE methods considered, along with currently funded efforts through industry (Electric Power Research Institute) and the DOE to develop inspection technologies for canisters. This limited the scope of NDE methods considered for the metal canister to visual testing, bulk ultrasound testing, guided ultrasonic wave testing, eddy current testing, and acoustic emission testing. The aging effects in metals considered include surface-breaking cracks and localized corrosion. The applicability of NDE methods to cracks in metal is determined on the basis of several studies to assess and document performance of NDE methods for detecting cracks in metallic components in light water reactors (LWRs). In these studies, crack detection was based on direct observation of a crack. Localized corrosion can infer the likelihood of crack formation or may infer that cracking already exists. In this scenario, cracks can also be detected indirectly through the observation of localized corrosion.

Acknowledgments

The work described in this report was sponsored by the U.S. Nuclear Regulatory Commission (NRC) under the contract number NRC-HQ-60-14-D-0020. Gratitude is extended to Bruce Lin who served as the NRC project manager and to Darrell Dunn and Ricardo Torres of the NRC who provided input on the content of the report. Gratitude is also reserved for Kay Hass of Pacific Northwest National Laboratory who helped edit and format this report.

Acronyms and Abbreviations

AASHTO	American Association of State Highway and Transportation Officials
ACI	American Concrete Institute
AE	acoustic emission
AET	acoustic emission testing
ASME	American Society for Mechanical Engineers
ASNT	American Society for Nondestructive Testing
ASTM	American Society for Testing and Materials
B&PV Code	Boiler & Pressure Vessel Code
BWR	boiling water reactor
COD	crack opening displacement
DOE	U.S. Department of Energy
DMW	dissimilar metal weld
DSC	dry shielded canister
DSS	dry storage systems
ECT	eddy current testing
EMAT	electromagnetic acoustic transducer
EPRI	Electric Power Research Institute
GPM	galvanostatic pulse measurement
GPR	ground penetrating radar
GUW	guided ultrasonic wave
HCP	half-cell potential
HSM	horizontal storage module
IAEA	International Atomic Energy Agency
ID	inner diameter
IE	impact echo
IGSCC	intergranular stress corrosion cracking
IR	impulse response
IRT	infrared thermography
ISFSI	independent spent fuel storage installation
ISI	inservice inspection
ITS	important to safety
LPR	linear polarization resistance
LWR	light water reactor
LWRS	Light Water Reactor Sustainability (program)
MsS	magnetostrictive sensor
NDE	nondestructive examination

NDT	nondestructive testing
NRC	U.S. Nuclear Regulatory Commission
OD	outer diameter
PAUT	phased-array ultrasonic testing
PDT	partially destructive testing
PINC	Program for the Inspection of Nickel Alloy Components
POD	probability of detection
PTZ	pan-tilt-zoom
PWR	pressurized water reactor
RM	resistivity measurements
SASW	spectral analysis of surface waves
SCC	stress corrosion cracking
SH	shear horizontal
SHRP 2	Second Strategic Highway Research Program
SNR	signal-to-noise ratio
SSCs	structures, systems, and components
TOFD	time-of-flight diffraction
TRB	Transportation Research Board
UPE	ultrasonic pulse echo
UPV	ultrasonic pulse velocity
USW	ultrasonic surface wave
UT	ultrasonic testing
Vg	group velocity
Vp	phase velocity
VT	visual testing

Definitions

Air Void*	A space in cement paste, mortar, or concrete filled with air
Aggregate*	Granular material, such as sand, gravel, crushed stone, crushed hydraulic cement concrete, or iron blast-furnace slag, used with a cementing medium to produce either concrete or mortar
Cement*	Any of a number of materials that are capable of binding aggregate particles together
Changes in Dimensions	Refers to reduction in actual thickness of concrete component as a result of material loss or to reduction in thickness of sound concrete as the result of degradation to a layer of concrete on the surface opposite to transducer placement
Concrete*	Mixture of hydraulic cement, aggregates, and water with or without admixtures, fibers, or other cementitious materials
Continuously Distributed Degradation	Refers to damage expressed as spatially smooth or gradual changes in concrete properties Contrasts with degradation that is expressed as a material discontinuity, such as cracking, delaminations, or voids Concrete properties of relevance in this report include elastic properties, strength, density, and concentration of moisture and chloride species
Crack*	A complete or incomplete separation of either concrete or masonry into two or more parts produced by breaking or fracturing
Delamination*	A planar separation in a material that is roughly parallel to the surface of the material; see illustration for a delamination in a wall in Figure I and a delamination in a slab in Figure II
Mass Concrete*	Any volume of concrete in which a combination of dimensions of the member being cast, the boundary conditions can lead to undesirable thermal stresses, cracking, deleterious chemical reactions, or reduction in the long-term strength as a result of elevated concrete temperature due to heat from hydration
Portland Cement*	A hydraulic cement produced by pulverizing portland-cement clinker and usually with addition of calcium sulfate to control setting
Portland-Cement Clinker*	A partially fused product of kiln that is ground to make cement
Rebar*	Colloquial term for reinforcing bar
Reinforcement*	Bars, wires, strands, fibers, or other slender element that are embedded in a matrix such that they act together to resist forces
Reinforced Concrete*	Structural concrete reinforced with no less than the minimum amount of prestressing steel or no prestressed reinforcement as specified in the applicable building code
Reinforcing Steel	Steel reinforcement (see definition of Reinforcement)
Vertical Crack	Surface-breaking crack that is oriented and propagates in the direction normal to the exposed surface; see illustration for a vertical crack in a wall in Figure I and a vertical crack in a slab in Figure II
Void	See definition for air void; see illustration for a void in a wall in Figure I and a void in a slab in Figure II

*Definition from ACI CT-13 (ACI 2013a)

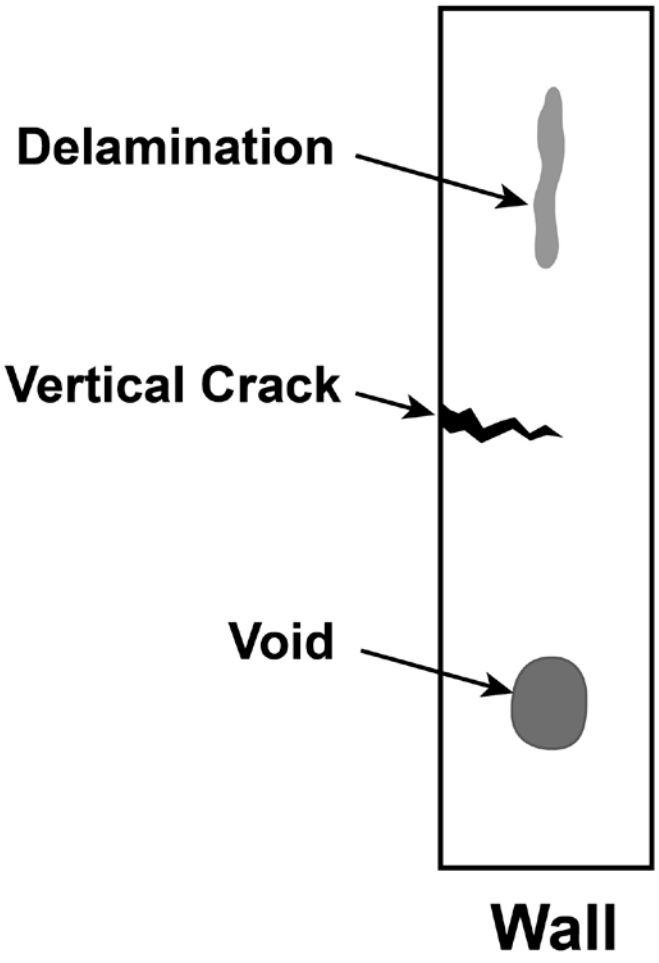

Figure I. Illustration of Delamination, Void, and Vertical Crack in a Concrete Wall Specimen

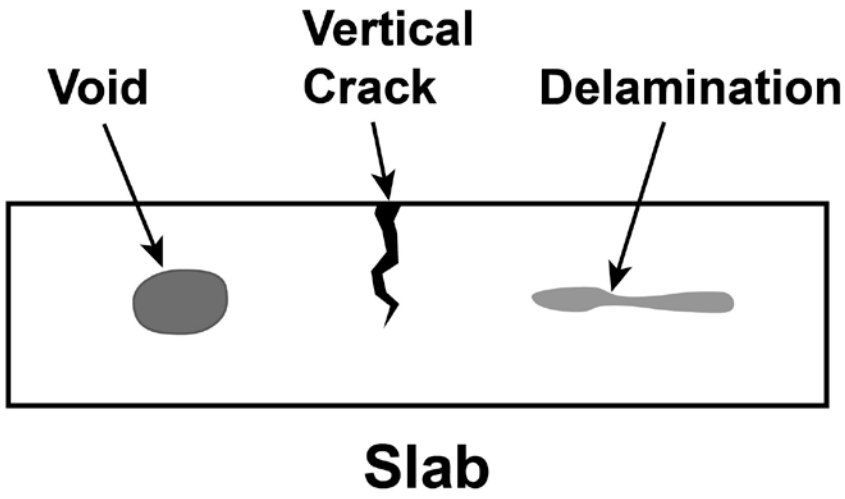

Figure II. Illustration of Delamination, Void, and Vertical Crack in a Concrete Slab Specimen

Contents

Figures

Tables

1.0 Introduction

In the United States, several dry storage systems (DSSs) for commercial spent nuclear fuel are approaching the end of their initial licensed or certified term. Many of these systems have originally been licensed or certified for 20 years, after which the licensing or certification may be renewed for periods up to 40 years, according to Title 10 of the Code of Federal Regulations (10 CFR), Part 72, "Licensing Requirements for the Independent Storage of Spent Nuclear Fuel, High-Level Radioactive Waste, and Reactor-Related Greater than Class C Waste." Guidance for review of renewal applications is provided in NUREG-1927, *Standard Review Plan for Renewal of Spent Fuel Dry Cask Storage System Licenses and Certificates of Compliance*. A review of aging effects that could affect important to safety (ITS) structures, systems, and components (SSCs) is required in renewal applications and applicants are required to address aging effects using either a time-limited aging analysis or an aging management program. The U.S. Nuclear Regulatory Commission (NRC) has recently prepared a revision to NUREG-1927 (NRC 2016) to clarify guidance on aging management expectations for renewal applications.

DSSs can be broadly classified as welded canister or bolted lid designs. Welded canister systems typically consist of a stainless steel shell (12.5 mm [~0.5 in.] thickness) into which the spent fuel is loaded prior to sealing by welding. The internal fuel basket and neutron poisons maintain the fuel geometry and provide criticality control. The welded canisters are then placed into a thick concrete overpack that provides physical protection for the welded canister and serves to shield the radiation emanating from the spent fuel. The bolted lid systems typically consist of a single integrated container with thick metal walls. Spent fuel is loaded into the container and a lid is bolted to close the container. A gas-tight seal is achieved through the use of O-rings and gaskets. The majority of DSSs deployed in the U.S. commercial nuclear industry are of the welded canister design and this report, specifically, focuses on the Transnuclear NUHOMS 80 and 102 DSSs. The NUHOMS 80 and 102 DSSs are horizontal systems such that the welded canister is oriented horizontally inside of the horizontal storage module (HSM). The NUHOMS 80 and 102 DSSs are nearly identical with the exception of their front shield doors and the use of metal liner over ventilation ports.

This report is intended to support NRC staff reviews of renewal applications for welded canister DSSs. Although the NUHOMS 80 and 102 system designs are specifically considered in this report, the information on nondestructive examination (NDE) methods and their applicability to aging effects in ITS SSCs included in Sections 2.0 and 3.0 are generally applicable to all welded canister DSSs that employ similar materials. The application to NUHOMS 80 and 102 system designs provides an example to highlight factors NRC staff should consider in reviewing proposed applications of NDE methods to welded canister DSS designs.

NDE methods are considered for both the welded canister (referred to as a DSC [dry shielded canister]) and the concrete overpack (referred to as the HSM). Several documents provide the basis for the NDE methods considered in this report for inspection of HSM concrete components. Some of the more influential documents include: ACI 349.3R, *Evaluation of Existing Nuclear Safety-Related Concrete Structures* (ACI 2002); ACI 228.2R-13, *Report on Nondestructive Test Methods for Evaluation of Concrete in Structures* (ACI 2013b); S2-R06A-RR-1, *Nondestructive Testing to Identify Concrete Bridge Deck Deterioration* (TRB 2013); ORNL/TM-2007/191, *Inspection of Nuclear Power Plant Structure-Overview of Methods and Related Application* (Naus 2009a); *Guidebook on Non-destructive Testing of Concrete Structures* (IAEA 2002), and *Non-destructive Testing of Nuclear Power Plant Concrete Structures - State of the Art Report* (Helmerich et al. 2013)). For the canister, the American Society for Mechanical Engineers (ASME) Boiler & Pressure Vessel Code (B&PV Code) is used primarily as the

basis for NDE methods considered, along with currently funded efforts through industry (Electric Power Research Institute, EPRI) and the U.S. Department of Energy (DOE) to develop inspection technologies for canisters.

This report supplements a report titled, *Managing Aging Processes in Storage*, (MAPS) under preparation by the Center for Nuclear Waste Regulatory Analyses at the Southwest Research Institute. The MAPS report provides a detailed accounting of aging degradation mechanisms and aging effects in DSS ITS SSCs. A renewal application should be clear regarding the NDE method to be applied for periodic inspection of specific DSS ITS SSCs. A review of a renewal application should consider the applicability of the specified NDE method to relevant aging degradation mechanisms in a specific ITS SSC and the feasibility of performing an adequate examination given practical constraints. In this report, an attempt is made to link NDE methods to aging effects for which they are applicable (and, thus, to corresponding aging degradation mechanisms) and to convey some practical bounds for deployment, where possible.

For metal components, studies have been conducted to quantify the performance of ultrasonic testing (UT) [including phased-array UT (PAUT)] and eddy current testing (ECT) for detecting linear flaws (cracks) in nuclear reactor pressure boundary components. Studies are currently ongoing to quantitatively assess the performance of visual testing for detecting cracks in reactor internal components. This information is referenced in Section 2.0, which provides an assessment of NDE methods for HSM and DSC SSCs. Such information is not as readily available in the literature for detection of localized corrosion, such as pitting and for flaws in concrete structures. The standard ASTM G46, *Standard Guide for Examination and Evaluation of Pitting Corrosion* (ASTM 2013a), provides an overview of methods for quantified measurements of extent of pitting in metals. The methods considered in the standard include visual, destructive, and nondestructive methods. In this standard, visual methods are classified separately from other NDE methods. The standard states that NDE methods can have difficulty detecting small pits and distinguishing pits from other surface blemishes. In the remainder of this document, visual methods will be considered a type of NDE method for the metal DSC.

Quantifying the performance of NDE methods for detecting flaws in concrete, in particular, is complex because of the heterogeneous nature of concrete, variability of constituents, and the multiple types of aging effects (i.e., cracks, voids, etc.) that are possible. In addition, the ability to detect many of these aging effects will be dependent upon the location and amount of reinforcing or embedded steel within the concrete, the thickness of the concrete member to inspect, and relative location of flaws with respect to reinforcing or embedded steel. NDE for concrete structures is currently a focus of the DOE Office of Nuclear Energy Light Water Reactor Sustainability (LWRS) program. Current emphasis of the LWRS program is placed on developing and evaluating technologies that can image the cross section of thick concrete structures, such as a reactor containment wall (Clayton et al. 2014; Clayton et al. 2013).

The rest of this report is organized as follows: Section 2.0 provides descriptions of NDE methods for HSM and DSC SSCs; Section 3.0 summarizes the applicability of the NDE methods to aging effects in concrete and metal components; Section 4.0 provides description of NUHOMS 80 and 102 HSM and DSC components while Section 5.0 provides an analysis of the ability to implement NDE methods on NUHOMS 80 and 102 HSMs; and Section 6.0 provides a summary of the aging effects and implementation analysis. Sections 3.0 and 5.0 are complementary in that information in both sections should be used to assess the appropriateness of an NDE method application for an aging effect in a specific HSM component. Finally, summary and conclusions are provided in Section 7.0.

2.0 Description of NDE Methods and Techniques for Concrete Testing and Canister Inspections

Brief descriptions of NDE methods for inspecting concrete and metal components are included in Sections 2.1 and 2.2, respectively. In addition to the descriptions of NDE methods, a brief discussion of sensor delivery to the surface of DSCs is provided in Section 2.3 and this is followed by a brief discussion on environmental compatibility for deployment of sensors for inspection of DSS components in Section 2.4. The information provided in this section provides the basis for summaries included in Sections 3.0, 5.0, and 6.0.

2.1 NDE Methods and Techniques for Concrete Testing

This section includes descriptions of NDE methods for performing augmented inspections of concrete structures following identification of indications by visual testing. Thus, visual testing is not described in this section. The American Concrete Institute (ACI) has published a guide for performing in-service visual inspections of concrete components [ACI 201.1R] (ACI 2008). The methods described here go beyond visual examination of the surface of concrete structures and are able to detect anomalies within the volume. The methods employ elastic, electromagnetic, nuclear, and electrical modalities for inspection. Three of the methods described are specific for inspecting corrosion of reinforcing steel. An effort is made in the following subsections to provide a basic description for each method, summarize relevant field or laboratory experience, identify influencing factors associated with instrumentation and the specimen and environment, and identify limitations associated with the methods. Information from this section is used to create a summary of the applicability of NDE methods for aging effects in concrete in Section 3.1. The information is also input to the implementation summary for application of NDE methods to NUHOMS HSM concrete components in Section 5.0.

2.1.1 Ultrasonic Pulse-Echo Testing

Ultrasonic pulse-echo (UPE) testing is based on detecting the reflection of acoustic energy from acoustic impedance discontinuities caused by defects in the concrete structure (see Figure 2.1). The technique is implemented by accessing only a single side of the concrete structure. The key components of a UPE test system are the transmitting and receiving transducer(s), a pulser, and a system for data acquisition, analysis, and display. An input pulse provided by the transmitter will propagate through a concrete test structure until the interface of a defect is encountered. The discontinuity in the acoustic impedance at this interface will cause a propagating input pulse to reflect and travel back towards the surface of the test structure where it is detected by the receiving transducer mounted in proximity to the transmitter. The location of a defect can be estimated based on the time delay observed for appearance of the reflected echo in the A-scan. Large aggregates have a significant scattering effect on the signals, thus restricting the method to relatively low-frequency inputs (50 kHz–200 kHz) (Naus 2009a, pp. 37-45; TRB 2013, p. 14).

Technology advancements have led to the development of low-frequency transducer arrays that can be dry-coupled to test structures and which incorporate advanced signal processing algorithms such as synthetic aperture focusing technique (SAFT). SAFT processes signals to correct for distortions in scanning images, as a result of transducer focusing distortion, to obtain images with improved resolution. SAFT can also be implemented with a transducer array in which each element in the transducer can be individually excited in sequence while all elements “listen” for echo signals. Using a 2-D matrix array allows SAFT imaging to be performed in 3-D.

A type of dry-coupled array system based on shear waves (S-waves) has been commercialized (see Figure 2.2) and is currently under evaluation by the U.S. DOE LWRS program (Clayton et al. 2014; Clayton et al. 2013). Cross-sectional images of test structures may be obtained from a 2-D matrix array implementing SAFT algorithms (Clayton et al. 2013). In addition, further advanced signal processing schemes are under development (Clayton et al. 2014).

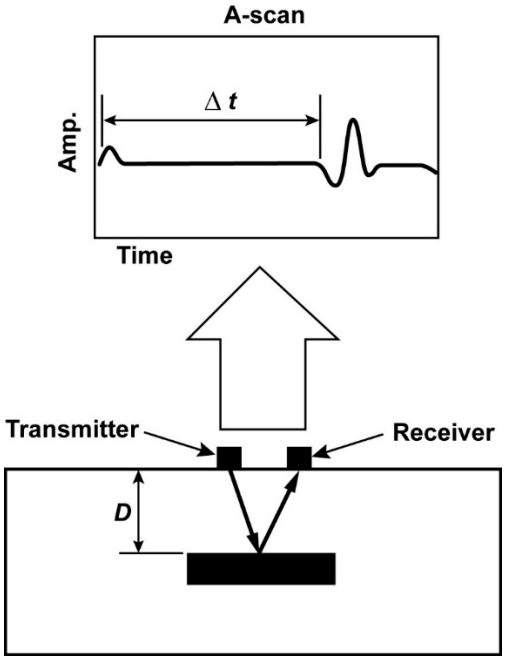

Figure 2.1. Illustration of the UPE Technique for Nondestructive Testing of Concrete

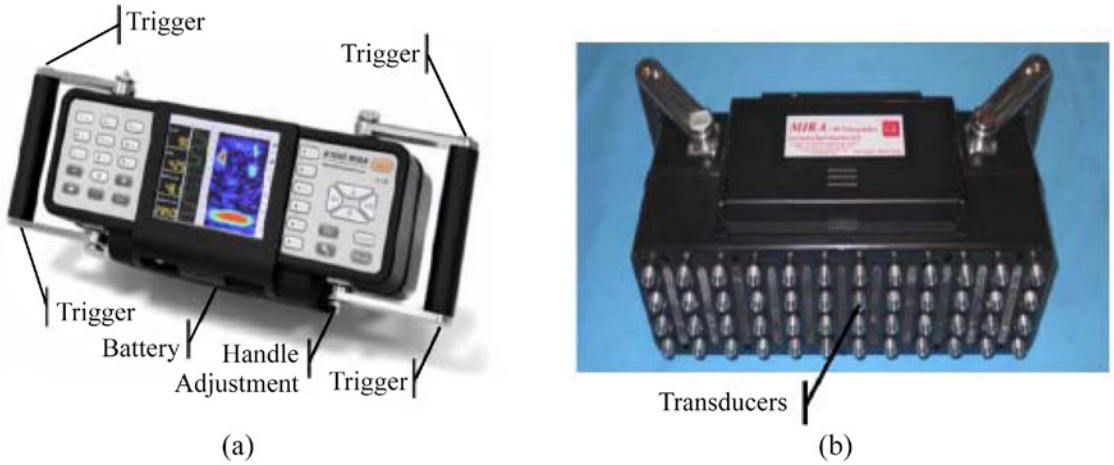

Figure 2.2. Photograph of Commercial UPE Array with Dry-Coupled Transducers (from Clayton et al. 2013)

2.1.1.1 Laboratory Experience

Ultrasonic arrays using dry-coupled transducers continue to be evaluated under the LWRS program (Clayton et al. 2014; Clayton et al. 2013). This work highlights that the ability to observe features behind embedded steel are significantly influenced by the bonding condition between the embedded steel and surrounding concrete. Debonding of embedded steel from the surrounding concrete results in very poor coupling between the steel and concrete and prevents transmission of ultrasound through the steel, resulting in "shadowing" of locations behind the debonded steel.

These tests were conducted on two 254 mm (10 in.) thick test structures simulating various degrees of rebar densities and with simulated voids and vertical cracks. Vertical cracks were simulated by triangular wedges that formed linear defects with 254 mm (10 in.) length and varied in depth linearly from the surface to a maximum depth of 76 mm (3 in.). Voids were simulated with cuboid geometries with length and width of 254 mm (10 in.) and 152 mm (6 in.), respectively, and depths of 76 mm (3 in.) and 152 mm (6 in.). This work indicated that it was possible to detect these simulated vertical cracks and voids using dry-coupled shear-wave array systems. However, the test blocks used in these studies were not designed to evaluate the influence of embedded reinforcing steel on the ability to detect such defects.

2.1.1.2 Field Experience

The commercial dry-coupled array system based on S-waves was incorporated in a test conducted in 2009 for concrete pavement on I-85 near Atlanta, Georgia (Hoegh et al. 2011). The test demonstrated the ability of the system to measure the thickness of the pavement deck up to 375 mm (15 in.) in thickness and detected delamination near the surface. Measurements were verified with core samples.

UPE is described as a candidate nondestructive testing (NDT) method for the second Strategic Highway Research Program (SHRP 2), but no evaluations of the technique were included in the laboratory and field validation studies (TRB 2013).

2.1.1.3 Influencing Factors Associated with Instrumentation

- Frequency – Transducers with center frequencies ranging from 50 kHz to 200 kHz are typically used (TRB 2013, p. 14). Within this range, it is preferable to use higher-frequency transducers for shorter path lengths and low-frequency transducers for longer path lengths because of attenuation.
- Coupling – The state-of-the-art in UPE testing of concrete is reflected in the development of dry-coupled array transducers, such as shown in Figure 2.2, which are based on the generation and propagation of S-waves. These systems do not require the use of a coupling material. This contrasts with earlier versions of UPE equipment that was based on the generation and propagation of compressional waves. In this case, it is necessary to fill the space between the transducer and concrete with viscous agents or water. This requirement is also applicable to the ultrasonic pulse velocity method (see Section 2.1.6) based on compressional waves (ASTM 2009b).

2.1.1.4 Influencing Factors Associated with Specimen and Environment

- Aggregate size – Large aggregates are associated with more scattering and attenuation of the signal; thus, requiring operation at lower frequencies (IAEA 2002, pp. 112-114).
- Embedded steel – Debonding of embedded steel from the surrounding concrete results in very poor coupling between the steel and concrete and prevents transmission of ultrasound through the steel, resulting in "shadowing" of locations behind the debonded steel (Clayton et al. 2013).

- Surface Conditions – Loose debris or material should be removed from locations where the transducer is to be placed in contact with the surface.

2.1.1.5 Limitations

- Most laboratory and field testing is performed on specimens with thicknesses of less than 375 mm (15 in.). This implies that UPE could be used to inspect portions of the concrete within 375 mm of the surface with currently available commercial technology. Deeper penetration may be possible with current instrumentation or with engineering modifications. However, such capability should be demonstrated.

2.1.2 Impact-Echo Testing

Impact-echo (IE) testing is a seismic or stress-wave technique that is performed by striking the surface of a test structure and measuring the response in close proximity. The impact excites longitudinal (compressional or P-wave), shear (S-wave), and surface-wave (R-wave) modes in the test structure with frequencies that can range from 1 to 60 kHz (IAEA 2002, p. 115). The P-wave and S-wave modes are reflected from internal reflectors and external boundaries. Although the technique can be applied to a variety of concrete structures, in principle, it has primarily been developed for the inspection of thin concrete structures approaching plate geometry (Carino 2001, pp. 5-6). The measurements are performed based on a frequency analysis of the signal provided by the P-wave echo from surfaces. For plate-like structures, this scenario is simplified because the number of reflecting surfaces is minimized and the reflecting surface is parallel to the surface that is struck. The analysis is based on the concept of plate thickness frequency. In essence, a peak will be observed in the frequency spectrum that is associated with resonant frequency for a plate with thickness, T. The resonant criteria is met when T is equal to half of the wavelength, $\lambda/2$. Thus,

$$f = \frac{V_P}{\lambda} = \frac{V_P}{2T}, \tag{2.1}$$

where f is the thickness frequency and V_P is the P-wave velocity. In addition, the depth, d, of a detected flaw can be determined from

$$d = \frac{V_P}{2f}. \tag{2.2}$$

Horizontally oriented flaws, such as delaminations and voids, are easiest to detect by the IE method (Carino 2001, p. 12). The depth of a flaw can be measured if its lateral dimension exceeds 1/3 of its depth. Flaws with lateral dimensions larger than 1-1/2 times their depth will have the effect of an infinite boundary and the frequency response will be equivalent to a plate with thickness equal to the flaw depth (Carino 2001, p. 12). For a flaw with lateral dimensions that do not exceed 1/3 of the flaw depth, it may still be possible to detect the flaw as a shift in peak frequency to lower value; however, the depth of the flaw cannot be measured. The minimum lateral dimension of a flaw that can be detected is approximately 1/4 of the flaw depth (Sansalone and Streett 1997). Finally, the minimum lateral dimension of a flaw that can be detected regardless of depth is equal to the wavelength associated with the maximum usable frequency (Sansalone and Streett 1997).

The frequency responses generated by these conditions are illustrated in Figure 2.3a)–d). As Figure 2.3a) and b) illustrate, the shift in peak frequency to a higher value is a result of the presence of a flaw with large lateral dimensions having the effect of an infinite boundary. Figure 2.3c) illustrates a sample response for a slab with a flaw with dimensions between 1/3 and 1-1/2 the slab thickness. In this case, two peaks can be observed in the frequency spectrum; one associated with the slab thickness, and the other peak associated with the flaw. Next, Figure 2.3d) illustrates the scenario in which the flaw dimensions are less than 1/3 of its depth. In this case, the flaw depth is not measurable but may be detectable based on a shift in peak frequency to lower values. Finally, Figure 2.3e) illustrates the scenario of a shallow delamination (within 100 mm [4 in.] of the impact surface). The low-frequency peak associated with shallow delaminations is attributed to flexural oscillations of the thin section of concrete above the delamination, causing it to vibrate like a constrained plate (Sansalone and Streett 1997, p. 99).

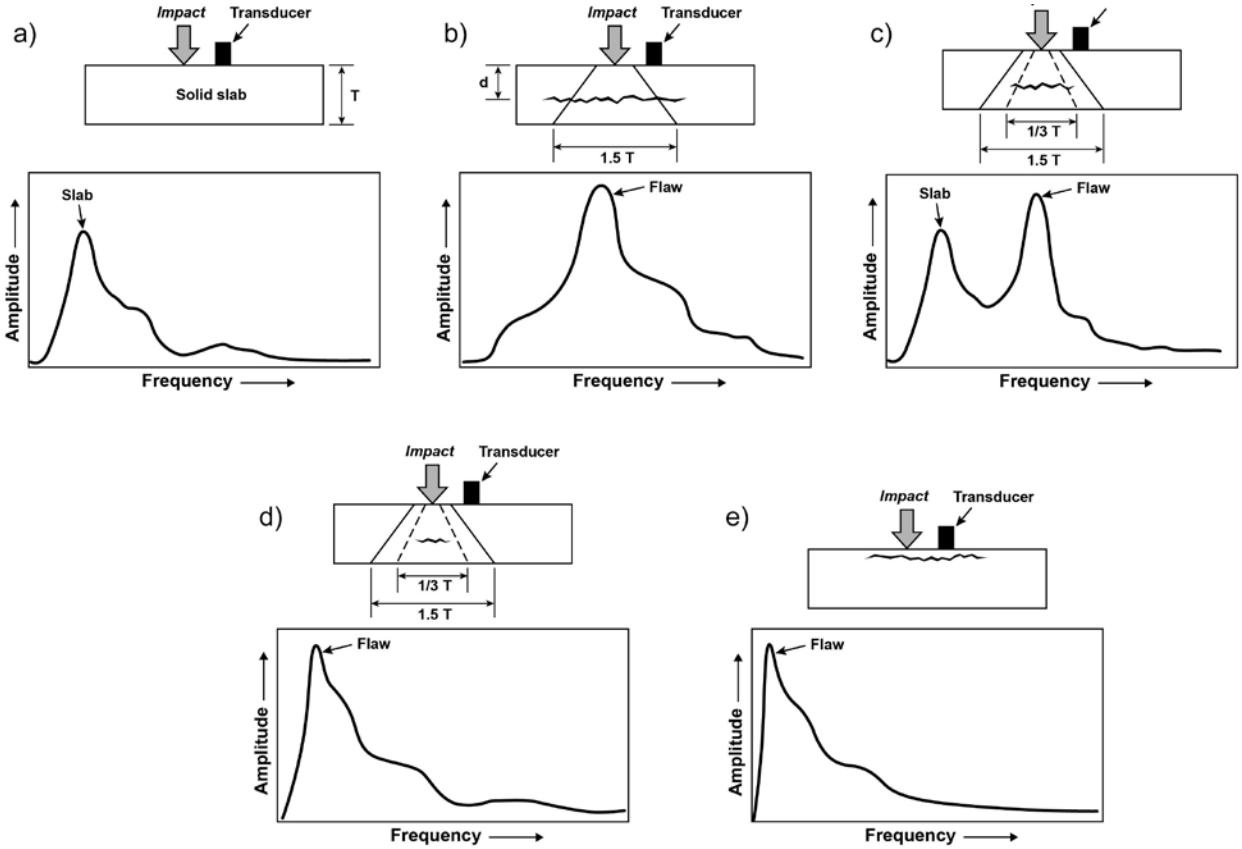

Figure 2.3. Illustration of Shift in the Peak Frequency of an Impact-Echo Response Caused by a Flaw

Sansalone and Streett (1997, pp. 123–134) also describe use of impact echo for measuring the depth of surface-breaking cracks in concrete. In this application, the impact source and receiver are placed on opposite sides of the crack. The presence of the crack blocks direct propagation of R-waves, P-waves, and S-waves from the impact source to the receiver. A diffracted P-wave is generated at the crack tip and the arrival time of this signal at the receiver may be used for estimating crack depth.

Standard ASTM C1383 exists for measuring the thickness of plate-like structures and is useful for the more general case of flaw detection (ASTM 2015c). In this standard, applicable plate-like structures are defined as having lateral dimensions that are at least six times their thickness.

2.1.2.1 Instrumentation and Implementation

Figure 2.4 depicts the implementation of a commercial impact-echo system. Steel balls mounted on spring steel rods are used for excitation while a nearby transducer measures the response. A PC records the signal and displays the frequency response.

Figure 2.4. Photograph Depicting the Implementation of Commercial Impact-Echo Testing Equipment (With permission of Impact-Echo Instruments, LLC[a])

The measurement can be affected by the distance between the impact location and the receiving transducer. If the distance is too large, then the response may be dominated by other modes besides the P-wave mode. If the distance is too small, then the response to the P-wave signal may be masked by the R-wave. Sansalone and Streett (1997) recommend a spacing of less than 40% of the depth.

Measurements are normally performed at several regularly spaced points along a line or rectangular grid. Many automated systems are designed for measuring on grid spacing from 5 cm to 10 cm (Helmerich et al. 2013).

Standard ASTM C1383 notes that suitable performance is achieved with a conical piezoelectric transducer, which is commercially available and which can be coupled to the test specimen using lead sheet (ASTM 2015c).

2.1.2.2 Field and Laboratory Experience

Several IE instruments were evaluated in SHRP 2 (TRB 2013). Technologies were evaluated according to several metrics including accuracy, precision, speed, ease-of-use, and cost. Overall, based on a composite score that considers all of these factors, IE testing was the second most suited method for delamination inspections behind radar testing (TRB 2013, p. 77). However, when considering only accuracy, IE testing scored the highest for delamination inspections, followed by infrared and radar testing (TRB 2013, p. 69).

[a] Impact-Echo Instruments, LLC, Ithaca, New York 14850; 607-756-0808.

Accuracy was assessed in laboratory validation studies which were performed on a fabricated bridge specimen and a recovered bridge specimen. The size of delaminations in the recovered bridge deck are not reported, but the size of simulated delaminations in the fabricated bridge deck ranged from 12 in. by 12 in. up to 24 in. by 48 in. (TRB 2013, p. 69).

2.1.2.3 Influencing Factors Associated with Instrumentation

- Impact duration – The impact duration determines the excitation frequency content and size of flaws that may be detected. Shorter impact durations cause higher-frequency components to be generated. Impact duration is a function of the type and size of impactor. Hammers are used for long and slender concrete members such as piles; whereas, spherical impactors (such as the impactor illustrated in Figure 2.4) with impact durations of 20 μs–80 μs are used for structural members less than 1 m (40 in.) thick. The impact duration, t_c, is a linear function of the impactor size (D – diameter) for an elastic impact (no crushing of concrete at impact location), $t_c \approx 4.3\ D$ where t_c is in μs and D has units of mm. Thus, for concrete structural members less than 1 m (40 in.) thick, the impactor diameter may be from 5 mm to 20 mm (0.2 in. to 0.8 in.). The maximum usable frequency in the impact signal is related approximately to the inverse of the impact duration (ACI 2013b, pp. 10-14). The minimum lateral dimension of a flaw that can be detected regardless of depth is equal to the wavelength associated with the maximum usable frequency (Sansalone and Streett 1997).
- Response of receiving transducer – The transducer should not have a resonant frequency that is close to the thickness frequency or anticipated frequency peaks to be measured (Carino 2001, p. 9).
- Coupling – Standard ASTM C1383 for measuring P-wave speed and the thickness of concrete components using the IE method notes that suitable performance is achieved with a conical piezoelectric transducer. In this case, coupling the transducer to the test piece with 0.25 mm thick lead sheet is recommended (ASTM 2015c).

2.1.2.4 Influencing Factors Associated with the Specimen and Environment

- Specimen geometry – The impact-echo technique was primarily developed for plate-like structures and standard ASTM C1383-15 ASTM (2015c) defines plate-like structures as having lateral dimensions of greater than six times the depth. Application to non-plate–like structures may result in modes generated by reflections from nearby boundaries resulting in a more complex frequency response. The detection of flaws requires understanding of the frequency response for the unflawed state (ACI 2013b, pp. 10-14).
- Specimen thickness – Thicker specimens are associated with a lower thickness frequency, which implies that longer impact durations are required and the lateral dimension of the minimum detectable flaw is larger. The minimum lateral dimension of a flaw that can be detected regardless of depth is equal to the wavelength associated with the maximum usable frequency (Sansalone and Streett 1997). Structural elements up to 1.5 m thick can be tested by IE (Sansalone and Streett 1997, p. 17).
- Embedded reinforcing steel – Reflection of P-waves from the concrete-steel interfaces of embedded steel bars can result in a cluster of peaks in the frequency spectrum characterized by the depth of the near and far interfaces of embedded steel with the concrete. If the ratio of bar diameter (D) to cover depth is less than 0.3, then the bars are not detected by IE signals. If the ratio is greater than 0.83, then the reinforcing steel dominates the IE response (Sansalone and Streett 1997, pp. 167-179).
- Compression wave speed – As can be seen in Eq. (2.1), the thickness frequency is directly proportional to the P-wave speed, which depends on the quality of the concrete. For quality concrete, typical P-wave speed may be approximately 4000 m/s.

- Surface Conditions – Standard ASTM C1383 for measuring P-wave speed and the thickness of concrete components using the IE method notes that surfaces should be dry and free of debris and dirt in the region where P-wave speed is to be determined. Loose debris or material should be removed before coupling the transducer to the test specimen. If surface roughness prevents adequate coupling, the surface should be ground so that adequate coupling can be achieved (ASTM 2015c).

2.1.2.5 Limitations

- Boundary conditions on structures of limited dimensions (i.e., structures that do not meet the definition of plate-like by standard ASTM C1383) will result in additional modes generated by reflections with boundaries that will result in a specific set of characteristic frequencies depending on the structure's shape and dimensions. The presence of a flaw can perturb these modes, making flaw detection possible. However, it is necessary to understand the frequency response for the unflawed case (ACI 2013b, pp. 10-14).
- Flaws at a depth of less than 10 cm cause flexural reflections at low frequencies, below the thickness frequency of the slab, which can make it difficult to estimate flaw depth (Helmerich et al. 2013, p. 66).

2.1.3 Impulse Response Testing

The impulse response (IR) method measures the dynamic response of a concrete structure in response to an applied impulse. Unlike the IE method that is based on excitation of thickness frequency modes above flaws and between top and bottom surfaces of slabs, the IR method is based on excitation of a bending vibration mode in the specimen. Whereas the measured frequency response of the IE method may be up to 60 kHz, the frequency response of the IR method is between 0–1 kHz.

A load cell in the hammer is used to measure the force spectrum associated with the impulse, while the receiver is used to record the velocity spectrum. The mobility spectrum is obtained by dividing the resulting velocity spectrum by the force spectrum. An illustration of a typical mobility spectrum is shown in Figure 2.5a). Information on the mechanical properties and integrity of the specimen can be obtained from analysis of the mobility spectrum, including (ASTM 2010):

- Dynamic stiffness – The slope of the mobility spectrum below 0.1 kHz represents compliance at the location of the test point. Dynamic stiffness is the inverse of compliance and is depending on the density and thickness of the plate structure, as well as the elastic modulus, as illustrated in Figure 2.5a).
- Mobility and damping – The test structure rigidity is directly related to the average mobility above 0.1 kHz [see Figure 2.5b)]. The rigidity is related to the structure thickness and quality of concrete. A reduction in thickness (i.e., delamination) will result in increased mobility. The presence of other aging effects such as cracking and honeycombing can result in increased mobility.
- Peak/mean mobility ratio – Debonding and delamination in a structure causes a decrease in the dynamic stiffness below 0.1 kHz and an increase in mean mobility from 0.1 to 1 kHz. The overall effect is that the peak mobility below 0.1 kHz becomes much greater than the mean mobility over 0.1 to 1 kHz, resulting in a mobility plot with a prominent peak at low frequency, as illustrated in Figure 2.5c).

ASTM C1740-10, "Standard Practice for Evaluating the Condition of Concrete Plates Using the Impulse Response Method," (ASTM 2010) provides guidance for implementing the IR testing method to concrete structures.

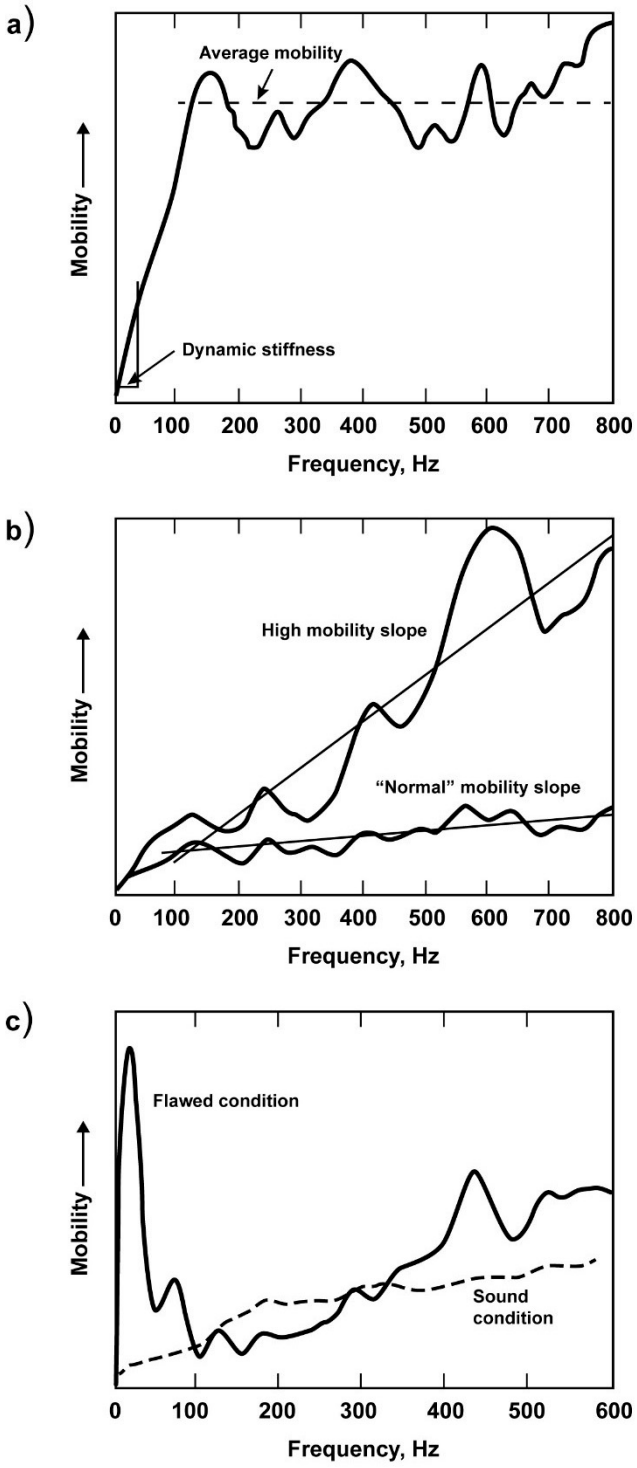

Figure 2.5. Illustration of Mobility Spectrums for IR Testing of a Plate-Like Structure Including Definitions of Dynamic Stiffness and Average Mobility Spectrum Features that Indicate a Flawed Condition.

2.1.3.1 Instrumentation and Implementation

The IR method is performed using a 3 lb. sledge hammer with a plastic tip and load cell to excite the structure and measure the force. The displacement velocity is measured with a velocity transducer (geophone) (ACI 2013b, pp. 15-17) [see Figure 2.6a)]. Modern systems include digital data acquisition equipment to record the force and velocity signals, develop the mobility spectrum, and display the results. IR measurements are performed by acquiring measurements at several points on a regularly spaced grid (typically 0.5 m–1.0 m spacing) as illustrated in Figure 2.6b) (ACI 2013b, pp. 15-17). A field system for structural testing became commercially available in 2002 (ACI 2013b, pp. 15-17).

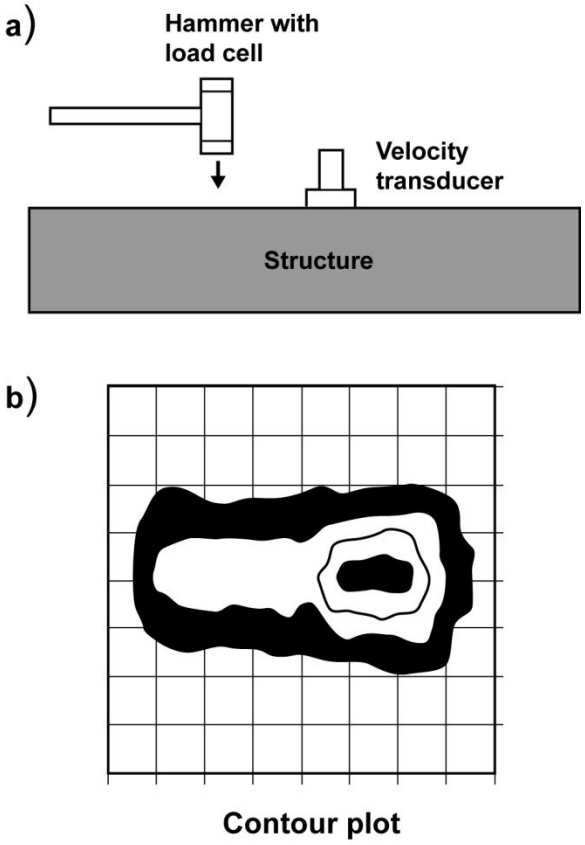

Figure 2.6. a) Illustration Depicting the Implementation of the IR Method and b) a Contour Plot Representing the Results of Measurements (e.g., dynamic stiffness, mobility, mobility ratio) Mapped for a Grid of Measurement Points

2.1.3.2 Field Experience

The IR method was evaluated in the field trial portion of SHRP 2, which was conducted on a highway bridge (TRB 2013). In this case, the IR technique was described as not being very successful at detecting delaminated areas (TRB 2013, p. 48).

IR was the primary inspection method used to evaluate the extent of delamination in the containment structure at the Crystal River Unit 3 nuclear plant and the measurements were validated by core sampling. The extent of delamination as determined by IR measurements encompassed an area of approximately 18.3 m (60 ft.) by 24.4 m (80 ft.) located at an average depth of 175 mm (7 in.) to 200 mm (8 in.) below the outer containment structure surface (Miller 2010).

2.1.3.3 Influencing Factors Associated with Instrumentation

- Impactor – The characteristics of the impactor (sledge hammer) affect the useful frequency range that is generated in the test structure. Guidance for impactor parameters, including impactor mass, size, and load cell response are provided in ASTM C1740-10.
- Response of receiving transducer – Standards for the frequency response of velocity transducers are provided in ASTM C1740-10. The standard specifies that the transducer should have a natural frequency of less than 15 Hz and constant response over the range from 15 Hz to 1 kHz.
- Coupling – The IR method is implemented using velocity transducers (geophones). No coupling material is necessary to couple the transducer to concrete (ASTM 2010).

2.1.3.4 Influencing Factors Associated with Specimen and Environment

- Specimen geometry – The interpretation of mobility spectrum as illustrated in Figure 2.5 assumes plate-like structures. The applicable definition of a plate-like structure for IR testing is the same as the definition provided in standard ASTM C1383-15 for impact-echo testing. This standard defines plate-like structures as having lateral dimensions of greater than six times the depth (ASTM 2015c). The standard for performing IR measurements was developed for plate-like structures (ASTM 2010). Measurements should not be made near the edges or boundaries of a test structure (within 300 mm [12 in.]) (ASTM 2010).
- Surface conditions – Standard ASTM C1740-10 specifies that the surface can be dry or wet, but not inundated and that loose debris or material should be removed in the location of test points and before the transducer is placed in contact with the surface. If surface roughness prevents adequate contact between the transducer and the surface or sufficient impact duration, grinding of the surface is recommended so that adequate contact and impulse durations can be achieved (ASTM 2010).

2.1.3.5 Limitations

- The IR method can detect gross defects in structures but is less reliable for the detection of smaller defects (TRB 2013, p. 19). The standard for performing IR measurements was developed for plate-like structures (ASTM 2010). Measurements should not be made near the edges or boundaries of a test structure (within 300 mm [12 in.]) (ASTM 2010).

2.1.4 Spectral Analysis of Surface Wave and Ultrasonic Surface Wave Testing

The spectral analysis of surface waves (SASW) is a technique for inspecting layered structures based on the propagation of surface Rayleigh waves (R-waves) (Nazarian et al. 1983). When propagating in layered structures with varying elastic properties, R-waves exhibit a phenomenon known as dispersion in which the velocity of the propagating R-wave varies based on the frequency and wavelength. A plot of velocity versus frequency or wavelength is known as a dispersion curve and information pertaining to the thickness and elastic moduli can be obtained by analysis of these dispersion curves. Penetration of the R-wave energy is on the order of the wavelength; thus, information on the profile of elastic properties as a function of depth in a structure can be obtained by applying an inversion process to dispersion curves (see Figure 2.7). Elastic properties such as Young's modulus (E) and the shear modulus (G) can be determined through relationships with the compressional and shear-wave velocities (i.e., V_P and V_S, respectively); which, in turn, relate to the R-wave velocity, V_R:

$$E = \rho(1+\nu)(1-2\nu)V_P^2/(1-\nu), \tag{2.3}$$

$$G = \rho V_S^2, \tag{2.4}$$

$$\nu = \left[0.5\left(V_P / V_S\right)^2 - 1\right] / \left[\left(V_P / V_S\right)^2 - 1\right], \tag{2.5}$$

$$V_P = \frac{1+\nu}{0.87+1.12\,\nu}\sqrt{\frac{2(1-\nu)}{1-2\nu}}V_R\ , \tag{2.6}$$

where ρ is the mass density and ν is the Poisson's ratio (Nazarian et al. 1983).

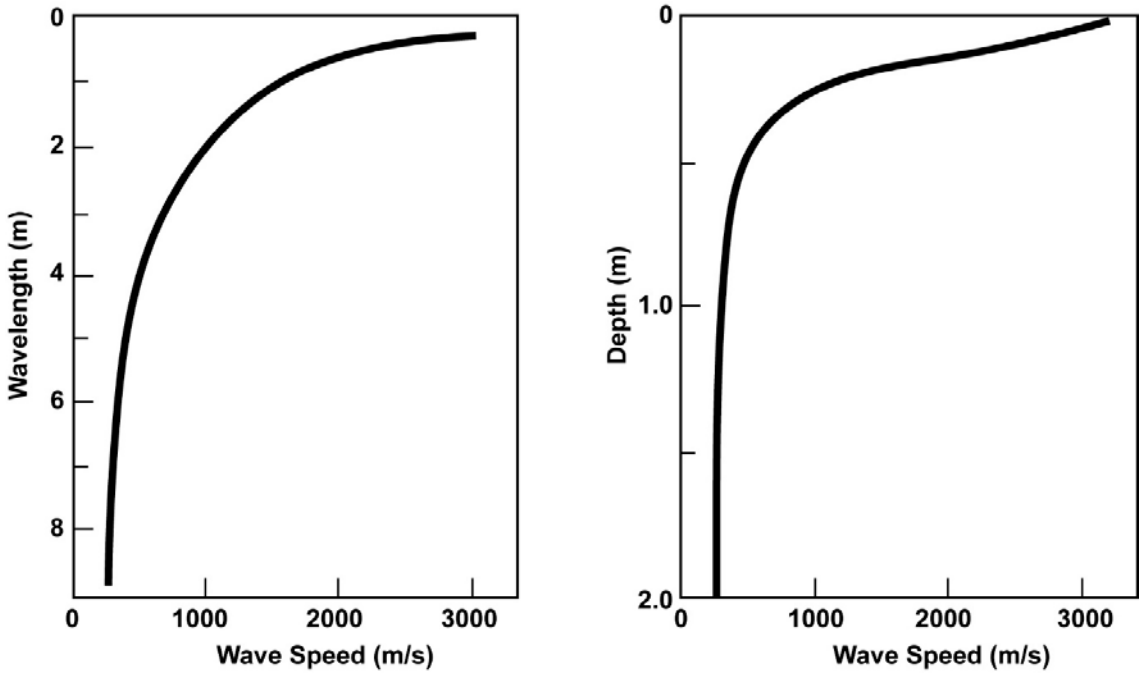

Figure 2.7. (left) Depiction of a Dispersion Curve Obtained by SASW Testing on a Multi-Layered Structure with Heterogeneous Elastic Properties and (right) Depiction of Velocity Profile as a Function of Depth Based on Inversion of the Dispersion Curve

In single-layer homogeneous structures, R-waves to do not exhibit dispersion and the measured V_R can be related directly to V_P and V_s through the relationships above. This case is satisfied for concrete structures for wavelengths less than the structure thickness. When the test structure thickness exceeds the wavelength, the velocity will depend only on the elastic properties of the structure and not on the thickness. This simplified scenario has been referred to as ultrasonic surface-wave (USW) testing (TRB 2013, p. 16).

The SASW (or USW) method involves a mechanical impact on the surface of the concrete structure to generate R-waves of different wavelengths that are picked up by transducers placed at fixed distances from the impact source, as illustrated in Figure 2.8. The velocity of each wavelength component is evaluated by calculating the phase difference between two receivers for each wavelength (ACI 2013b, pp. 14-15).

The influence of reflected R-waves and reflected S-waves and P-waves from boundaries was investigated by Sheu et al. (1988). Reflections can cause fluctuations to appear in the dispersion curves. To minimize the influence of reflections from edges, Sheu et al. (1988) recommend placement of the source between the boundary edge and receivers when the transducer array is oriented perpendicular to the edge. When the edge is oriented parallel to the transducer array, it is recommended to position the array very close to

the boundary so that reflected waves are in phase with the source waves, or positioning the array as far from the reflecting boundary as possible so that reflected waves experience more attenuation and are of low amplitude.

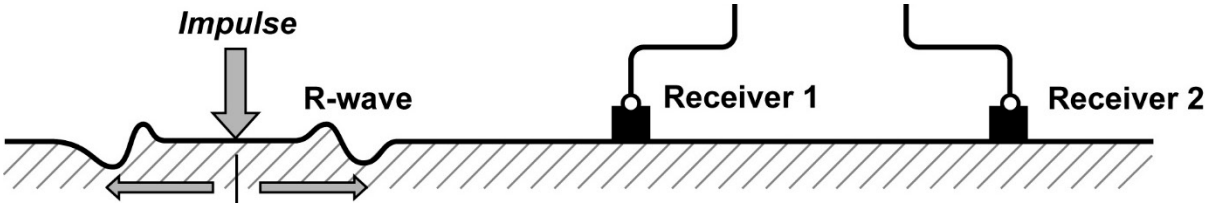

Figure 2.8. Schematic of SAWS (or USW) Method with Source Impact to Excite an R-wave with Circular Wave Front and Pair of Receivers (geophones) to Measure the R-wave Velocity Based on Phase Difference between the Two Transducers

The SASW testing method can be combined with the IE testing method for examining concrete structures (Kim et al. 2002; Kim et al. 2006). In this case, SASW can be used to directly measure the compressional wave velocity in situ to improve the accuracy of locating delaminations via IE testing. In these studies, a value of $\nu = 0.2$ is assumed, which is estimated to limit the possible error in compressional wave velocity measurement to 5% (Kim et al. 2002).

2.1.4.1 Instrumentation and Implementation

The source and receiving transducers are usually spaced such that the distance from the source to the nearest receiver is equal to the distance between the receiving transducers. When investigating concrete pavements and structural members, the receivers are located relatively close together with the closest spacing of about 0.15 m. The spacing is increased by a factor of two for subsequent tests. Tests are also performed by reversing the position of the source relative to the receivers as a check of the phase measurement (ACI 2013b, pp. 14-15).

Two modes for conducting the tests include the common source and common receiver midpoint methods, as illustrated in Figure 2.9. The common source method is depicted in the top of Figure 2.9, while the common receiver midpoint method is depicted in bottom of Figure 2.9 (Nazarian et al. 1995, pp. 5-7). A combination of geophones and accelerometers may be used for application to concrete pavements, while small accelerometers are typically used for application to concrete structural members (ACI 2013b, pp. 14-15). As depicted in Figure 2.9, the measurement location remains fixed as determined by the midpoint between the receivers, for each set of measurements in the common receiver midpoint method. In the common source method, the receiver midpoint moves for each subsequent location, indicating that the location of the sample changes for each subsequent measurement. It would appear that the common source method may provide a more global assessment of the concrete but may average out local variations because the concrete that is sampled changes with subsequent measurements. Conversely, the common receiver midpoint method samples a region of concrete more consistently and so the method appears to be more localized.

The source must be capable of generating R-waves over a wide range of frequencies while simultaneously minimizing the generation of P-wave or S-wave energy (Nazarian et al. 1983). In this case, a small hammer, or even smaller impactor or vibrator, is required so that a short-duration pulse is produced with sufficient energy at frequencies up to approximately 50 to 100 kHz (ACI 2013b, pp. 14-15). For USW testing, the frequency range of interest is limited to a narrow high-frequency range as such that the surface-wave penetration does not exceed the thickness of the structure under test (TRB 2013, p. 16). Typically, velocity transducers (geophones) or accelerometers are used as receivers (ACI 2013b, pp. 14-15).

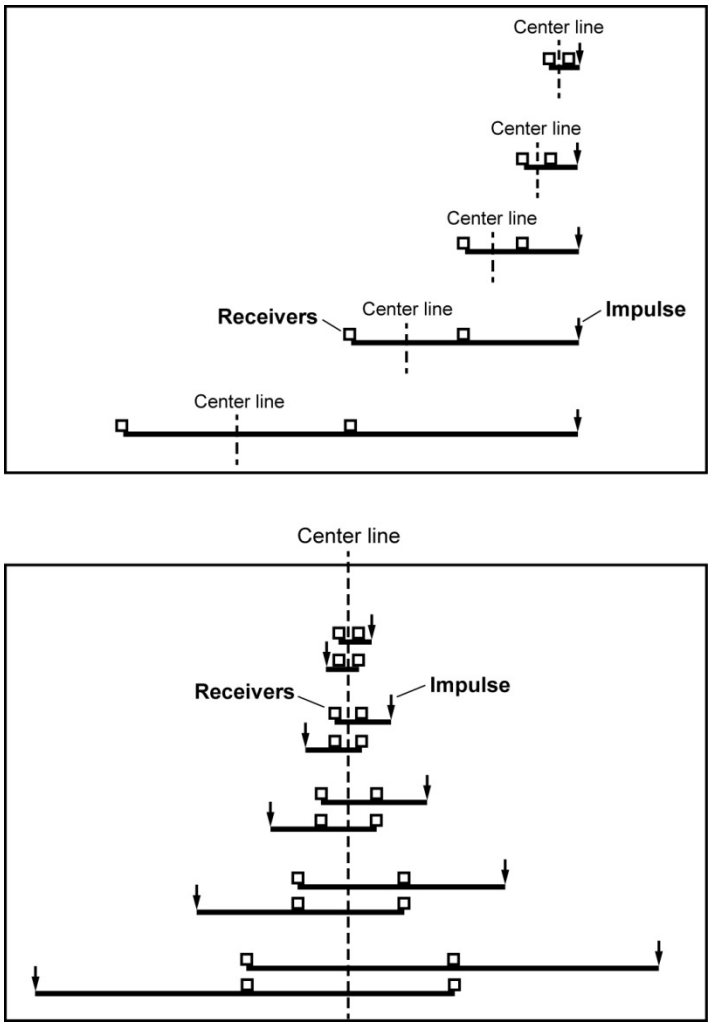

Figure 2.9. Schematic of the (top) Common Source and (bottom) Common Receiver Midpoint Methods for Conducting SASW (or USW) Testing

2.1.4.2 Field or Laboratory Experience

SASW and USW technologies were evaluated in SHRP 2 (TRB 2013). USW technologies were used to measure the elastic properties of concrete structures while SASW technologies were applied for measuring the depth of vertical cracks, and an IE-USW technology was evaluated for delamination detection capability (TRB 2013, p. 69).

With respect to measuring the degradation of concrete properties, the USW technique performance was rated much better than any other techniques or methods evaluated based on accuracy (TRB 2013, p. 69) and based on a composite score consisting of factors such as speed, cost, repeatability, and ease-of-use (TRB 2013, p. 77). Other methods that were evaluated in SHRP 2, and considered applicable to measuring degradation of concrete properties, included radar and IE testing.

In the field validation testing portion of SHRP 2, USW testing also exhibited capability to detect delaminations as areas of measured low elastic moduli. These areas correlated well with areas where delaminations were detected by other methods (TRB 2013, p. 48). The complete true state in the field

validation testing is unknown, but comparisons to other NDE methods used in the study suggest that the specimen had delaminations with areas of approximately 10 ft. by 10 ft. or smaller.

Finally, SASW techniques rated highest for measuring depth of vertical cracks in terms of accuracy (TRB 2013, p. 69) and based on a composite score consisting of factors such as speed, cost, repeatability, and ease-of-use (TRB 2013, p. 77).

2.1.4.3 Influencing Factors Associated with Instrumentation

- Impactor – The characteristics of the impactor affect the useful frequency range that is generated in the test structure. Typically, a greater impactor mass will result in excitation of a lower frequency range. The desired range of frequencies is dictated by the desired depth of the penetration. In this case, the low end of the frequency range (longest wavelengths) should include components that are compatible with inspecting at the deepest desired depth for SASW testing. For USW testing, interest is focused on a narrower frequency range sufficiently high that all wavelength components are less than the thickness of the component under test.
- Response of receiving transducer – No known standard exists for receivers used for surface-wave testing of concrete. However, their response should be compatible with the frequency range of interest for the inspection.
- Coupling – The SASW method is implemented using velocity transducers (geophones) or accelerometers. No coupling material is necessary to couple the transducer to concrete.

2.1.4.4 Influencing Factors Associated with Specimen and Environment

- Specimen geometry – Reflections can cause fluctuations to appear in the dispersion curves. To minimize the influence of reflections from edges, Sheu et al. (1988) recommend placement of the source between the boundary edge and receivers when the transducer array is oriented perpendicular to the edge. When the edge is oriented parallel to the transducer array, it is recommended to position the array very close to the boundary so that reflected waves are in phase with the source waves, or positioning the array as far from the reflecting boundary as possible so that reflected waves experience more attenuation and are of low amplitude.
- Surface conditions – Specimen surface conditions can be important for techniques based on propagation of surface waves. Although dust and small debris would not be expected to impact SASW and USW measurements, other conditions such as standing water or contact with other structures, may have an influence. Loose debris or material should be removed from the location where the transducer will be mounted.
- Specimen thickness – For SASW testing, a greater specimen thickness will require a lower frequency range of excitation for penetration to greater depth and will require greater spacing between transducers. This will require access to a large surface area for measurements (Naus 2009a, pp. 37-45).

2.1.4.5 Limitations

- SASW testing of thick members requires greater spacing between receivers. Thus, testing of thick structural members require access to large surface areas (Naus 2009a, pp. 37-45). A minimum depth of 50 mm (2 in.) is required to measure reduced strength and elastic properties in damaged concrete layers (ACI 2013b, pp. 14-15).

2.1.5 Audio Methods

Audio methods (or sounding methods) are essentially elastic wave tests performed in the audible frequency range (generally considered to be 20 Hz–20 kHz). Sounding methods are based on striking the surface of a concrete structure and listening to the audible noise to characterize the condition. Deteriorated areas of concrete are discerned by a "dull" or "hollow" sound that results from low-frequency flexural oscillations (usually in the 1 kHz–3 kHz range) that are caused by the deflection of the thin section of concrete above the delamination causing it to vibrate like a constrained plate (Sansalone and Streett 1997, p. 99; TRB 2013, pp. 25-28). Solid areas of concrete will produce a characteristic "ringing" sound when impacted (TRB 2013, pp. 25-28). These methods are used to detect delaminated, debonded, or cracked areas in concrete structures such as bridge decks. Sounding methods may miss small delaminations and are usually limited to an effective region of penetration not exceeding the concrete cover depth. The methods are relatively fast and are typically performed over a grid to map the structure to provide a profile of delaminations (Naus 2009a, pp. 37-45).

Guidance for performing sounding testing of concrete bridge decks is provided by standard ASTM D4580, "Standard Practice for Measuring Delaminations in Concrete Bridge Decks by Sounding," (ASTM 2012c). The standard identifies three procedures for performing sounding including: electromechanical sounding, chain drag, and rotary percussion. The electromechanical sounding procedure employs an electric-powered tapping device, whereas the chain drag procedure is the procedure noted above and is performed by noting dull or hollow sounds while dragging a chain over the concrete surface. The chain drag may be substituted with tapping the bridge deck with a steel rod or hammer. The rotary percussive procedure is performed using percussive units attached to an axle. Tapping devices on the percussive units strike the concrete as the rotary percussive units are rolled over the surface of the concrete.

Sounding methods using hammers or by chain dragging are referred to as the most common methods for detection of delaminations in concrete bridge decks. Chain dragging can be performed in a much more rapid manner than hammer sounding; thus, it is used to rapidly inspect large surface areas. Hammer sounding is used to inspect much smaller areas and is used to more accurately define the boundaries of delaminated regions. While chain dragging is limited to horizontal surfaces, hammer sounding may be implemented on both horizontal and vertical surfaces (TRB 2013, pp. 25-28).

Hammer sounding and chain dragging are also considered to be very operator-dependent. The interpretation of the sound can also be operator-dependent and the signals generally are not quantified. An exception includes the electric-powered tapping device method as specified in standard ASTM D4580, which specifies the use of sonic receivers and a recorder also capable of basic noise filtering (ASTM 2012c).

2.1.5.1 Instrumentation and Implementation

The chain drag technique is performed using several segments of linked steel chain, as specified in ASTM D4580. The chain drag can be substituted by tapping with a hammer or with steel rods. The dimensions of the steel rod are specified in ASTM D4580. No specifications are provided for hammers (ASTM 2012c). Photographs of chain dragging and hammer sounding being implemented on a concrete bridge deck are provided in Figure 2.10 (TRB 2013, pp. 25-28).

The electric-powered tapping device method incorporates tapping wheels capable of tapping the bridge deck surface at a rate of 33 times/sec. (ASTM 2012c). Further, sonic receivers are to be used to record the signals (ASTM 2012c).

The rotary percussion method employs hardened steel rotary percussion units that are fit onto an axle to be rolled over the surface to be tested (ASTM 2012c).

Figure 2.10. Depiction of Chain Dragging (left) and Hammer Sounding (right) on a Bridge Deck (TRB 2013, p. 27)

2.1.5.2 Field or Laboratory Experience

Hammer sounding was performed on a few NUHOMS HSMs (model HSM-15) at Calvert Cliffs and no defect areas were found using this method (EPRI 2015a). It is not clear which components of the HSMs were tested.

Hammer sounding was performed as part of baseline inspections performed on all NUHOMS HSMs (model HSM-80) containing Three Mile Island fuel at Idaho National Laboratory (INL) in 2008. It is not clear if any defect areas were discovered as a result of hammer sounding (EPRI 2015a).

Chain dragging and hammer sounding were evaluated in SHRP 2 (TRB 2013). Based on accuracy for inspection of delaminations, chain dragging and hammer sounding was rated lower than radar testing, IE testing, and infrared thermography (IRT) testing (TRB 2013, p. 69). Accuracy was assessed in laboratory validation studies that were performed on a fabricated bridge specimen and a recovered bridge specimen. The size of delaminations in the recovered bridge deck are not reported, but the size of simulated delaminations in the fabricated bridge deck ranged from 12 in. by 12 in. up to 24 in. by 48 in. (TRB 2013, p. 69). When chain dragging and hammer sounding for inspection of delaminations was evaluated based on a composite score consisting of factors such as speed, cost, repeatability, and ease-of-use, it was rated above USW testing and tied with IRT testing. However, it still rated below radar testing and IE testing (TRB 2013, p. 77).

2.1.5.3 Influencing Factors Associated with Instrumentation

- Coupling – Use of sonic receivers is to be implemented for audio methods employing electric-powered tapping devices. These are to consist of wheel-mounted hydrophones coupled to the test structure through soft tires and oil within the wheel (ASTM 2012c). No coupling material is necessary to couple the transducer to concrete.

2.1.5.4 Influencing Factors Associated with Specimen and Environment

- Geometry and thickness – Chain dragging and hammer sounding can be applied to specimens of essentially any geometry and are not heavily influenced by specimen thickness. However, the

methods are usually limited to an effective region of penetration not exceeding the concrete cover depth (Naus 2009a, pp. 37-45). While chain dragging is limited to horizontal surfaces, hammer sounding may be implemented on both horizontal and vertical surfaces (TRB 2013, pp. 25-28).

- Environmental noise – Other sources of audible noise (e.g., traffic) can interfere with interpretation of audible sounding signals.
- Surface conditions – Use of sonic receivers is to be implemented for audio methods employing electric-powered tapping devices. These are to consist of wheel-mounted hydrophones coupled to the test structure through soft tires and oil within the wheel (ASTM 2012c). Loose debris or material should be removed from the surface where the wheel mounted hydrophones will be in contact with the surface.

2.1.5.5 Limitations

- Audio methods have limited penetration depth (typically not exceeding cover depth). In addition, chain dragging and hammer sounding methods are operator-dependent and rely on the subjective interpretation of sound and deteriorated concrete regions (Naus 2009a, pp. 37-45).

2.1.6 Ultrasonic Pulse Velocity Testing

Ultrasonic pulse velocity (UPV) testing is based on measuring the travel time over a known path length for a pulse of ultrasonic compressional waves (P-waves). The schematic of a UPV system is shown in Figure 2.11 (ACI 2013b, pp. 7-9). It is most useful when carrying out comparative surveys of concrete quality in or between similar concrete structures. Some primary uses of UPV include determination of the uniformity of concrete in and between members, measurement of the changes in concrete properties over time, the estimation of concrete strength, and the determination of elastic properties of the concrete. UPV can also be used for detection of internal defects such as voids or cracks (IAEA 2002, pp. 100-112). The effects of different defects on travel time of ultrasonic pulses are illustrated in Figure 2.12 (TRB 2013, pp. 7-9). The sensitivity of ultrasonic pulse velocity to defect size is determined by the size of the sound beam and wavelength. Assuming a velocity in concrete of 4000 m/s and frequency of 50 kHz, the wavelength is 80 mm (3 in.). It is reported that it is possible to use UPV to detect defects with projected sizes of approximately 100 mm (4 in.) or greater (IAEA 2002, pp. 100-112). The reliability of crack detection is significantly impacted by the presence of water filling cracks or contact between crack faces, which can allow ultrasonic energy to propagate through the faces with little resistance (IAEA 2002, pp. 100-112).

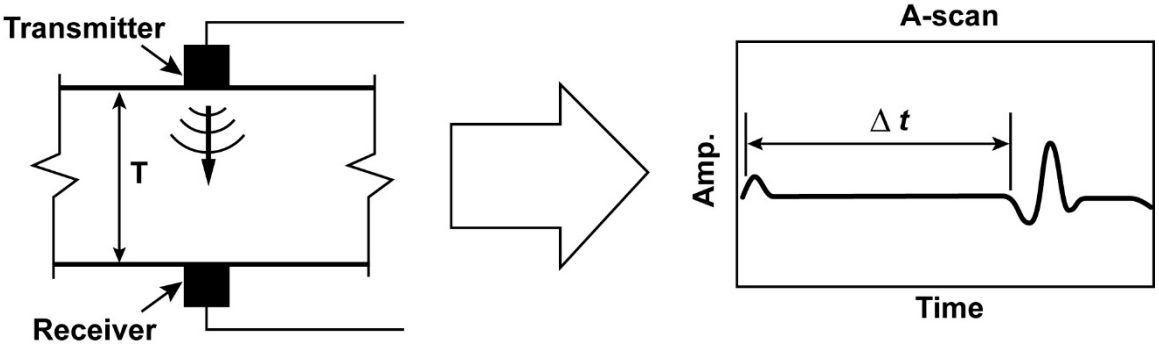

Figure 2.11. Schematic of Through-Transmission Test System

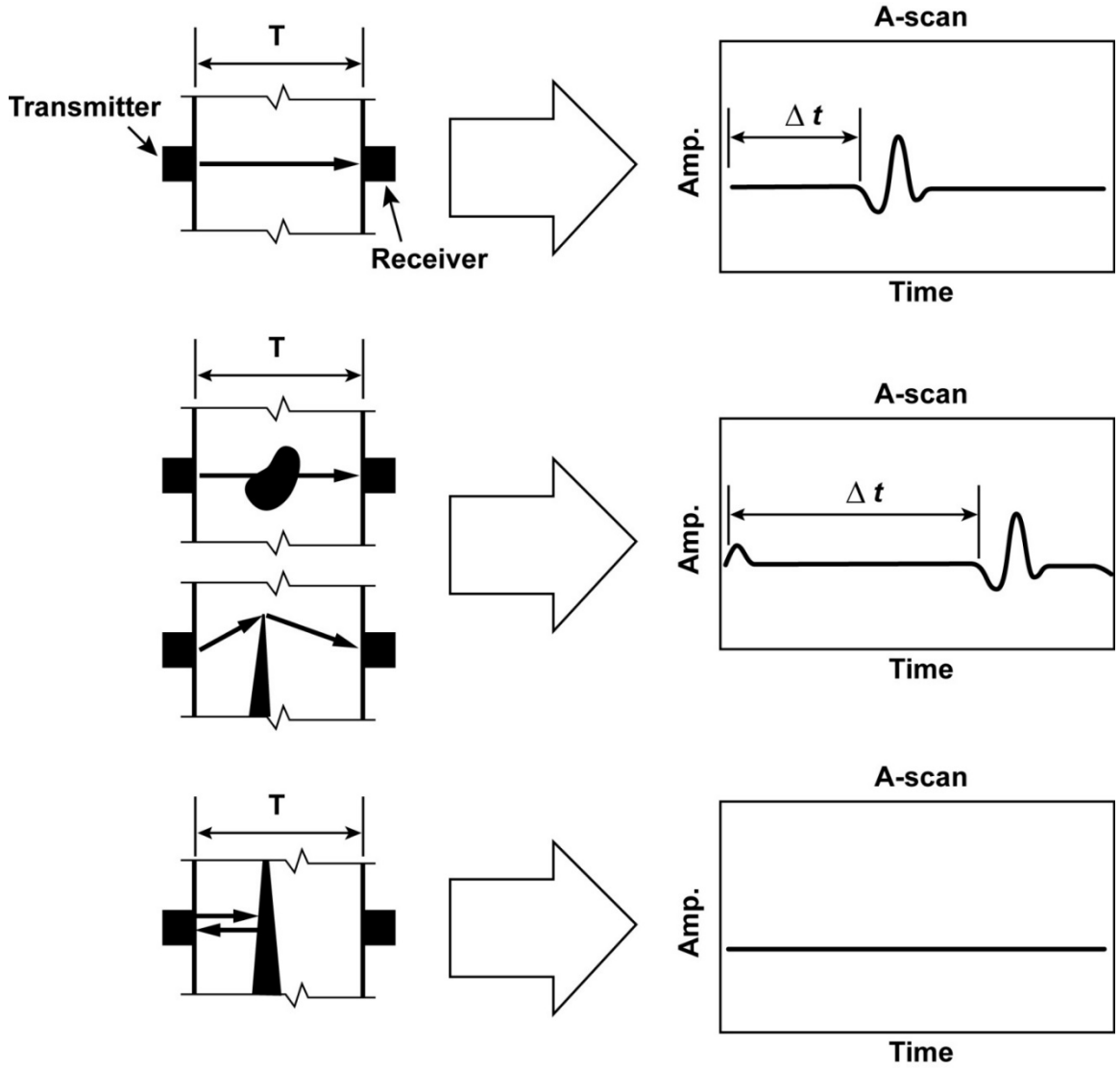

Figure 2.12. Illustration of the Effects of Different Defects on Travel Time of Ultrasonic Pulses

Figure 2.11 depicts a "direct transmission" configuration, which requires that transducers be able to access both sides of a concrete member. However, alternative configurations for UPV are possible. For instance, an "indirect transmission" or "surface transmission" configuration is depicted in Figure 2.13, which shows that it is possible to conduct UPV measurements when only single-sided access is possible (IAEA 2002, pp. 100-112). The indirect transmission method is reported to be less sensitive than the direct transmission method with received signal amplitudes reported to be on the order of 2% to 3% of those produced by direct transmission (IAEA 2002, pp. 100-112). Also, the measured pulse velocity for the indirect transmission method is more heavily influenced by concrete near the surface than the direct transmission method. As a result, the measured pulse velocity for the indirect transmission method is lower in comparison to measured pulse velocity by the direct transmission method (IAEA 2002, pp. 100-112). The contact area of the transducers contributes to uncertainty in the path length for the indirect transmission configuration. To reduce this uncertainty, a series of measurements can be made with different separation distances between the transducers (see Figure 2.14). The slope of a straight line through data points of transit time versus separation distance can be used to estimate the mean measured pulse velocity. A discontinuity or change in slope of this line is an indication of a surface crack or

presence of a surface layer of concrete of inferior quality (IAEA 2002, pp. 100-112). The reason for this change in slope is depicted in Figure 2.13, which shows that for a degraded surface layer on top of sound concrete, two paths exist for the signal transmission between the transmitter and receiver. For close transducer spacings, the transit time for the path along the concrete surface is shorter. As transducer spacing is increased, the transit time along the path interior to the concrete at the interface between damaged and sound concrete will be shorter. If the concrete quality is homogeneous, the transit time at the surface will always be the shortest and there will be no deflection in the line. The depth of the degraded surface layer can be determined from the location of the deflection of the slope of transit time versus separation distance of transducers. ACI 228.2R (ACI 2013b, pp. 7-9) indicates that the indirect transmission mode is primarily used for measuring the depth of damaged surface layers of concrete (e.g., by fire or freeze-thaw). ACI 228.2R also states that the technique is only applicable if the upper layer has a slower wave speed than the lower layer.

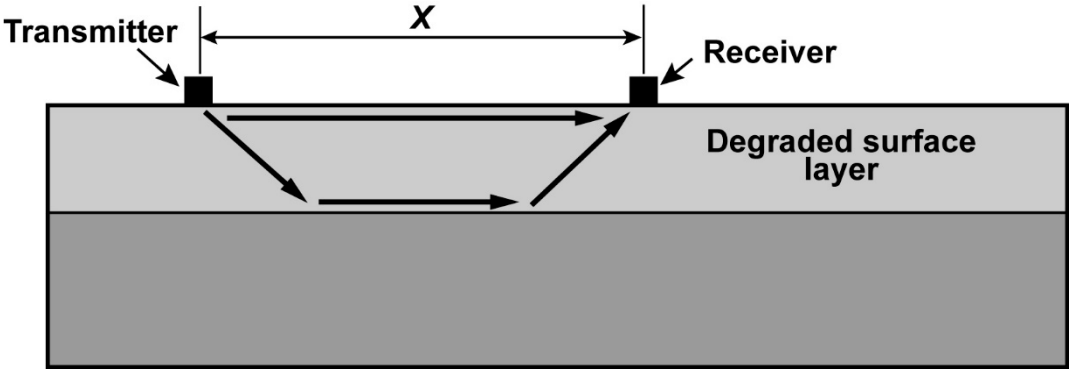

Figure 2.13. Depiction of Indirect UPV Configuration

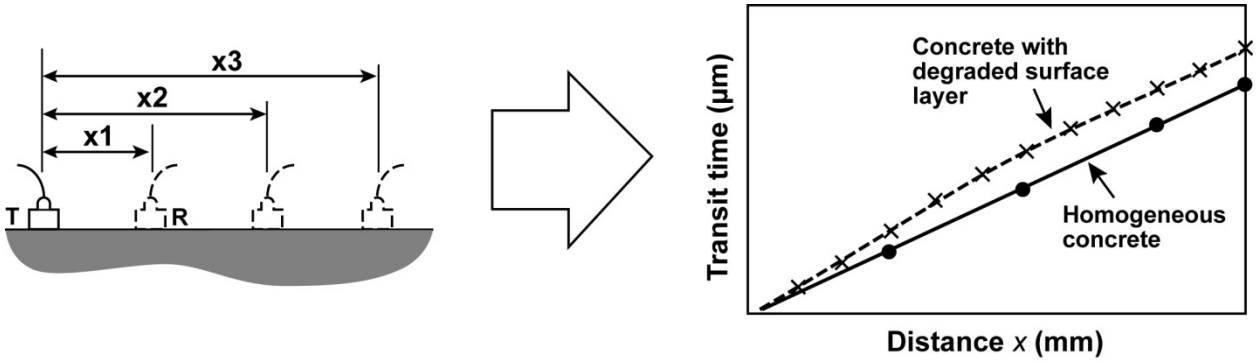

Figure 2.14. Depiction of Series of Measurements for Indirect Transmission Configuration and Plot of Transit Time versus Separation Distance for Transducers (IAEA 2002, p. 108)

The UPV technique can also be used measure concrete properties such as strength and elastic modulus. Strength and velocity are proportional; thus, variations in measured velocity over a concrete component can provide indication of regions of relatively greater and less strength. A qualitative classification of concrete quality based on UPV is provided in Table 2.1. Obtaining an actual estimate of strength from UPV measurements requires correlation of UPV with relevant specimens of known strength. This is performed by fabricating specimens with similar concrete specifications to the component under test or removing core samples from the component under test. The accuracy of concrete compressive strength measurements using UPV is reported to be approximately ± 20% (Naus 2009a, pp. 37-45).

Table 2.1. Qualitative Classification of Concrete Quality According to UPV

Compressional Wave (P-wave) Velocity (m/s)	Concrete Quality
>4500	Excellent
3500–4500	Good
3000–3500	Doubtful
<3000	Poor

2.1.6.1 Instrumentation and Implementation

UPV application requires transmitting and receiving transducers, a pulser for generating the signals in the transmitter, and an amplifier for the received signal. ASTM C597, "Standard Test Method for Pulse Velocity Through Concrete," specifies that transmitter transducers should have resonant frequencies from 20–100 kHz (ASTM 2009b). For most applications, 50 kHz resonant frequency transducers are suitable, whereas low resonant frequency transducers (20 kHz) are used for mass concrete. Received signals are input to an oscilloscope for measuring the transit time. A viscous coupling agent is required to fill in air gaps between the concrete surface and the contact surfaces of the transducers to ensure efficient transfer of energy between the concrete and transducers.

2.1.6.2 Influencing Factors Associated with Instrumentation

The requirements for a suitable pulse velocity device are given in ASTM C597 (ASTM 2009b). The influencing factors of UPV testing associated with instrumentation include:

- Frequency – Transducers of various resonant frequencies have been used, with 50 kHz to 60 kHz transducers being the most common. It is preferable to use high-frequency transducers for shorter path lengths and low-frequency transducers for longer path lengths due to attenuation. Generally, lower-frequency transducers are used for mass concrete (10–20 kHz) and higher-frequency transducers (> 100 kHz) are used for thinner members where accurate travel times have to be measured (IAEA 2002, pp. 100-112).
- Coupling – Coupling to fill the space between the transducer and concrete can be typically provided by viscous agents or water. Standard ASTM C597 notes that quality of the coupling is very important for the accuracy and range of the UPV method and that repeat measurements should be performed at the same location to minimize errors due to inadequate coupling (ASTM 2009b).

2.1.6.3 Influencing Factors Associated with Specimen and Environment

- Composition – There are many variables associated with specimens that influence the ultrasonic pulse velocity. These include aggregate size, type, and gradation; cement type; water-to-cementitious materials ratio; admixtures; degree of compaction; curing conditions and age of the concrete; concrete temperature; moisture content; size and shape of specimen; and presence of reinforcement (Naus 2009a). However, many of these influencing factors are only important when attempting to correlate velocity to concrete strength quantitatively. For comparative surveys, however, many of these factors will not be important unless they vary spatially or with time.
- Embedded steel reinforcement – The velocity in reinforcing steel is greater than in the cement, which can make the velocity appear greater for paths that intersect reinforcing steel than for measurements taken along adjacent paths that do not intersect any steel. It is recommended that measurements be taken over paths that do not intersect reinforcing steel (Naik et al. 2004, pp. 8-1 through 8-15).

- Aggregate size – Attenuation increases with aggregate size, which may demand use of lower frequency or shorter path. Minimum specimen thickness (path length) is influenced by aggregate size because of the stochastic nature of aggregate sizes and shapes. The minimum recommended path length for concrete having maximum aggregate size of 45 mm (1.8 in.) is 150 mm (6 in.). The minimum recommended path length is shorter for smaller aggregate sizes (Naik et al. 2004, pp. 8-1 through 8-15).
- Specimen size – UPV testing is not constricted by the size of the test specimen, unless its smallest dimension approaches the wavelength at the testing frequency. At 50 kHz, this is approximately 80 mm (3 in.). For most applications, 50 kHz resonant frequency transducers are suitable, whereas low resonant frequency transducers (20 kHz) are used for mass concrete (ASTM 2009b).
- Surface conditions – The minimum necessary path length can be influenced by the variability introduced by surface conditions. Surfaces that have been cast against formwork or a mold are preferred for transducer contact versus surfaces formed by other means (i.e., troweling), which may have properties differing from those of the bulk structure. A minimum path length of 150 mm (6 in.) is recommended for direct transmission involving one unmolded surface and a minimum of 400 mm (16 in.) for indirect transmission along one unmolded surface (IAEA 2002, pp. 100-112). Loose material or debris should be removed from the location on the surface at which transducers are to be mounted.

2.1.6.4 Limitations

- Depending on the size of the area to be measured, application of the UPV technique can be time-consuming because it only takes point measurements. Although the UPV technique can be deployed by two-sided (direct transmission) or single-sided (indirect transmission) access, it has been noted that the indirect transmission configuration is less sensitive than the direct transmission configuration and requires greater path length.

2.1.7 Infrared Thermography Testing

Infrared thermography (IRT) is a form of nondestructive testing that relies on anomalous variations in the emission of electromagnetic radiation from the surfaces of test objects within the infrared spectrum (wavelength ranging from 0.7 μm to 14 μm). In the case of concrete testing, bulk material properties such as density, thermal conductivity, and specific heat capacity are influenced by the presence of subsurface defects such as voids and delaminations. Thus, the flow of heat into or out of a concrete structure can be perturbed by the presence of such defects. As a consequence, deteriorated regions of concrete structures can develop surface temperatures that deviate 1°C to 3°C from the surrounding areas when ambient conditions are favorable (ACI 2013b, pp. 51-53). ASTM D4788-03, "Standard Test Method for Detecting Delaminations in Bridge Decks Using Infrared Thermography," describes the use of infrared thermography for detecting delaminations in concrete bridge decks (ASTM 2013b). Primary advantages of the method are that surface contact is not required and that relatively large surface areas can be inspected (ACI 2013b, pp. 51-53).

Practically, IRT testing is performed by heating up a structure and then viewing the area of interest with an infrared camera while the structure cools down. Conversely, it can also be performed on a structure that has been cooled and then viewed while heating up (see Figure 2.15).

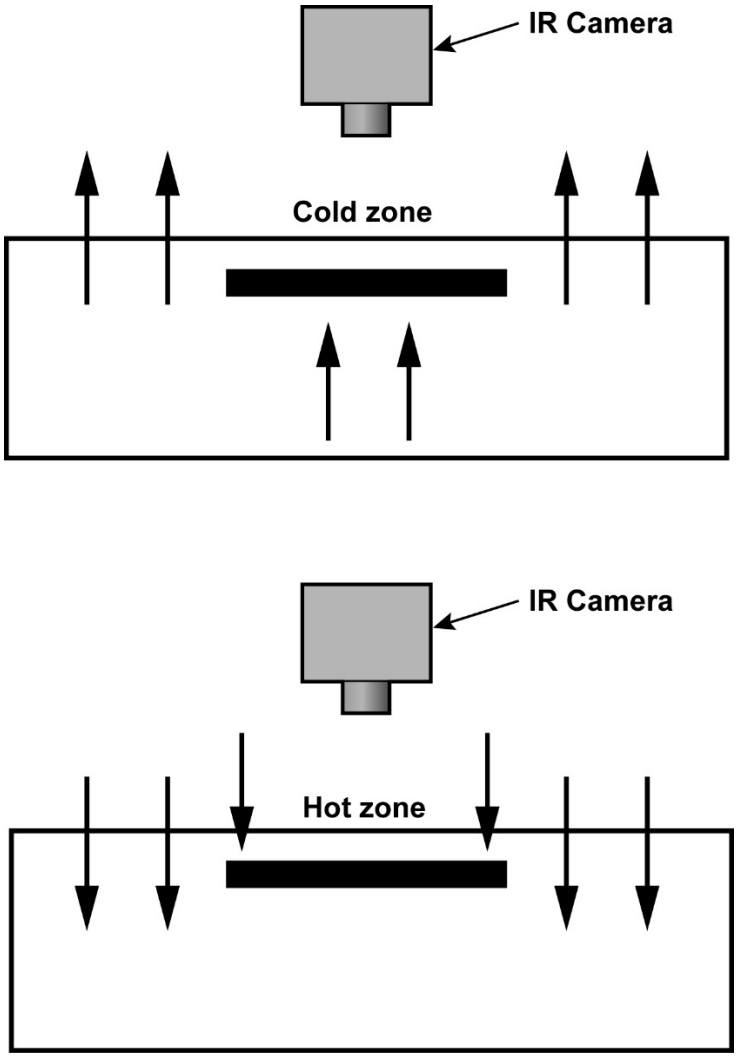

Figure 2.15. Depiction of IRT Testing Performed in the Case of Heat Flowing Out (top) or Heat Flowing In (bottom) to a Structure

IRT testing can be performed in an active or passive mode in which active mode IRT testing refers to the use of an active heating device to heat up the structure. Impulse thermography is a type of active IRT that has been studied for civil structure applications (Weritz et al. 2005). Passive mode IRT testing relies on solar illuminance to provide the source of heat necessary for IRT testing. Optimum contrast can be achieved via solar illuminance during maximum heating or cooling cycles; thus, it is ideal to perform passive IRT at sunrise or sunset (Renshaw et al. 2014). Active IRT allows greater control over the heating source, in comparison to passive IRT, which can enable enhancement of inspection performance. However, active mode IRT measurements are localized, whereas passive IRT is a way to capture thermographic images of much larger surface areas. Standard ASTM D4788-03 for bridge deck inspections is based on performing passive IRT relying on solar illuminance for heating (ASTM 2013b). An obvious drawback of solar illuminance is that it can be affected by several environmental factors such as cloud cover, rain, wind, and shadows from nearby structures (Renshaw et al. 2014).

2.1.7.1 Instrumentation and Implementation

The basic instrumentation for IRT testing includes an infrared scanner/detector and equipment to capture and record thermal video images. The infrared scanner captures infrared energy in the short (3 to 5.6 µm) and long (8 to 12 µm) wavelength ranges (ASTM 2013b). Thermal energy is not efficiently transmitted through the atmosphere at wavelengths between these two bands (Rao 2008). The infrared scanner should have a minimal resolution 0.2°C under ambient air conditions (ASTM 2013b). However, cameras for long wavelength range imaging can achieve temperature resolution down to 0.08°C (Clark et al. 2003). Figure 2.16 includes photographs that depict the use of an infrared camera to view bridge deck specimens (TRB 2013, pp. 25-27).

Figure 2.16. Depiction of IRT Testing on a Bridge Deck (TRB 2013, pp. 25-27)

2.1.7.2 Field and Laboratory Experience

IRT testing was evaluated in SHRP 2 (TRB 2013). Based on accuracy for inspection of delaminations, IRT testing was rated lower than IE testing, but rated higher than chain dragging/hammer sounding and radar methods (TRB 2013, p. 69). Accuracy was assessed in laboratory validation studies that were performed on a fabricated bridge specimen and a recovered bridge specimen. The size of delaminations in the recovered bridge deck are not reported, but the size of simulated delaminations in the fabricated bridge deck ranged from 12 in. by 12 in. up to 24 in. by 48 in. (TRB 2013, p. 69). When IRT testing for delamination inspections was evaluated based on a composite score consisting of factors such as speed, cost, repeatability, and ease-of-use, it was rated above USW testing and tied with chain dragging/hammer sounding. However, it still rated below radar testing and IE testing (TRB 2013, p. 77).

2.1.7.3 Influencing Factors Associated with Instrumentation

For passive IRT testing, the instrumentation factors that can influence results will be associated with the imaging system. Thermal energy is transmitted in the short (3 to 5.6 μm) and long (8 to 12 μm) wavelength ranges (ASTM 2013b) and the IRT camera system should be able to capture and process energy in these wavelength ranges. The wavelength range of interest is dependent on the temperature conditions as the longer wavelengths are preferred when target temperatures are approximately below room temperature and the short wavelength range is preferred for environments where large temperature differences exist (Clark et al. 2003). The minimal temperature resolution of the infrared camera system will impact sensitivity as it relates to the smallest temperature differential that can be observed. Testing based on emissions from the long wavelength range allow detection of smaller temperature differences. Although standards specify that the infrared scanner should have a minimal resolution 0.2°C under ambient air conditions (ASTM 2013b), cameras for long wavelength range imaging can achieve temperature resolution down to 0.08°C (Clark et al. 2003). It is seen that the maximum differential temperature between deteriorated and sound concrete regions decreases as the depth of the delaminations increase (ACI 2013b, pp. 51-53).

2.1.7.4 Influencing Factors Associated with Specimen and Environment

The influencing factors that impact measurements during IRT testing are concrete surface emissivity, surface temperature, concrete thermal conductivity, concrete volumetric-heat capacity, thickness of the heated layer, and intensity of incident solar radiation. The environmental conditions such as ambient temperatures, wind, and surface moisture present at the time of testing also affect measurements (ACI 2013b, pp. 51-53). Optimum weather conditions include clear skies, dry surface, mild wind, and strong solar illuminance. The following guidelines are recommended to minimize environmental influences on testing (ACI 2013b, pp. 51-53):

- Removal of debris from the test surface
- No standing water, ice, or snow should be present
- Surface should be dry at least 24 hours before testing
- Testing should only be conducted with wind speeds at 15 mph or below
- The ground temperature should be above freezing (0°C) [32°F])
- Clear skies are required even when testing at night

The standard ASTM D4788 recommends several hours of sunshine exposure for inspecting concrete and for detecting delaminations in asphalt-covered concrete bridge decks. However, the amount of time required will vary for different applications (ACI 2013b, pp. 51-53).

Optimum contrast can be achieved via solar illuminance during maximum heating or cooling cycles (Renshaw et al. 2014). The suggested best time for doing infrared surveys is soon after sunrise or after sunset. The concrete surface can become thermally saturated and the thermal anomalies can fade if testing is performed too long after a thermal change (ACI 2013b, pp. 51-53).

2.1.7.5 Limitations

- The capability of IRT testing is significantly influenced by the depth of flaws and the thickness of the specimen under test. It becomes less effective in the detection of subsurface flaws as the thickness of the object increases. It is seen that the maximum differential temperature between deteriorated and sound concrete regions decreases as the depth of the delaminations increase (ACI 2013b, pp. 51-53). Thus, deep flaws are difficult to detect.
- The method does not provide information about the depth of detected flaws (TRB 2013, p. 25).
- IRT is vulnerable to several environmental factors as discussed in Section 2.1.7.4.

2.1.8 Acoustic Emission Testing

Acoustic emission (AE) testing refers to the passive monitoring of structures for degradation through sensing of elastic waves that are generated by the rapid release of energy associated with a given degradation mechanism. In reinforced concrete structures, AE can be sensitive to cracking processes, slip friction between the concrete and reinforcing steel, and the fracture or debonding of fibers in fiber-reinforced concrete (Mindess 2004). Others note that AE can be indirectly sensitive to the corrosion of reinforcing steel through detection of cracking that occurs in response to the expansion caused by the build-up of corrosion products on the surface of reinforcing steel (Gostautas et al. 2005; Ohtsu et al. 2007).

An interesting phenomenon associated with AE of several materials is the Kaiser effect. The Kaiser effect refers to the absence of AE activity in a material until it is stressed to a level that exceeds the previous peak load stress. The Kaiser effect is clearly observed in metals; however, in concrete, the effect exhibits greater complexity (Mindess 2004). Mindess (2004) states that while there is evidence of a Kaiser effect in concrete, it is only present below 75% to 85% of the ultimate strength of the concrete. Further, reference is made to work by Nielsen and Griffin (1977) in which it is reported that the Kaiser effect is short-lived, existing only if rest between load cycles is limited to a few hours. The Kaiser effect forms a partial basis for a recommended practice for testing concrete structures by AE in Japan (Ohtsu et al. 2007).

AE is implemented by mounting piezoelectric transducers on the surface of the test structure. The sensors may be epoxied or otherwise attached to the surface ensuring adequate coupling (see Figure 2.17). AE sensors pick up elastic energy that is generated by active degradation, which then propagates through the structure. Several sensors are often deployed to enable monitoring of larger regions and/or to enable source localization. The transducers may have a wide-band frequency response or a resonant frequency response. However, wide-band transducers are more vulnerable to the pick up of sources of environmental noise. Resonant frequency transducers may have the benefit of naturally filtering out sources of extraneous noise; however, it may be difficult to predict the optimal frequency response for a specific application and some testing may be required. Most AE investigations of concrete employ sensors that are tuned to the frequencies in the 50 kHz to 2 MHz range (Mindess 2004). Less attenuation of AE signals is experienced at low frequencies; however, the monitoring is more susceptible to sources of noise from the environment. At higher frequencies, sources of noise from the environment are less problematic, but greater attenuation of the signals is observed (Mindess 2004).

The interpretation of structural integrity from AE testing is based mostly on the intensity of emissions, which is determined by the number of signals and their magnitudes. One method for determining the deterioration of a structure is based on computation of two intensity-based metrics referred to as the historic index, $H(t)$, which is a function of time, t, and severity index, S_r, (Golaski et al. 2002). The historic index represents changes in signal strength and is expressed as,

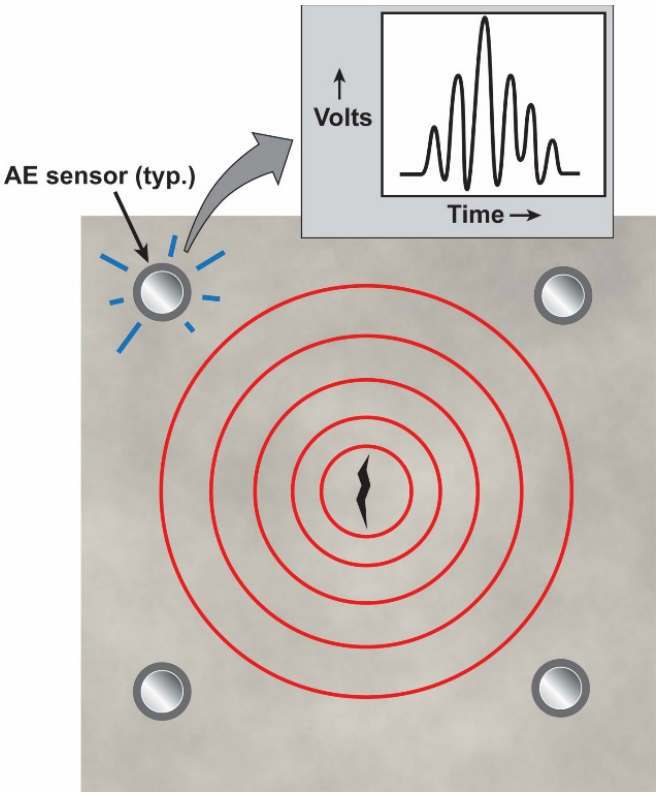

Figure 2.17. Depiction of AE Testing of a Concrete Structure Including Array of Sensors and Conversion of Burst of Elastic Energy from Degradation into Electrical Signal

$$H(t) = \frac{N}{N-K} \frac{\sum_{i=K+1}^{N} S_{Oi}}{\sum_{i=1}^{N} S_{Oi}}, \tag{2.7}$$

where N is the number of hits observed up to time t, S_{Oi} is the signal strength of the i-th signal, and K is empirically derived. The severity index is defined as the average strength of the 50 largest signals and is expressed as,

$$S_r = \frac{1}{50} \sum_{i=1}^{i=50} S_{Oi} \, . \tag{2.8}$$

The condition of a structure can be interpreted based on mapping the historic and severity indices of sensors utilized in a test on a 2-D plot as illustrated in Figure 2.18a).

Another method for qualifying the state of a concrete structure based on AE activity is based on indices referred to as the "Calm Ratio" and the "Load Ratio" (Ohtsu et al. 2007). The Load Ratio is a metric based on the Kaiser effect in concrete and is defined as the ratio of the load at the onset of AE activity to the previous load at which onset of AE activity was observed. The Kaiser effect is associated with sound concrete but is not apparent in damaged concrete. For sound concrete, the Load Ratio can be greater than 1.0 and the Load Ratio can be less than 1.0 for concrete that is damaged. The Calm Ratio is the ratio of

cumulative AE activity observed during unloading portion of a cycle to the cumulative AE activity observed for a full loading cycle. A low Calm Ratio is associated with sound concrete (Ohtsu et al. 2007). Qualifying the damage of a concrete structure by analysis of Load Ratio and Calm Ratio is incorporated in a recommended practice for testing concrete structures by AE in Japan (Ohtsu et al. 2007). A depiction of the relationship between the Load Ratio, Calm Ratio, and state of a concrete structure is provided in Figure 2.18b).

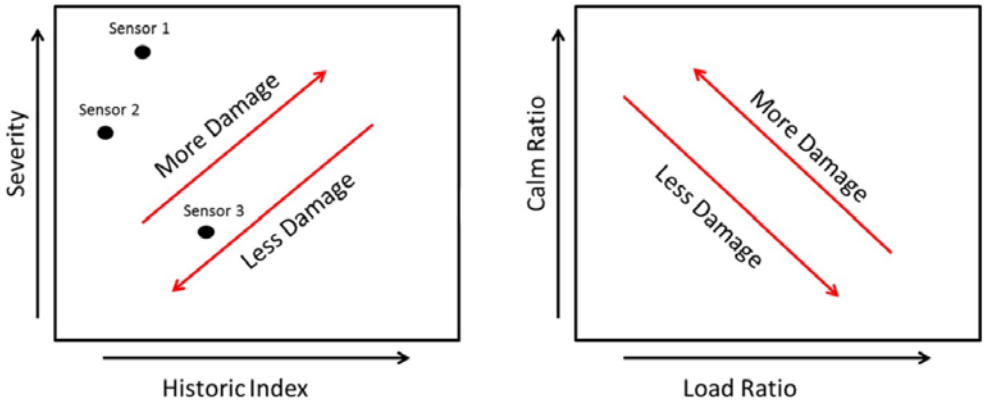

Figure 2.18. a) 2-D Plot of Historic vs. Severity Indices for Observed AE Sensor Activity to Qualify the State of Damage and b) a 2-D Plot of the Calm Ratio vs. Load Ratios to Qualify the State of Damage

Parameterization of AE signals is often applied in an attempt to simplify analysis and/or classify signal origin. Similar to frequency-based discrimination of noise, signals can be based on other parameters such as amplitude, duration, etc. in an attempt to filter relevant signals away from non-relevant signals. An illustration of AE signal parameterization is provided in Figure 2.19, displaying multiple features that may be used for signal classification.

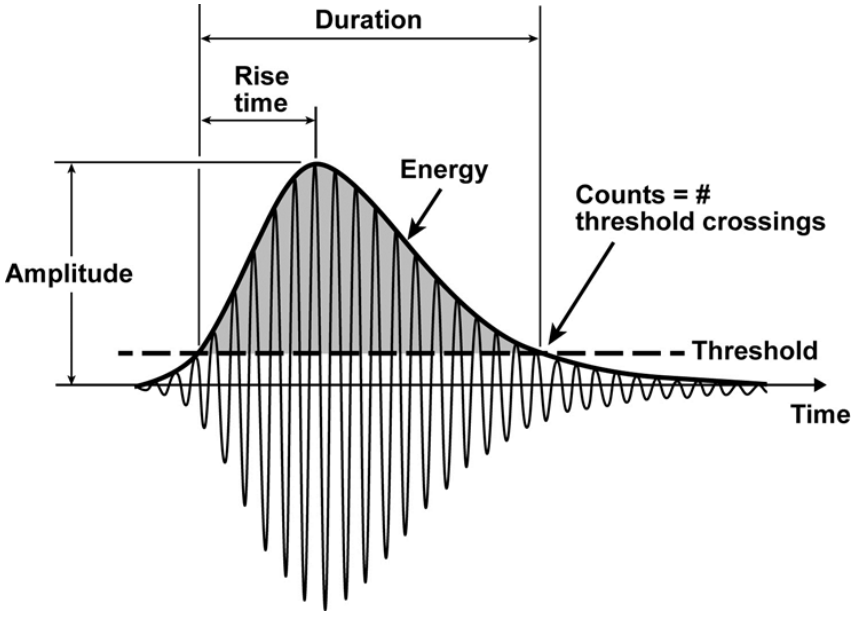

Figure 2.19. Illustration of AE Signal Parameterization

Location algorithms allow locating the source of AE signals. When an array of sensors is implemented, the location of signal origination may be determined by triangulation. Zonal location can also be implemented with sensor arrays. In this case, the approximate location of degradation is ascertained by comparing the relative activity observed by sensors in the array. Zonal location may be the only practical way of locating the source of AE activity when the speed of elastic wave propagation cannot be accurately known.

Standard ASTM E1932, "Standard Guide for Acoustic Emission Examination of Small Parts," is applicable to AE testing of small parts or defined regions of larger structures. Qualifications for applicability of the standard include low AE signal attenuation in the region to be monitored. In addition, the standard assumes a controlled or measured stress is applied to the structure being monitored (ASTM 2012a).

2.1.8.1 Instrumentation and implementation

Equipment required for AE testing includes sensors, preamplifiers, a data acquisition system, and computer for visual interface. Commercial systems are available. Typically, piezoelectric sensors are employed that may have a wide-band or resonant frequency response. Resonant transducers can be more sensitive than wide-band transducers, but the resonant frequency must be selected to provide optimal response. AE investigations of concrete typically employ sensors that are tuned to the frequencies in the 50 kHz to 2 MHz range (Mindess 2004). For perspective, two AE sensors are shown in the photograph in Figure 2.20. Typical sensor dimensions are approximately 45 mm (0.75 in.) in diameter and 25 mm (1 in.) in height.

Figure 2.20. Photograph of AE Sensors Bonded to Concrete Surfaces (Courtesy of Paul Ziehl, University of South Carolina)

The signal from typical piezoelectric transducers may be on the order of 100 μV and these signals are typically amplified by 40 dB or 60 dB with a preamplifier (Mindess 2004). Signals from the preamplifier are fed to the data acquisition system, which can usually accommodate multiple channels. An amplitude-based discrimination is applied at the input channels by setting the "Threshold" as illustrated in Figure 2.19. This serves as an initial filter of noise.

Yuyama et al. (2007) state that sensors resonant at 60 kHz and 150 kHz can be applied with spacings up to 2.0 m and 0.5 m, respectively, while maintaining adequate sensitivity for monitoring reinforced concrete. Mindess (2004) recommends sensor spacing of 0.4 m for ordinary concrete.

2.1.8.2 Influencing Factors Associated with Instrumentation

- Resonant frequency – Most AE investigations of concrete employ sensors that are tuned to the frequencies in the 50 kHz to 2 MHz range (Mindess 2004). Less attenuation of AE signals is experienced at low frequencies; however, the monitoring is more susceptible to sources of noise from the environment. At higher frequencies, sources of noise from the environment are less problematic, but greater attenuation of the signals is observed (Mindess 2004).
- Sensor spacing – With greater attenuation, sensors must be spaced closer together, reducing the volume that can be monitored. Yuyama et al. (2007) state that sensors resonant at 60 kHz and 150 kHz can be applied with spacings up to 2.0 m and 0.5 m, respectively, while maintaining adequate sensitivity for monitoring reinforced concrete. Mindess (2004) recommends sensor spacing of 0.4 m for ordinary concrete.
- Coupling – Sensors must be adequately coupled to the surface of the specimen to ensure efficient transmission of signals from the specimen to the sensors (usually with a viscous coupling agent such as silicone grease) (Mindess 2004). Guidance for coupling sensors to test structures may be found in standard ASTM E650 (ASTM 2012b), "Standard Guide for Mounting Piezoelectric Acoustic Emission Sensors."

2.1.8.3 Influencing Factors Associated with Specimen and Environment

- Age – More mature cements show increased permissivity to the transmission of acoustic waves. Thus, attenuation decreases with age of concrete (Mindess 2004).
- Specimen size – Specimen size appears to influence AE activity with smaller specimens giving rise to a greater amount of AE activity than larger specimens (Mindess 2004).
- Extraneous noise – AE testing is inherently sensitive to sources of noise from the environment, which can be caused by wind, rain, traffic, etc. In addition, friction from surfaces in contact can also contribute noise that must be discriminated from degradation. However, strategies generally exist for discriminating these noise sources from signals of interest.
- Surface conditions – Loose material or debris should be removed from the location of sensor mounting. Guidance for coupling sensors to test structures may be found in standard ASTM E650 (ASTM 2012b).

2.1.8.4 Limitations

- Extensive laboratory testing is required to validate AE testing for field testing. Mindess (2004) states, "While AE is very useful laboratory technique for the study of concrete properties, its use in the field remains problematic." Nair and Cai (2010) state: "Although numerous techniques of AE data assessment have been proposed and proven useful in laboratory trials, very rarely have any of them been reported viable for practical onsite monitoring."

- The literature reviewed in this section indicates that active loads are required to stimulate a sufficient AE response from a concrete structure. Standard ASTM E1932, "Standard Guide for Acoustic Emission Examination of Small Parts," assumes that a controlled or measured stress is applied to the part being monitored (ASTM 2012a).

2.1.9 Ground Penetrating Radar Testing

Ground penetrating radar (GPR) is an NDT method based on the use of electromagnetic waves to interrogate below the surface of a structure to discern if anomalies are present. From a physics standpoint, it parallels the UPE method in that measurements are based on interpretation of pulses of energy that are launched into a structure and reflected back to a receiver. Reflections are produced where strong discontinuities in material properties exist. For GPR testing, the material properties that most significantly influence the propagation of electromagnetic waves include the dielectric constant and electrical conductivity. It is worthwhile to note contrasts between the propagation of elastic and electromagnetic energy in concrete, particularly with respect to interfaces such as concrete-air and concrete-steel interfaces. Whereas an air-filled discontinuity will cause nearly total reflection of elastic energy because of the negligible acoustic impedance of air compared to concrete, an air-filled discontinuity will only result in the reflection of approximately 50% of incident electromagnetic radiation launched by GPR. Therefore, GPR has the ability to penetrate beyond air-filled discontinuities (ACI 2013b, pp. 53-61).

Conversely, a concrete-steel interface will result in almost total reflection of incident electromagnetic energy because of the negligible electrical conductivity of concrete in comparison to steel. In addition, the polarity of GPR signals experience a reversal in polarity at concrete-steel interfaces. Thus, GPR is particularly suited for locating embedded steel in concrete. However, the strong reflections from embedded steel can obscure signals from less significant reflectors in the test structure and from layers of embedded steel located deeper within the test structure (ACI 2013b, pp. 53-61). The ability to penetrate beyond a layer of reinforcing steel depends on the size of the rebar, the rebar spacing, and the cover depth. In one source, it is stated that features below a layer of embedded reinforcing steel cannot be detected when the rebar size is 32 mm (1.26 in.) diameter or greater and the spacing is at 200 mm (8 in.) given a frequency of 1 GHz and a cover depth of 25 mm (1 in.) to 50 mm (2 in.) (ACI 2013b, pp. 53-61). Another source states that it is possible to detect below a mesh of reinforcing steel that is 12 mm (0.5 in.) in diameter and spaced at 150 mm (6 in.) at 900 MHz (IAEA 2002, pp. 137-151).

Ignoring the influence of embedded steel, the depth to which a GPR signal is able to penetrate is influenced by the signal frequency and the conductivity of the concrete test structure, which will be primarily influenced by moisture content and the presence of chlorides. Frequencies used for GPR testing can range from 400 MHz to 2.6 GHz although testing at frequencies below 500 MHz is usually reserved for massive concrete structures such as a concrete dam (ACI 2013b, pp. 53-61). Typical penetration depths range from 0.5 m to 2 m (20 in. to 80 in.) for antenna frequencies ranging from 1 GHz to 500 MHz. A trade-off exists between the achievable penetration depth and resolution as increases in frequency improve achievable resolution but decrease the penetration ability of the GPR signal (ACI 2013b, pp. 53-61).

GPR testing of concrete can be performed using an air-coupled or ground-coupled antenna. Air-coupled antennas can be mounted on a vehicle for performing rapid inspection of concrete bridge decks or pavements (ACI 2013b, pp. 53-61; TRB 2013, pp. 19-21). The ground-coupled antenna is usually integrated into a hand-held or cartable system for targeted inspections or surveying smaller areas (ACI 2013b, pp. 53-61).

Two relevant standards for GPR testing of concrete include ASTM D6087-08, "Standard Test Method for Evaluating Asphalt-Covered Concrete Bridge Decks Using Ground Penetrating Radar" (ASTM 2015b) and ASTM D4748-10, "Standard Test Method for Determining the Thickness of Bound Pavement Layers Using Short-Pulse Radar" (ASTM 2015a).

2.1.9.1 Instrumentation and Implementation

As previously noted, GPR testing of concrete can be performed using an air-coupled or ground-coupled antenna, depending on the application. The air-coupled configuration usually consists of a horn antenna mounted approximately 150 mm (6 in.) to 500 mm (20 in.) above the test structure (ACI 2013b, pp. 53-61). A bow tie antenna is normally used for the ground-coupled scenario. For this case, the spacing between the antenna and the test structure should be no more than 1/10 of a wavelength to achieve adequate coupling of the signal (IAEA 2002, pp. 137-151). Frequencies used for GPR testing can range from 400 MHz to 2.6 GHz, and pulses are generated with durations typically ranging from 1 to 3 ns (ACI 2013b, pp. 53-61). A photograph depicting ground-coupled GPR testing is provided in Figure 2.21.

Figure 2.21. Depiction of GPR Testing on Transportation Infrastructure (TRB 2013)

Besides the antennas, other equipment considered essential to GPR testing includes the control unit, which controls and powers the antenna pulses and collects and amplifies received signals. Data can be sent to a visual display and a digital storage device for additional analysis (ACI 2013b, pp. 53-61). Data can be represented in several formats including B-scan type images in which the signal amplitude is color-coded and recorded as a function time for several positions along a one-dimensional linear scan of position. The result resembles a contour plot with the time along one axis and linear position along the second axis.

2.1.9.2 Field and Laboratory Experience

Air-coupled and contact GPR technologies were evaluated in SHRP 2 (TRB 2013). GPR technologies were used to inspect for delaminations and corrosion of reinforcing steel (TRB 2013, p. 69).

With respect to inspections for delaminations, GPR performance was rated just ahead of chain dragging but behind both IRT testing and IE testing (TRB 2013, p. 69). Accuracy was assessed in laboratory validation studies that were performed on a fabricated bridge specimen and a recovered bridge specimen. The size of delaminations in the recovered bridge deck are not reported, but the size of simulated delaminations in the fabricated bridge deck ranged from 12 in. by 12 in. up to 24 in. by 48 in. (TRB 2013,

p. 69). However, when rating is based on a composite score consisting of factors such as speed, cost, repeatability, and ease-of-use, GPR is rated the highest (TRB 2013, p. 77). For rebar corrosion detection, GPR testing was rated the lowest in performance based on accuracy for the methods evaluated (TRB 2013, p. 69). Other methods evaluated included half-cell potential (HCP) and galvanostatic pulse measurement (GPM) testing. Nevertheless, when rating is based on a composite score as described above, GPR is again rated the highest (TRB 2013, p. 77). In the SHRP-2 study, GPR was also considered applicable for detecting concrete degradation, but its score was low for this application (TRB 2013, p. 77).

GPR testing was performed as part of baseline inspections conducted on all NUHOMS HSMs (model HSM-80) containing Three Mile Island fuel at Idaho National Laboratory (INL) in 2008. GPR testing was performed primarily to locate reinforcing steel and it is not clear if any defects were detected as a result of this testing. Further, it is not clear which components of the HSM-80 were inspected (EPRI 2015a).

2.1.9.3 Influencing Factors Associated with Instrumentation

- Frequency – Frequency is a primary influencing factor as it relates to the depth of penetration and the thickness of objects that may be inspected. Frequencies below 500 MHz are usually reserved for massive concrete structures such as a concrete dam (ACI 2013b, pp. 53-61). Typical penetration depths range from 0.5 m to 2 m (20 in. to 80 in.) for antenna frequencies ranging from 1 GHz to 500 MHz (ACI 2013b, pp. 53-61). The resolution, which would relate to the smallest detectable defect, is also related to frequency, decreasing as the frequency increases. For dry concrete, the resolution is approximately 59 mm (2.3 in.) at 1.5 GHz and is 176 mm (7 in.) at 500 MHz (ACI 2013b, pp. 53-61).
- Pulse duration – The duration of the radar pulse limits the minimum thickness of a structure that may be interrogated with GPR as it will be impossible to resolve reflections if the structure is too thin. For a 1.5 ns pulse duration, this estimated minimum thickness is estimated to be 45 mm (1.7 in.). The minimum thickness can vary from 39 mm (1.54 in.) to 117 mm (4.6 in.) for frequency ranging from 1.5 GHz to 500 MHz, respectively (ACI 2013b, pp. 53-61). This can impact the ability to detect defects that are close to the surface of a structure.

2.1.9.4 Influencing Factors Associated with Specimen and Environment

- Moisture – Moisture has a much higher dielectric constant than other concrete constituents (besides reinforcing steel). Thus, moisture infiltration into any defects will increase the reflection coefficient from defects, enhancing their detectability. For typical air-filled defects in concrete, the reflection coefficient is approximately 50% (ACI 2013b, pp. 53-61). Moisture content and chloride concentration increase the conductivity of concrete resulting in greater attenuation of propagating electromagnetic pulses, which reduces the penetration depth of GPR signals (ACI 2013b, pp. 53-61). These effects of moisture are drastically reduced if the moisture freezes (TRB 2013, pp. 19-21).
- Embedded reinforcing steel – The ability to penetrate beyond a layer of reinforcing steel depends on the size of the rebar, the rebar spacing, and the cover depth. In one source, it is stated that features below a layer of embedded reinforcing steel cannot be detected when the rebar size is 32 mm (1.26 in.) diameter or greater and the spacing is at 200 mm (8 in.) given a frequency of 1 GHz and a cover depth of 25 to 50 mm (1 to 2 in.) (ACI 2013b, pp. 53-61). Another source states that it is possible to detect below a mesh of reinforcing steel that is 12 mm (0.5 in.) in diameter and spaced at 150 mm (6 in.) at 900 MHz (IAEA 2002, pp. 137-151). For concrete covers up to 150 mm (6 in.), the minimum rebar spacing at which individual bars are resolvable increases with increasing cover depth. For concrete cover depth greater than 150 mm (6 in.), the minimum spacing is unaffected by cover depth and depends mostly on rebar size (ACI 2013b, pp. 53-61).

2.1.9.5 Limitations

- For concrete structures that are heavily reinforced, GPR has limited ability to penetrate beyond the first layer of embedded reinforcing steel. Further, because approximately 50% of electromagnetic energy incident on a concrete-air interface is transmitted through, GPR has limited ability to detect delamination-type defects unless they are filled water or other material that enhances the contrast of the defect. The contrast enhancement effected by the presence of water is significantly reduced if the water is frozen (TRB 2013, pp. 19-21).
- GPR cannot be used to quantifiably estimate mechanical properties of the concrete or the amount of moisture or chlorides present in concrete, despite being influenced by these factors (TRB 2013, pp. 19-21). Because of the large number of properties that can affect the dielectric constant and conductivity of concrete, it is difficult to isolate what factors may be impacting the GPR signal. Also, GPR cannot measure cross-section loss of rebar with the level of sensitivity needed to be useful for corrosion monitoring (TRB 2013, pp. 19-21).
- Finally, GPR cannot resolve defects located closer than 1/3 of a wavelength to the surface because of the inability to resolve reflected pulses. This distance can vary from 39 mm to 117 mm (1.54 in. to 4.6 in.) for frequency ranging from 1.5 GHz to 500 MHz, respectively (ACI 2013b, pp. 53-61).

2.1.10 Radiographic Testing

Radiographic testing (RT) of concrete is based on measuring the attenuation of an incident beam of X-rays or gamma rays due to scattering or absorption as the radiation passes through the structure. An image collector is placed on the opposite side of the structure from the source and detects the penetrating radiation, registering a two-dimensional image. A location of decreased thickness or density will result in greater exposure (darkening) of the film recording a shadow image of the anomaly (see Figure 2.22). RT may be used to locate reinforcing steel, voids, and cracks in concrete structures (IAEA 2002, pp. 82-99).

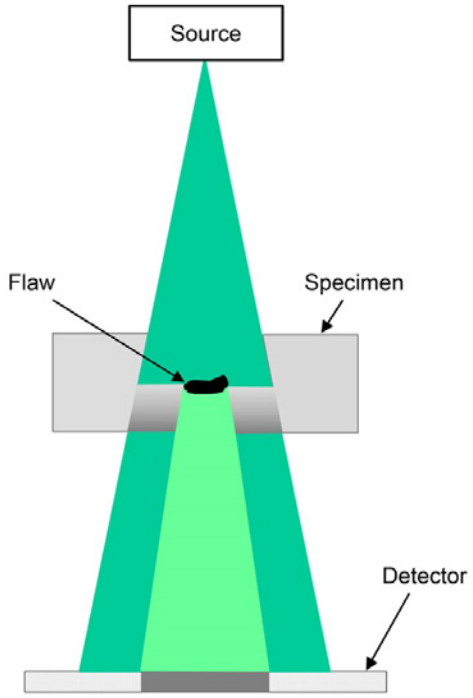

Figure 2.22. Illustration of a Radiographic Examination and Interaction of Source X-rays with Density Discontinuities such as Voids

In addition, techniques have been developed for estimating the depth of reinforcing steel and voids by RT based on shifts in the shadows produced on film or other detectors from exposures at two different source locations (IAEA 2002, pp. 82-99). The choice of using X-rays or gamma rays depends on the application as there are relative advantages and disadvantages to using either source type. X-rays can be generated by X-ray tube or linear accelerator. Perhaps the most significant factor influencing the choice of source type for radiography of concrete structures is the structure thickness. X-ray tubes are preferred for many research applications where the concrete specimen thickness can be controlled. Options are generally limited to radioisotopic sources and linear accelerators for field applications because of the thickness of most field structures. A linear accelerator mounted on a movable crane has been developed and deployed in the field for concrete bridge inspections (Mitchell 2004). A radioisotopic source is generally preferred to deployment of a linear accelerator; however, as Table 2.2 indicates, no other options may exist for performing radiography on concrete structures exceeding 500 mm (20 in.) in thickness. Besides the difficulty in deploying a linear accelerator in the field, high-energy X-rays generated by linear accelerator can suffer from beam hardening, which is a shift in the energy spectrum to high energies as a result of lower energy photons getting filtered out of the spectrum by scattering (ACI 2013b, pp. 23-28). A comparison of some of the advantages and disadvantages of deploying a radioisotopic source versus linear accelerator X-ray source is provided in Table 2.3.

Table 2.2. Summary of Maximum Concrete Thickness Range for Radioisotopic and X-ray Sources

Source	Maximum Concrete Thickness	Reference
Ir-192 (several energies from 0.21 to 0.61 MeV)	250 mm (10 in.)	IAEA (2002, pp. 82-99)
Co-60 (1.173 and 1.332 MeV)	500 mm (20 in.)	IAEA (2002, pp. 82-99)
Linac @ 10 MeV (X-ray)	1000 mm (40 in.)	Mitchell (2004)
Linac @ 18 MeV (X-ray)	1600 mm (63 in.)	IAEA (2002, pp. 82-99)

Table 2.3. Comparison of Radioisotopic Sources and Linear Accelerator X-ray Sources

Characteristic	Comparison of Radioisotopic Source to X-ray Source
Intensity	X-ray sources can be generated with intensities on the order of 10^4 greater than can be achieved with radioisotopic sources
Energy spectrum	X-ray spectrum is polychromatic; radioisotopic sources can be monocromatic
Power required?	X-ray sources require power; radioisotopic sources do not
Ability to turn “on” and “off”	X-ray sources can be turned “on” and “off”; radioisotopic sources cannot
Portability	Radioisotopic sources are dimensionally small relative to X-ray sources

Geometric unsharpness refers to a loss in definition of a radiograph as a result of the finite size of the source and/or other geometric factors of the exposure setup. It refers to a blurring or smearing of the boundaries associated with actual discontinuities in the object, as illustrated in Figure 2.23. The formula for geometric unsharpness can be expressed as,

$$Ug = \frac{s * b}{a - b}, \tag{2.9}$$

where *Ug* is the geometric unsharpness, *s* is the source diameter, *b* is the object-to-detector distance, and *a* is the source-to-detector distance. Geometric unsharpness can be minimized by decreasing the source diameter, ensuring the detector is located as close to the object as possible, or increasing the source-to-detector distance; however, increasing the source-to-detector distance results in a reduction of intensity (IAEA 2002, pp. 82-99).

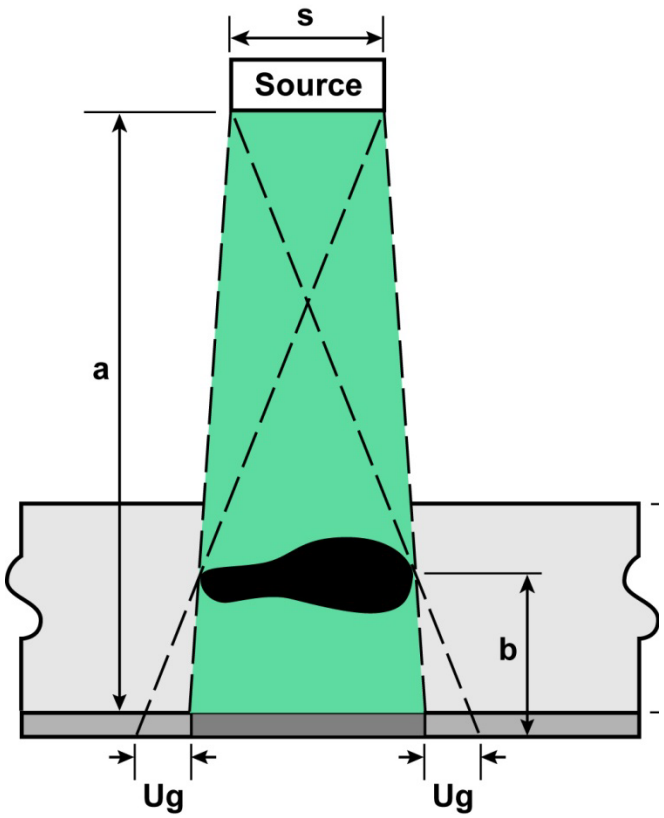

Figure 2.23. Illustration of Geometric Unsharpness (*Ug*) (IAEA 2002, pp. 82-99)

2.1.10.1 Instrumentation and Implementation

X-rays for radiography are generated as a result of bremsstrahlung radiation emanating from the impingement of high velocity electrons into a metal anode. In an X-ray tube, electrons are emitted from a cathode (e.g., heated filament) in a vacuum tube and accelerated to high velocity by application of a high-voltage source across the cathode and anode. To maintain the stability of the generated X-ray beam and lifetime of the anode, a means of cooling the anode and/or rotating the anode is incorporated into the tube (IAEA 2002, pp. 82-99). Tubes capable of generated a source of X-rays with energies of several hundred keV (~500 keV) are commercially available; however, cost increases significantly with increasing energy. Much higher X-ray energies can be achieved with linear accelerators, which can generate X-rays with energies up to 10's of MeV (IAEA 2002, pp. 82-99; Mitchell 2004).

Radioisotopic sources of gamma rays can also be used as a source for radiography. Typical sources, as outlined in Table 2.2, have energies ranging from several hundred keV to greater than 1 MeV. Some of the relative merits and disadvantages to using radioisotopes versus X-rays are summarized in Table 2.3.

The radiographic image is usually recorded by exposing film to the source radiation that manages to penetrate through the test specimen. In addition to film, digital methods for recording images have been

developed, such as storage phosphor plates and flat panel digital detector arrays. While the use of digital recording devices is routine in the medical industry, their use for NDE applications in the commercial nuclear sector are not widespread (Meyer et al. 2012).

Shielding around the source may be used to direct or collimate the beam of radiation and lead intensifier screens may be used in front of the detector to enhance the image (IAEA 2002, pp. 82-99).

2.1.10.2 Influencing Factors Associated with Instrumentation

- Source energy – Source energy will determine the penetrability and maximum thickness of structures that are feasible to radiograph. Table 2.2 summarizes several sources and the maximum thickness that may be radiographed by each source type.
- Configuration – Configuration of the radiograph setup will influence image quality and geometric unsharpness. In this case, important parameters include the source diameter, the source-to-detector distance, and the object-to-detector distance. Image quality can be improved by minimizing source size, maximizing source-to-detector distance, and minimizing object-to-detector distance. However, this must be balanced with the need to maintain sufficient intensity at the detector.

2.1.10.3 Influencing Factors Associated with Specimen and Environment

- Specimen thickness – Specimen thickness influences radiography by limiting the source that may be applied and influencing the amount of time necessary for exposure. An increase in thickness for a given configuration will lead to increased attenuation of the incident radiation beam and less intensity at the detector. This will increase the time needed for exposure or may prohibit the use of certain types of sources. Table 2.2 summarizes several sources and the maximum thickness that may be radiographed by each source type.

2.1.10.4 Limitations

- Radiography presents unique burdens that must be addressed including potential health risks posed by the use of ionizing radiation and high-voltage sources, and handling and disposal of radioisotopic sources, where they are employed (IAEA 2002, pp. 82-99).
- X-ray sources for examining thick concrete sections in the field are expensive and performing the measurements can be time-consuming (IAEA 2002, pp. 82-99; Mitchell 2004).
- Radiography is relatively insensitive to thin voids or delaminations oriented perpendicular to the source beam. As the overall thickness of a structure increases, the relative influence of thin voids or delaminations to the beam attenuation becomes small (IAEA 2002, pp. 82-99; Mitchell 2004).

2.1.11 Nuclear Methods for Testing of Concrete

This section covers nuclear methods for testing of concrete integrity, which may also be referred to as radiometric methods. Like radiography, radiometry is based on measuring the attenuation of radiation after propagation through a region of concrete. However, whereas radiography may employ the use of film, imaging plates, or even digital panel detectors to record a 2-D spatial registration of the response, responses from radiometry testing are usually overall measurements of intensity corresponding to attenuation for the sampled volume. Radiometry testing can be distinguished by source type (either gamma ray or neutron) and gamma-ray radiometry can be performed in either through-transmission (see Figure 2.24) or backscattering mode (see Figure 2.25). Both modes of gamma-ray radiometry are used primarily to measure the density of concrete through attenuation of the gamma-ray source due to Compton scattering (primarily for energies from 60 keV to 15 MeV), and photoelectric absorption (below 60 keV) (IAEA 2002, pp. 152-161). Figure 2.25 illustrates that shielding is required between the

source and detector for the backscatter mode to ensure all gamma rays collected by the detector have a path through the concrete. The two modes of gamma radiometry depicted in Figures 2.24 and 2.25 show the source and detector outside of the concrete structure, although devices exist for the intent of placing the source and/or detector inside of the concrete structure; such devices require drilling one or more holes in the concrete to accommodate access for each measurement (IAEA 2002, pp. 152-161).

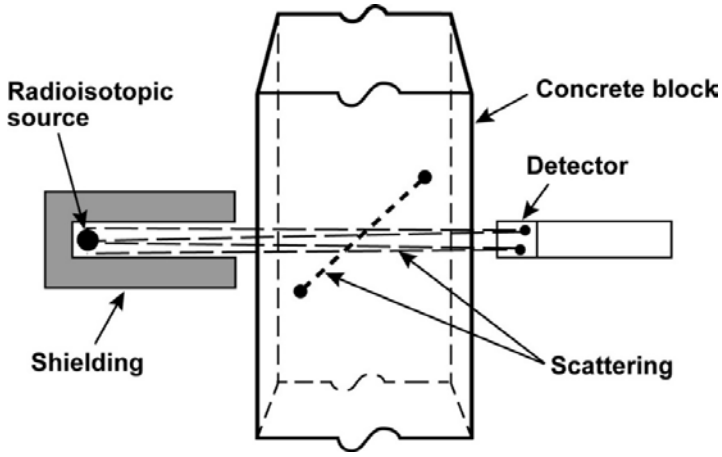

Figure 2.24. Illustration of Gamma-Ray Radiometry Performed in Through-Transmission Mode (IAEA 2002, pp. 152-161)

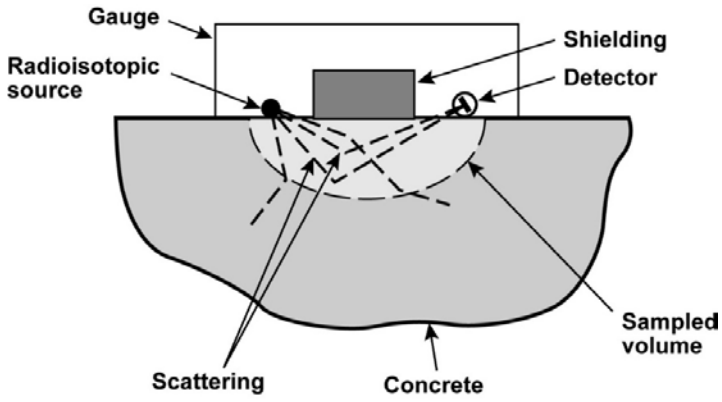

Figure 2.25. Illustration of Gamma-Ray Radiometry Implemented in Backscattering Mode (IAEA 2002, pp. 152-161)

The advantage of the backscatter mode is that access to only a single side of the concrete structure is necessary; however, the backscatter mode is only able to access a layer of concrete near the surface approximately 40 mm to 100 mm (1.6 in. to 4 in.) in depth (ACI 2013b, pp. 23-28). For typical commercial backscatter systems, nearly all of the response can be attributed to the first 50 mm (2 in.) of concrete adjacent to the source and detector, and concrete beyond 75 mm (3 in.) has almost no influence on the detected signal (IAEA 2002, pp. 152-161). The actual arrangement of the source, detector, and shielding can influence the thickness to which gamma radiometry is sensitive (IAEA 2002, pp. 152-161). Through-transmission mode requires access to both sides of a concrete structure and the measurement of attenuation is integrated along the total path length. Gamma-ray radiometry is sensitive to the aggregate composition because the cross section for photoelectric absorption is proportional to the atomic number (Z) raised to the fourth power. The backscatter mode is even more sensitive to aggregate composition because only photons that are scattered one or more times are picked up by the detector. In through-transmission mode, the detector signal is dominated by photons that travel in nearly a straight line

between source and detector, experiencing minimal scattering interactions. Both modes are normally implemented using a sealed radioisotopic source and a detector, which is usually a Geiger-Muller (G-M) tube gas detector, although solid-state sodium iodine scintillation detectors have been used as well (IAEA 2002, pp. 152-161). The typical radioisotopic source used for density measurements is ^{137}Cs (662 keV). Other sources that are used include ^{226}Ra (equivalent to 750 keV emission) and ^{60}Co (1.173 and 1.332 MeV) (IAEA 2002, pp. 152-161).

Neutron source radiometry devices are useful for measuring moisture content in concrete structures. For elastic interactions, neutrons experience the greatest energy transfer in collisions with hydrogen atoms, because of the similarity in masses. The most convenient neutron sources include sealed sources such as ^{241}AmBe, which has a fast neutron spectrum (energy greater than 10 keV) (IAEA 2002, pp. 152-161). Interactions with hydrogen in concrete convert the fast neutrons into thermal neutrons (energies below 0.5 eV). The thermal neutrons are then captured in detectors that contain isotopes with large cross sections for neutron-gamma interactions. The resulting gamma rays are detected through their ionizing interactions with a gas. Typical detectors that may be used in a neutron radiometry device for moisture measurements include gas-filled BF^3 or ^{3}He detectors (IAEA 2002, pp. 152-161). A neutron source device for moisture measurements only requires single-sided access to concrete structures as the source and detectors are located on the same side, similar to the gamma-ray backscatter configuration in Figure 2.25. However, shielding between the source and detector is not required because the detectors are not sensitive to the energy spectrum of fast neutrons generated by the source. Neutron source devices sample a greater volume in comparison to backscatter gamma-ray devices. Neutron source devices have a relatively deep penetration in comparison to backscatter gamma-ray source devices as neutron source devices may sample concrete up to 350 mm (14 in.) into a structure (IAEA 2002, pp. 152-161).

2.1.11.1 Instrumentation and Implementation

Portable gamma-ray source devices for density measurements are normally implemented using a sealed radioisotopic source and one or two detectors, which are typically G-M tube gas detectors, although solid-state sodium iodine scintillation detectors have been used as well (IAEA 2002, pp. 152-161). The G-M tube detectors are better suited for field applications because of ruggedness; however, sodium iodine detectors are more efficient and enable the discrimination by gamma-ray energy (IAEA 2002, pp. 152-161). The typical radioisotopic source used for density measurements is ^{137}Cs (662 keV). Other sources that are used include ^{226}Ra (equivalent to 750 keV emission) and ^{60}Co (1.173 and 1.332 MeV) (IAEA 2002, pp. 152-161). Spacing between the source and detector(s) is typically on the order of 254 mm (10 in.) (Mitchell 2004). Illustrations of the through-transmission and backscatter configurations are provided in Figures 2.24 and 2.25. Shielding is required between the source and detector for the backscatter configuration to ensure all gamma rays collected by the detector have a path through the concrete.

Portable neutron source devices for moisture measurements have a configuration similar to the backscatter configuration for gamma-ray source devices as shown in Figure 2.25 except that no shielding is required between the source and detector. This is because the most convenient neutron sources have fast neutron sources (energies > 10 keV) and the detectors are only sensitive to neutrons that have been moderated to the thermal energy spectrum (energies < 0.5 eV) through scattering events with hydrogen atoms attached to water molecules in concrete. Typical detectors that may be used in a neutron radiometry device for moisture measurements include gas-filled BF^3 or ^{3}He detectors (IAEA 2002, pp. 152-161).

2.1.11.2 Field and Laboratory Experience

The outcomes of a round robin-test conducted on roller compacted concrete (RCC) included measures of single-operated, single-instrument precision and multi-operator, multi-instrument precision for density

measurements with a gamma-ray source device. The standard deviation of the former was measured to be 8.0 kg/m^3 while the standard deviation of the latter was measured to be 16.0 kg/m^3 (ASTM 2013c). The test included five different commercial instruments and five different operators.

2.1.11.3 Influencing Factors Associated with Instrumentation

For a given instrument, there may be few adjustable parameters because the radioisotopic sources cannot be tuned; however, the overall instrument configuration including shielding layout and detector configuration can influence the response (IAEA 2002, pp. 152-161).

2.1.11.4 Influencing Factors Associated with Specimen and Environment

- Embedded reinforcing steel – Reinforcing steel can influence the signal of gamma-ray source devices for density measurements and the measurements should be conducted in a way that ensures that reinforcing steel does not intersect the sampled volume (ASTM 2013c).
- Concrete density – The sampled volume for gamma-ray devices is influenced by the density of the concrete in such a way that the sampled volume will decrease for regions with greater density (ASTM 2013c).
- Aggregate composition – Gamma-ray radiometry is sensitive to the aggregate composition because the cross section for photoelectric absorption is proportional to the atomic number (Z) raised to the fourth power. The backscatter mode is even more sensitive to aggregate composition because only photons that are scattered one or more times are picked up by the detector (IAEA 2002, pp. 152-161).

2.1.11.5 Limitations

- Sensitivity of gamma-ray source devices to aggregate composition means that absolute measurements of density require calibrations on specimens with similar aggregate composition to the structure undergoing testing. Difficulties or burdens associated with this may limit use of measurements to qualitative comparisons of measurements at different locations or over time.
- Heavy reinforcement may limit the effectiveness of through-transmission gamma-ray devices and limit the application of backscatter devices to regions above the outermost layer of reinforcement (ASTM 2013c). Further, through-transmission techniques require access to both sides of the structure and possibly boring of holes into the concrete.
- The volume of concrete sampled with gamma-ray and neutron source devices is not well-defined and is influenced by factors associated with instrumentation and the test specimen (ASTM 2013c).
- NDE methods based on scattering of gamma rays or neutrons may be impacted because the measurements are based on the same forms of radiation emanating from the fuel source. The overall impact may be to limit the achievable signal-to-noise ratio (SNR) with gamma-ray and neutron scattering techniques.
- Finally, radiometric measurements present unique burdens that must be addressed including health risks posed by the radioisotopic source and disposal of the radioisotopic sources at the end of an instrument's lifecycle (IAEA 2002, pp. 82-99).

2.1.12 Half-Cell Potential Measurements

The HCP method is used to evaluate corrosion activity of steel reinforcement in concrete. HCP measurements can provide an indication of the likelihood that reinforcing steel is undergoing corrosion. Under alkaline conditions (pH of approximately 12.5), a passive film oxide layer will exist on the reinforcing steel, protecting it from undergoing corrosion. Deterioration of the protective film due to

carbonation or ingress of chloride ions can create conditions allowing corrosion of reinforcing steel to occur (Carino 2004). When the reinforcing steel is not undergoing corrosion, there is no flow of electrons and ions. When a reinforcing bar is corroding, the ferrous ions move into the surrounding concrete; the electrons left behind in the bar give the bar a negative charge that is detected by HCP (ACI 2013b, pp. 32-35).

HCP measurements are performed by measuring the potential of a portion of embedded reinforcing steel with respect to a reference half-cell in electrical contact with the concrete surface. The half-cell consists of a metal anode immersed in a metal ion solution. Electrical coupling between the concrete surface and the half-cell solution is achieved via porous membranes and by wetting the surface of the concrete at the point of contact. The positive electrode of high impedance volt meter is attached to the reinforcing steel while the negative electrode is connected to the half-cell anode. A more negative potential reading will indicate a greater likelihood of corrosion (ACI 2013b, pp. 32-35). An illustration of the HCP measurement on reinforcing steel is provided in Figure 2.26. A copper/copper-sulfate half-cell is most typical, although other anode metal/electrolyte combinations may be used. The value of the potential difference reading between the reinforcing bar and half-cell anode will depend on the type of anode metal/electrolyte combination used. ASTM C876-09, "Standard Test Method for Corrosion Potentials of Uncoated Reinforcing Steel in Concrete," specifies that other standard half-cells can be used, such as silver/silver chloride reference electrodes, which is often used for measurements on concrete submerged in seawater. However, potentials measured by electrodes other than copper/copper-sulfate should be converted to the copper/copper-sulfate equivalent potential (ASTM 2009a).

HCP measurements are normally obtained at several locations on a concrete surface, often on a regularly spaced grid of points. The spacing between measurement points should be such that that readings between adjacent points are maintained between 100 mV and 150 mV (IAEA 2002, pp. 56-60). The grid of measurements can be used to generate a contour plot of equipotential surfaces for visualizing the results with areas where the potential gradient is strongest representing areas with greatest likelihood for corrosion. Results may also be represented as a cumulative frequency diagram. It is used to determine the percentage of measurements that are more negative than a certain cut-off value (ACI 2013b, pp. 32-35). A HCP measurement device that incorporates the reference cell inside of a wheel for quick inspection of multiple sites of a bridge deck is illustrated in Figure 2.27 (TRB 2013, pp. 21-22).

2.1.12.1 Instrumentation and implementation

The procedure for HCP measurements requires a direct electrical connection to the reinforcing steel and positive terminal of a high impedance voltmeter. This may require drilling a hole into the concrete if the reinforcing steel is not otherwise accessible. The negative terminal of the high impedance voltmeter is connected to the anode of a standard reference cell. Electrical contact is achieved between the reference cell solution (cathode) and surface of the concrete via porous membrane and ensuring the surface of the concrete is wetted at the point of measurement (see Figure 2.26). The standard reference cell typically consists of a copper anode immersed in a copper-sulfate solution. However, other electrode types may be employed, such as silver/silver chloride reference electrodes. Potentials measured by electrodes other than copper/copper-sulfate should be converted to the copper/copper-sulfate equivalent potential (ASTM 2009a).

Measurements are obtained at several points on the surface of the concrete; often on a regularly spaced grid pattern (IAEA 2002, pp. 56-60). ASTM C876–09 recommends a spacing of 1.2 m unless the potential difference between adjacent measurements exceeds 150 mV, in which closer spacing is recommended (ASTM 2009a). The measurements can be visualized by a plotting the equipotential surfaces on a 2-D contour plot or they may be depicted on a cumulative frequency diagram representing the portion of measurements that exceed some cut-off value (ACI 2013b, pp. 32-35).

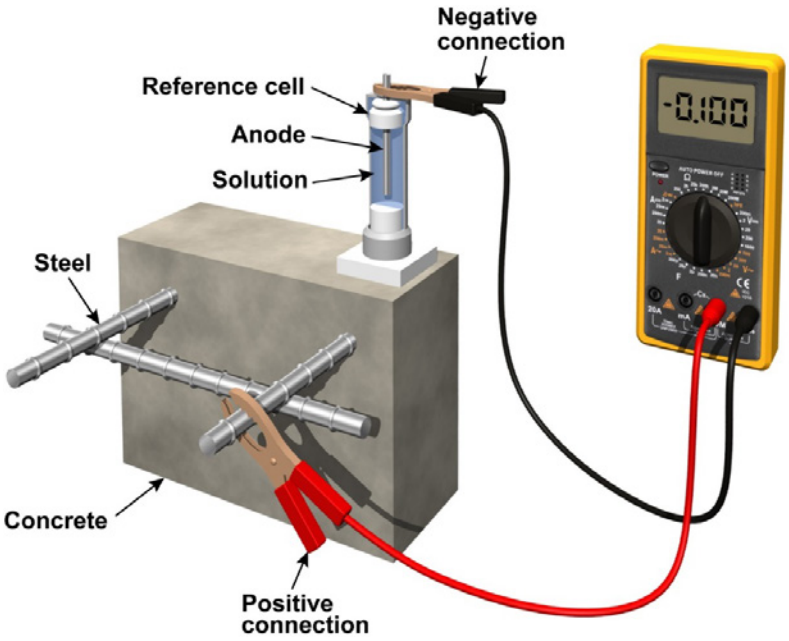

Figure 2.26. Depiction of HCP Measurement on Reinforcing Steel Showing Electrical Connections between the Reference Cell, Concrete Surface, Voltmeter, and Reinforcing Steel

Figure 2.27. HCP Testing Incorporating Reference Cell in a Wheel for Faster Implementation on a Bridge Deck (TRB 2013, pp. 21-22)

2.1.12.2 Field and Laboratory Experience

HCP testing was evaluated in SHRP 2 to observe the corrosion of reinforcing steel (TRB 2013, pp. 21-22). For rebar corrosion, HCP testing tied with resistivity testing for the highest rating based on accuracy for the methods evaluated (TRB 2013, p. 77). In this case, accuracy was based on the ability to discriminate regions where corrosion activity existed from regions where there was no, or low, corrosion activity. Other methods evaluated included GPM testing and GPR testing. When the rating is based on a composite score consisting of factors such as speed, cost, repeatability, and ease-of-use, HCP testing is rated below resistivity testing but above GPR and GPM testing (TRB 2013, p. 77).

2.1.12.3 Influencing Factors Associated with Instrumentation

The major parameters associated with instrumentation that may influence HCP measurements include the type of reference cell used and the electrical contacts between the reference cell and the concrete surface and between the positive terminal of the voltmeter and the reinforcing steel.

- Electrical contacts – The concrete surface may require pre-wetting particularly if the half-cell reading fluctuates with time when it is placed in contact with the concrete. The whole surface may be wetted, or just the locations where measurements are to be obtained (IAEA 2002, pp. 56-60).
- Type of reference cell – Potentials measured by electrodes other than copper/copper-sulfate should be converted to the copper/copper-sulfate equivalent potential (ASTM 2009a).

2.1.12.4 Influencing Factors Associated with Specimen and Environment

- Concrete resistivity – HCP measurements are influenced by the concrete resistivity, which is influenced by the moisture content and chloride content of the concrete. Valid HCP measurements can only be obtained if the concrete is sufficiently moist; thus, it is important to be able to recognize when there is insufficient moisture for a valid measurement. A corrosion specialist is required to interpret HCP measurements under conditions of a) concrete saturated with water, b) concrete carbonated to depth of the reinforcement, or c) when the reinforcing steel is galvanized (ACI 2013b, pp. 32-35).
- Cover depth – Correcting for the influence of cover depth on HCP measurements is not straightforward as it has not been extensively researched (IAEA 2002, pp. 56-60). It is noted that concrete cover depths greater than 75 mm (3 in.) can result in loss of ability to observe spatial variations in corrosion activity (ASTM 2009a).

2.1.12.5 Limitations

- HCP does not provide a direct measure of the corrosion rate and only provides an indication that corrosion is likely (IAEA 2002, pp. 56-60).
- Electrical contact is required between the positive terminal of the high impedance voltmeter and the embedded reinforcing steel, which may require drilling a hole into the concrete in order to access it (IAEA 2002, pp. 56-60).
- HCP cannot be applied if the reinforcing steel has an epoxy coating. Further, all of the reinforcing steel must be electrically connected (ACI 2013b, pp. 32-35).

2.1.13 Linear Polarization Resistance Measurements

Linear polarization resistance (LPR) measurements provide a measure of the corrosion current (*Icorr*), which is directly related to the corrosion rate. The corrosion current can be estimated from the following relationship,

$$Icorr = B / Rp \,, \tag{2.10}$$

where B is a constant and Rp is the polarization resistance, which has units of $\Omega \times cm^2$ (ACI 2013b, pp. 38-42). A value for B of 26 mV can typically be used for corroding steel in concrete though the constant can vary by a factor of 2. The polarization resistance, Rp, is what is measured by LPR methods and it is determined by measuring the amount of current, Δi , required to induce a small change in the potential of the corroding steel bar, ΔE, where,

$$Rp = \Delta E / \Delta i \,. \tag{2.11}$$

ΔE is measured by the HCP method discussed in Section 2.1.12 (ACI 2013b, pp. 38-42). The linear relationship in Eq. (2.11) is only valid when ΔE is kept below 20 mV (IAEA 2002, pp. 168-169).

2.1.13.1 Instrumentation and Implementation

The general setup for LPR measurements is shown in Figure 2.28, which shows the electrical connectivity between three electrodes including 1) a reference half-cell; 2) the reinforcement (also called the working electrode); and 3) the counter electrode, which supplies the polarization current to the bar. Voltmeters and current meters are connected to measure voltages and currents (ACI 2013b, pp. 38-42). To implement LPR, it is necessary to locate the reinforcing steel and estimate cover depth with a cover meter. The counter electrode should be centered over the reinforcing steel when making a measurement. In addition, it is necessary to estimate the surface area of the working electrode (i.e. projected surface area of reinforcing steel located beneath the counter electrode) (ACI 2013b, pp. 38-42). A significant uncertainty is associated with the area of the working electrode (reinforcing steel) that is impacted by the flow of current from the counter electrode. The flow of current along straight paths between the counter electrode and working electrode cannot necessarily be assumed. As a result, many commercial devices may include a "guard" or "auxiliary" electrode to help confine the flow of current beneath the working electrode (Carino 2004). A photograph of LPR testing being conducted in the field is provided in Figure 2.29.

LPR can be implemented in one of two major modes: 1) galvanostatic mode in which the potential of the working electrode is monitored in response to a steady applied current between the working electrode and counter electrode, and 2) potentiostatic mode in which the amount of current required to maintain a fixed working electrode potential is measured. The galvanostatic pulse method (GPM) is a variation of LPR in which the potential is measured in response to a short-duration pulse of current (ACI 2013b, pp. 38-42).

2.1.13.2 Field and Laboratory Experience

A study of three commercial LPR instruments was conducted in the 1990s on bridge structures. Two of the LPR instruments incorporated guard electrodes. It was noted that all devices successfully distinguished between active and passive sites and that they could all successfully locate corrosion (ACI 2013b, pp. 38-42).

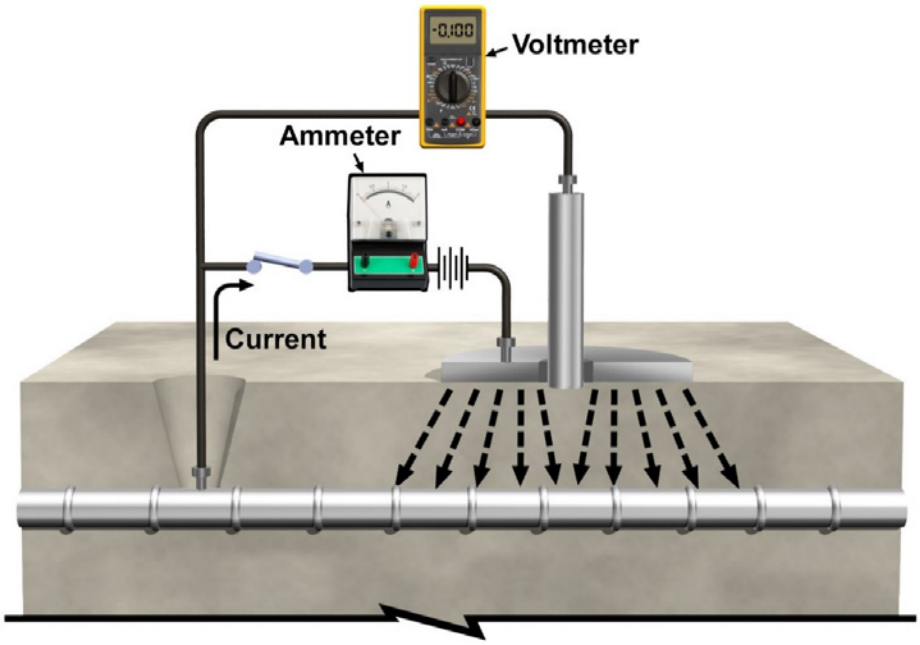

Figure 2.28. Depiction of LPR Measurement on Reinforcing Steel Showing Electrical Connections between the Reference Cell, Concrete Surface, Voltmeter, and Reinforcing Steel, and Counter Electrode (IAEA 2002, pp. 168-169)

Figure 2.29. LPR Testing Conducted in the Field (TRB 2013, pp. 22-24)

LPR testing (galvanostatic pulse mode) was evaluated in SHRP 2 to observe the corrosion of reinforcing steel (TRB 2013, pp. 22-24). For rebar corrosion, LPR testing was rated lower than HCP and resistivity testing and higher than GPR testing based on accuracy for the methods evaluated (TRB 2013, p. 77). In this case, accuracy was based on the ability to discriminate regions where corrosion activity existed from regions where there was no, or low, corrosion activity. When the rating is based on a composite score consisting of factors such as speed, cost, repeatability, and ease-of-use, LPR testing is rated lowest for corrosion inspections behind HCP, resistivity and GPR testing (TRB 2013, p. 77).

2.1.13.3 Influencing Factors Associated with Instrumentation

LPR requires the use of a half cell and is subject to the same influences associated with instrumentation as HCP measurements.

- Electrical contacts – The quality of electrical contact between the half cell and concrete surface, which may require pre-wetting (IAEA 2002, pp. 56-60).
- Type of reference cell – Potentials measured by electrodes other than copper/copper-sulfate should be converted to the copper/copper-sulfate equivalent potential (ASTM 2009a).
- Current pulse duration – The duration of the applied current must be sufficient to obtain a reliable reading and is typically between 30 s to 100 s depending on how actively the steel is corroding (ACI 2013b, pp. 38-42). GPM measurements can be performed much more quickly (on the order of 10 s); however, the polarization resistance is found to increase with pulse duration—meaning that corrosion rates can be overestimated if pulse durations are too short, although methods have been developed to correct polarization resistances measured with short pulse durations (ACI 2013b, pp. 38-42).

2.1.13.4 Influencing Factors Associated with Specimen and Environment

- Concrete resistivity – HCP measurements performed as part of LPR testing are influenced by the concrete resistivity, which is influenced by the moisture content and chloride content of the concrete. Valid HCP measurements can only be obtained if the concrete is sufficiently moist; thus, it is important to be able to recognize when there is insufficient moisture for a valid measurement. A corrosion specialist is required to interpret HCP measurements under conditions of a) concrete saturated with water, b) concrete carbonated to depth of the reinforcement, or c) when the reinforcing steel is galvanized (ACI 2013b, pp. 32-35).
- Cover depth – LPR measurements can be influenced by the effect of cover depth on HCP measurements. As noted in 2.1.12.4, HCP measurements is not straightforward as it has not been extensively researched (IAEA 2002, pp. 56-60). It is noted that concrete cover depths greater than 75 mm (3 in.) can result in loss of ability to observe spatial variations in corrosion activity (ASTM 2009a).

2.1.13.5 Limitations

- LPR measurements are sensitive to several factors related to the ambient environment such as temperature and moisture; thus, several measurements should be performed to capture the seasonal variations in the measurements (Carino 2004).
- Significant error can be introduced in the estimation of the surface area of the working electrode (reinforcing steel) exchanging current with the counter electrode. It is noted that significant error can persist even for devices with guard electrodes, except at high corrosion rates (IAEA 2002, pp. 168-169).
- The constant parameter, B, in Eq. (2.10) is a source of inherent uncertainty that can be off by a factor of two depending on the corrosion activity.
- In general, a corrosion specialist should be consulted to interpret LPR measurement results (ACI 2013b, pp. 32-35).

2.1.14 Resistivity Measurements

Resistivity measurements (RM) can be performed on concrete to indirectly assess the likelihood of corrosion, similar to HCP testing. Resistivity testing can also have an important role as a supplemental

measurement to HCP testing because the interpretation of HCP results is dependent on the resistivity of the concrete. Although there is no ASTM standard for performing RM on concrete, the typical configurations include a four-probe or four-electrode setup, also referred to as a Wenner probe and a two-electrode configuration (ACI 2013b, pp. 35-36). An illustration of the Wenner probe configuration is provided in Figure 2.30. The outer two electrodes are used to inject an alternating current into the concrete structure while the potential drop across the inner two electrodes is measured with a volt meter. The two-electrode measurement of resistivity is performed as part of LPR testing discussed in Section 2.1.13. In this case, the potential drop that forms between the reinforcing steel and the counter electrode for a set current flow from the counter electrode to the reinforcing steel can be used to estimate the concrete resistivity below the counter electrode. This method requires knowledge of the cover depth (ACI 2013b, pp. 35-36). However, unlike the Wenner probe method, the two-probe method requires direct contact with the reinforcing steel. Estimation of concrete resistivity by the two-probe method is distinct from an LPR measurement, which measures the polarization resistance of the reinforcing steel and which is calculated from Eq. (2.11).

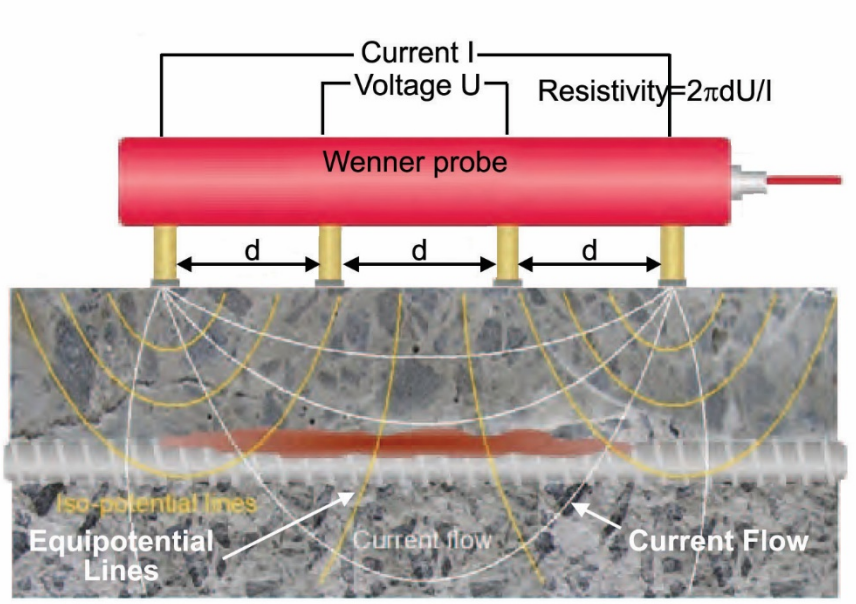

Figure 2.30. Illustration of the Four-Probe Method for Measuring the Resistivity of Concrete (TRB 2013, pp. 24-25)

In general, the relationship between the resistivity of a conductor, ρ, and the total resistance of the conductor, R, can be expressed as,

$$R = \rho \frac{L}{A} \tag{2.12}$$

where L is the length of the conducting region and A is the cross-sectional area of the conducting region. R is expressed in Ω (ohms) and a typical unit for ρ is Ω-cm. For the Wenner probe, an expression has been derived to relate resistivity to the injected current in the outer electrodes (I) and the measured voltage between the inner electrodes (V),

$$\rho = \frac{2\pi dV}{I}. \tag{2.13}$$

In this formula, *d*, is the electrode spacing. This formula assumes that the concrete is homogenous and that the structure under testing is semi-infinite (ACI 2013b, pp. 35-36). Table 2.4 indicates the qualitative relationship between concrete resistivity values and the corrosion rate often observed for different conditions of resistivity (TRB 2013, pp. 24-25).

Table 2.4. Relationship Between Resistivity and the Corrosion Rate (TRB 2013, pp. 24-25)

Resistivity (kΩ-cm)	Corrosion Rate
<5	Very high
5–10	High
10–20	Moderate–low
>20	Low

2.1.14.1 Instrumentation and Implementation

As noted, the four-probe (or Wenner probe) is a typical instrument for performing RM on concrete. A diagram of the probe is provided in Figure 2.30, which shows that alternating current is injected through the outer electrodes, and the potential drop to form across the inner electrodes is measured. A photograph of the Wenner probe application to a bridge deck is provided in Figure 2.31 (TRB 2013, pp. 24-25). Pre-wetting of the concrete surface and/or application of conductive gel can be used to improve the electrical contact of the Wenner probe electrodes and the surface of the concrete (IAEA 2002, pp. 76-78). Alternatively, resistivity may be measured by the two-probe method incorporated into an LPR instrument, as described in Section 2.1.13.1.

Figure 2.31. Photograph of Application of the Four-Probe (Wenner probe) Method in the Field (TRB 2013, pp. 24-25)

2.1.14.2 Field and Laboratory Experience

Resistivity testing was evaluated in SHRP 2 to observe the corrosion of reinforcing steel (TRB 2013, pp. 24-25). For rebar corrosion, resistivity testing tied with HCP testing for the highest rating based on accuracy for the methods evaluated (TRB 2013, p. 77). In this case, accuracy was based on the ability to discriminate regions where corrosion activity existed from regions where there was no, or low, corrosion activity. Other methods evaluated included HCP testing, GPM testing, and GPR testing. When the rating is based on a composite score consisting of factors such as speed, cost, repeatability, and ease-of-use, resistivity testing is rated the highest (TRB 2013, p. 77).

2.1.14.3 Influencing Factors Associated with Instrumentation

- Electrode spacing – The electrode spacing, *d*, is the primary parameter associated with the Wenner probe that can be adjusted. The spacing influences the region of concrete that is being measured and can influence the scatter in the measurements. At smaller electrode spacing, measurements are increasingly influenced by the heterogeneous nature of the concrete and the stochastic effects related to aggregate size and shape. If electrode spacing is too large, then the measurements may be influenced by edge effects associated with the finite size of the structure under test. In addition, it becomes more difficult to avoid the presence of reinforcing steel within the sampled region. An electrode spacing of 50 mm (2 in.) is considered adequate for testing most concrete structures as long as the thickness is 200 mm (8 in.) or greater (IAEA 2002, pp. 76-78). Further, the distance to the edge of the structure from the point of measurement should be at least twice the electrode spacing (ACI 2013b, pp. 38-42).
- Electrical contacts – Measurements may also be influenced by the quality of the electrical contact between the probe electrodes and the concrete surface, in which case, pre-wetting of the concrete surface and/or application of conductive gel may be advisable (IAEA 2002, pp. 76-78).

2.1.14.4 Influencing Factors Associated with Specimen and Environment

Specimen factors that may influence the ability to obtain accurate RM include aggregate size and distribution and the presence of reinforcing steel.

- Aggregate size and distribution – The aggregate size and distribution can cause significant scatter in measurements because of the relatively high resistivity of individual aggregate particles in comparison to surrounding cement. This requires the electrode spacing to be large enough so that stochastic effects associated with the size and arbitrary distribution of aggregate are averaged (IAEA 2002, pp. 76-78).
- Embedded reinforcing steel – The effect of reinforcing bars is to indicate a much lower resistivity than actual for the concrete. RM should be performed with the probe situated between reinforcing bars. The effect of cover depth appears to have greater influence than bar diameter. It may be possible to correct for the effect of reinforcing steel when the size of the bars and locations are known (ACI 2013b, pp. 38-42).
- Surface conditions – RM can also be impacted if a thin surface layer of resistivity different than the bulk resistivity is present (ACI 2013b, pp. 38-42).

2.1.14.5 Limitations

- Several material properties contribute to the overall resistivity of concrete such as moisture content, the presence of ions, and the porosity of concrete; and it is not possible to delineate the contribution of each to the overall measurement of resistivity (TRB 2013, pp. 24-25).
- Deviations from the assumption of the homogeneity and semi-infinite extent of the structure will result in errors in the estimation of resistivity by Eq. (2.13).
- Like LPR measurements, RM can be influenced by ambient environmental factors so several measurements may need to be performed to account for seasonal variations in resistivity.

2.1.15 Summary of Relevant NDE Technology Scores From SHRP 2 Program

A significant amount of information regarding field or laboratory experience is obtained from assessments of NDE methods for inspecting concrete bridge decks. In particular, data obtained from field and laboratory trials is provided in the report S2-R06A-RR-1, *Nondestructive Testing to Identify Concrete Bridge Deck Deterioration* (TRB 2013). This report documents work performed under the SHRP 2 and data from two summary tables in this report (Tables 7.1 and 7.8) are referenced frequently throughout Section 2.1. Relevant portions of these tables are provided below as Table 2.5 and Table 2.6 for the convenience of the reader in comparing the relative performance of individual NDE methods as observed in the SHRP 2 study. The accuracy of NDE methods was assessed in laboratory validation studies that were performed on a fabricated bridge specimen and a recovered bridge specimen. The size of delaminations in the recovered bridge deck are not reported, but the size of simulated delaminations in the fabricated bridge deck ranged from 12 in. by 12 in. up to 24 in. by 48 in. (TRB 2013, p. 69). Table 2.5 includes the summary of rankings based on accuracy performance in SHRP 2. The true state of the specimen in the field validation testing was not determined so it could not be used for accuracy assessment. However, the field validation testing was used to assess other relevant factors associated with the deployment of NDE methods in the field, including such as speed, cost, repeatability, and ease-of-use. Overall composite rankings that are based on these factors and accuracy are provided in Table 2.6.

Table 2.5. Grading of NDE Methods Based on Accuracy in SHRP 2 Study (TRB 2013, p. 69)

Defect	Technology	Average Grade
Delamination	GPR	1.7
	IE	2.8
	IE-USW	2.8
	Infrared	2.2
	Chain dragging	1.6
Rebar Corrosion	GPM-HCP	2.4
	GPR	1.6
	HCP	2.2
Crack Depth	SASW	2.3
	SWT	3.0
	TOFD	1.6
Concrete Degradation	USW	3.8

Table 2.6. Overall Value of NDE Methods in Bridge Deck Deterioration Detection (TRB 2013, p. 77)

Deterioration Type	Delamination	Corrosion	Vertical Cracks	Concrete Degradation
Impact Echo	3.0	0.0	1.0	1.0
Ultrasonic Surface Waves	2.7	0.0	2.4	3.3
Ground-Penetrating Radar	3.1	3.1	0.0	1.0
Half-Cell Potential	0.0	3.3	0.0	0.0
Galvanostatic Pulse Measurement	0.0	2.8	0.0	0.0
Electrical Resistivity	0.0	3.6	0.0	0.0
Infrared Thermography	2.9	0.0	0.0	0.0
Chain Dragging/Hammer Sounding	2.9	0.0	0.0	0.0

2.2 NDE Methods and Techniques for Inspection of Stainless Steel Components

NDE methods for inspecting degradation in metal components are summarized in this section. The methods described in this section include visual testing (Section 2.2.1), bulk ultrasound testing (Section 2.2.2), guided ultrasonic wave testing (Section 2.2.3), eddy current testing (Section 2.2.4), and acoustic emission testing (Section 2.2.5). The descriptions are written with the primary focus on inspections of DSCs to detect forms of localized corrosion and cracking that initiate on the outer surface. The ASME B&PV Code is used primarily as the basis for NDE methods considered, along with currently funded efforts through industry (EPRI) and the DOE to develop inspection technologies for canisters.

2.2.1 Visual Testing

A comprehensive overview of visual testing (VT) can be found in Volume 9 of the ASNT Nondestructive Testing Handbook (ASNT 2010). VT is perhaps the most prevalent form of nondestructive testing. Visual testing refers to the examination of a component or material using the unaided human eye or with the aid of a variety of tools to enhance the inspection capability. Such aids may include lenses, fiber-optic light guides, cameras, special lighting equipment, etc. In the nuclear power industry, VT is one of the NDE methods sanctioned by the ASME B&PV Code for performing examinations of nuclear facility structural components (ASME 2007b). VT is used for remote surveys of piping and pressure vessels in reactor systems (Cumblidge et al. 2007). Different categories of VT are defined in the ASME B&PV Code, such as VT-1 for pitting/cracking detection and VT-3 for general/mechanical condition assessment. A VT-2 type visual inspection is performed to identify signs of component leakage.

Industry-led activities such as the Boiling Water Reactor Vessel and Internals Project-03 (EPRI 2005) and the Materials Reliability Program-227 (EPRI 2015b) provide additional guidance for the implementation of visual inspection methods for the purposes of detecting cracking in reactor vessel internals. This guidance is generally included in procedures developed by the various providers of visual examination to the nuclear power industry. In addition to reactor components, visual testing is also used for inspection of containment structures at nuclear power plants. Subsections IWE and IWL of ASME B&PV Code Section XI specify inspection requirements for metal containments (MC) and concrete containment (CC) components respectively. A "tiered" approach to inspection is specified for MC and CC components requiring suspected areas of degradation to be re-inspected with greater vigor to verify and characterize the degradation. The types of visual inspections referred to for these circumstances are "general visual" and "detailed visual" examinations (ASME 2007b). In this case, the general visual examination is performed first and a detailed visual inspection is only performed if signs of degradation are observed

during the general visual examination and the detailed visual examination is focused on the region of concern. In the case of MC components, ultrasonic testing may also be performed following a general visual or detailed visual examination.

A survey of several commercial vendors' websites indicates that the most common application of radiation-hardened cameras is the inspection and monitoring of nuclear power facilities including underwater operation to monitor fuel storage in spent fuel pools. The other major application is in the inservice inspection (ISI) of reactor vessel internals. In both cases, there is a need for camera systems that are radiation-tolerant, and for the real-time video to be relayed to a remote monitor. Further, access restrictions may limit the maximum size of the camera that can be used. This is particularly true with the inspection of appurtenances within the reactor vessel.

Limited studies have been performed to understand the adequacy of visual inspection for application to reactor internal inspections and the factors that can influence performance and reliability. Most of this work has been conducted through literature review and parametric study as documented in NUREG/CR-6860 (Cumblidge et al. 2004) and NUREG/CR-6943 (Cumblidge et al. 2007). A cooperative research effort between the NRC, EPRI, and PNNL is ongoing with respect to understanding how well remote visual testing methods can perform for inspection of reactor vessel internal components. Even so, these studies focus on the ability of VT to detect cracks on surfaces exposed to light water reactor (LWR) environments and do not directly address the detection of localized corrosion (via precursors such as pitting or corrosion products) on surfaces exposed to atmospheric conditions.

2.2.1.1 Instrumentation and Implementation

A review of radiation-hardened camera products from several vendor websites indicates that primary packages include pan-tilt-zoom type (PTZ) and tube cameras (Meyer et al. 2013b). An illustration of a PTZ camera is provided in Figure 2.32 and illustrations of tube cameras are provided in Figures 2.33 and 2.34, respectively. Figure 2.34 is an illustration of a tube camera with a 90° tilt mirror accessory, which may enable usage in locations where access is restrictive. The PTZ cameras have the ability to rotate in pan and tilt directions and to zoom to adjust the field of view. A photograph of a PTZ camera is provided in Figure 2.35. This particular camera system is 98 mm (3.9 in.) wide and approximately 196 mm (7.7 in.) in length. The video signal can be relayed to a monitor located away from the camera and the video signals can also be recorded.

Radiation-hardened cameras come in a variety of technologies including charge-coupled device, complementary metal–oxide–semiconductor, Chalnicon, and charge injection device. Temperature ratings for cameras are fairly modest with the highest temperature rating at 70°C in water and 40°C–50°C being more typical for operation in air. Depending on the shielding and the camera type, the total exposure limit for gamma radiation spans from 1 MRad to 200 MRad. Figure 2.36 summarizes commercially available radiation-hardened camera systems with maximum lateral dimension less than 100 mm (4 in.) by their specifications for radiation tolerance and temperature rating. Figure 2.37 summarizes commercially available radiation-hardened camera systems with maximum lateral dimension less than 100 mm (4 in.) by their specifications for radiation tolerance and camera resolution. In this case, the maximum lateral dimension is the diameter for tube-type cameras or the maximum of width or height for PZT cameras.

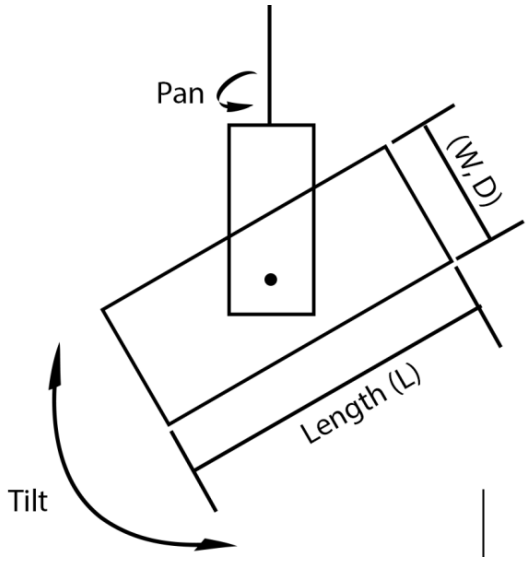

Figure 2.32. Illustration of a Pan/Tilt/Zoom Camera System (Meyer et al. 2013b)

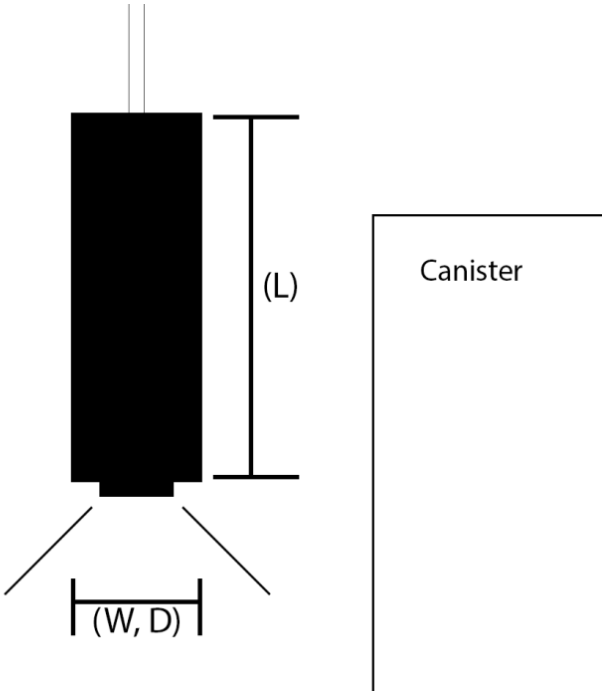

Figure 2.33. Illustration of Tube Camera Suspended by Power Cable (Meyer et al. 2013b)

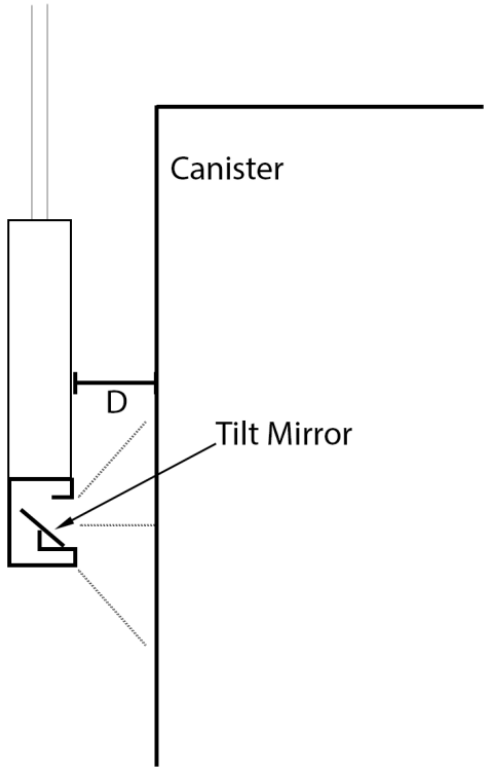

Figure 2.34. Illustration of Tube Camera with Tilt Mirror Accessory to Alter Viewing Direction (Meyer et al. 2013b)

Figure 2.35. Photograph of the GE PTZ 100 Camera

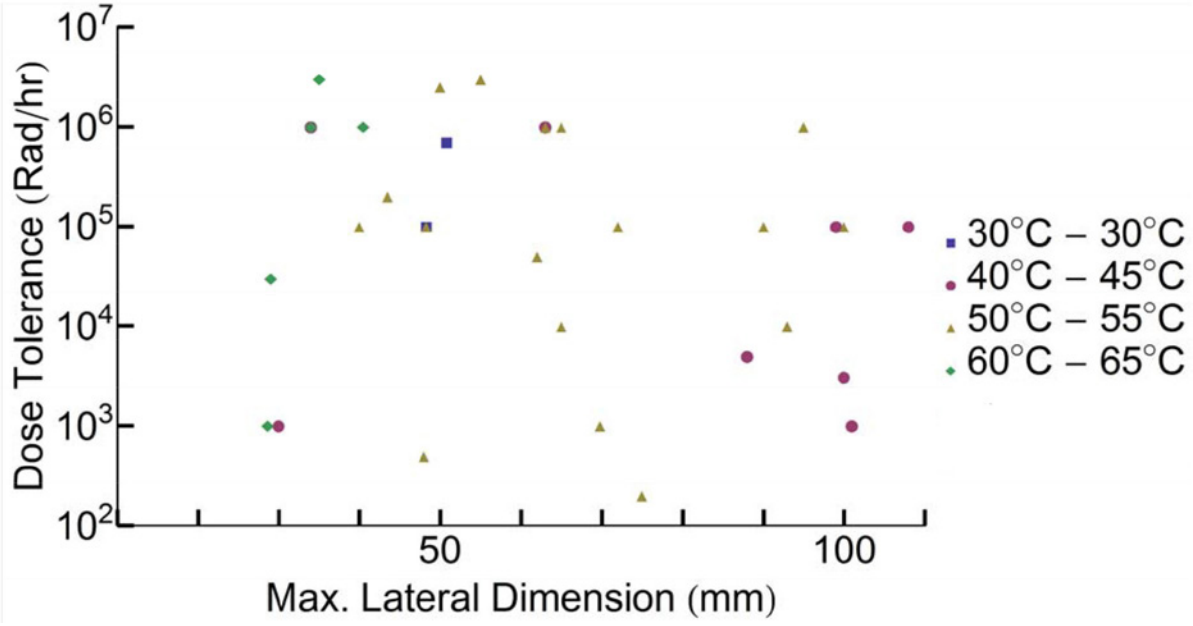

Figure 2.36. Summary of Specifications by Dose Tolerance and Temperature Rating for Several Commercially Available Radiation-Hardened Camera Systems with Maximum Lateral Dimension of 100 mm (4 in.) or Less

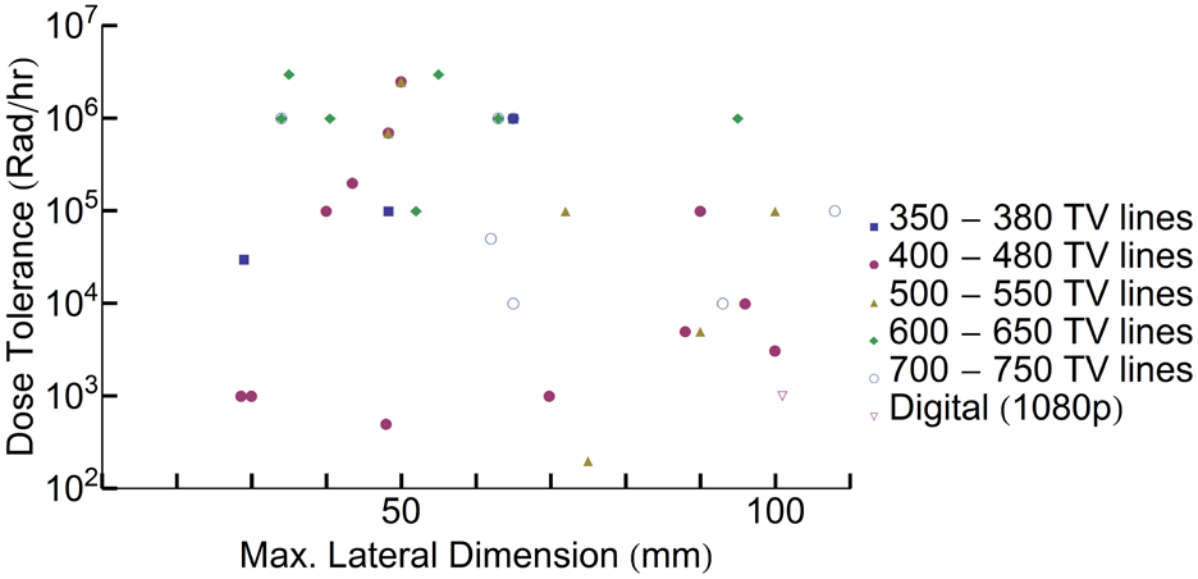

Figure 2.37. Summary of Specifications by Dose Tolerance and Camera Resolution for Several Commercially Available Radiation-Hardened Camera Systems with Maximum Lateral Dimension of 100 mm (4 in.) or Less

Many of the camera systems used for ISI applications provide color output and are standard definition cameras, although vendors are moving to providing radiation-tolerant, high-definition color camera systems. Such cameras provide improved clarity and may improve the ability to detect cracking per manufacturer claims. However, such claims still need to be verified. Tube-type cameras are also occasionally used in ISI (especially in locations where access may be tight), and provide monochromatic outputs.

In addition to cameras, boroscopes may also be utilized to inspect surfaces that might otherwise be difficult to access. Conventionally, a borescope refers to rigid or flexible light guide to transmit optical information to a remotely located sensor. Rigid borescopes usually consist of a series of relay lenses and other optical components to transfer an image from the objective lens to the eyepiece. Flexible borescopes use coherent fiber-optic bundles to transfer an image from the objective lens to the eyepiece. Typically, a coaxial arrangement of fiber-optic bundles is employed with an outer bundle that transfers a source of light to the object for illumination, while the inner bundle is used to transfer the image back to the eyepiece (ASNT 2010). The disadvantage of flexible borescopes in comparison to rigid borescopes is that the resolution is limited by the number of fibers that can be incorporated into the bundle. Systems also exist with miniature cameras mounted to the end of a long cable. Information of the image can be transmitted through the cable back to a monitor for viewing or device for recording. The means for remotely manipulating the camera also exists, allowing tilting or rotating of the miniaturized camera. A photograph of this type of system is provided in Figure 2.38.

Figure 2.38. Photograph of GE Mentor IQ Video Borescope

2.2.1.2 Performance Estimations and Field Experience

The detection performance for remote VT can be influenced by many factors. However, according to Cumblidge et al. (2007, p. 2.7), the influence of all factors can be described by their effect on three main parameters that impact flaw detection—contrast between flaws and background, flaw recognition, and flaw discrimination. An overview of several factors that can influence remote VT detection performance and how they influence detection performance is provided in Section 2.2.1.3. Given favorable conditions, a camera can theoretically detect cracks less than a micron in opening (and roughly a millimeter in length); however, this comes at a cost of very small field of view (due to high required magnification) and long inspection time.

Cumblidge et al. (2007, p. 7.1) concluded that crack opening displacement (COD) had the largest impact on detection reliability. Some commercial inspection cameras are quoted as being able to detect features below 100 μm in size, although this specification is highly conditional (Cumblidge et al. 2004). A review of the available literature suggests that cracks with a COD greater than 100 μm are detectable under most conditions, while cracks with a COD less than 20 μm cannot be detected reliably except under the most favorable conditions (Cumblidge et al. 2007). The detectability of cracks with CODs between these limits is dependent on all of the influencing factors mentioned in Sections 2.2.1.3 and 2.2.1.4 below. A cooperative research effort between the NRC, EPRI, and PNNL is ongoing. The scope of this effort is to quantify the performance of current industry practice regarding remote VT inspections of reactor components and to determine if improved capabilities are needed.

The Swedish Nuclear Power Inspectorate (SKI) (now part of the Swedish Radiation Authority [SSM]) has performed a systematic evaluation of service-induced crack characteristics (Ekstrom and Wåle 1995; Wåle 2006). Cracks are assessed according to crack type and material, with several different crack types considered in the analysis. Several flaw parameters were catalogued, including COD. The mean COD for stress corrosion cracking (SCC) cracks analyzed ranged from 16–30 μm.

For chloride-induced SCC (CISCC), studies suggest that significant pitting corrosion may precede the formation of large cracks (Caseres and Mintz 2010; He et al. 2014). Analysis of field occurrences of CISCC at nuclear power facilities indicates that pitting was present in many of the occurrences, but not all occurrences (Lareau 2014; NRC 2012). Multiple studies have considered automated or semi-automated analysis of localized corrosion based on visual attributes such as discoloration and texture (Choi and Kim 2005; Codaro et al. 2002; Pidaparti et al. 2013). These works are focused on characterization and do not attempt to define or quantify detection performance.

2.2.1.3 Influencing Factors Associated with Instrumentation

The following discussion is not a comprehensive discussion of the factors that influence VT performance but provides a summary of the outcomes of studies performed with respect to crack detection in reactor internal components and documented in NUREG/CR-6943 (Cumblidge et al. 2007).

- Camera movement – Camera scanning speed is identified as a controllable factor that most impacts the quality of remote VT inspections (Cumblidge et al. 2007, p. 7.1). Cumblidge et al. (2007, p. 7.1) makes a recommendation that stationary cameras or slowly moving cameras be used for remote VT inspections because a high scanning speed can have a severe impact on detection capability and can cause blurring (Figure 2.39). At scan rates below approximately 6 mm/sec. (0.24 in./sec.), image quality experiences minimal distortion. At scan rates above 25 mm/sec. (1.0 in./sec.), a significant degradation in image quality is observed for a radiation-hardened PTZ system (Cumblidge et al. 2007, pp. 4.10-4.11).

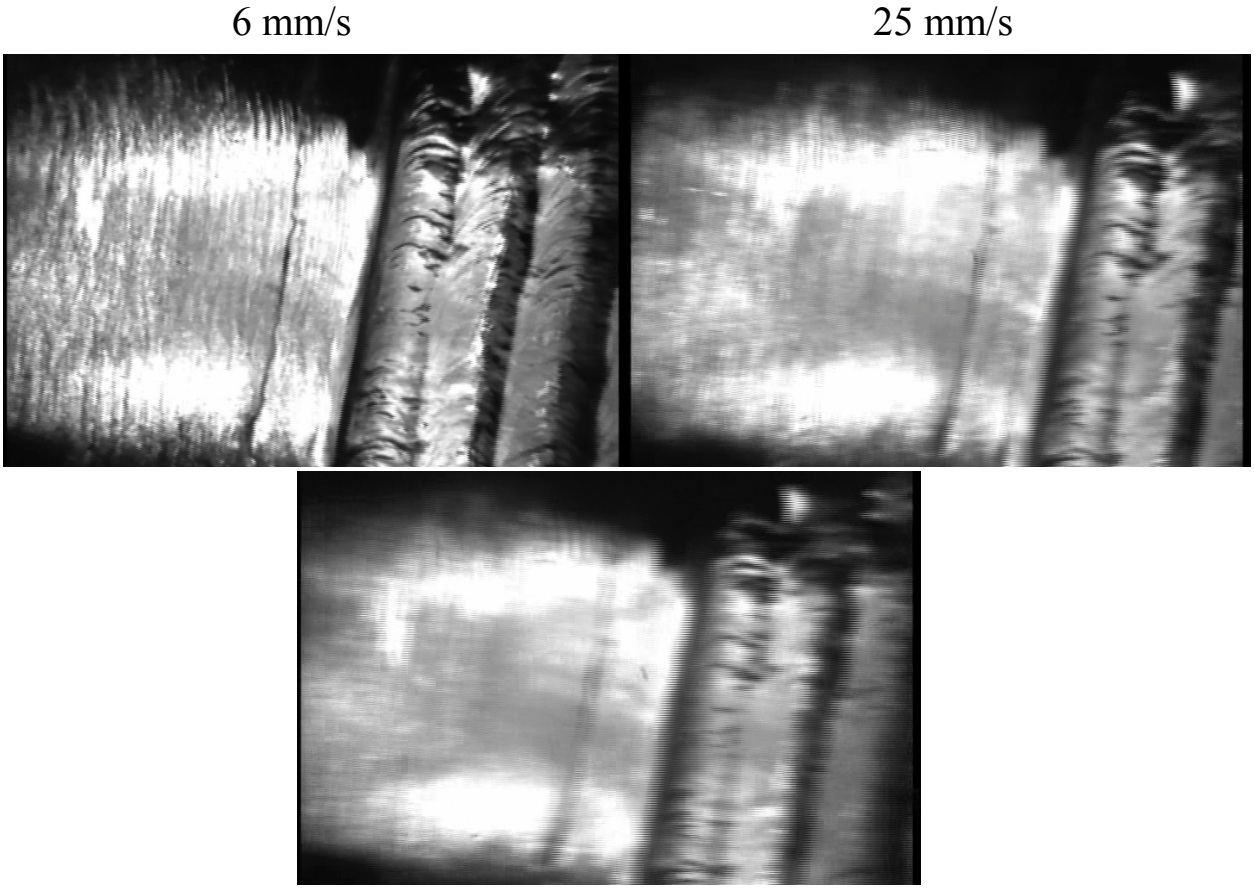

Figure 2.39. Photographs Illustrating How Greater Camera Scan Speeds can Degrade Image Quality and Crack Detection Performance by Remote VT (Cumblidge et al. 2007, Fig. 4.6)

- Lighting conditions – Camera lighting is identified as the next most important factor that impacts detection performance behind COD and camera scanning speed (Cumblidge et al. 2007, p. 7.1). Lighting can be impacted by the source type including the use of onboard or auxiliary systems and use of specular versus diffuse systems. A limited set of lighting systems were examined in NUREG/CR-6943 (Cumblidge et al. 2007, pp. 3.1-3.3 and 4.4-4.7). In the context of inspections performed on reactor components, it is noted that the common practice is the use of one or two fixed spotlights. Detection capability is much better when the spotlights are aligned parallel to crack orientation than when they are aligned perpendicular to crack orientation (Cumblidge et al. 2007, p. 4.4). A diffuse on-axis light was determined to be the most effective but it is acknowledged that the system would not be very practical for use in reactor environments (Cumblidge et al. 2007, p. 7.1). Overall, diffuse lighting is preferable to the bare bulb (incandescent or LED) spotlights because the spotlights provide uneven lighting and tend to produce more glare than diffuse light sources (Cumblidge et al. 2007, p. 4.7). Figure 2.40 includes photos of different lighting sources on the same surface to illustrate the difference between diffuse and bare bulb spot lighting styles. Lighting can also be arranged to provide bright field or dark field images. In bright field imaging, the component surface or background is illuminated. The crack faces redirect light that reflects off of their surfaces resulting in darkness associated with the crack and providing contrast with the illuminated background. In dark field imaging, lighting is applied at an angle so that the background is illuminated to a lesser extent and the crack faces reflect light into the camera lens. In this case, the

crack appears bright and provides contrast to the dark background. Often, lighting at an angle can result in a combination of bright field and dark field effects (Cumblidge et al. 2007, pp. 2.12-2.14). This is illustrated in Figure 2.41, which includes photographs of a crack image obtained with direct lighting above the surface and a crack imaged with lighting from the side. The direct lighting condition provides a bright field image of the crack, while side lighting results in mixed bright field and dark field effects. It is noted that if spotlighting must be used, then providing lighting at several angles and perspectives to the surface can be used to enhance crack detection through dark field effects (Cumblidge et al. 2007, pp. 4.13-4.15).

- Camera resolution and magnification – Camera resolution refers to the number of pixels an image is projected onto. Magnification refers to an image enhancement in which an increased portion of the detector pixels are dedicated to capturing a smaller physical object area. For a given resolution, increased magnification necessarily decreases the field of view, which increases the time required for inspection. In addition, high magnification results in loss of context and fiduciaries (Cumblidge et al. 2007, pp. 4.3–4.4). Camera resolution can influence detection performance through effects on contrast between flaws and background, flaw recognition capability, and flaw discrimination capability. Inadequate resolution can result in poor image sharpness. The reduced sharpness can "blur" flaw boundaries negatively impacting contrast and masking recognizable features of flaws making it difficult to discriminate between flaws and superficial marks (Cumblidge et al. 2007, p. 7.1).

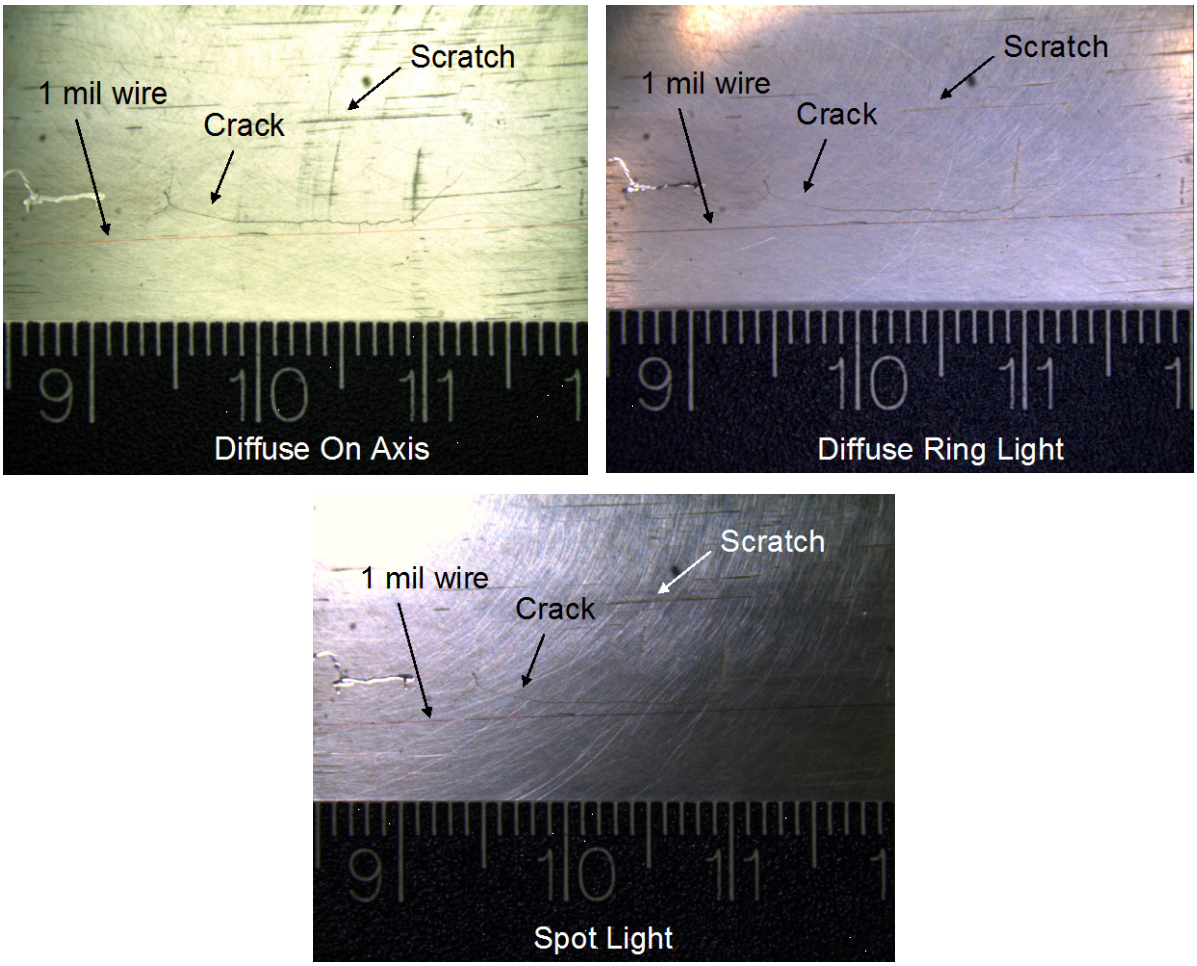

Figure 2.40. Photographs Illustrating the Effect of Three Light Sources (diffuse on axis, diffuse ring light, and spot light) on Image Quality and Ability to Detect Cracks with Remote VT

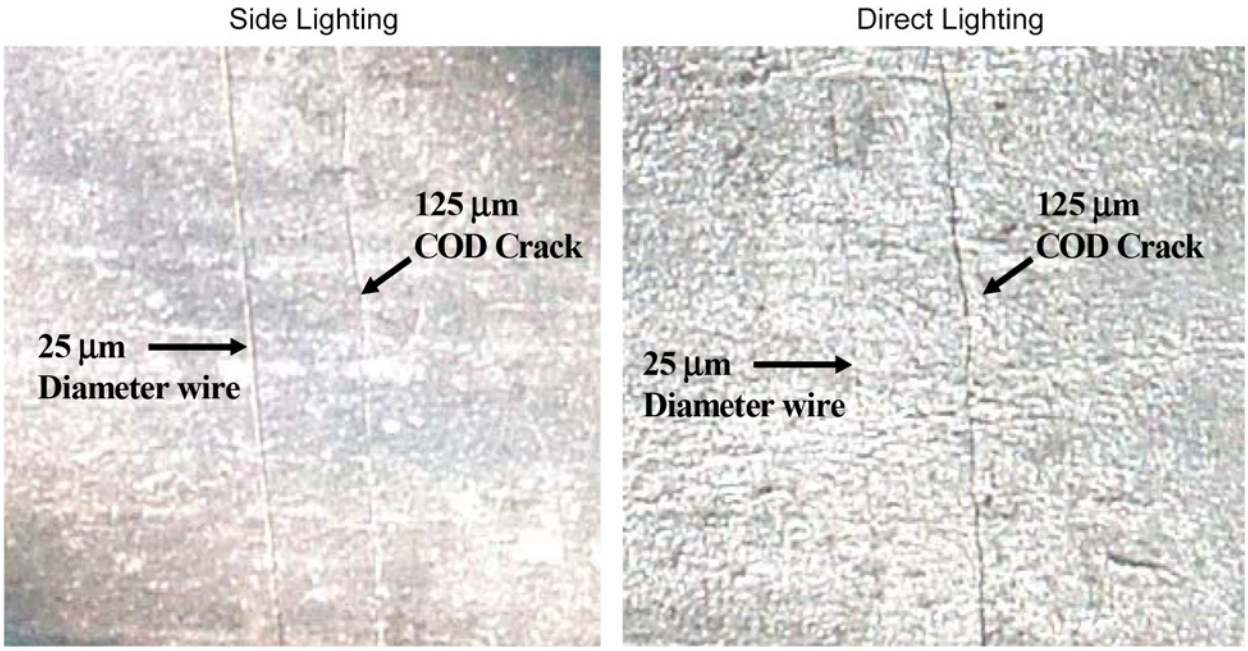

Figure 2.41. Photograph Illustrating Bright Field and Dark Field Imaging Effects by Applying Light Sources at an Angle to the Surface

- Viewing angles – It is noted in Cumblidge et al. (2007) that, although diffuse lighting conditions are ideal, practical application results in a mixture of diffuse and specular light reflection for surfaces. Whereas diffuse reflection essentially means that an equal amount of light scatters off a surface in all directions, specular reflection results in an angular dependence. To minimize the influence of viewing angle, it may be advisable to perform inspections at multiple angles.
- Recording devices – From the ongoing research activity between NRC, EPRI, and PNNL, it is known that there is a potential for degradation of the image in recorded video data compared to live video stream during remote visual examination. This degradation is related to the high compression ratios that attempt to reduce the size of the video files recorded.

2.2.1.4 Influencing Factors Associated with Specimen and Environment

- Crack opening displacement – Cumblidge et al. (2007, p. 7.1) concluded that COD had the largest impact on detection reliability. Some commercial inspection cameras are quoted as being able to detect features below 100 μm in size, although this specification is highly conditional (Cumblidge et al. 2007). A review of the available literature suggests that cracks with a COD greater than 100 μm are detectable under most conditions, while cracks with a COD less than 20 μm cannot be detected reliably except under the most favorable conditions (Cumblidge et al. 2007). The detectability of cracks with CODs between these limits is dependent on all of the influencing factors mentioned in Sections 2.2.1.3 and 2.2.1.4.
- Flaw orientation – Flaw orientation was not considered in the parametric study by Cumblidge et al. (2007). If the camera has a viewpoint directly above the surface (not at an angle) and diffuse light sources are used, then flaw orientation would not be expected to have a significant influence on detection capability. However, it has been noted that when paired spotlights are used for illumination, detection capability is much better when the spotlights are aligned parallel to crack orientation than when they are aligned perpendicular to crack (Cumblidge et al. 2007, p. 4.4).

- Access – Access to the canister can have significant influence on visual inspection results (if it is located in a difficult-to-access area, the camera may have to be placed at a large standoff and/or at oblique viewing angles). Figures 2.42 and 2.43 show photo-realistic renderings of views from a camera inserted into the front inlet ventilation port of an HSM Model 80 or 102 viewing toward the rear of the module, and for a camera inserted into the back inlet ventilation port viewing up at the canister near the rear of the HSM. Figure 2.42 indicates that attempting to view the rear of the canister from a front inlet requires significant standoff and an oblique viewing angle. In addition, canister support structures block the view of a significant portion of the canister surface and lighting intensity drops near the rear end of the canister. While standoff can potentially be compensated for with sufficient magnification and resolution, it is more difficult to mitigate the influences of oblique viewing angle, poor lighting intensity, and view obstructions. Figure 2.43 shows that by inserting a camera into the rear inlet vent, the rear portion of the canister can be viewed at angles closer to the normal of the surface and this placement of a camera results in less stand-off distance. Also, the lighting intensity appears more uniform in this image.

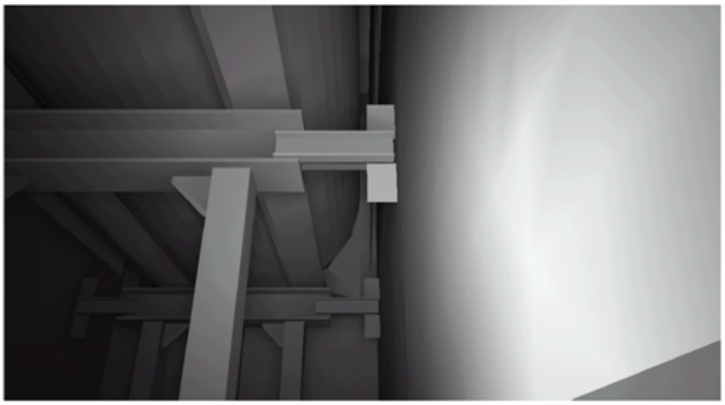

Figure 2.42. Photo-Realistic Rendering of View from Camera Inserted into Front Inlet Vent Viewing Toward Back of HSM

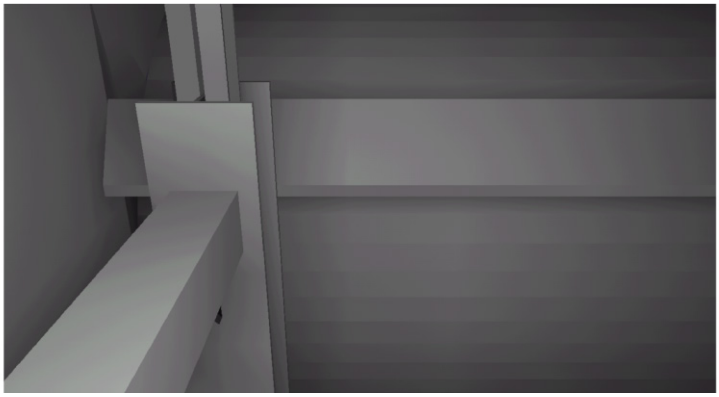

Figure 2.43. Photo-Realistic Rendering of View from Camera Inserted into Back Inlet Vent Viewing Up at the Canister in the Back End of the HSM

- Cleanliness – Cleaning may be required to remove material deposits that prohibit viewing of the surface to be inspected. Current ISI procedures in most reactor vessel internals inspection require a cleaning assessment to determine if the deposits and/or staining are expected to interfere with the ability to detect cracks, especially for components that are flaw intolerant.

- Surface conditions – Scratches, machine marks, weld crowns, etc. can interfere with or act to camouflage actual flaws by producing contrasts that look like real flaws, or produce shadowing that can obscure a flaw. Overall surface specularity can also influence inspection performance. In general, cracks are observed to have lower contrast on specimens that are highly specular versus specimens that are only somewhat specular (Cumblidge et al. 2007, pp. 4.13–4.14). Figure 2.44 shows photographs of approximately same size cracks (COD of 12 μm) on three different surfaces. Scratches, marks or other patterns can make flaw detection more difficult.

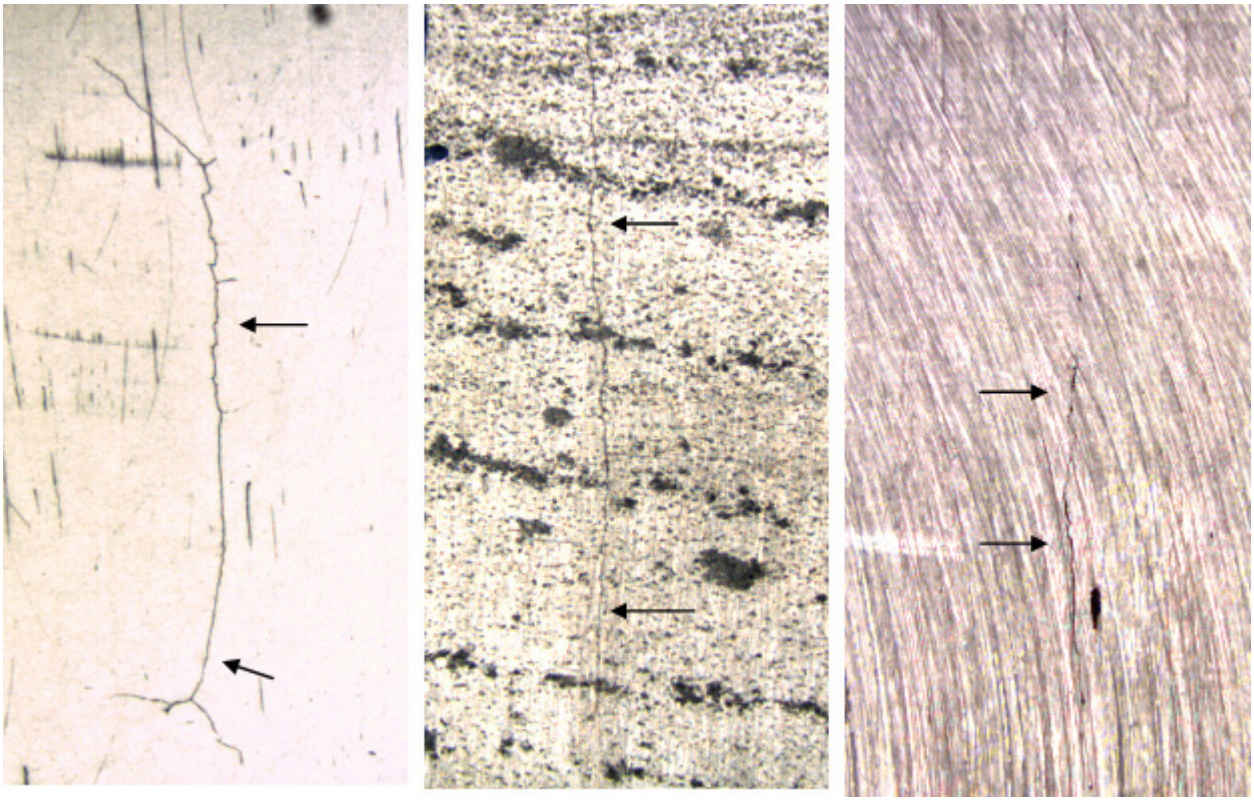

Figure 2.44. Photograph Illustrating the Influence of Surface Conditions on the Ability to Detect Cracks by Remote VT. All cracks are approximately 12 μm COD. From Cumblidge et al. (2007, Fig. 4.10).

2.2.1.5 Limitations

- Environmental compatibility – In the case of remote VT, a survey of specifications of several commercial cameras systems for radiation environments is included in Figure 2.36. Strategies may be employed to operate systems in environments that exceed specified limits for short duration and/or to replace equipment when failure occurs.

2.2.2 Bulk Ultrasonic Testing

Bulk ultrasonic testing refers to the techniques of injecting ultrasonic body waves into specimens for the detection of flaws or other imperfections by sensing the ultrasonic energy scattered by the flaws or imperfections. The scattered ultrasonic energy is converted to electrical signals, which can be immediately viewed or recorded for later analysis. Bulk ultrasonic waves may propagate in solid materials in either longitudinal (compressional) or shear-wave modes. Longitudinal waves are polarized such that the direction of displacement or pressure fluctuations are oriented along the direction of wave

propagation, while shear waves are polarized such that pressure fluctuations are perpendicular to the direction of wave propagation. Two different shear-wave polarizations are possible and defined in Figure 2.45 as shear (S-waves) and shear horizontal (SH-waves). SH-waves are a special type of S-waves in which the displacement vector is parallel to interfaces or boundaries. Figure 2.45 provides a schematic illustration of possible transmission and reflection scenarios when longitudinal or shear waves are incident on a solid-solid or solid-gas interface.

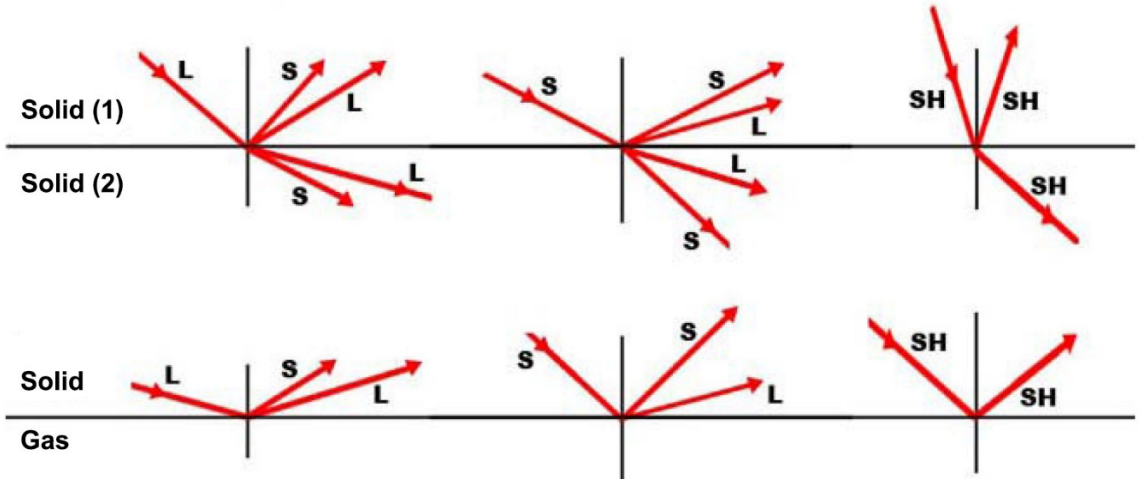

Figure 2.45. Schematic Illustration of the Multiple Types of Mode Conversions that Occur when Longitudinal (L), Shear (S), or Shear Horizontal (SH) Waves are Reflected from an Interface

Bulk waves interact with an interface between two mediums according to Snell's law and as a consequence, because the longitudinal wave velocity is greater than the shear-wave velocity, the longitudinal wave is refracted at a larger angle. Fundamental science and physics aspects related to ultrasonic wave sources, propagation, and scattering are covered in several textbooks including those by Ensminger and Bond (2011), Cheeke (2002), and Rose (1999). Several practical considerations related to ultrasonic examinations for materials characterization and NDE applications are provided in the American Society for Nondestructive Testing (ASNT) *Nondestructive Testing Handbook*, Volume 7 (ASNT 2007). An overview of several nondestructive examinations of welds using UT techniques is provided by Moran et al. (2010), and several ultrasonic crack sizing techniques for inner diameter (ID) surface-connected flaws are described in Davis (1998) and Cumblidge et al. (2010).

UT is typically performed by through-transmission (transducer on opposite sides of a component) or pulse-echo mode (a single transducer located on only one side). Pitch-catch mode (also referred to as dual mode or transmit-receive mode) employs two separate transducers located on a single side of a component for signal transmission and receiving. All three of these techniques are illustrated in Figure 2.46. The pitch-catch mode is commonly used for inspecting materials that are naturally noisy and is more commonly used for nuclear power plant (NPP) inspections than through-transmission mode. Materials can present natural sources of noise to a UT examination if the material is a heterogeneous mixture of regions with distinct acoustic properties. The boundaries between these regions represent a discontinuity in acoustic impedance that can result in reflections of the acoustic signal. Cast austenitic stainless steel (CASS) is an example of a material that can be challenging to inspect by UT techniques because fabrication processes of CASS lead to the formation of a macrostructure of uniform or randomly oriented grains with varying acoustic properties. The pulse-echo and pitch-catch modes are able to measure both the transit time and attenuation of signals; whereas, the through-transmission mode only allows measurement of signal attenuation. As a consequence, pulse-echo and pitch-catch modes can

provide more information about flaws including flaw location, length, and flaw depth. A further disadvantage of through-transmission techniques relative to pulse-echo and pitch-catch is that they require access to both the inside and outside component surfaces.

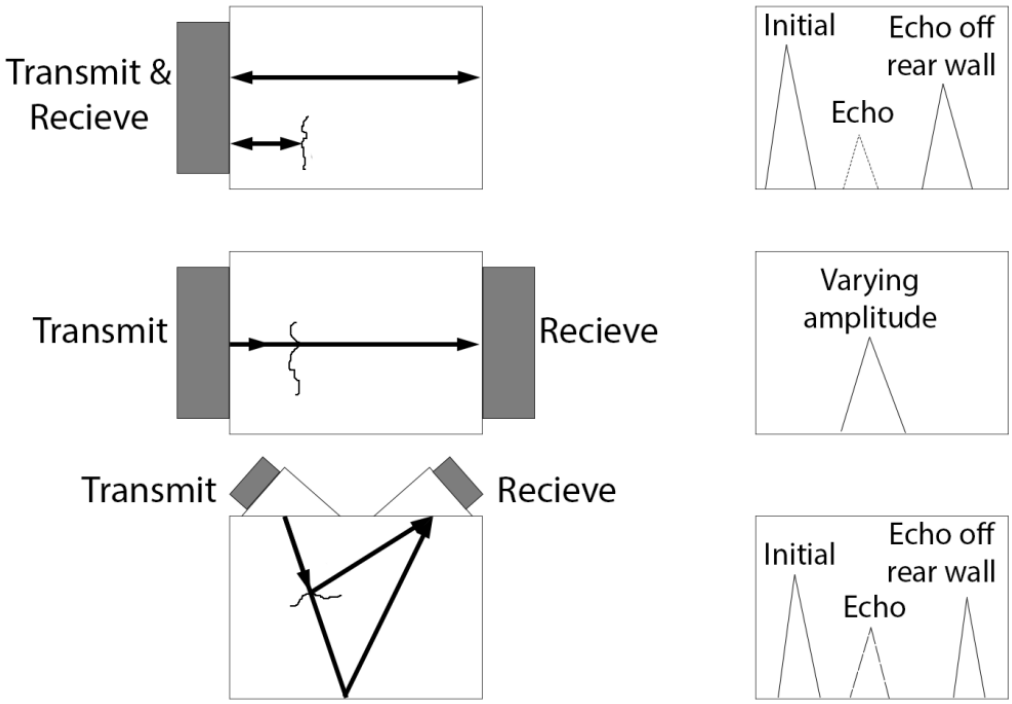

Figure 2.46. Typical Ultrasonic Testing Techniques: a) pulse-echo, b) through-transmission, and c) pitch-catch

2.2.2.1 Angle Beam Examinations

Ultrasonic inspections may be performed using transducers oriented normal to the surface of a component or at an angle. The latter scenario is typical for weld inspections where ultrasonic energy at appropriate angles is needed to ensure significant interaction of the beam with the planar crack face. Angle beam transducers are commonly fabricated to generate longitudinal or shear waves at 30°, 45°, and 60° in stainless steel material (ASNT 2007).

2.2.2.2 V-Path Examinations

In the nuclear power industry, service-induced flaws in Class 1 safety piping and vessels typically manifest as ID surface-connected cracks. Pulse-echo or pitch-catch mode inspections can be employed using angle beam transducers to detect and characterize back-surface-connected flaws using a half-V beam path as illustrated in Figure 2.47. For front-surface-connected flaws, these inspections may be conducted using a full-V beam as illustrated in Figure 2.48. A corner trap reflection is indicated in both figures, although the beam can return to the transducer upon reflection from the crack face. Detection of corner trap signals is often used to identify the base of a crack and aid in depth sizing.

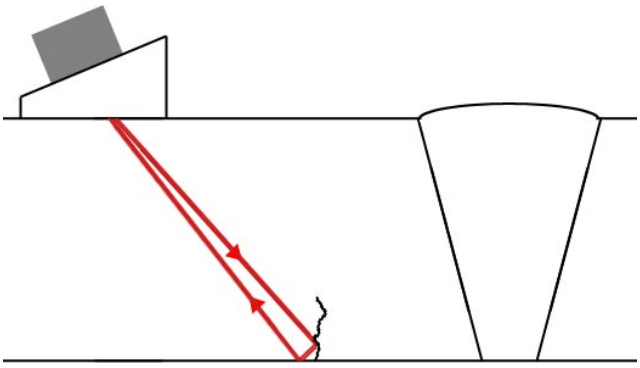

Figure 2.47. Illustration of Half-V Path Technique for Examination of Back Surfaces and Detection of Back-Surface-Connected Flaws

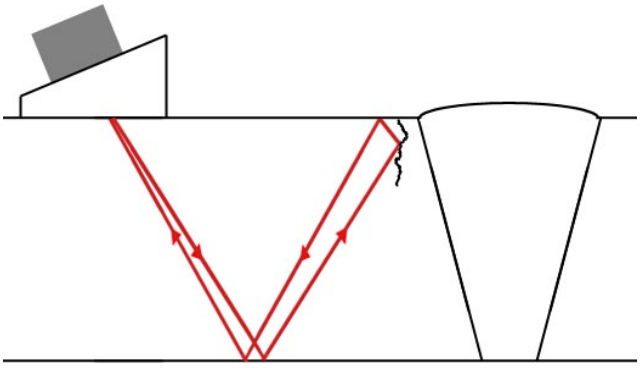

Figure 2.48. Illustration of Full-V Path Technique for Examination of Front Surfaces and Detection of Front-Surface-Connected Flaws

2.2.2.3 High-Angle L-Wave Mode Examinations

High-angle longitudinal mode (L-mode) examinations can be performed to detect and help characterize large back-surface-connected cracks (greater than 50 percent through wall) by sampling material located in the region near the front surface of the component under test (ASNT 2007). In practice, the technique is commonly employed using an L-wave refracted at 70° as illustrated in Figure 2.49 and Figure 2.50. This technique may be more effective at detecting and sizing flaws emanating from the same scanning surface (Figure 2.50) because material near the front surface is preferentially sampled.

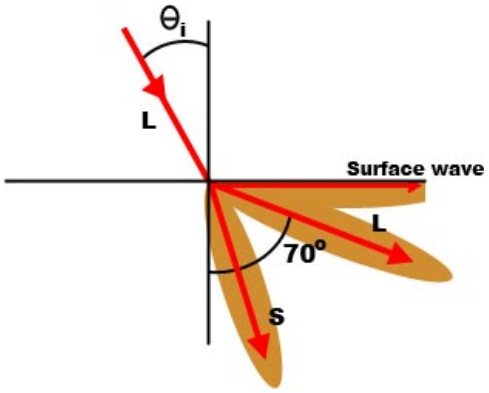

Figure 2.49. Vector Depiction of High-Angle (70 degrees) Longitudinal (L-mode) Refraction and Accompanying Side Lobe Surface Wave

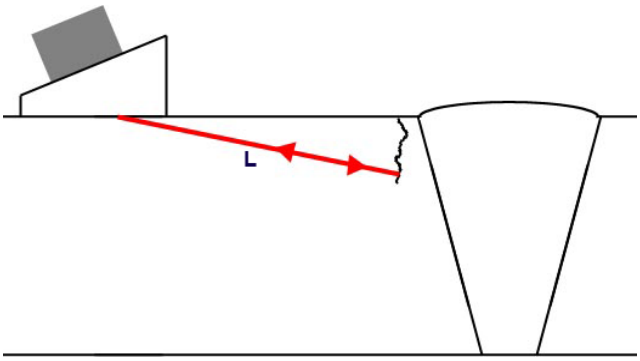

Figure 2.50. Illustration of High-Angle L-mode Examination Technique for Detection of Front-Surface-Connected Flaws

2.2.2.4 Tip-Diffracted Signals and Flaw Sizing

Sizing of flaws is based on amplitude drop methods, as depicted for length sizing in Figure 2.51, or detection of a tip-diffraction signal, with tip-diffraction techniques being the standards for depth sizing. Interaction of the incident sound beam energy on the face of a crack will impart an oscillation, or vibration, along this face. This vibration energy propagates along the face of the crack until it reaches the tip where the energy is re-emitted into the bulk material as a spherical wave front (see Figure 2.52). The re-emitted signal is referred to as the tip-diffracted signal and a portion of the signal travels back to the transducer, which may afford detection. An accurate technique for depth sizing of flaws involves measuring the relative time-of-arrival (TOA) of the corner-reflected signal from the base of a flaw and the tip-diffracted signal. The tip-diffracted signal is normally very weak compared to the corner-reflected signal and can be difficult to detect in practice, especially in highly attenuative materials. Crack branching can impact sizing accuracy as multiple crack tips may result in the emission of several tip-diffracted signals that are smaller in amplitude than if only one branch is present; this lowers the SNR of these diffracted signals making it more difficult to resolve the crack tip of interest (typically the deepest tip for use in structural integrity assessment) (see Figure 2.53).

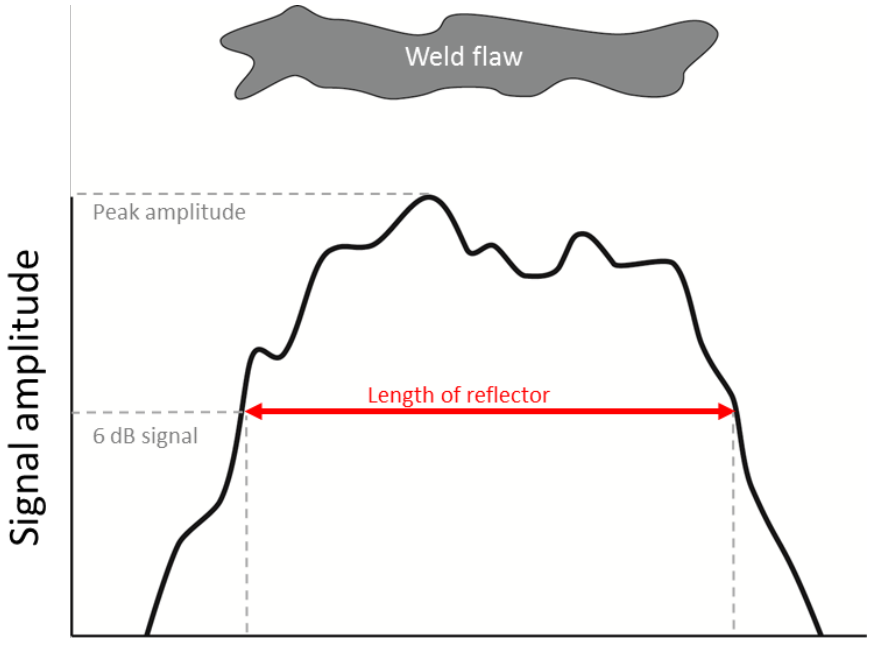

Figure 2.51. Illustration of Amplitude Drop Method for Flaw Sizing

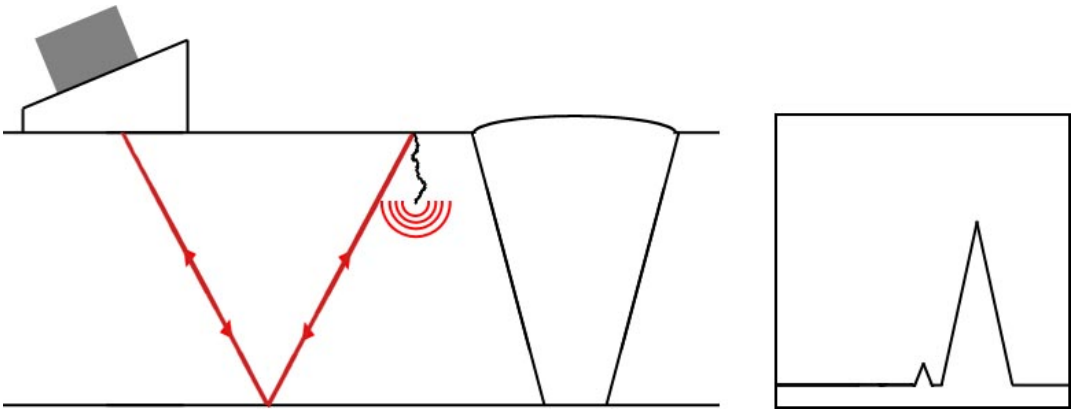

Figure 2.52. Illustration of the Excitation of a Tip-Diffracted Signal Because of Interaction of Incident Beam with Base of Crack

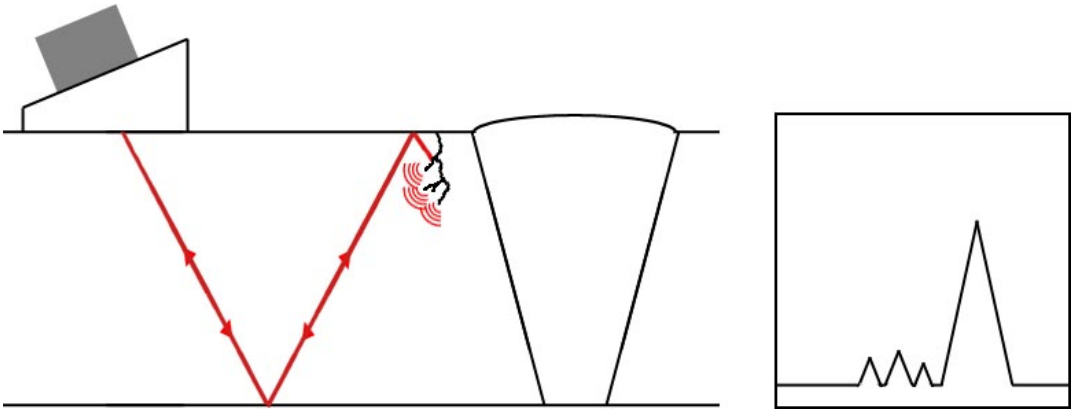

Figure 2.53. Illustration of How Multiple Tip-Diffracted Signals from Branching Cracks May Make It Increasingly Difficult to Resolve Crack Tip Signals of Interest

2.2.2.5 Time-of-Flight Diffraction Technique

The time-of-flight diffraction (TOFD) technique is a dual-probe method using one probe for transmitting and the other probe for receiving (Figure 2.54). The transmitter introduces a high-angle L-wave near the second critical angle, which induces a so-called "lateral wave" that propagates along the surface of the component between the pair of transducers. Additionally, a "creeping wave" is also developed that runs for a short distance along the opposite surface of the component being examined. With no flaws present, the receiver will pick up a back-wall echo and the transmitted lateral wave. The transit time information for the back-wall signal and lateral wave can enable crack detection and location. In the case of front-surface cracks, crack detection and location will be based on the lateral wave echo. Depth sizing may be accomplished by detection and transit time analysis of a tip-diffracted signal. The illustration in Figure 2.54 displays a TOFD response from a non-surface-breaking flaw. The TOFD response, in this case, includes the front wall and back-wall echoes as well as tip-diffraction signals from both ends of the flaw. Figure 2.54 illustrates this response in both A-scan (middle) and B-scan (bottom) views.

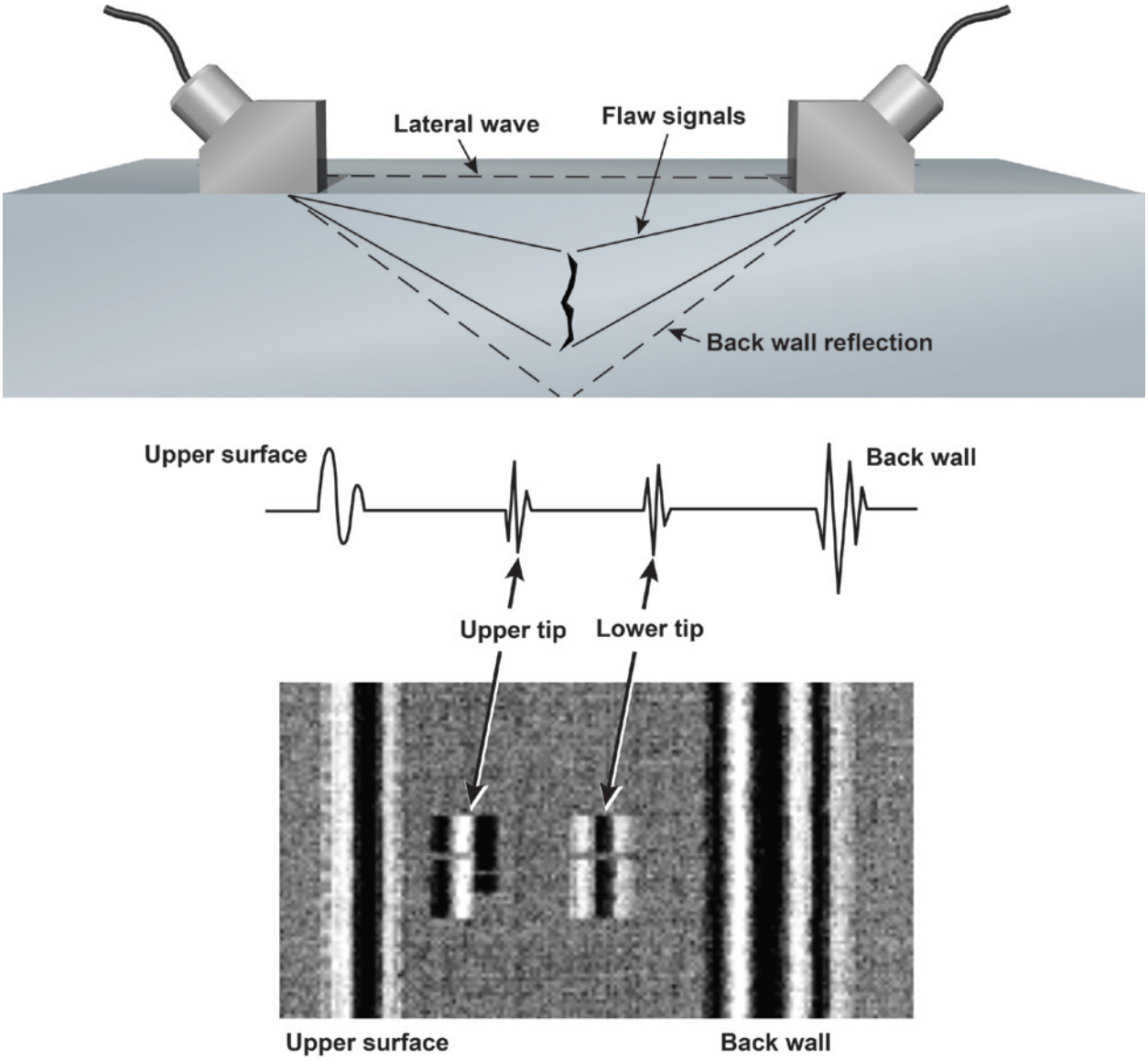

Figure 2.54. Diagram of Time-of-flight Diffraction Technique

2.2.2.6 Phased Ultrasonic Array Technique

Phased ultrasonic arrays rely on applying specific time delay sequences (known as delay laws) to an array of multiple piezoelectric elements to cause phase shifting of emitted sound fields and a pattern of constructive and deconstructive interference to produce electronically focused sound fields and to steer a beam as illustrated in the diagram of Figure 2.55. This can help minimize the impact of relative probe-flaw orientation as phased-array probes can rapidly sample a flaw from multiple angles. The multi-view scans can be combined with signal processing electronics to build up images of the flaw as depicted in Figure 2.56. The A-scan image in Figure 2.56 represents signal amplitude versus time for a single probe position. The B-scan image represents signal amplitude plotted versus time and linear position. Finally, the S-scan (sectorial scan) image in Figure 2.56 represents signal amplitude plotted as a function of time and refraction angle.

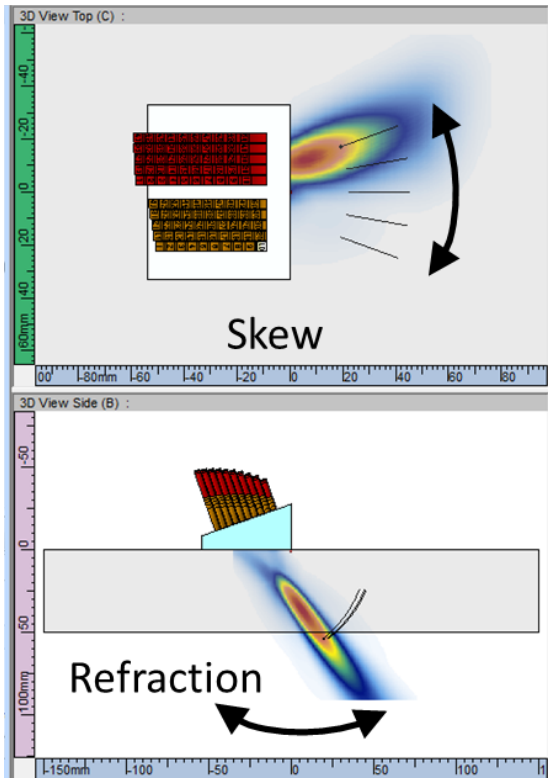

Figure 2.55. Illustration of Beam Skew and Beam Refraction Directions for Matrix PAUT Probe

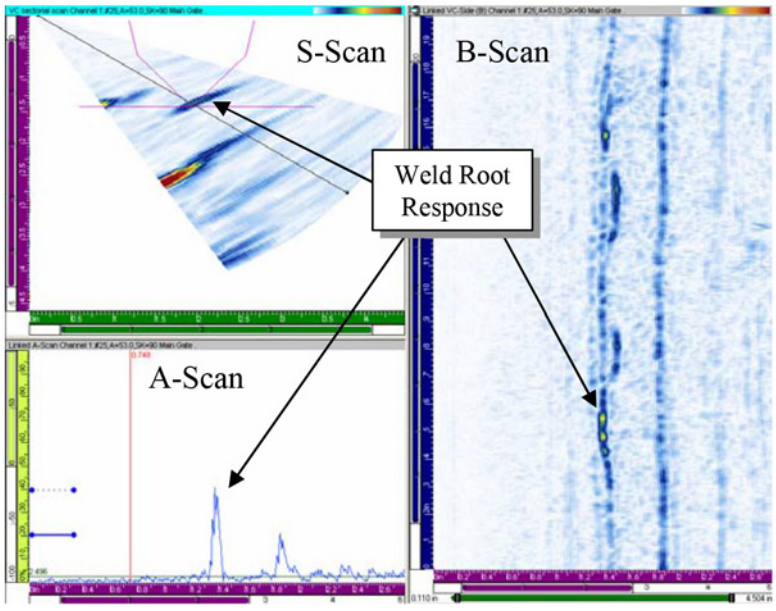

Figure 2.56. Diagram of Phased-Array Response Image Display (Anderson et al. 2007)

Array probes can have multiple configurations including linear, matrix, or annular element configurations. Phased-array probes are less compact than single-element transducers because they incorporate multiple sensing elements. A significant advantage of phased-array techniques over conventional techniques is that the ultrasonic beam may be steered electronically, enabling scanning at multiple angles and depths without physical adjustment of the transducer orientation or position. Further,

in PAUT, the energy can be focused at the desired region of inspection. With conventional UT sensors, the beam simply diverges in the far field with increasing distance from the transducer. As a result, PAUT can provide a better SNR in comparison to conventional UT. PAUT is often implemented using dual-mode transducers, which are also referred to as transmit-receive (TR) transducers. This transducer configuration employs separate transducers for transmitting and receiving signals, but the transducers are arranged such that they function together like a pulse-echo system. In TR transducers, the transmit and receive sensors are electrically and acoustically isolated (see Figure 2.57) resulting in improved SNR.

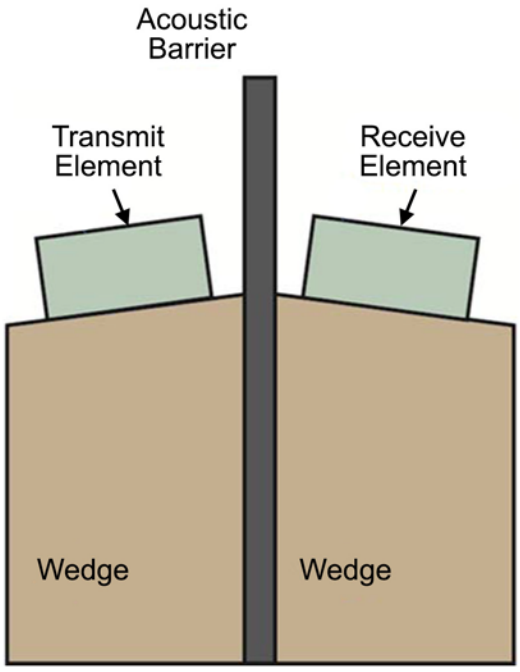

Figure 2.57. Illustration of a Transmit-Receive Probe

2.2.2.7 Instrumentation and Implementation

A typical UT system consists of transducer(s), a pulser, an amplifier, a receiver, couplant, and a device to record/display the signal. The pulser is an electronic device that can produce high-voltage electrical pulses. The transducer generates high-frequency ultrasonic energy in response to the electrical signal provided by the pulser. Typical frequencies used to inspect stainless steel and nickel-base alloy materials commonly used in nuclear vessel welds are generally between 0.5 and 2.25 MHz. The sound energy is introduced and propagates through the materials of interest. When there is a discontinuity (such as a crack) in the sound path, part of the energy will be reflected back from the flaw surface. The reflected wave signal is transformed into an electrical signal by the receiving transducer where it is input to a receiver and amplifier and displayed on a screen.

A photograph of single-element contact transducers that may be used for conventional UT or TOFD is provided in Figure 2.58. A pair of contact transducers mounted to acrylic wedges for high-angle beam TOFD inspection is shown in Figure 2.59. Finally, a photograph of TR transducer for performing PAUT inspections is provided in Figure 2.60. In this case, a transmit-receive shear-wave (TRS) probe is shown with operating frequency of 5.0 MHz.

A portable pulser/receiver unit is shown in Figure 2.61 for manual UT inspections. However, UT inspections may also be implemented with automated scanning and encoding to register responses with locations, as illustrated for the TOFD example in Figure 2.59. Further, considerably more complex electronics and signal processing are required for PAUT inspections. A photograph of typical data acquisition hardware with computer interface for PAUT inspections is provided in Figure 2.62.

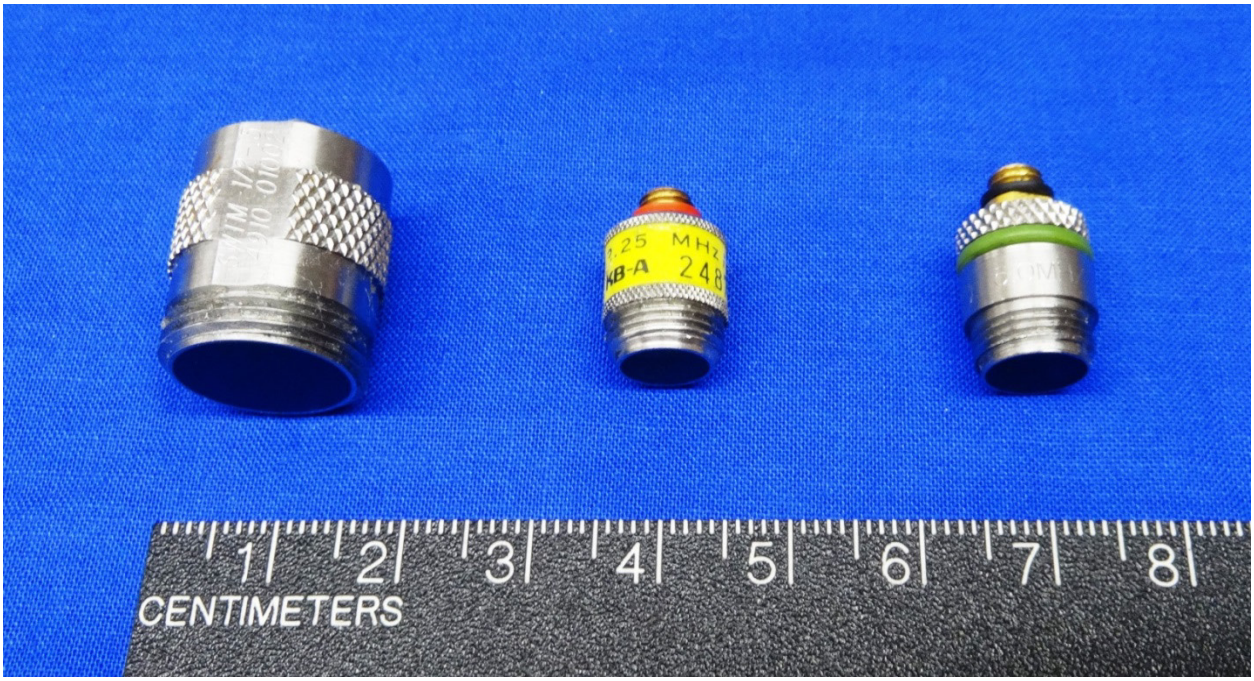

Figure 2.58. Photograph of Contact Ultrasonic Transducers for Performing Conventional UT or TOFD. The transducers have resonant frequencies of 500 kHz (left), 2.25 MHz (middle), and 5.0 MHz (right).

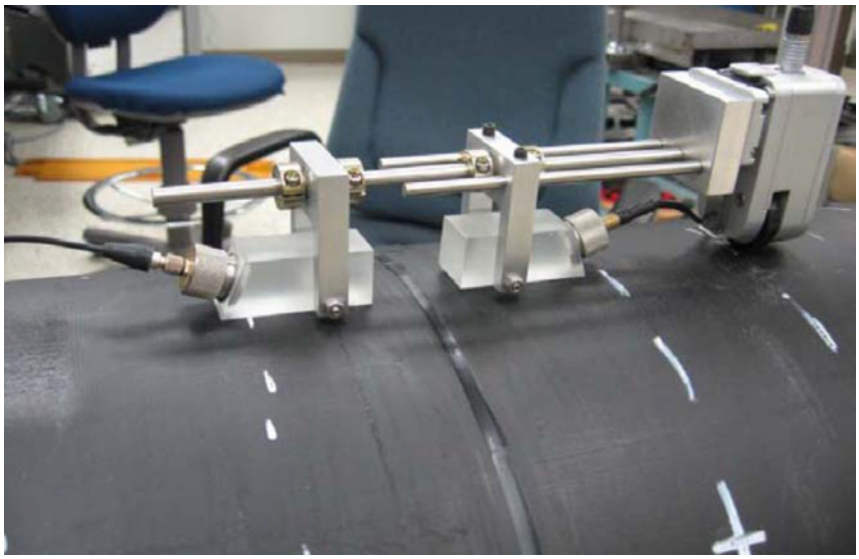

Figure 2.59. Pair of Contact Transducers Mounted to Acrylic Wedges for TOFD Inspection

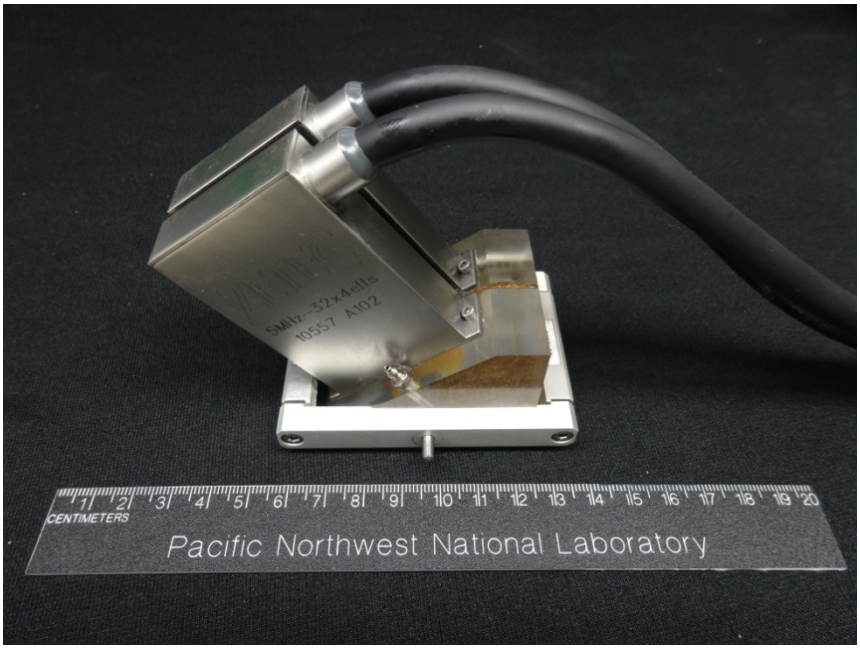

Figure 2.60. 5-MHz TRS Phased-Array Probe on Wedge Assembly

Figure 2.61. Photograph of a Portable Pulser/Receiver Unit for Manual UT Inspections.

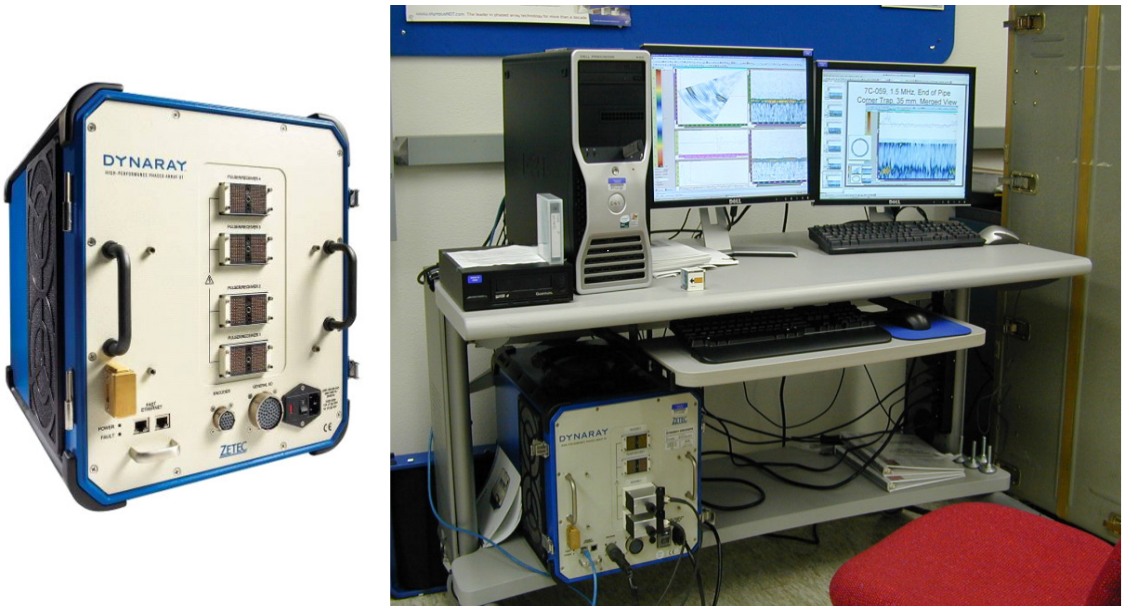

Figure 2.62. Photograph of Data Acquisition Hardware for PAUT and Integration with Computer Interface

2.2.2.8 Performance Estimations

The detection performance of NDE methods applied to metal components is often expressed in terms of probability of detection (POD), which expresses the POD as a function of a parameter, *a*, considered of consequence for the application. POD is often expressed as a function of flaw depth for nuclear components, but can also be expressed as a function of other flaw parameters such as flaw length and COD. An illustration of a POD curve is provided in Figure 2.63.

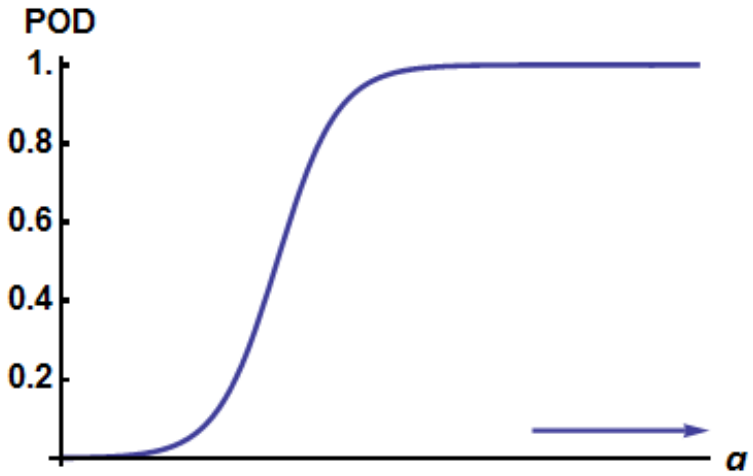

Figure 2.63. Illustration of POD Curve Used to Measure Performance of NDE Methods

Major reliability studies of bulk UT for inspection of wrought stainless steel components of nuclear power plants are documented in several NUREGs. Studies include the Piping Inspection Round Robin (PIRR) (Heasler and Doctor 1996), the Mini Round Robin (MRR) (Heasler et al. 1990), and the Programme for Inspection of Steel Components III Austenitic Stainless Steel Testing Study (PISC III AST). A comparison of the results for all three studies is included in NUREG/CR-6795 (Heasler and

Doctor 2003). In PIRR, test specimens were inspected that included 250 mm (10 in.) diameter Schedule 80 (1.51 cm [0.6 in.]) wall thickness and Schedule 80s (1.27 cm [0.5 in.]) wall thickness samples of rolled and welded 304 stainless steel pipe. In this report, the results from all three studies are combined to predict a POD of 90 percent for flaws that are 10 mm (0.4 in.) deep and a 70 percent POD for flaws that are 5 mm (0.2 in.) deep. This combined analysis included intergranular stress corrosion cracking (IGSCC), thermal fatigue, mechanical fatigue, and EDM notch defects. These studies focused on cracking that resulted from exposure of components to LWR environments; thus, the cracks were ID-connected (i.e., back-surface-connected from perspective of transducer).

Detection performances for more advanced techniques including PAUT and low-frequency synthetic aperture focusing technique were documented for a study evaluating the performances of these techniques for performing far-side inspections of welds (Anderson et al. 2011). The samples included specimens from 610 mm (24 in.) diameter wrought 304 stainless steel piping with 36 mm (1.4 in.) wall thickness and 711 mm (28 in.) diameter wrought 304 stainless steel piping with thickness ranging from 20–41 mm (0.8–1.6 in.). In this report, phased-array UT is described as having the best detection performance, and it is noted that better performance is observed for inspections performed using longitudinal modes versus shear modes. These studies also focused on cracks that were ID-connected (i.e., back-surface-connected from perspective of transducer).

Performance assessments of conventional UT, PAUT, and TOFD techniques continue under the Program for Assessing the Reliability of Emerging Nondestructive Techniques (PARENT) program. PARENT includes an international consortium of participants.[(a)]

2.2.2.9 Influencing Factors Associated with Instrument

- Frequency – Typical frequencies used to inspect stainless steel and nickel-base alloy materials commonly used in nuclear vessel welds are generally between 0.5 and 2.25 MHz (Moran et al. 2010). High-frequency transducers have shorter wavelengths, which increase the sensitivity and resolution, but experience greater attenuation. Lower-frequency transducers have longer wavelength and deeper penetration into the material, but less sensitivity and resolution.
- Ultrasonic wave modality and insonification angle – Ultrasonic inspections may be performed using transducers oriented normal to the surface of a component (normal incidence scan) or at an angle (angle beam scan). The normal incidence or 0-degree scan is typically not used for crack detection as usually there is some surface feature that does not allow for continuous contact and is usually oriented so that the crack face is parallel to the beam direction of normal incidence probes. The angle beam scan is typical for weld inspections aimed at detecting and characterizing service-induced cracks because they usually have a perpendicular orientation. If the cracks intersect the front surface, which is the case for atmospheric SCC, then bouncing sound or using a full-V technique is preferred. The fine-grain microstructures of parent and weld materials in wrought stainless steel components facilitate the use of shear waves. Shear waves ensure that minimum mode-converted signals will be produced during the skipping of sound off of the back surface (V-path techniques). Additionally, shear waves are more sensitive to potential flaws because of their shorter wavelengths (for the same frequency) than longitudinal waves (Moran et al. 2015).
- Couplant (contact of transducer) – In order to transmit ultrasonic energy efficiently into the specimen, the probe must be coupled to the stainless steel surface by means of a liquid (e.g., water) or gel or solid coupling interface.

(a) Meyer, R. M. and P. G. Heasler, "Results of Blind Testing for the Program to Assess the Reliability of Emerging Nondestructive Techniques," under preparation.

2.2.2.10 Influencing Factors Associated with Specimen and Environment

- Specimen (material - microstructure, surface roughness) – Because the DSCs are wrought stainless steel, then a higher frequency may be selected as there is less scatter and attenuation of the sound field by large grain boundaries and material heterogeneities. This enables the use of frequencies at the high end of the 0.5 and 2.25 MHz range mentioned in Section 2.2.2.9, and possibly higher. This is in contrast to cast stainless steels, which can exhibit an anisotropic microstructure and large grain boundaries to scatter the sound field. The effect of grain size on scattering can be minimized by selecting a frequency so that the wavelength is significantly larger than the grain size. The surface roughness and state of the weld crown (ground flush, smoothed, as-welded) also influence how well the transducer will stay coupled to the material and limit access to the inspection volume.
- Flaw characteristics – A review of flaw characteristics that can impact bulk UT detection and sizing of flaws is provided by Kemppainen and Virkkunen (2011). Flaw characteristics that can influence detection and sizing of flaws include flaw orientation, flaw size, flaw opening or width through depth, fracture surface roughness, and the presence of water or debris (e.g., corrosion products) inside of flaws. The influence of these flaw characteristics on detection and sizing of flaws with bulk UT is summarized in Table 2.7.
- Access – Environmental factors that influence ultrasonic inspection are component access to surfaces where transducers need to be placed and have enough space for scanning. Access to opposite side of the weld (or flaw) will determine what type of ultrasonic technique is needed. For instance, TOFD inspection requires access to both sides of the weld to complete the evaluation. Pulse-echo techniques require access to only one side of a weld. Access restrictions may also limit the extent to which equipment to facilitate automated scanning and encoding of inspection data may be implemented.

2.2.2.11 Limitations

- The compatibility of instrumentation with environmental stressors (notably, temperature and gamma and neutron radiation exposure) near the canister surface should be evaluated. The environment near the canister surface will be a function of the initial loading conditions and the time after loading at which the inspection is to be performed.
- The physical morphology of SCC flaws can influence how well they can be detected by UT techniques. Very tight cracks with significant portions of crack faces in contact can transmit a portion of the incident sound field, leaving less signal to be transmitted back to the transducer.

2.2.3 Guided Ultrasonic Wave Testing

Guided ultrasonic waves (GUW) involve the introduction of ultrasonic energy with wavelengths on the same order as the dimension of the component under inspection and observing the reflection of that energy from flaws or other discontinuities in the component. As a consequence, boundary conditions significantly influence the propagation of GUW energy, and the component under inspection may support the propagation of several modes. The mode formation is the result of constructive and destructive interferences resulting from the multiple reflections of energy off of component boundaries. Each of these modes experience dispersion that can result in significant variation of phase (Vp) and group velocity (Vg) with respect to frequency. Rigorous derivations for propagating GUW modes in several relevant geometries can be found in standard texts, including the text by Rose (1999).

Table 2.7. Summary of Effects of Flaw Characteristics on Detection and Sizing

Flaw Characteristic	Influence on Detection and Sizing
Flaw Orientation	Detection of flaws oriented normal to the surface through depth is detected primarily through specular reflection. As the tilt orientation of the flaw increases, detection becomes increasingly reliant on diffusely scattered signals (Kemppainen and Virkkunen 2011, p. 151). Flaw orientation with respect to welds is known to impact detection and sizing of flaws in some reactor components. However, this primarily relates to flaws located in welds. In this case, a sound field must propagate primarily through weld material to detect flaws oriented perpendicular to the weld. For flaws oriented parallel to welds, the sound field propagates mostly in base material.
Flaw Opening	Echo signals increase in amplitude with increased crack width and decrease as the crack closes. As flaw width increases, a point of saturation is reached where the echo signal amplitude is at maximum and no longer increases with width. Studies on mechanical fatigue cracks indicate that saturation occurs at 10 μm–20 μm (Kemppainen and Virkkunen 2011, pp. 146–147). Flaw opening can vary over a fracture surface and flaw opening can often be less near the ends and tips of a flaw. If the width is small enough, it may allow propagation of ultrasonic energy through the fracture surface where crack width is small. This can lead to flaw under sizing. Further crack tip diffraction signals are also influenced by crack opening, with smaller openings resulting in decreased tip diffraction signal amplitudes (Kemppainen and Virkkunen 2011, p. 151).
Fracture Surface Roughness	Increase in fracture surface roughness will reduce forward scatter and specular reflection of ultrasonic energy. More of the energy is spatially spread and diffusely scattered. Thus, specular signals are degraded while diffuse signals are enhanced relative to a smooth flaw (Kemppainen and Virkkunen 2011, pp. 145–146). Flaw sizing based on amplitude drop methods and detection of tip diffraction signals is adversely affected by increasing surface roughness. Surface roughness results in significant variability of the amplitude response along the flaw dimension making it difficult to identify edges. Further, diffusely scattered fields can mask or interfere with tip diffracted signals (Kemppainen and Virkkunen 2011, pp. 145–146).
Flaws Filled with Water or Debris	The presence of water in flaws increases the transparency of flaws to ultrasonic energy and adversely impacts detection and sizing. The effect of the presence of debris or oxides can be similar; however, debris and oxide particles can also prevent a crack from closing and trap air between crack faces (Kemppainen and Virkkunen 2011, p. 152).
Flaw Size	The effect of flaw size is not considered in Kemppainen and Virkkunen (2011). However, it is well known that a larger area of crack face will reflect more ultrasonic energy and provide a more likely target for detection.
Flaw Branching	The effect of flaw branching is also not considered in Kemppainen and Virkkunen (2011). However, it is known that branching leads to multiple crack tips, which can complicate sizing and identification of the crack tip associated with the deepest portion of the flaw. Further, branches may exhibit tilt and fracture surface roughness.

The interaction with material boundaries has significant consequences when contrasted with bulk waves, in a couple of respects. First, with bulk wave testing, only two modes (longitudinal and shear) are excitable; whereas, for GUW, an infinite number of modes are excitable. Second, bulk wave modes are dispersion-less, which means the mode velocity is independent of frequency. In contrast, most GUW modes experience dispersion. The types of GUW modes excited will depend on the frequency-thickness product for the component under test and the component geometry where thickness refers to the thickness of the component under test and frequency is the frequency of the propagating GUW signal. For thicker

planar geometries, Lamb waves and SH waves can be generated. SH wave modes are distinguished by a displacement vector that is parallel to the component surface and perpendicular to the direction of propagation, as depicted in Figure 2.64. Lamb waves often refer to modes with displacement vectors that are within the plane defined by the direction of wave propagation and plate thickness (see Figure 2.65).

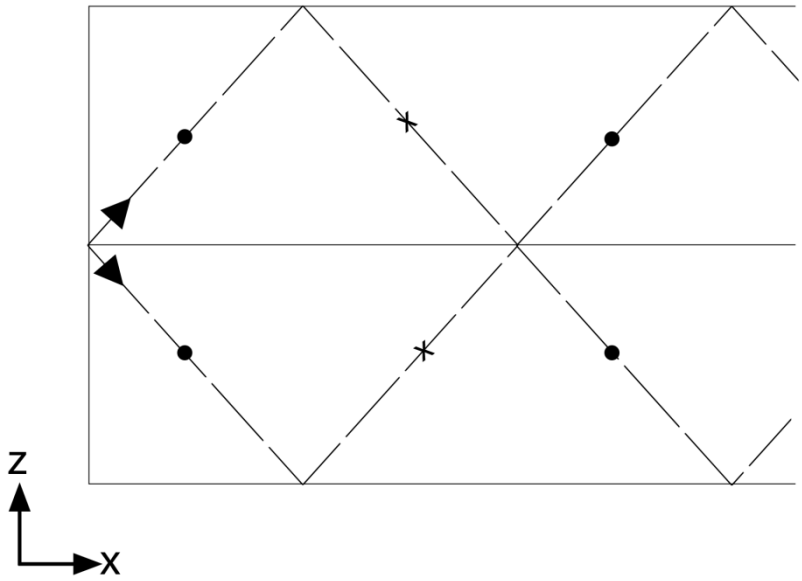

Figure 2.64. Vector Representation of SH Wave Propagation Along the x-direction of a Planar Component in the Sagittal Plane

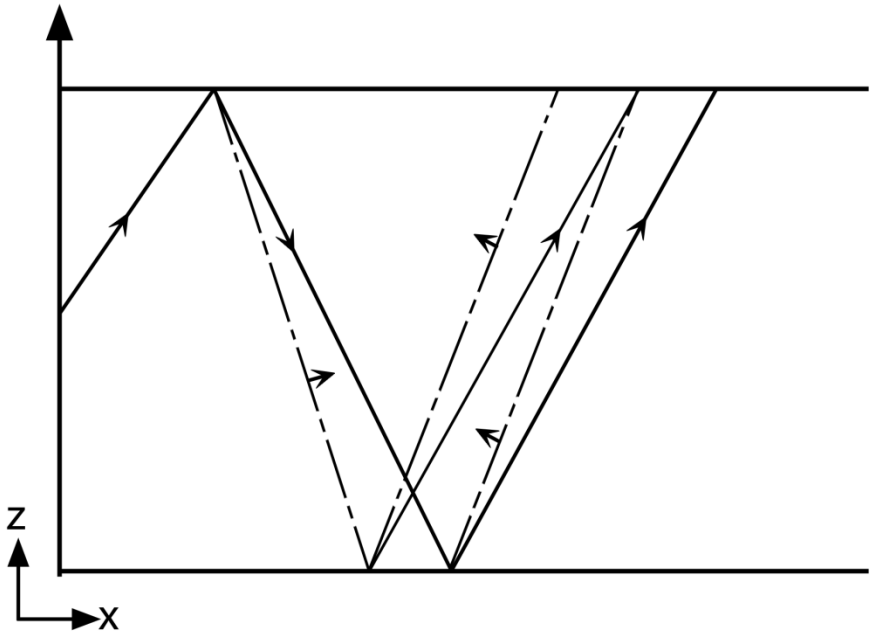

Figure 2.65. Vector Representation of Lamb Wave Propagation Along the x-direction of a Planar Component

The potential to simultaneously excite multiple modes that experience dispersion can create interference and complicate signal interpretation. An analysis of dispersion relationships is usually conducted in the design of GUW systems and before testing to identify frequency ranges and configurations that will minimize the excitation of undesirable modes. Examples of dispersion relationships for the phase velocity of Lamb waves and SH waves in 12.7 mm (0.5 in.) thick planar components are provided in Figure 2.66 and Figure 2.67, respectively. Figure 2.66 shows that a minimum of two modes (A0 and S0) will be excited when testing with Lamb waves and that all of the modes experience dispersion over the depicted frequency range, although to varying extent. The A0 and S0 modes refer to the fundamental antisymmetric and symmetric modes, respectively. The graphics in Figure 2.68 illustrate the nature of symmetric and antisymmetric wave modes in a planar component as the antisymmetric wave modes exhibit asymmetry in the displacement with respect to the mid-plane, while symmetric wave modes exhibit symmetry in the displacement with respect to the mid-plane. Figure 2.67 shows that at lower frequencies, it is possible to excite just the fundamental SH mode (SH0) and that this mode exhibits dispersion-less behavior. Lamb waves may include a displacement vector that is out-of-plane, thus, experiencing greater attenuation as a function of propagation distance than SH wave modes. As guided wave modes can only form after several interactions with component boundaries, a near-field, or dead-zone, exists near GUW transducers. Thus, transducer placement must be such that the targeted region of inspection is located beyond the near-field, which is typically on the order of several inches. The plots in Figure 2.66 and Figure 2.67 are generated for a plate that is 12.7 mm (0.5 in.) thick; however, curves can be translated to other thicknesses by considering the horizontal axis to represent the frequency-thickness (MHz-inches) product by multiplying the frequency values by the ratio of the current assumed plate thickness (12.7 mm) to the new plate thickness.

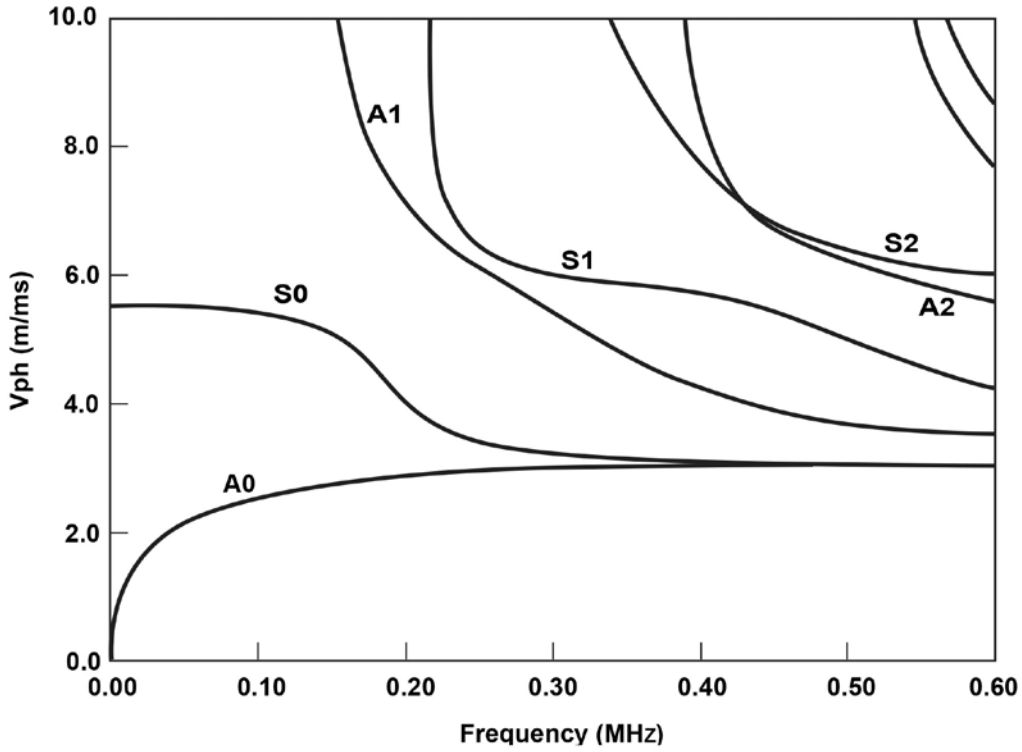

Figure 2.66. Dispersion Relationships for the Phase Velocity (Vp) of Lamb Waves Excited in a 12.7 mm (0.5 in.) Planar Steel Component

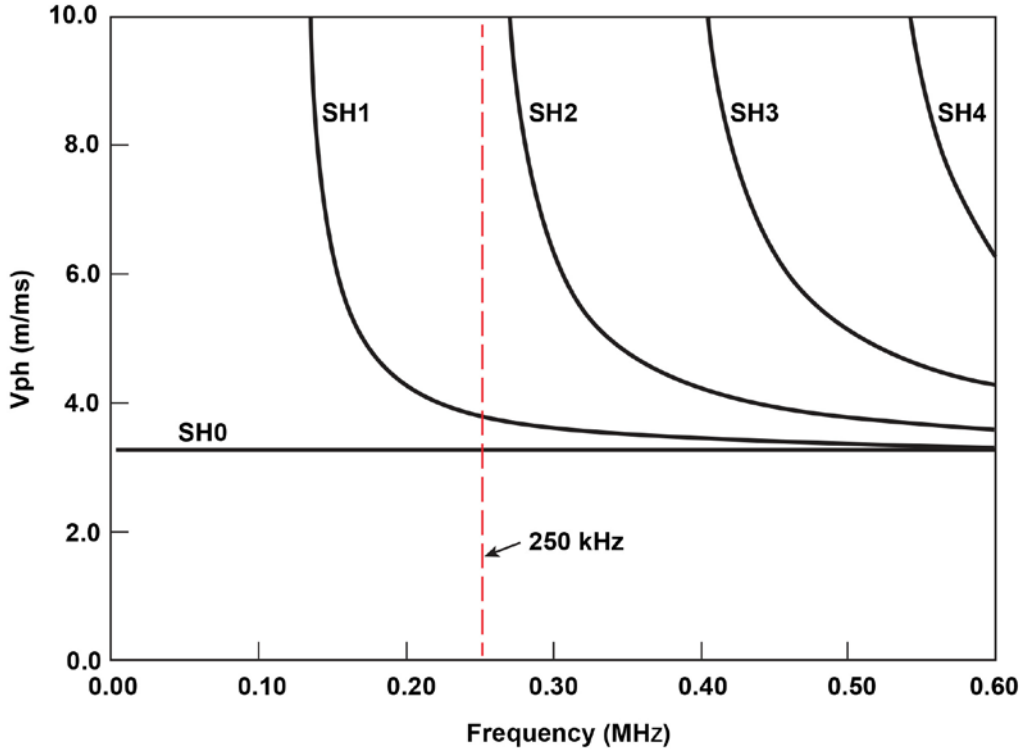

Figure 2.67. Dispersion Relationships Calculated for the Phase Velocity (Vp) of the Several SH Modes (SH0 to SH4) in a 12.7 mm (0.5 in.) Planar Steel Component

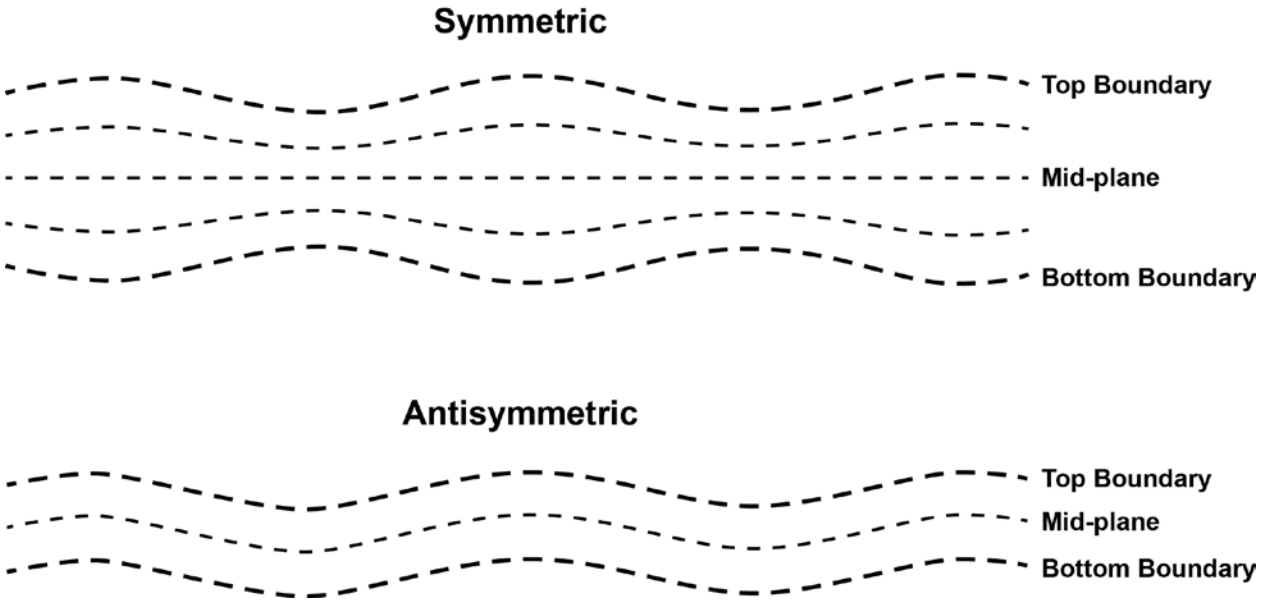

Figure 2.68. Depiction of Antisymmetric and Symmetric Modes in Planar Components. The figure indicates that symmetric wave modes exhibit symmetry in displacement about the component mid-plane while asymmetric modes exhibit asymmetry about the mid-plane.

The same types of transducers used for other types of UT can be used for GUW, including transducers made from piezoelectric or piezo-composite materials. In addition, guided waves may be generated using electromagnetic acoustic transducers (EMATs) or magnetostrictive sensors (MsSs). With EMATs, GUW

detection and generation is facilitated by the Lorentz force mechanism. The EMAT transducer and receiver both consist of a permanent magnet or electromagnet and a coil. The transmitter induces eddy currents in the test component through radio-frequency excitation. The induced eddy currents interact with the magnetic field from the coil to produce a Lorentz force and generate guided waves. Detection is achieved through the reverse process. EMATs are contactless transducers, making them relatively insensitive to surface conditions, and can be applied through thin coatings of insulating material. EMATs preferentially generate SH modes. The MsS sensing mechanism is based on the force in ferromagnetic materials generated by strains associated with the motion of magnetic domains (Kittel 1949). The technique may be contactless for the inspection of ferromagnetic materials and can be applied to the inspection of other materials with the aid of an intermediate strip of ferromagnetic material in direct contact with the test component to convert magnetic domain motion to elastic wave motion.

Guided wave equipment can be deployed as either a pulse-echo technique using a single transducer or as a pitch-catch technique using one exciting and one detecting transducer.

2.2.3.1 Instrumentation and Implementation

At present, commercial GUW systems for inspection of canisters do not exist. However, efforts in this respect are being pursued by EPRI and through a U.S. DOE Integrated Research Project (IRP) that is led by Penn State. Both efforts are engaging Structural Integrity Associates, Inc. (SIAI) to develop a short-range guided wave inspection technology based on horizontally polarized shear waves (SH0 and SH1 modes) excited using EMATs and operating at 250 kHz (see Figure 2.69).[(a)] A photograph of a transmit-receive pair of EMATs on a stainless steel plate is provided in Figure 2.69(A) (Van Velsor et al. 2014).

Received signals are input to an amplifier and typically fed to a digital oscilloscope or other digital recording device. One method for displaying GUW data is the B-scan, which is a contour plot of signal amplitude with respect to scan direction and time. Strong reflections can be observed in the B-scan and located by relating time to position through the signal velocity. A B-scan image showing the reflection from a notch in a stainless steel plate using the EMAT sensors described above is shown in Figure 2.69(C) (Van Velsor et al. 2014).

2.2.3.2 Performance Estimations

The performance of EMAT systems under development have not yet been thoroughly evaluated. However, the detection sensitivity may be estimated based on other work with GUW testing. These efforts indicate that flaws smaller than 5 percent of the sound field cross section are generally not detectable. According to finite element models, the wavelength has a significant impact on the detection limit as well, such that surface notches less than 1/40 the depth of the wavelength are theoretically undetectable (Alleyne and Cawley 1992).

2.2.3.3 Influencing Factors Associated with Instrument

- Frequency or wavelength – The frequency (or wavelength) determine the location on dispersion curves (Figure 2.66 and Figure 2.67) for operation and, thus, determine which modes may be excited for a plate of given thickness. Generally, a higher frequency (shorter wavelength) will result in excitation of a larger number of modes, which complicates signal interpretation as multiple modes can interfere with each other. According to finite element models, the wavelength has a significant impact on the detection limit as well, such that surface notches less than 1/40 the depth of the wavelength are theoretically undetectable (Alleyne and Cawley 1992).

(a) MS Lindsay, Structural Integrity Associates, Inc. (SIAI), private communications, January 2016.

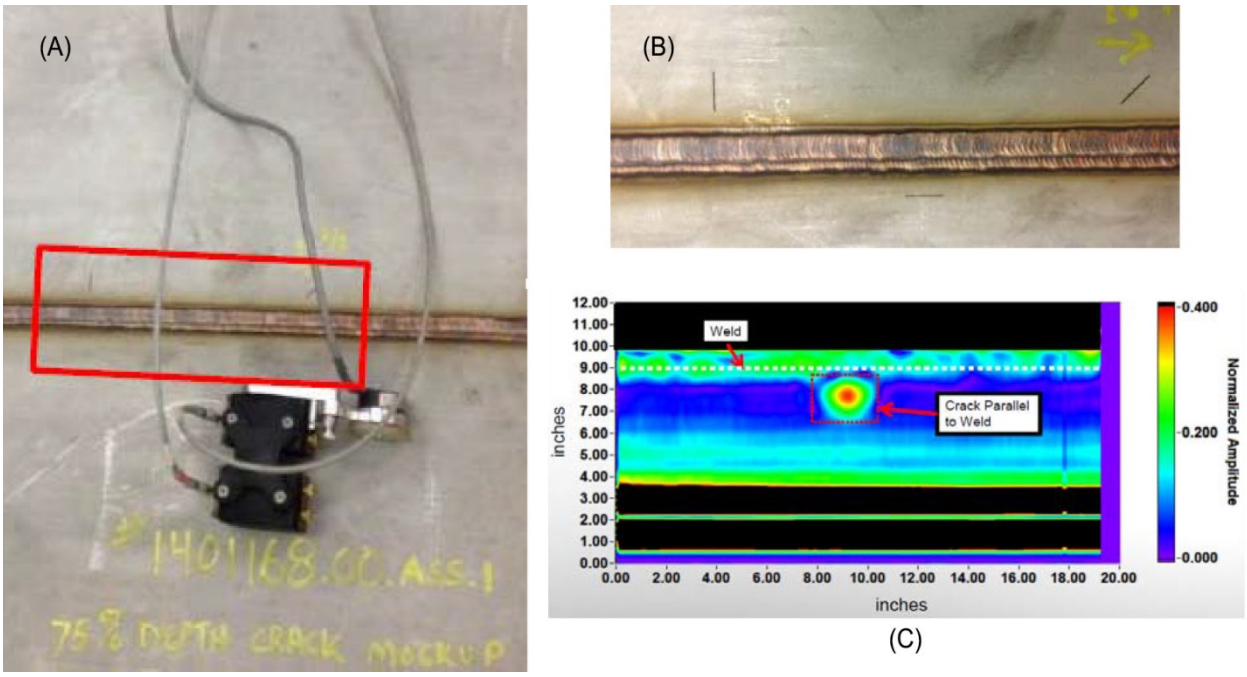

Figure 2.69. Photo of (A) EMAT Transducers on Mock-up Plate and (B) Close-up of Notches Used to Simulate Cracks in the Weld Heat-Affected Zone (HAZ). A B-scan Plot of the Signals Received (C) Illustrates the Ability of the System to Detect the Simulated Defect (Van Velsor et al. 2014). Reprinted with permission of the Electric Power Research Institute and Structural Integrity Associates, Inc.

- Mode types – Generally, GUW inspection of thick plates can be performed via Lamb wave excitation or the excitation of SH waves, which are less sensitive to crack orientation because the displacement vector is perpendicular to the plane of the wave vector and plate thickness. Therefore, significant interactions with cracks oriented parallel or perpendicular to the wave vector are anticipated. With Lamb waves, the displacement vector is in the same plane as the wave vector and the plate thickness; thus, limited sensitive to cracks that are parallel to the wave vector is anticipated.[(a)] Generally, SH waves may be generated with EMATs or MsSs whereas Lamb waves are often generated with piezoelectric or piezocomposite transducers.
- Transducer type – As mentioned, the type of transducer can dictate the type of modes that get excited within a test structure. However, there are further impacts. For instance, EMATs do not require the use of couplant and are considered contactless. They are relatively insensitive to surface conditions and can be used to obtain measurements through thin surface coatings; however, they are less efficient that piezoelectric or piezocomposite materials resulting in a lower SNR. MsS transducers also do not require use of couplant but require intimate contact of a ferromagnetic strip with the test structure.

2.2.3.4 Influencing Factors Associated with Specimen and Environment

- Thickness – The canister thickness will influence mode excitation considering the dispersion curves in Figure 2.66 and Figure 2.67. The plots in Figure 2.66 and Figure 2.67 are generated for a plate that is 12.7 mm (0.5 in.) thick; however, curves can be translated to other thicknesses by considering the horizontal axis to represent the frequency-thickness (MHz-inches) product by multiplying the

(a) C. Lissenden, Penn State University, private communications, January 2016.

frequency values by the plate thickness (12.7 mm). If, instead, the thickness is 25 mm (1 in.) then the frequencies on the horizontal axis of Figure 2.66 and Figure 2.67 would halve and 250 kHz would become 125 kHz.

- Welds or other features – Welds or other features can interfere with reflections from flaws, especially if flaws are located near these sources of reflections. This is partially illustrated in Figure 2.69(C) where the reflection from the weld is clearly visible.
- Space constraints – Space constraints can also influence the performance of GUW testing. For EMAT transducers, for instance, transducer size increases with decrease in desired operating frequency and increase in desired magnetic field strength.
- Surface deposits or texture – Surface roughness due either to deposits or surface texture can degrade SNR and performance.

2.2.3.5 Other Limitations

- The compatibility of instrumentation with environmental stressors (notably, temperature and gamma and neutron radiation exposure) near the canister surface should be evaluated. The environment near the canister surface will be a function of the initial loading conditions and the time after loading at which the inspection is to be performed.

2.2.4 Eddy Current Testing

In practice, an eddy current probe consists of one or more coils with the axis alignment perpendicular to the inspection surface normal. An alternating current source is applied to the one or more coils, generating magnetic fields. These magnetic fields induce eddy currents in the conducting materials when the probe is positioned nearby (see Figure 2.70). Flaws and defects in the test material impede the flow of eddy currents manifesting as a change in the measurable eddy current coil impedance. The depth of penetration of an induced eddy current field is not uniformly distributed throughout the test material but is most dense near the surface and decreases in magnitude with distance from the surface (Hagemaier 1990). The effective zone for flaw detection of the eddy current field is defined by the value of the standard depth of penetration, or the skin depth,

$$\delta = \sqrt{\frac{1}{\pi \, \mathrm{f} \, \sigma \, \mu}} \tag{2.14}$$

which provides a measure of the depth to which eddy current fields can penetrate in a test material. This is the distance down from the surface of the material where the eddy current energy density has decreased by 37%. As can be seen from Eq. (2.14) this quantity depends on the coil frequency, f, and electrical conductivity, σ, of the test material (μ is the magnetic permeability). Electrical conductivity, σ, describes the ability of a material to conduct electric current. As the conductivity of a material increases, the resistance to the flow of eddy currents in the material decreases. Magnetic permeability, μ, is the ability of a material to concentrate magnetic lines or, in other words, the ease with which a material can be magnetized. Nonferrous metals such as brass, aluminum, copper, and austenitic stainless steels have essentially the same numeric relative permeability as that of a vacuum or air; that being 1. The skin depth up to frequencies of 10 MHz may be observed in Figure 2.71 for several materials, including 304 stainless steel. From 100 kHz to 500 kHz, the value of the skin depth is approximately 1 mm to 3 mm (0.04 in. to 0.12 in.). Due to the limited depth of penetration, ECT is primarily limited to surface examinations and is classified as a surface examination technique in article IWA-2000 of the ASME B&PV Code, in Division 1, Section XI, which includes rules for the ISI of LWRs.

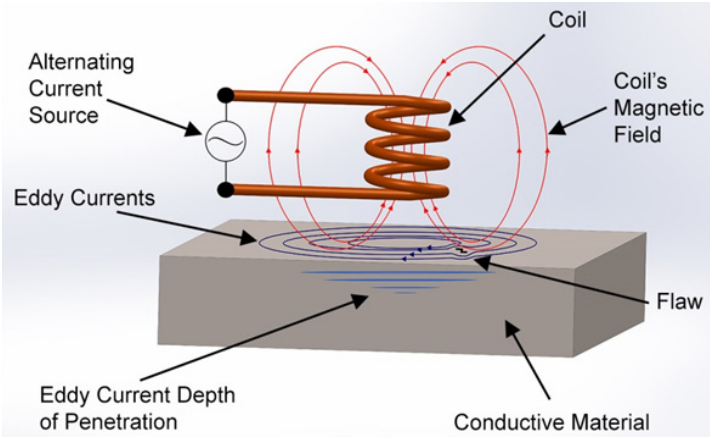

Figure 2.70. Depiction of a Single Coil Eddy Current Probe with an Alternating Current Excitation, Induced Magnetic Fields, and Induced Eddy Currents and Disturbance of Eddy Current Flow Caused by Existence of a Defect

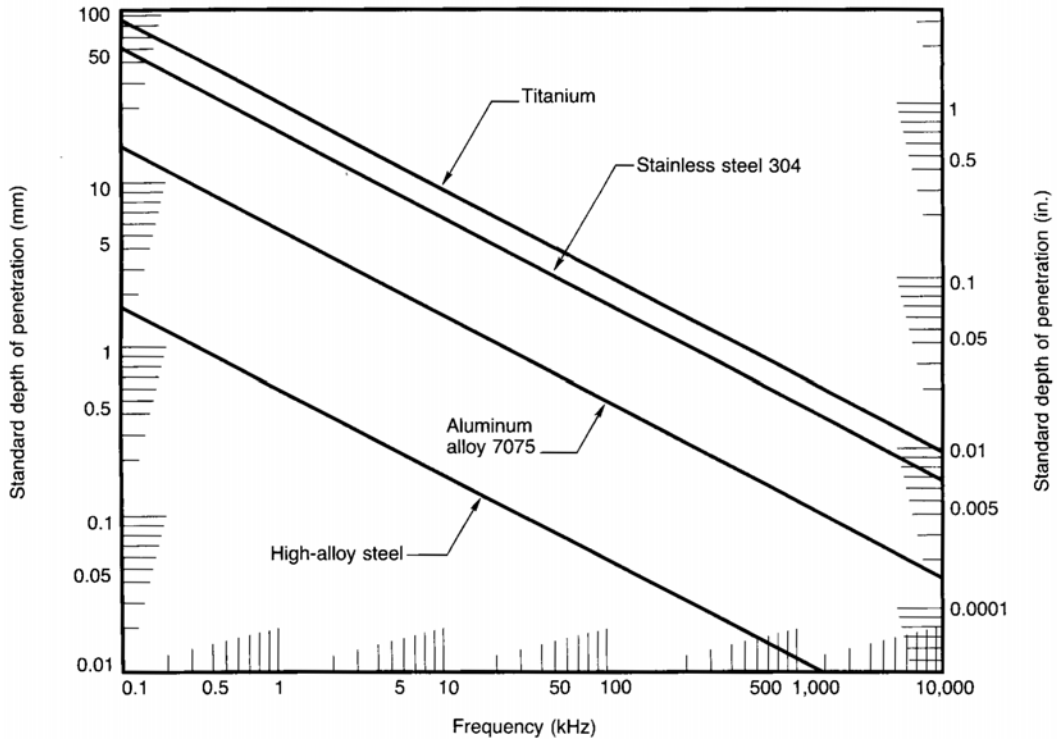

Figure 2.71. Eddy Current Testing Standard Depth of Penetration for Assorted Materials of Varying Conductivity as a Function of Frequency (from Hagemaier 1990)

The eddy current response manifests as an electrical impedance signal,

$$Z = R + jX, \tag{2.15}$$

where R is resistance and X is reactance of the coil. The response can be plotted in the impedance plane (see Figure 2.72) where R and X are horizontal and vertical axes, respectively. Figure 2.72 indicates that as the coil is brought from air to the surface of non-magnetic materials, such as stainless steel, R increases and X decreases. When the coil is so far away from the surface that none of the magnetic flux lines

intersect the test material surface, the coil will exhibit its empty coil reactance. As the coil is brought closer to the material surface, the coil's magnetic flux lines begin to penetrate into the surface of the test specimen, generating eddy currents in the test specimen which result in an a canceling magnetic flux that reduces the overall coil reactance. The reactance will continue to decrease as more of the flux lines intersect the surface of the material until the coil is in contact with the surface. The resistance increases because the potential difference applied to the coil must be used to drive the current in the coil and the eddy currents in the adjacent test material. The presence of a crack will interrupt eddy currents in the material, resulting in a decrease in R and increase in X.

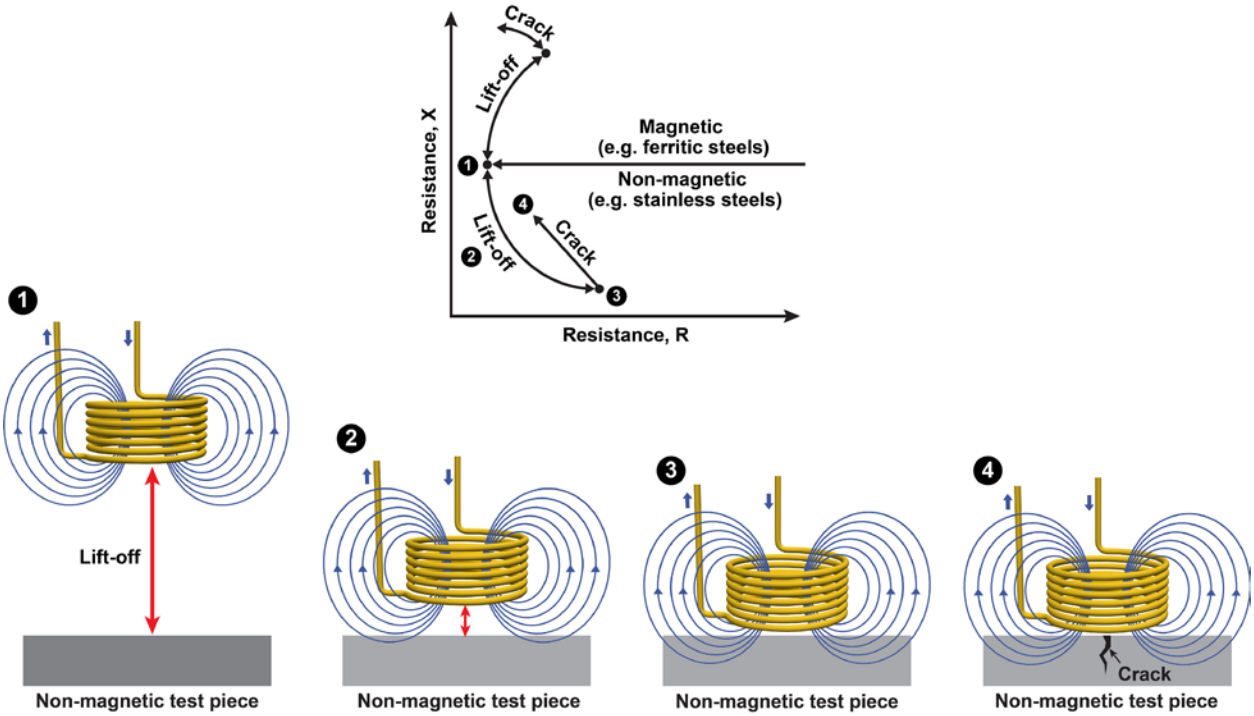

Figure 2.72. Illustration of the Effect of Lift-off and Crack-like Defects on Eddy Current Responses in the Impedance Plane

The probe in Figure 2.70 represents an absolute eddy current probe in which one sensing coil is employed. Another common configuration is known as the differential probe, which consists of two coils that are sensing two different (but closely spaced) regions of the test specimen (see Figure 2.73). The two coils are connected so that their signals cancel when there are no defects or impedance anomalies in the material. When defects or other impedance anomalies are encountered, an unbalance occurs. When the defect is crack-like, a scan of the differential probe over the crack produces a Lissajous figure (figure-8 shape).

Multi-coil probes can also include separate coils for the generation of eddy current fields in the test material and for detection of the fields at the surface, as illustrated in Figure 2.74. These types of probes may also be referred to as reflection probes, driver-pickup, exciter-pickup, or send-receive probes. This contrasts with probes in which the same coil is used for both field generation and for signal reception.

Array type probes can be fabricated containing multiple channels to enable more rapid scanning of surfaces as illustrated in Figure 2.75. Such probes can have diverse form factors and can be designed to conform to the geometry of the test piece surface.

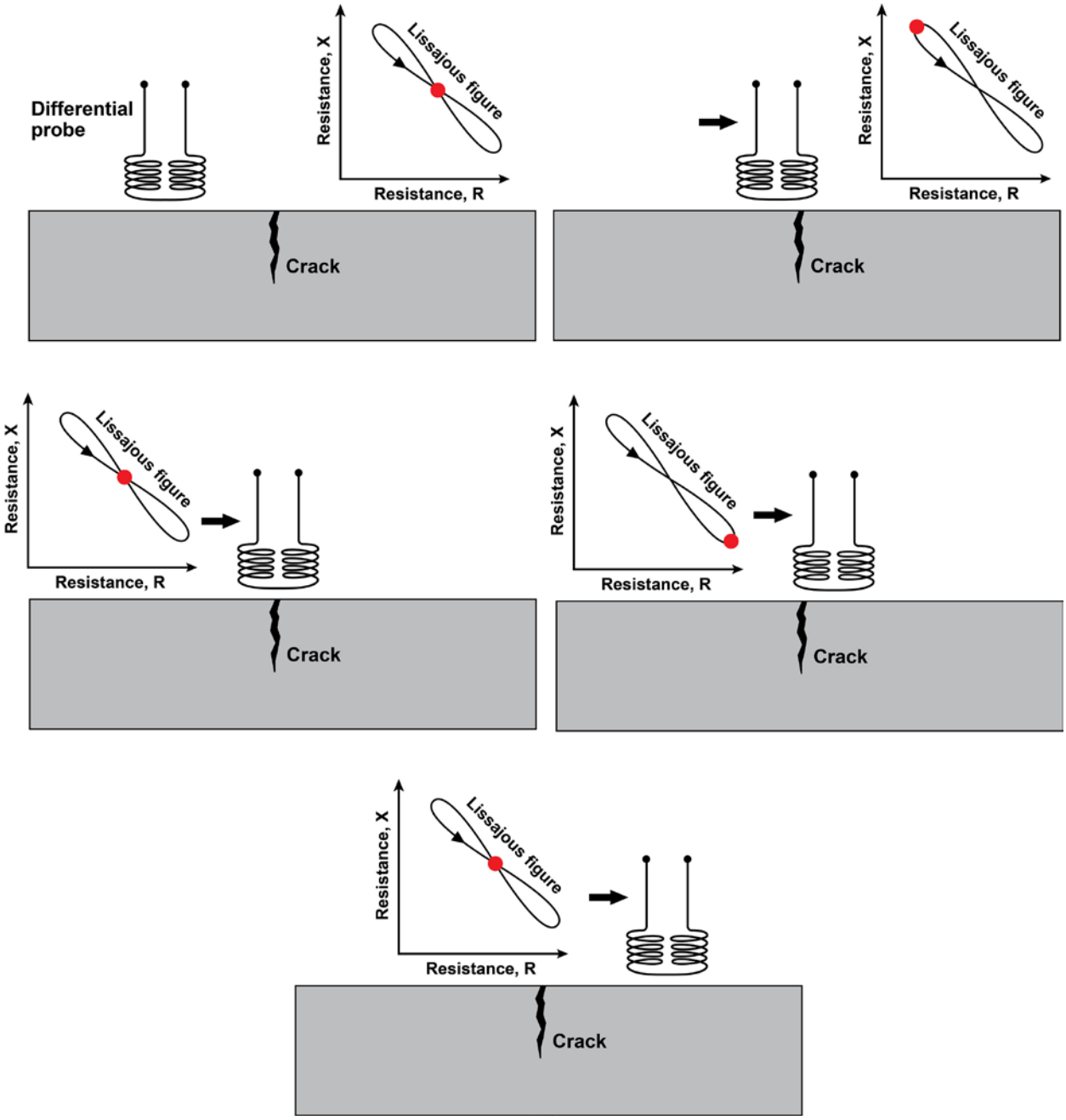

Figure 2.73. Depiction of Differential Probe and Response in Form of a Lissajous Figure

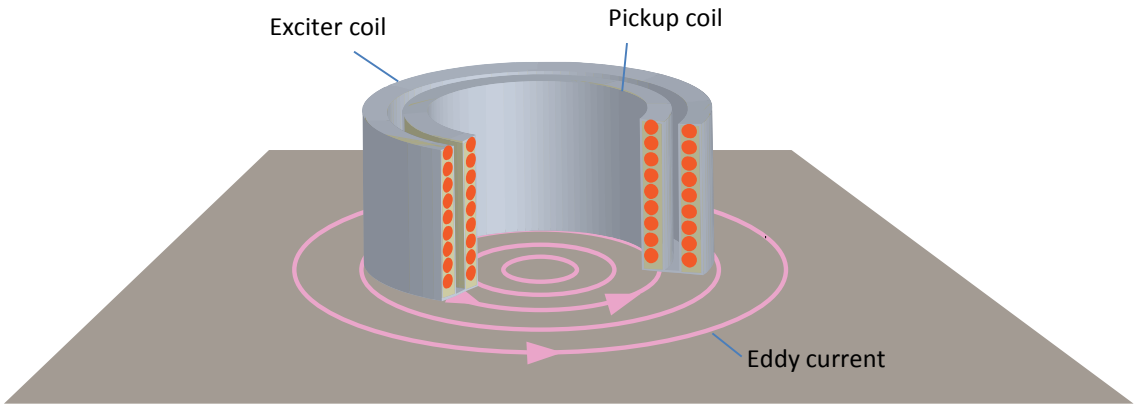

Figure 2.74. Wire-Coil-Based Reflection Probe Setup Showing Cross Section of the Two Coils. Two circuits are used to drive the two coils, each of which is a pancake-type coil.

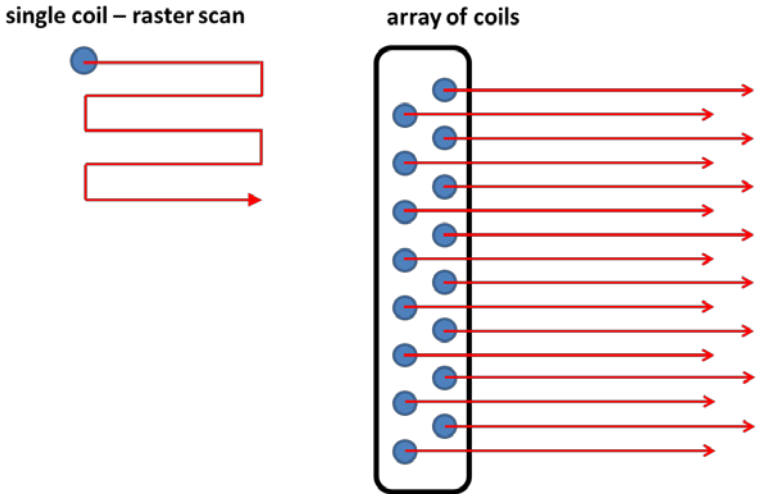

Figure 2.75. Illustration of Single Coil Raster Scan and Multi-Coil Array

2.2.4.1 Instrumentation and Implementation

Instrumentation for ECT includes a probe and equipment for driving the probe and for data acquisition and display. Circuitry is included in data acquisition devices to convert the resistive and reactive components of impedance into voltage signals. EPRI is currently working with Eddyfi to develop a multiple coil array probe with flexibility to fit the contour of the outer diameter (OD) of a dry storage canister (Renshaw 2014). A prototype under development is shown in Figure 2.76.

ECT data may be encoded or non-encoded. Encoded data refers to a method that is incorporated for relating a signal to the position at which it was acquired. Data can be displayed in multiple fashions, including representation in an impedance plane, as illustrated in Figure 2.72, or by plotting signal amplitudes as a function of position as is indicated in Figure 2.77. In this figure, the signal amplitude is coded by color with green representing the background, defect-free condition of test pieces. The data in Figure 2.77 is collected with a prototype array probe similar to that shown in Figure 2.76.

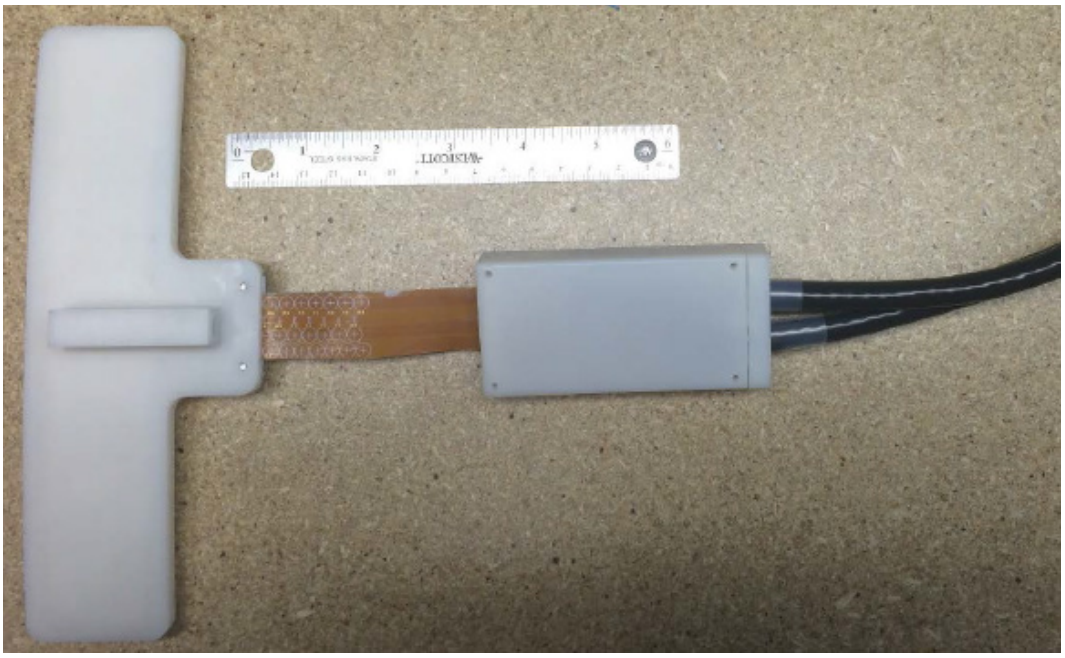

Figure 2.76. Photograph of a Prototype Eddy Current Array Probe Under Development Designed to Contour to the Surface of a Dry Storage System Canister and Fit in the Annular Space Between the Canister and Overpack (Renshaw 2014). Reprinted with permission of the Electric Power Research Institute.

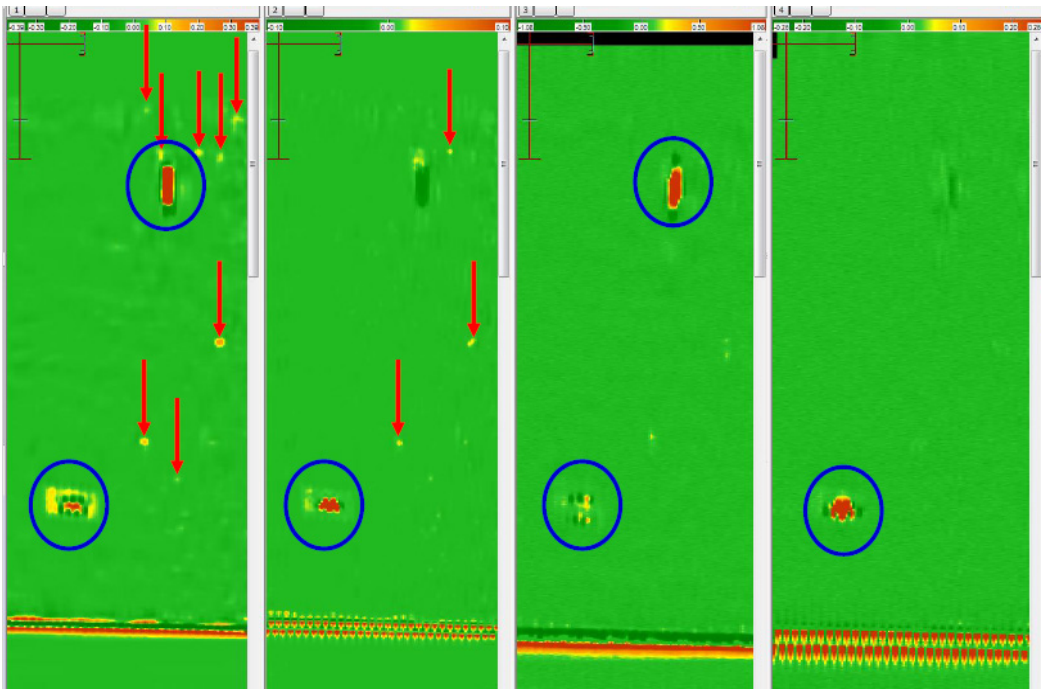

Figure 2.77. Contour Representation of Output from Four Different Channels of Prototype Eddy Current Array Probe (Renshaw 2014). Reprinted with permission of the Electric Power Research Institute.

Devices for delivering sensors to the canister surface through ventilation ports in the overpack are also being supported by the industry. This is briefly described in Section 2.3.

2.2.4.2 Performance Estimations

ECT have been evaluated as part of the NRC's Program for the Inspection of Nickel Alloy Components (PINC) (Cumblidge et al. 2010). The POD data for procedures applied to dissimilar metal weld (DMW) test blocks in PINC is provided in Table 2.8. The performance results for DMW test blocks indicate that ECT has a better performance for detection of shallow flaws (i.e., ~5 mm [0.2 in.]) than bulk UT (Cumblidge et al. 2010, p. 4.17). The flaws utilized in PINC DMW test blocks include weld solidification cracks and some laboratory grown SCC flaws. It should be noted that the flaws used in PINC were implanted on the ID surface and that inspections by bulk UT were performed from the OD surface. In the case of dry storage canisters, it is expected that cracks will initiate on the OD surface and that all inspections will be performed by accessing the OD surface regardless the NDE method applied.

Table 2.8. Probability of Detection Summary for Procedures on DMW Test Blocks in PINC (Cumblidge et al. 2010)

	POD for Flaw Depths of				
Procedure	5 mm (0.2 in.)	10 mm (0.39 in.)	15 mm (0.59 in.)	False Call Probability	ID/OD
Eddy Current	0.88	1.00	1.00	0.17	ID
Conventional UT and Phased-Array UT	0.62	0.94	0.99	0.14	OD
Conventional UT	0.36	0.51	0.67	0.23	OD
Phased-Array UT	0.36	0.51	0.66	0.24	OD
Conventional UT and TOFD	0.44	0.53	0.61	0.35	OD

2.2.4.3 Influencing Factors Associated with Instrument

- Frequency – The choice of frequency dictates the skin depth of the eddy current energy density as shown in Figure 2.71 (lower frequency means deeper penetration) with the trade-off between frequency and sensitivity to defect sizes (higher frequency improves sensitivity to shallower flaws). Frequencies of 100 kHz to 500 kHz are common with the value of the skin depth at approximately 1 mm to 3 mm (0.04 in. to 0.12 in.).
- Probe lift-off and tilt – Probe lift-off refers to the separation distance between the coil and the test piece surface. The quality of results depends on the ability to maintain a consistent lift-off distance. Lift-off variability will introduce noise to the ECT signal. Probe tilt can have a similar impact on signal quality as lift-off and refers to a condition in which a coil axis is no longer perpendicular to the test piece surface. Figure 2.72 illustrates the effect of lift-off on the eddy current signal in the impedance plane. For a probe on a steel surface, lift-off will manifest as an increase in X and decrease in R.
- Scanning – If scanning is part of the ECT procedure, the scanning parameters such as scanning speed and stability of the scan system can affect the signal quality.

2.2.4.4 Influencing Factors Associated with Specimen and Environment

- Surface conditions – Adverse surface condition may degrade performance by causing probe lift-off and tilt. Examples of such surface conditions may include geometrical features of welds that are not ground flush, surface deposits, and surface roughness. The presence of non-relevant surface imperfections (e.g., scratches) may interfere with the performance by introducing false calls.
- Variability of material conductivity and permeability (σ and μ) – In stainless steel canisters, the most likely locations for spatial variation in σ and μ will include welds and transition regions between base metals and welds. Temperature variations will also result in variation of σ and μ. In this case, the conductivity, σ, will increase with decreasing temperature.

2.2.4.5 Limitations

- The compatibility of instrumentation with environmental stressors (notably, temperature and gamma and neutron radiation exposure) near the canister surface should be evaluated. The environment near the canister surface will be a function of the initial loading conditions and the time after loading at which the inspection is to be performed.

2.2.5 Acoustic Emission Testing

Acoustic emission refers to the generation of elastic energy in a material resulting from stress accumulation and relaxation. The shedding of stress by a material because of crack extension or corrosion can result in detectable AE facilitating the monitoring of materials for damage through coupling of AE transducers to the surface of the test material (see Figure 2.78). AE is unique compared to other NDE technologies in that it is sensitive to the dynamic processes of damage progression.

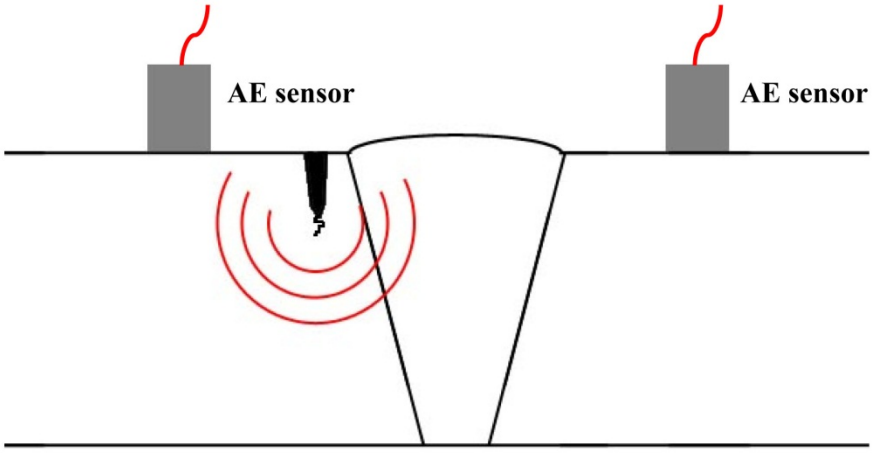

Figure 2.78. Depiction of Acoustic Emission Generation by Crack Extension and Detection by Acoustic Emission Sensors Coupled to the Surface of a Component

Several source mechanisms are possible for the generation of AE during SCC degradation, the origins of which are related to mechanical fracture or corrosion processes (Yuyama 1986). Sources associated with mechanical fracture include brittle crack jumps, plastic deformation, decohesion of inclusions or precipitates, martensitic transformation, twinning, microcracking, and slip deformation. Corrosion-related sources include dissolution of metal, evolution of hydrogen gas bubbles, and cracking or breakdown of oxide films (see Figure 2.79). The emissivity of these sources depends significantly on the material and exact crack growth or corrosion process taking place. A review of several studies exploring the emissions from various physical processes associated with crack growth and corrosion are provided in Meyer et al.

(2013b). In this report, it is noted that cracking in brittle materials produces more intense acoustic emissions than cracking in ductile materials. As a consequence, hydrogen embrittlement at crack tips can work to strengthen the intensity of acoustic emissions emanating as the crack grows. Localized corrosion processes can also generate acoustic emissions. In this case, emissions can be generated by the breakdown or spalling of thick oxide films (several microns thick) (Yuyama 1986).

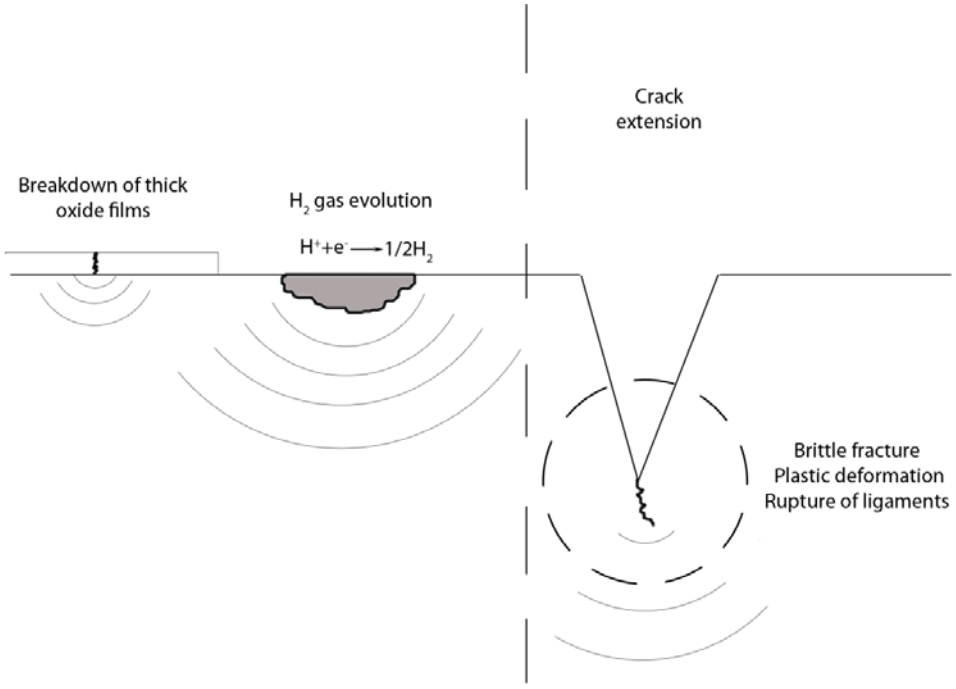

Figure 2.79. Depiction of Possible Acoustic Emission Sources Associated with Corrosion and Stress Corrosion Cracking Phenomena in Metals

The potential to monitor the degradation of structural components in nuclear power facilities by acoustic emission testing (AET) has been considered as well. Some of the challenges encountered for nuclear power structural monitoring applications include the dependence of emission strength on material and stress condition, the presence of significant noise at low frequencies (≤ 0.2 MHz) from flowing reactor coolant, and the distortion of the source signals by sensor response functions, which limited the ability to discriminate the source of the emission (Bentley 1981; Macleod et al. 1991; Runow 1985; Scruby 1987). The viability of implementing AE to continuously monitor IGSCC flaws in pressure boundary components during the operation of nuclear power plants has been demonstrated at the Limerick Unit 1 reactor (Hutton et al. 1993). In this field demonstration, the AE sensors were coupled to the component of interest through metal waveguides to isolate the sensitive piezoelectric materials from the environment at the surface of the component.

As discussed in Section 2.1.8, parameterization of AE signals is often applied in an attempt to simplify analysis and/or classify signal origin. Similar to frequency-based discrimination of noise, signals can be based on other parameters such as amplitude, duration, etc., in an attempt to filter relevant signals away from non-relevant signals. An illustration of AE signal parameterization is provided in Figure 2.19, displaying multiple features that may be used for signal classification.

AET may be performed using an array of sensors arranged near the region of interest as illustrated in Figure 2.17 of Section 2.1.8. The use of an array of sensors allows for localization of the source of emissions, which is useful for focusing monitoring on a region with known degradation. Section XI of the

ASME B&PV Code, "Rules for In-service Inspection of Nuclear Power Plant Components," Division I, governs the use of AE as part of inservice examinations of nuclear power plant components. The use of AE for volumetric examinations is discussed in paragraph IWA-2234 (ASME 2007b). Paragraph IWA-2234 restricts flaw monitoring with AE to monitoring the growth of existing flaws that have been characterized using other NDE technologies (e.g., via ultrasonic examinations).

2.2.5.1 Instrumentation and Implementation

Equipment required for AET includes sensors, preamplifiers, a data acquisition system, and computer for visual interface. Commercial systems are available. Typically, piezoelectric sensors are employed that may have a wide-band or resonant frequency response. Resonant transducers can be more sensitive than wide-band transducers, but the resonant frequency must be selected to provide optimal response. AE sensors are commercially available in in a variety of packages with standard transducers having diameters of approximately 19 to 38 mm (¾ to 1½ in.) and heights from approximately 12.5 to 63 mm (½ to 2½ in.). Miniature sensors are also available with diameters as small as 3.8 mm (0.15 in.) and height as small as 2.54 mm (0.1 in.). Standard models are rated for operation at temperatures up to 177°C and high-temperature models are available that can exceed 500°C (PAC 2005).

The signal from typical piezoelectric transducers may be on the order of 100 μV, and these signals are typically amplified by 40 dB or 60 dB with a preamplifier (Mindess 2004). Signals from the preamplifier are fed to the data acquisition system, which can usually accommodate multiple channels. An amplitude-based discrimination is applied at the input channels by setting the "threshold" as illustrated in Figure 2.19. This serves as an initial filter of noise.

Some transducers are also available with integrated preamplifiers. These sensors are limited to temperatures of 85°C (PAC 2005). A photograph of an array of AE sensors set up to monitor fatigue crack growth in a stainless steel pipe is shown in Figure 2.80.

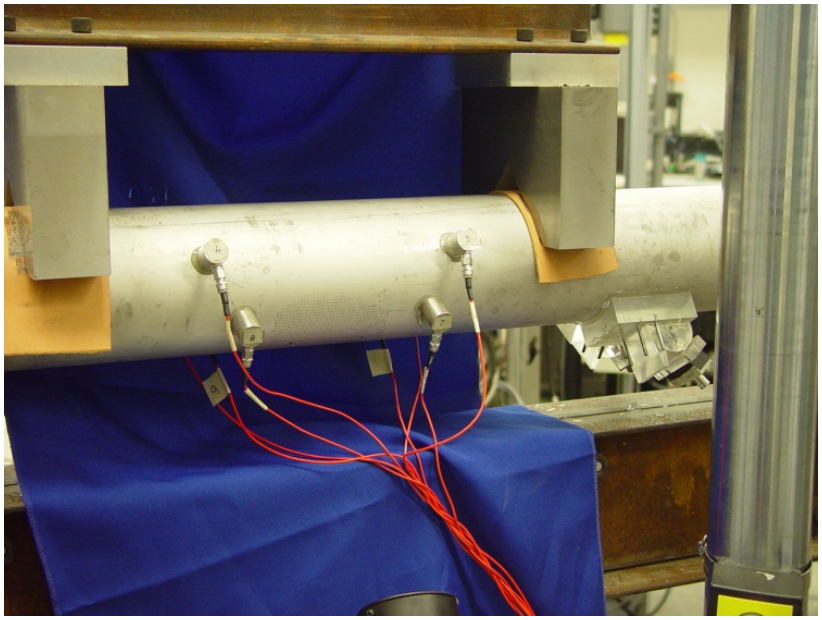

Figure 2.80. Experimental Setup of AE Instrumentation to Monitor Fatigue Crack Initiation and Growth in a 10.2 cm (4 in.) Diameter Stainless Steel Pipe

2.2.5.2 Influencing Factors Associated with Instrumentation

- Frequency – Most AE investigations of concrete employ sensors that are tuned to the frequencies in the 50 kHz to 2 MHz range (Mindess 2004). Less attenuation of AE signals is experienced at low frequencies; however, the monitoring is more susceptible to sources of noise from the environment. At higher frequencies, sources of noise from the environment are less problematic, but greater attenuation of the signals is observed (Mindess 2004).
- Coupling – The quality of the coupling of AE sensors to the test structure can influence the sensitivity. Sensors can be bonded to a test structure by adhesive or bonded by pressure contact with suitable coupling interface. Sometimes, metal waveguides may be implemented to minimize exposure of sensitive sensor elements to environmental conditions. Use of waveguides will introduce additional signal distortion and attenuation. In addition, the delay introduced by waveguides can have an impact on localization capability.

2.2.5.3 Influencing Factors Associated with Specimen and Environment

- Ductility – The intensity and detectability of AE signals is dependent on the ductility of the test material. Fracture of brittle material results in larger AE signals than cracking in ductile material. Further, the attenuation of AE signals is greater in ductile material than brittle material.
- Pressurization – AE activity can be enhanced in components that are highly pressurized as the pressurization can drive crack growth and more energetic fracture.
- Noise – AET is particularly vulnerable to sources of noise in the environment. Noise from flowing coolant has been a particular challenge in nuclear power facilities.

2.2.5.4 Limitations

- AET depends on several factors such as the material properties, type of expected degradation, external noise sources, and the level to which a component is energized. The capability to monitor chloride-induced SCC or localized corrosion in dry storage canisters has not yet been evaluated or demonstrated.

2.3 Delivery of NDE Sensors

In addition to the development of inspection technologies, industry and the DOE are also sponsoring efforts to develop devices for delivering sensors to the canister surface. For instance, EPRI has contracted with a vendor to develop a robotic device to deliver sensors to the surface of a canister in a vertical DSS system with access through the overpack vents. A photograph of a robotic device crawling up the annulus between the stainless steel canister and overpack of a cut-away dry storage cask system is provided in Figure 2.81. The delivery system in Figure 2.81 is provided as an example and could potentially be designed to accommodate payloads to support deployment of different NDE methods.

2.4 Environmental Compatibility

The compatibility of NDE instrumentation with the environment of DSC systems can also influence their deployment. This is most important for NDE instruments applied to inspect the metal canister because instrumentation will be much closer to the radiation and heat source. A conservative analysis estimates peak temperatures of approximately 225°C and gamma radiation exposures as high as 10^4 Rad/hr. (Meyer et al. 2013a). However, this assumes loading to design basis heat loads and represents the conditions immediately after loading. Canisters will be typically loaded with heat loads significantly below their

design basis limit. Further, significant decay of the heat generation rate and radiation source will occur over the first 25–30 years of storage. Thus, actual temperatures and radiation fields for measurements on canisters are likely to be much lower than those noted above. However, some analysis to understand the environmental conditions before deployment of equipment near canisters is likely to be beneficial for planning and performing inspections.

Figure 2.81. Photograph of a Robotic Delivery System Located Between the Stainless Steel Canister and Overpack of a Cut-Away Dry Storage Cask System at the Palo Verde Energy Education Center – Buckeye, Arizona (EPRI 2016). Reprinted with permission of the Electric Power Research Institute.

Environmental compatibility is not expected to present significant challenges for the deployment of NDE instrumentation for concrete structures because one of the intended functions of the thick concrete structures is to limit radiation exposure at the outer surfaces to modest levels. However, NDE methods based on scattering of gamma rays or neutrons may be impacted because the measurements are based on the same forms of radiation emanating from the fuel source. The overall impact may be to limit the achievable signal-to-noise ratio with gamma-ray and neutron scattering techniques.

3.0 Aging Effects

This section provides a summary of the NDE methods organized by their applicability to aging effects in concrete and stainless steel components. The information summarized in this section is based on information compiled for the various NDE methods in Section 2.0. Section 3.1 provides the summaries for concrete components considering aging effects of delaminations (horizontally oriented planar flaws) and voids, vertically oriented cracks, continuously distributed degradation in concrete, corrosion of embedded steel, and changes in concrete component dimensions. Section 3.2 provides summaries for stainless steel components considering aging effects of cracking (stress corrosion cracking, more specifically) and localized corrosion. This section is complemented by Section 5.0 and Table 5.1 through Table 5.3, specifically, which summarizes implementation considerations for NDE methods on NUHOMS 80 and 102 HSM components. The summary in Section 5.0 is formed based on information in Section 2.0 and in Section 4.0, which includes descriptions of NUHOMS 80 and 102 HSM components. Upon confirmation of applicability of an NDE method to a target aging effect, Section 5.0 should be consulted to determine if implementation on the desired component or region is feasible.

3.1 Summary of NDE Methods Applicability to Aging Effects in Concrete

This section includes summaries of NDE methods organized by their applicability to the aging effects in concrete. The information is organized in tables for the aging effects of delaminations (horizontally oriented planar flaws) and voids, vertically oriented cracks, continuously distributed degradation in concrete, corrosion of embedded steel, and changes in concrete component dimensions. Each table includes rows for each applicable NDE method for a particular aging effect with a column for comments regarding pertinent limitations of each method and a column indicating if application for a given aging effect is considered a primary or secondary application for an NDE method. In this regard, a primary application refers to an intended or dominant application for an NDE method. Designation as secondary application acknowledges a basis for sensitivity of an NDE method to an aging effect; however, the usefulness or the experience in applying the NDE method for an aging effect designated as a secondary application may be limited. For instance, in theory GPR could be used to measure moisture and chloride concentrations in concrete based on the influence of these factors on dielectric constant. In practice, the dielectric constant is influenced by several other factors besides moisture and chloride concentration that are difficult to account for, which limits the usefulness of GPR for this purpose.

The summary of NDE methods for aging effects is included in the following tables as specified:

- The summary of NDE methods for delaminations and voids is included in Table 3.1.
- The summary of NDE methods for vertical cracks is included in Table 3.2.
- The summary of NDE methods for continuously distributed degradation is included in Table 3.3.
- The summary of NDE methods for corrosion of embedded steel is included in Table 3.4.
- The summary of NDE methods for detection of changes in dimensions is included in Table 3.5.

Summaries of NDE methods applicable to detection of both delaminations and voids in concrete are combined in Table 3.1 because both defect types manifest as material discontinuities within the interior of concrete structures and result in similar NDE responses. In this case, it may be expected that a void will produce a response equivalent to a delamination with size equal to the area of the void projected into the perspective of the sound field. Delaminations are thin material discontinuities that are parallel to the

surface and can also be characterized as horizontally oriented cracks and two-dimensional defects. Voids are three-dimensional defects that can have a variety of shapes depending on how the void was formed.

Continuously distributed degradation in Table 3.3 refers to damage expressed as spatially smooth or gradual changes in concrete properties. This contrasts with degradation expressed as material discontinuities such as cracks, delaminations, and voids. In Table 3.5, the term "changes in dimensions" is used to refer to a reduction in actual thickness of concrete as a result of material loss or a reduction in the thickness of the concrete that is structurally sound from the surface opposite to which the transducers are applied (the surface that is not visible). For the case of a surface layer of damaged concrete on the surface that is accessible to transducers, the indirect UPV method may be used and this is covered under Table 3.3, which summarizes NDE methods applicable to detection of continuously distributed degradation in concrete.

The performances of many NDE methods were tested in the field trial portion of SHRP 2, which was conducted on a highway bridge (TRB 2013, p. 48). The existence of delaminations was verified by core sampling but information on the actual area of delaminations is not provided. Thus, while it was possible to assess the capability of methods to detect delaminations in the field sample, it is not possible assess the influence of delamination size on detection or to evaluate the ability of a method to accurately profile the area of a delamination.

Table 3.1. Summary of NDE Methods Applicable to Detection of Delaminations and Voids in Concrete

NDE Method	Primary or Secondary Application	Comments
Ultrasonic Pulse Echo	Primary	Most laboratory and field testing is performed on specimens with thickness of <= 375 mm (15 in.). Although many HSM components may have a greater thickness, this implies that currently available instruments can inspect regions within 375 mm of the surface. The UPE technique is applied by taking point measurements; thus, measurements are localized in nature. No field experience was included in the literature reviewed for the UPE technique. In laboratory testing, the technique was able to detect voids with perpendicular areas to the sound field of 10 in. by 6 in. The voids were located at depths of 3 in. and 6 in., respectively (Clayton et al. 2014).
Ultrasonic Pulse Velocity – direct transmission	Secondary	The obstruction of a UPV signal by delamination may result in loss of signal at the receiver, which does not provide information regarding the location of a flaw. It is reported that it is possible to use UPV to detect defects with projected sizes (i.e., projected to the perspective of the incident sound field) of approximately 100 mm (4 in.) or greater (IAEA 2002, pp. 100-112).

NDE Method	Primary or Secondary Application	Comments
Impact Echo	Primary	The standard for performing IE measurements was developed for plate-like structures (ASTM 2010). The minimum lateral dimension of a flaw that can be detected is approximately 1/4 of the flaw depth (Sansalone and Streett 1997). The minimum lateral dimension of a flaw that can be detected regardless of depth is equal to the wavelength associated with the maximum usable frequency (Sansalone and Streett 1997). When considering only accuracy, IE testing scored the highest for delamination inspections, followed by infrared and radar testing in SHRP 2 (TRB 2013, p. 69). Accuracy was assessed in laboratory validation studies that were performed on a fabricated bridge specimen and a recovered bridge specimen. The size of delaminations in the recovered bridge deck are not reported, but the size of simulated delaminations in the fabricated bridge deck ranged from 30.5 by 30.5 cm (12 by 12 in.) up to 61 by 122 cm (24 by 48 in.) (TRB 2013, p. 69).
Impulse Response	Primary	The technique is generally more applicable to "mass" concrete structures such as dams and containment structures. The standard for performing IR measurements was developed for plate-like structures (ASTM 2010). The IR method can detect gross defects in structures but is less reliable for the detection of smaller defects (TRB 2013, p. 19). For perspective, IR inspections of the containment structure at the Crystal River Unit 3 nuclear plant were validated by core sampling. The extent of delamination as determined by IR measurements encompassed an area of approximately 18.3 m (60 ft.) by 24.4 m (80 ft.) located at an average depth of 175 mm (7 in.) to 200 mm (8 in.) below the outer containment structure surface (Miller 2010). The IR technique was described as not being very successful at detecting delaminated areas in the field trial portion of SHRP 2, which was conducted on a highway bridge (TRB 2013, p. 48). Measurements should not be made near the edges or boundaries of a test structure (within 300 mm [12 in.]) (ASTM 2010).
Spectral Analysis of Surface Waves and Ultrasonic Surface Waves	Secondary	In the field validation testing portion of the second Strategic Highway Research Program, USW testing exhibited capability to detect delaminations as areas of measured low elastic moduli. These areas correlated well with areas where delaminations were detected by other methods (TRB 2013, p. 48). The complete true state in the field validation testing is unknown, but comparisons to other NDE methods used in the study suggest that the specimen had delaminations with areas of approximately 3 m by 3 m (10 ft. by 10 ft.) or smaller (TRB 2013, p. 48).

NDE Method	Primary or Secondary Application	Comments
Audio Methods	Primary	Audio methods have limited penetration depth (typically not exceeding cover depth). In addition, chain dragging and hammer sounding methods are operator-dependent and rely on the subjective interpretation of sound and deteriorated concrete regions (Naus 2009a, pp. 37-45). Chain dragging and hammer sounding were evaluated in SHRP 2 (TRB 2013). Based on accuracy for inspection of delaminations, chain dragging and hammer sounding was rated lower than radar testing, IE testing, and IRT testing (TRB 2013, p. 69). Accuracy was assessed in laboratory validation studies that were performed on a fabricated bridge specimen and a recovered bridge specimen. The size of delaminations in the recovered bridge deck are not reported, but the size of simulated delaminations in the fabricated bridge deck ranged from 30.5 by 30.5 cm (12 by 12 in.) up to 61 by 122 cm (24 by 48 in.) (TRB 2013, p. 69)
Infrared Thermography	Primary	The capability of IR testing is significantly influenced by the depth of flaws and the thickness of the specimen under test. It becomes less effective in the detection of subsurface flaws as the thickness of the object increases. It is seen that the maximum differential temperature between deteriorated and sound concrete regions decreases as the depth of the delaminations increase (ACI 2013b, pp. 51-53). Thus, deep flaws are difficult to detect. Based on accuracy for inspection of delaminations, IRT testing was rated lower than IE testing, but rated higher than chain dragging/hammer sounding and radar methods in SHRP 2 (TRB 2013, p. 69). Accuracy was assessed in laboratory validation studies that were performed on a fabricated bridge specimen and a recovered bridge specimen. The size of delaminations in the recovered bridge deck are not reported, but the size of simulated delaminations in the fabricated bridge deck ranged from 30.5 by 30.5 cm (12 by 12 in.) up to 61 by 122 cm (24 by 48 in.). (TRB 2013, p. 69).
Ground Penetrating Radar	Primary	For concrete structures that are heavily reinforced, GPR has limited ability to penetrate beyond the first layer of embedded reinforcing steel. GPR has limited ability to detect delamination-type defects unless they are filled with water or other material that enhances the contrast of the defect. The contrast enhancement effected by the presence of water is significantly reduced if the water is frozen (TRB 2013, pp. 19-21). GPR cannot resolve defects located closer than 1/3 of a wavelength to the surface due to the inability to resolve reflected pulses. This distance can vary from 39 mm (1.54 in.) to 117 mm (4.61 in.) for frequency ranging from 1.5 GHz to 500 MHz, respectively (ACI 2013b, pp. 53-61). GPR performance was rated just ahead of chain dragging but behind both IRT testing and IE testing in SHRP 2 (TRB 2013, p. 69). Accuracy was assessed in laboratory validation studies that were performed on a fabricated bridge specimen and a recovered bridge specimen. The size of delaminations in the recovered bridge deck are not reported, but the size of simulated delaminations in the fabricated bridge deck ranged from 30.5 by 30.5 cm (12 by 12 in.) up to 61 by 122 cm (24 by 48 in.) (TRB 2013, p. 69).

NDE Method	Primary or Secondary Application	Comments
Acoustic Emission	Primary	Active loads are required to stimulate a sufficient AE response from a concrete structure. Standard ASTM E1932, "Standard Guide for Acoustic Emission Examination of Small Parts," assumes that a controlled or measured stress is applied to the part being monitored (ASTM 2012a). Extensive laboratory testing is required to validate AE testing for field applications.
Radiography	Primary	Radiography is relatively insensitive to thin voids or delaminations oriented perpendicular to the source beam. As the overall thickness of a structure increases, the relative influence of thin voids or delaminations to the beam attenuation becomes small (IAEA 2002, pp. 82-99; Mitchell 2004).

Table 3.2. Summary of NDE Methods Applicable to Detection of Vertical Cracks in Concrete

NDE Method	Primary or Secondary Application	Comments
Spectral Analysis of Surface Waves	Secondary	SASW techniques rated highest for measuring depth of vertical cracks in terms of accuracy (TRB 2013, p. 69) and based on a composite score consisting of factors such as speed, cost, repeatability, and ease-of-use (TRB 2013, p. 77).
Ultrasonic Pulse Velocity – indirect transmission	Secondary	The reliability of crack detection is significantly impacted by presence of water filling cracks or contact between crack faces, which can allow ultrasonic energy to propagate through the faces with little resistance (IAEA 2002, pp. 100-112).
Impact Echo	Secondary	Sansalone and Streett (1997, pp. 123-134) describe use of impact echo for measuring the depth of surface-breaking cracks in concrete based on arrival time of diffracted P-wave signal at receiver.
Acoustic Emission	Primary	Active loads are required to stimulate a sufficient AE response from a concrete structure. Standard ASTM E1932, "Standard Guide for Acoustic Emission Examination of Small Parts," assumes that a controlled or measured stress is applied to the part being monitored (ASTM 2012a). Extensive laboratory testing is required to validate AE testing for field applications.

Table 3.3. Summary of NDE Methods Applicable to Detection of Continuously Distributed Degradation in Concrete

NDE Method	Primary or Secondary Application	Property Application	Comments
Spectral Analysis of Surface Waves and Ultrasonic Surface Waves	Primary	**Elastic properties** such as Young's modulus (E) and the shear modulus (G) based on R-wave velocity	SASW testing of thick members requires greater spacing between receivers. Thus, testing of thick structural members require access to large surface areas (Naus 2009a, pp. 37-45). Closest spacing for receivers approximately 0.15 m (5.91 in.) (ACI 2013b, pp. 14-15). A minimum depth of 50 mm (1.97 in.) is required to measure reduced strength and elastic properties in damaged concrete layers (ACI 2013b, pp. 14-15).
Ultrasonic Pulse Velocity	Primary	**Strength and Elastic Modulus** based on P-wave velocity	The UPV technique is applied by taking point measurements. Although the UPV technique can be deployed by two-sided (direct transmission) or single-sided (indirect transmission) access, the indirect transmission configuration is less sensitive than the direct transmission configuration and requires greater path length. It is recommended that measurements be taken over paths that do not intersect reinforcing steel (Naik et al. 2004, pp. 8-1–8-15). ACI 228.2R (ACI 2013b, pp. 7-9) indicates that the indirect transmission mode is primarily used for measured the depth of damaged surface layers of concrete.
Ground Penetrating Radar	Secondary	**Moisture and Chloride content** based on conductivity and dielectric constant	GPR cannot be used to quantifiably estimate mechanical properties of the concrete or the amount of moisture or chlorides present in concrete, despite being influenced by these factors (TRB 2013, pp. 19-21). Due to the large number of properties that can affect the dielectric constant and conductivity of concrete, it is difficult to isolate what factors may be impacting the GPR signal.

NDE Method	Primary or Secondary Application	Property Application	Comments
Gamma Radiometry	Primary	**Density** through attenuation of gamma radiation	Gamma-ray radiometry can be performed in either through-transmission or backscattering mode. The backscatter mode is only able to access a layer of concrete near the surface approximately 40 mm (1.6 in.) to 100 mm (4 in.) in depth (ACI 2013b, pp. 23-28). Heavy reinforcement may limit the effectiveness of through-transmission gamma-ray devices and limit the application of backscatter devices to regions above the outermost layer of reinforcement (ASTM 2013c). The volume of concrete sampled with gamma-ray and neutron source devices is not well-defined and is influenced by factors associated with instrumentation and the test specimen (ASTM 2013c). Sensitivity of gamma-ray source devices to aggregate composition means that absolute measurements of density require calibrations on specimens with similar aggregate composition to the structure undergoing testing. Difficulties or burdens associated with this may limit use of measurements to qualitative comparisons of measurements at different locations or over time.
Neutron Radiometry	Primary	**Moisture** through scattering of neutrons	Neutron source devices sample a greater volume in comparison to backscatter gamma-ray devices. Neutron source devices have a relatively deep penetration in comparison to backscatter gamma-ray source devices as neutron source devices may sample concrete up to 350 mm (13.78 in.) into a structure (IAEA 2002, pp. 152-161). The volume of concrete sampled with gamma-ray and neutron source devices is not well-defined and is influenced by factors associated with instrumentation and the test specimen (ASTM 2013c).

Table 3.4. Summary of NDE Methods Applicable to Detection of Corrosion of Embedded Steel in Concrete

NDE Method	Primary or Secondary Application	Comments
Half-Cell Potential	Primary	HCP does not provide a direct measure of the corrosion rate and only provides an indication that corrosion is likely (IAEA 2002, pp. 56-60). Electrical contact is required between the positive terminal of the high impedance voltmeter and the embedded reinforcing steel, which may require drilling a hole into the concrete in order to access it (IAEA 2002, pp. 56-60).

NDE Method	Primary or Secondary Application	Comments
Linear Polarization Resistance	Primary	LPR measurements are sensitive to several factors related to the ambient environment such as temperature and moisture; thus, several measurements should be performed to capture the seasonal variations in the measurements (Carino 2004).
Resistivity Measurements	Primary	Several material properties contribute to the overall resistivity of concrete such as moisture content, the presence of ions, and the porosity of concrete; and it is not possible to delineate the contribution of each to the overall measurement of resistivity (TRB 2013, pp. 24-25).
Ground Penetrating Radar	Secondary	GPR cannot measure cross-sectional loss of rebar with the level of sensitivity needed to be useful for corrosion monitoring (TRB 2013, pp. 19-21). For rebar corrosion detection, GPR testing was rated the lowest in performance based on accuracy for the methods evaluated (TRB 2013, p. 69).
Acoustic Emission	Secondary	It is noted that AE can be indirectly sensitive to the corrosion of reinforcing steel through detection of cracking that occurs in response to the expansion caused by the build-up of corrosion products on the surface of reinforcing steel (Gostautas et al. 2005; Ohtsu et al. 2007). Extensive laboratory testing is required to validate AE testing for field applications.

Table 3.5. Summary of NDE Methods Applicable to Detection of Changes in Dimensions of Concrete Structures

NDE Method	Primary or Secondary Application	Comments
Ultrasonic Pulse Echo	Primary	Most laboratory and field testing is performed on specimens with thickness of <= 375 mm (15 in.). The UPE technique is applied by taking point measurements and would be sensitive to localized dimensional changes.
Ultrasonic Pulse Velocity – Direct Transmission	Primary	If P-wave velocity is known, then thickness can be determined from arrival time of signal at receiver. The UPV technique would be sensitive to localized dimensional changes.
Impact Echo	Primary	The standard for performing IE measurements was developed for plate-like structures (ASTM 2010). The opposite boundary of the structure will give a frequency response that resembles the response from a large delamination (Carino 2001, p. 12). The IE technique would be sensitive to changes of dimensions that affect a significant area of the component under test.
Spectral Analysis of Surface Waves	Primary	Information pertaining to the thickness and can be obtained by analysis of dispersion curves. The SASW technique would be sensitive to changes of dimensions that affect a significant area of the component under test.

3.2 Summary of NDE Methods Applicability to Aging Effects in Stainless Steel

This section includes summaries of NDE methods organized by their applicability to the aging effects in stainless steel components considering aging effects of cracking (SCC) and localized corrosion. A summary of NDE methods applicable to detection of SCC in stainless steel is included in Table 3.6 and a summary of NDE methods applicable to detection of localized corrosion is included in Table 3.7.

Table 3.6. Summary of NDE Methods Applicable to Detection of Stress Corrosion Cracking in Stainless Steel

NDE Method	Comments	References
Visual Testing	COD is most influential flaw feature on POD. SCC-type flaws may feature COD below reliable detection range for typical cameras used for field inspection of reactor components.	Cumblidge et al. (2007) Cumblidge et al. (2004)
Eddy Current Testing	Better performance than UT for surface-breaking flaw detection, particularly for shallow flaws. In PINC, ECT exhibited a POD of 88% for 5 mm (0.2 in.) deep flaws and a POD of 100% for 10 mm (0.4 in.) deep flaws. Typical component thickness in this study was 30 mm to 40 mm (1.6 in.) and flaws initiated on the ID surface.	Cumblidge et al. (2010, p. 4.17)
Bulk Ultrasound (UT)	90% POD for 10 mm (0.4 in.) deep flaws. 70% POD for 5 mm (0.2 in.) deep flaws. For austenitic stainless steel piping with 12 mm (0.5 in.) and 15 mm (0.6 in.) wall thickness and IGSCC flaws. These POD values were obtained with data from studies before PAUT became relevant. Also, this data is based on flaws that initiate on the ID surface of piping components.	Heasler and Doctor (2003)
Guided Ultrasonic Waves	Flaws smaller than 5% of the sound field cross section are generally not detectable.	Lowe and Cawley (2006)
Acoustic Emission Testing	SCC-type degradation does not produce a large AE response Signals will experience significant attenuation in ductile SS canister. Canisters are not expected to provide high-energy source (pressurization) to drive AE response. The capability to monitor chloride-induced SCC or localized corrosion in dry storage canisters has not yet been evaluated or demonstrated.	Meyer et al. (2013b)

Table 3.7. Summary of NDE Methods Applicable to Detection of Localized Corrosion in Stainless Steel

NDE Method	Comments	References
Visual Testing	Multiple studies have considered automated or semi-automated analysis of localized corrosion based on visual attributes such as discoloration and texture associated with pitting or accumulation of corrosion products.	Codaro et al. (2002) Choi and Kim (2005) Pidaparti et al. (2013)
Acoustic Emission Testing	Acoustic emissions can be generated by the breakdown or spalling of thick oxide films (several microns thick). The breakdown of oxide films on the order of nanometers thick are not detectable (Yuyama 1986).	Meyer et al. (2013b)
Eddy Current Testing	The sensitivity of ECT to superficial surface blemishes (such as scratches) and surface texture implies potential for sensitivity to localized corrosion such as pitting. The data image in Figure 2.77 demonstrates that ECT can detect small pits in stainless steel.	

4.0 Description of HSM and Canister Components

This section provides descriptions of DSC and HSM components for the NUHOMS 80 and 102 DSS. The descriptions are focused on conveying physical constraints associated with accessing a particular SSC for performing an inspection. In addition, for concrete components, other details considered relevant to an inspection are described including the presence, size, and density of embedded steel and the thickness of individual components. An overview description of the DSC and HSM SSCs is provided in Section 4.1 and identifies individual SSCs to be described in greater detail. The independent spent fuel storage installation (ISFSI) and base pad are described in Section 4.2, the concrete slabs and walls of the HSM are described in Section 4.3, the shield door is described in Section 4.4, the inlets and outlets are described in Section 4.5, the heat shields are described in Section 4.6, and the DSC support structure is described in Section 4.7. A summary of parameters for concrete structures considered relevant to NDE is provided in Section 4.8. Finally, a description of the DSC exterior is provided in Section 4.9.

4.1 Overview

The NUHOMS storage system is a transportation and storage system that includes a DSC and HSM. The DSC assembly provides a containment boundary for the spent fuel assemblies. It is composed of a cylindrical stainless steel shell with top and bottom cover plates. The cover plates are welded to the cylindrical shell. The DSC houses the basket assembly, neutron absorbers for criticality control, spent nuclear fuel assemblies, shield plugs, and supporting structural components. Figure 4.1 shows a typical DSC canister.

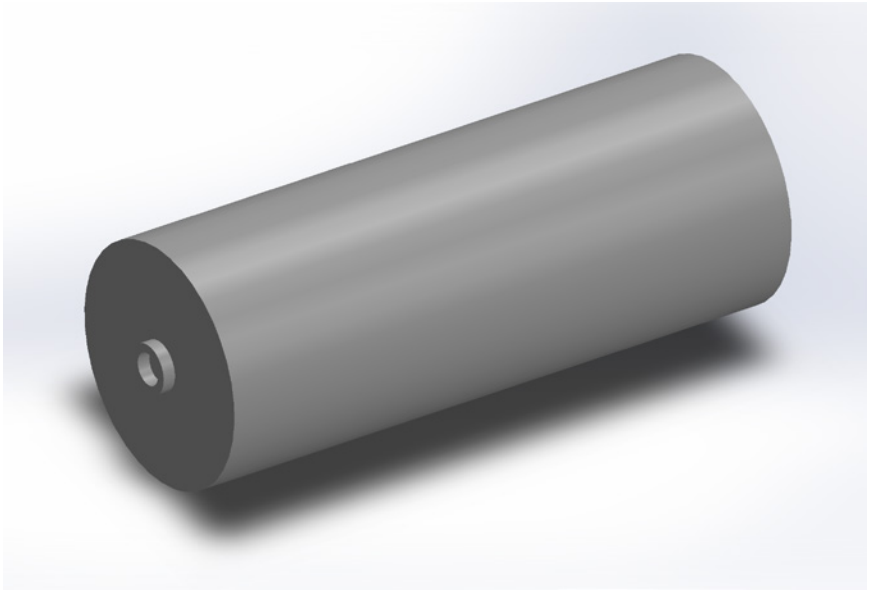

Figure 4.1. Typical Dry Shielded Canister

Spent nuclear fuel is loaded into the DSC and transported to ISFSI locations in a transfer cask. The DSC is then removed from the transfer cask and loaded into a HSM located at the ISFSI. The HSM assembly is a reinforced concrete structure that stores the DSC horizontally. A typical HSM includes heat shields, and a steel support structure that the DSC is installed on. In addition to providing confinement and shielding, the storage system also allows for heat removal of the spent fuel through natural convection within the

HSM assembly. Ambient air enters the HSM through inlets, circulates around the DSC, and exits through outlet openings at or near the roof of the HSM assembly.

There are several different configurations of the HSM design. This discussion focuses on the "standardized NUHOMS" HSM design, also known as the Model 80 and Model 102 design. Figure 4.2 gives an overall view of the HSM Model 80 and HSM Model 102 configuration (Greene et al. 2013). The HSM Model 80 and HSM Model 102 are similar designs, with the difference being that the Model 102 door is fabricated from reinforced concrete and includes thin steel liners along the inlet and outlets. The HSM Model 80 door design consists of encased concrete with steel liners on all faces. The rest of the discussion will focus primarily on the HSM Model 80 design. The following sections described the components of the HSM Model 80 assembly, and a general overview of the various DSCs compatible with the HSM Model 80. Concrete components are classified as thick or thin components, where a thick component has a thickness of greater than 500 mm (20 in.).

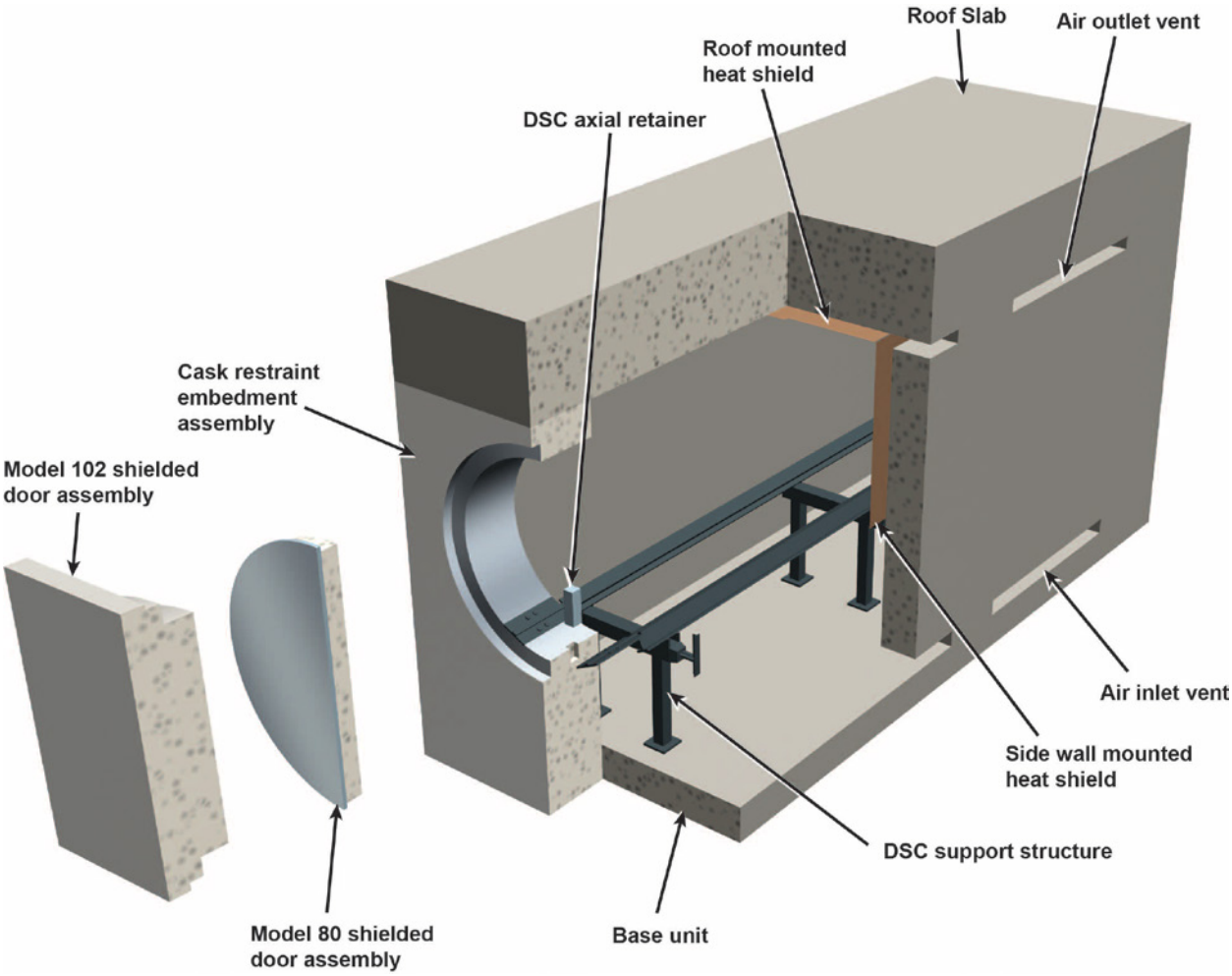

Figure 4.2. HSM Models 80 and 102

4.2 ISFSI/Base Pad

The ISFSI is typically a concrete storage pad for spent fuel storage modules. The HSMs are located in an array configuration on the storage/base pad. The base pad is a reinforced concrete slab, and varies in size depending on the site-specific ISFSI layout. A typical HSM array has the modules located in rows, with an HSM assembly having a neighboring module located on each side (unless it is an end unit) and the back of the assembly sits up against the back of an adjacent assembly facing the opposite direction. At the ends of each array are end walls that provide additional shielding. End walls are also placed at the back of single module row HSM arrays. The end walls ensure that all exposed outer walls, including the roof and front wall, form a thick concrete barrier that acts as biological shielding.

The end walls and base pad are classified as a thick concrete for the HSM Model 80. A typical gap of several inches is placed between neighboring HSM Model 80 assemblies along an array row, creating a narrow alleyway between modules. This allows ambient air to enter and exit a module. There is no gap between the back walls of adjacent modules in a double row of HSM Model 80 arrays. Figure 4.3 shows a typical double row array with HSM Model 80.

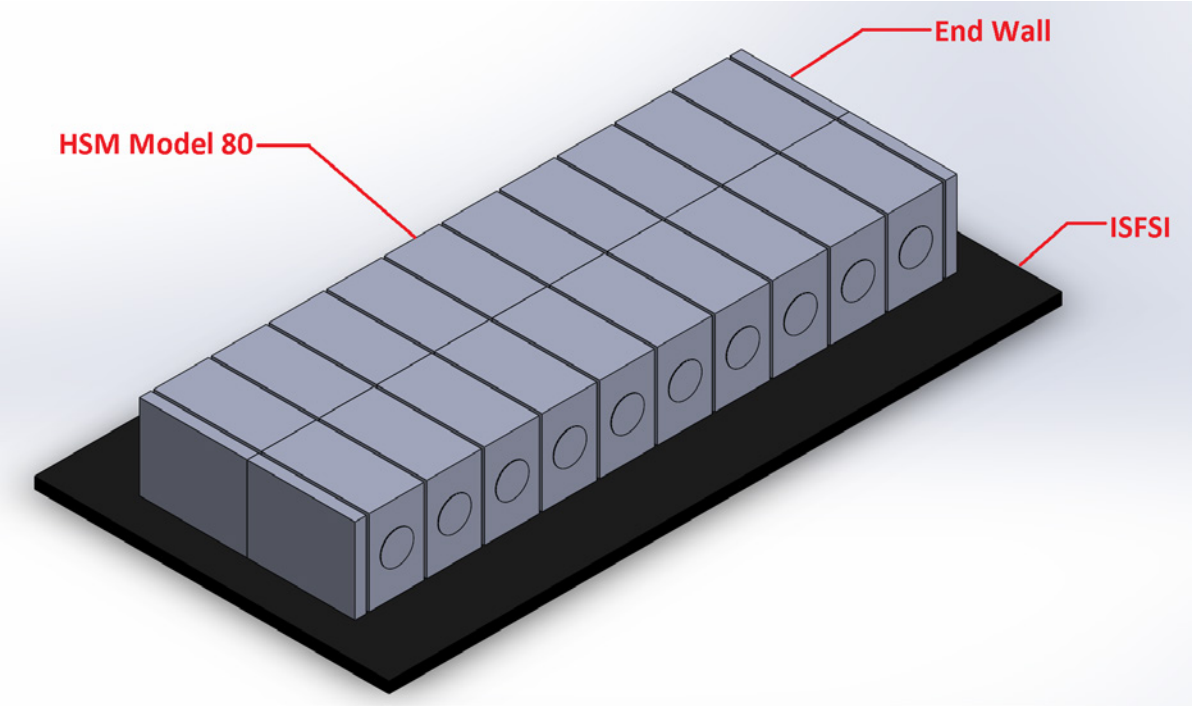

Figure 4.3. Typical Double Array Configuration for HSM Model 80 Assemblies

4.3 Concrete Walls and Slabs

The HSM is made up of a front wall, back wall, two side walls, roof slab, and floor slab—all consisting of reinforced concrete. The concrete reinforcement is designed to meet minimum and maximum reinforcement requirements of ACI 349 (Code Requirements for Nuclear Safety-Related Concrete Structure and Commentary) (ACI 1980). A typical HSM reinforcement uses rebar with spacing of 150 to 300 mm (6 to 12 in.). The roof slab and front wall are required to be thick concrete parts regardless of the array configuration at the ISFSI, because these components are always considered exposed walls. This ensures proper shielding of the overall array of assemblies.

For the HSM Model 80, the back wall, side walls, and floor slab are classified as thin concrete parts. During assembly of the HSM Model 80 the concrete front wall, back wall, side walls, and floor slab are poured as a single component, referred to as the base unit. The roof slab is attached to the base unit through four steel roof attachment angle assemblies located at the upper corners of the module. A DSC support structure is attached to the floor slab, front wall, and one of the side walls. Inlets and outlets are located on the side walls. The front wall has an access opening that is slightly larger than the diameter of the DSC. See Figures 4.4 and 4.5.

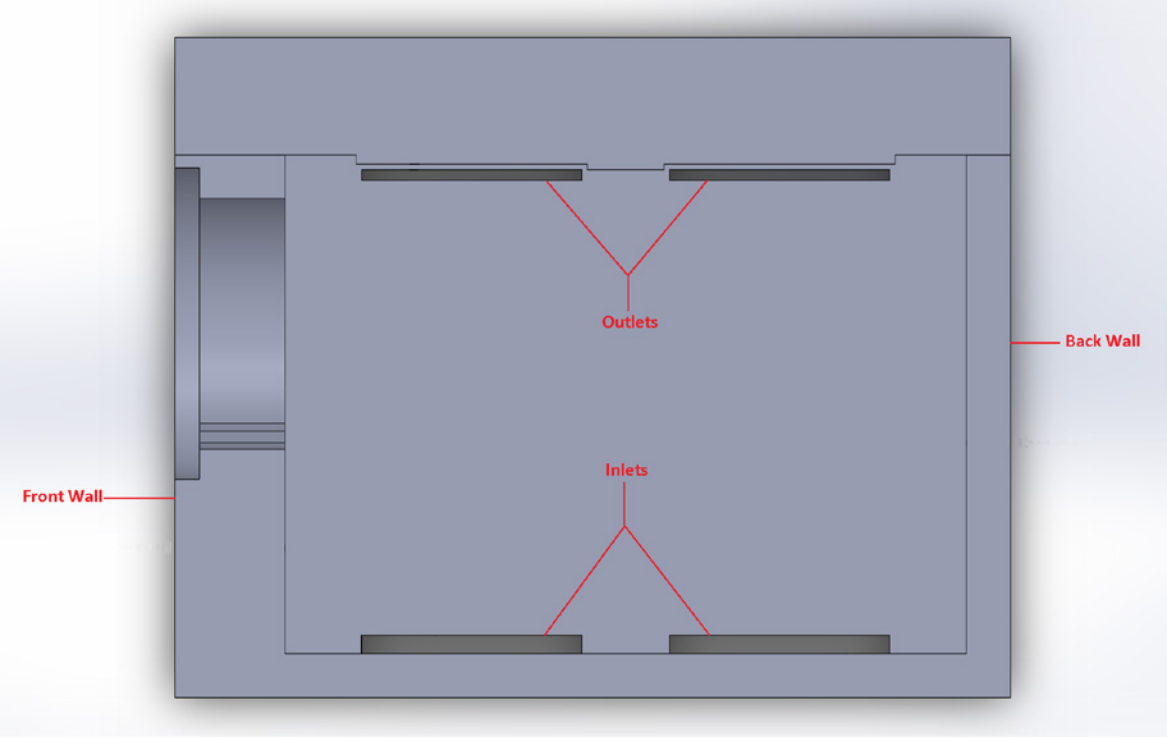

Figure 4.4. Axial Cross Section of the HSM Models 80/102

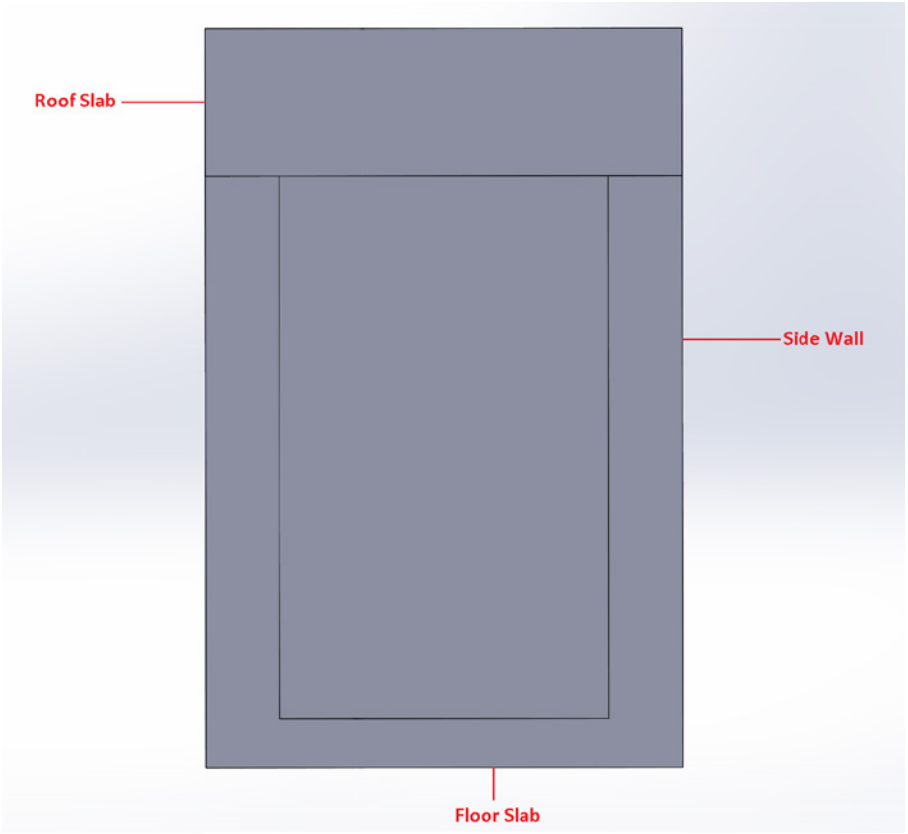

Figure 4.5. Radial Cross Section of the HSM Models 80/102

4.4 Shield Door

The door to the HSM is located in the front wall and provides access for transferring the DSC into and out of the HSM. It is attached to the front wall with four bolt clamps. The door is heavily shielded to minimize radiation exposure. A composite door is used for the HSM Model 80 assembly. The composite door has a steel outer lining and an inner concrete core. It is classified as a thin part. For the HSM Model 102 assembly, the shield door does not have a steel outer lining and is classified as a thick part.

4.5 Inlets and Outlets

The spent fuel housed within the HSM is cooled by natural convection with the environment. Ambient air enters through the inlets, circulates around the DSC, and exits through the outlets. Typically, the inlets are located near the ground and the outlets are located in or near the roof of the module.

In the HSM Model 80, there are four inlets located in the side walls (two per side wall) near the floor slab. Each side wall also has two outlets (four total per module) located near the roof slab. The inlets and outlets have rectangular openings with lengths much greater than heights. The heights of inlets and outlets are several inches and the heights of inlet vents are typically greater than the heights of outlets. The inlet and outlets are partially shielded by the neighboring module or end wall. Bird screens cover the narrow alley way formed between neighboring modules.

4.6 Heat Shields

Heat shields are located within the HSM to protect the concrete walls and ceiling from direct thermal radiation from the hottest external surfaces along the DSC. Typically, the hottest location is along the top axial surface of the DSC. The heat shields also increase the overall surface area for convection heat transfer.

The HSM Model 80 has a metal heat shield assembly hanging over the top and sides of the DSC, shielding the concrete components from the hottest DSC temperatures. Figure 4.6 shows an isometric view of the heat shield assembly within an HSM Model 80. The heat shield assembly is attached to the roof slab and side walls with bolt assemblies. A typical gap of a few inches separates the heat shield from side walls and roof components.

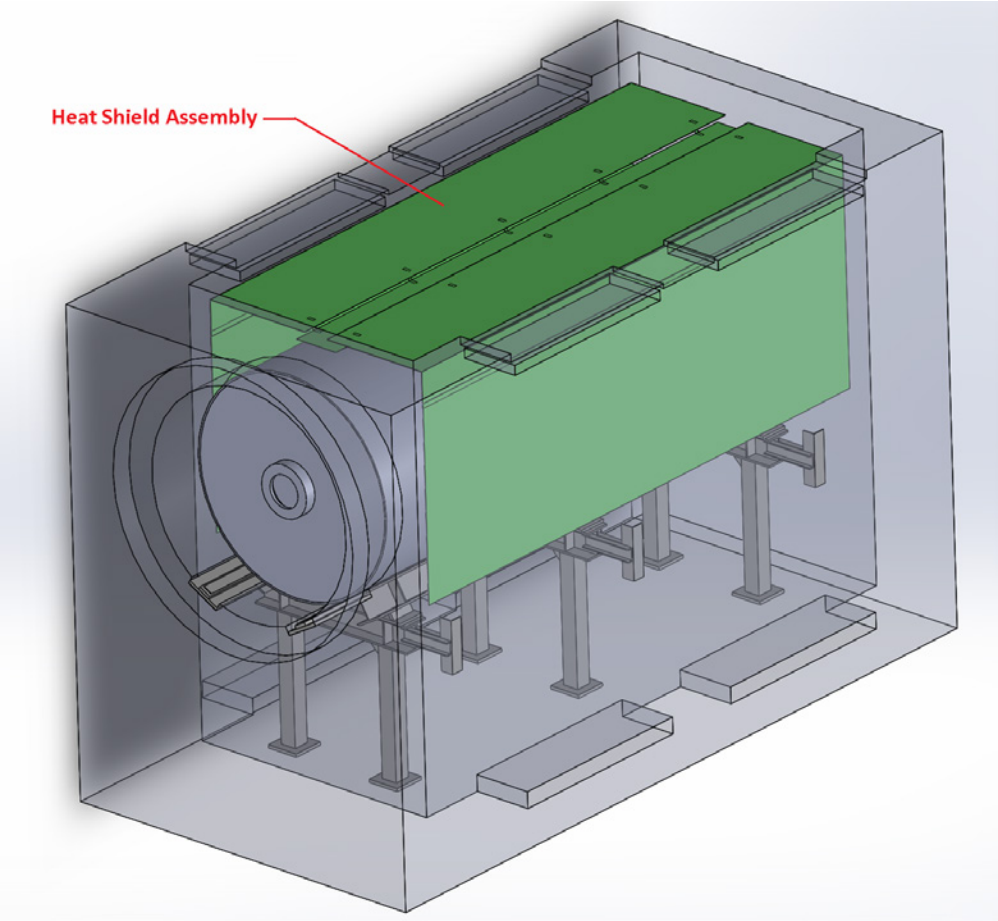

Figure 4.6. Heat Shield Assembly Shown in Green for HSM Model 80 (roof slab removed for clarity)

4.7 DSC Support Structure

The DSC rests on the support rails, which are held up by steel frames. The frames anchor the support rails to the HSM. The frames and support rails are referred to as the DSC support structure. Support rails are typically composed of carbon steel or high-strength low-alloy (HSLA) steel with stainless steel strips for wear and galling resistance located at the top of the rails that contact the DSC.

Figure 4.7 shows the DSC support structure for HSM Model 80. As shown in the figure, the rails are supported vertically and horizontally by three moment-resisting braced frames. These frames are anchored to the concrete floor slab and one of the side walls. The support rails also extend into the access opening of the front wall. During assembly of the modules, the rails are leveled to be parallel with the floor slab and then welded to plates bolted to the access opening in the front wall. This anchors the rails to the front wall, in addition to being anchored to the floor and side wall.

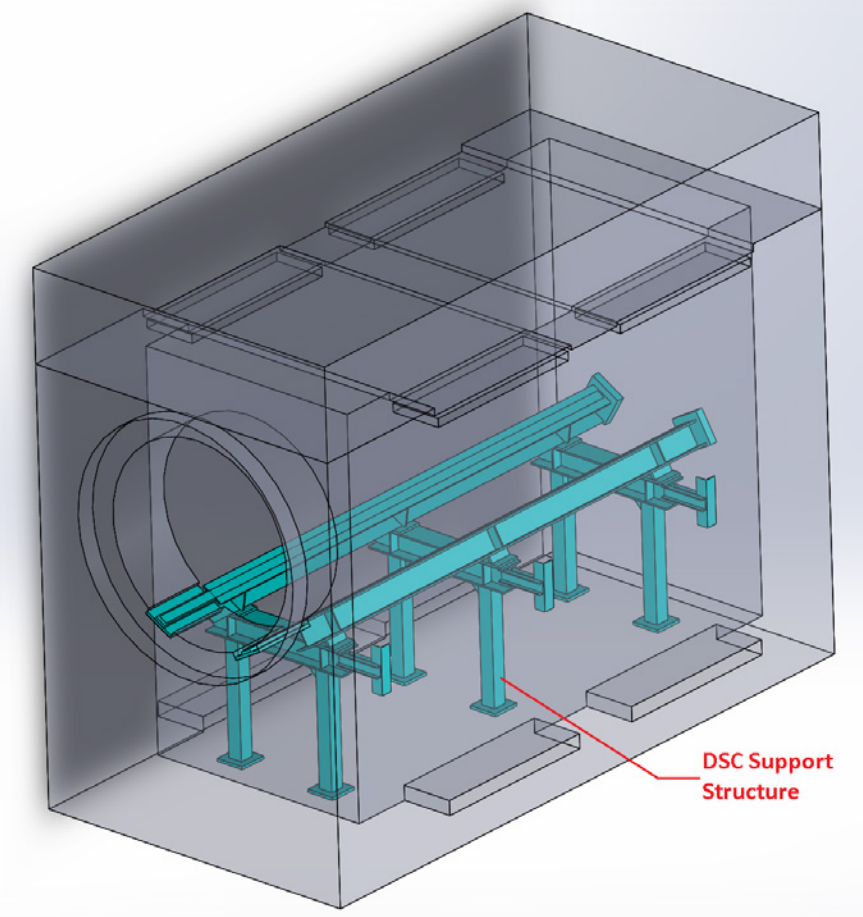

Figure 4.7. DSC Support Structure Shown in Blue for HSM Model 80 (heat shield and DSC removed for clarity)

4.8 Summary of Concrete Structure Parameters

Several characteristics typical of bridge deck, dam, and reactor concrete containment structures are tabulated and compared to characteristics for HSM Models 80 and 102 concrete components in Table 4.1. This comparison highlights similarities and distinctions between HSM Models 80 and 102 concrete components and other concrete structures, which can aid in identifying potentially relevant NDE methods. Descriptions of typical bridge deck, dam, and reactor concrete containment structures are provided in Appendix A.

Table 4.1. Tabulated Summary of Several Parameters of Typical Concrete Bridge Deck, Dams, and Reactor Concrete Containment Structures along with a Summary of Parameters for HSM Models 80 and 102 Concrete Components

	Thickness, mm (in.)	Embedded Steel Spacing, mm (in.)	Cover Depth, mm (in.)	Orientation
HSM Sidewalls	< 500 (20)	150–300 (6–12)		Vertical
HSM Roof Slab	> 500 (20)	150–300 (6–12)		Horizontal
HSM Front Wall	> 500 (20)	150–300 (6–12)		Vertical
HSM Back Wall	< 500 (20)	150–300 (6–12)		Vertical
HSM Floor Slab	< 500 (20)	150–300 (6–12)		Horizontal
HSM End Wall	> 500 (20)	150–300 (6–12)		Vertical
Typical Bridge Deck	175–267 (7–10.5)	125–200 (5–8)	~50 (2)	Horizontal
Typical Dam Structure	>= 300 (12) (rockfill/earthfill membranes)	< = 300 (12)	50–80 (2–3) minimum	Vertical
Typical Reactor Containment Wall	1.37 m (4.5 ft.)	150–300 (6–12)	38–80 (1.5–3)	Vertical

4.9 DSC Exterior

The exterior of the DSC is made up of a cylindrical stainless steel shell with top and bottom plate assemblies attached at each end. A containment boundary is formed by welding the plate assemblies to the cylindrical shell. The welding process leaves circumferential weld lines at the top and bottom of the DSC. The shell is fabricated from multiple stainless steel plates, butt welded together to form a cylinder. The location and number of the welds can vary. Typically, a DSC will have both longitudinal and circumferential butt welds along the cylindrical shell. The welds are typically double V-groove welds hand ground flush on the outside. Figure 4.8 provides an illustration of a typical DSC shell and welds.

The HSM Model 80 can store a variety of different DSC assemblies and fuels. Either PWR or BWR fuel assemblies can be stored within the module. The PWR canisters have an overall length of approximately 4.73 m (186.2–186.55 in.), and have a diameter of 1.7 m (67.19 in.). The overall length of a BWR DSC varies around 5 m (195.92–196 in.), and a diameter approximately 1.8 m (67.19–67.25 in.) (Greene et al. 2013).

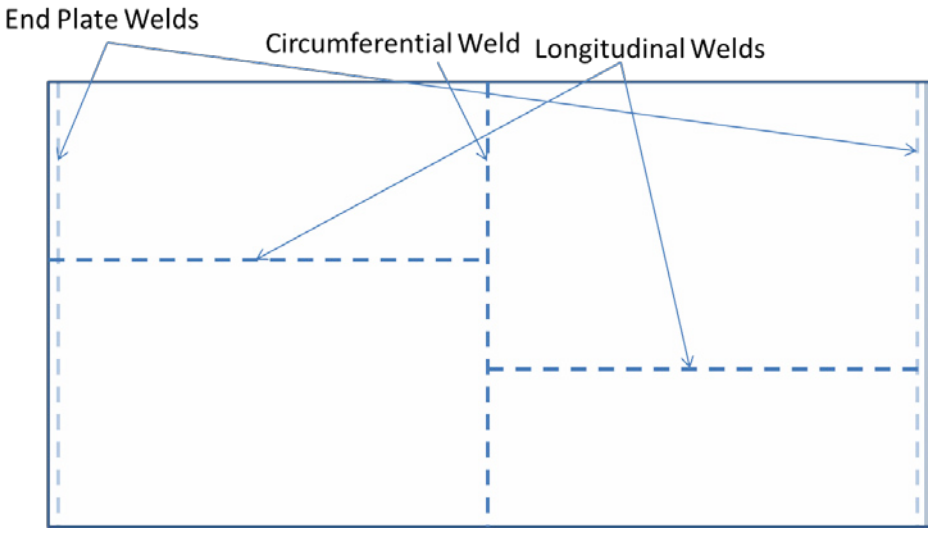

Figure 4.8. Typical NUHOMS DSC Assembly

5.0 Implementation of NDE Methods and Techniques on NUHOMS 80 and 102 HSM Components

This section summarizes implementation considerations from NDE methods on NUHOMS 80 and 102 HSM components. Applicability of the NDE methods to aging effects is discussed in Section 3.0. Information from Section 3.0 should be used in conjunction with information in this summary in reviewing the appropriateness of applicability of NDE methods to specific aging effects and implementation on specific HSM components. The information summarized in Section 3.0 is based on information summarized for the various NDE methods and techniques in Section 2.0. The summary in this section is formed based on information in Section 2.0 and in Section 4.0, which includes descriptions of NUHOMS 80 and 102 HSM components. The information summary is included in three tables (Tables 5.1, 5.2, and 5.3, respectively). Table 5.1 summarizes implementation considerations for several NDE methods including whether single- or double-sided access is required, the sampling depth, and other considerations specific to each method. Table 5.2 includes remarks related to implementation of each NDE method on front wall, roof slab, and end wall structures, while Table 5.3 includes remarks related to implementation of each NDE method on side wall, back wall, floor slab, and base pad structures.

From the descriptions in Section 4.0, it is clear that the outer surfaces of the front wall, roof slab, and end wall are generally unobstructed and accessible. Two-sided access to the end wall structure and single-side access to the side wall structures becomes possible if instrumentation can access gaps between HSM modules. Finally, the floor slab and back-wall structures are not accessible unless the canister is removed from the HSM. Removal of the canister from the HSM would also make portions of the side wall and front wall accessible from the inside.

Table 5.1. Summary of Implementation Considerations for NDE Methods for Inspecting Concrete Structures

NDE Method	Single or Two-Sided Access Requirement	Sampling Depth Potential	Other Relevant Considerations
Ultrasonic Pulse Echo	Single-sided	Demonstrated up to 375 mm (15 in.)	Debonding of reinforcing steel can cause shadowing of regions on the far side of reinforcing steel.
Impact Echo	Single-sided	Can be performed on members up to 1.5 m thick (Sansalone and Streett 1997, p. 17)	If the ratio of rebar diameter to cover depth is less than 0.3, then the bars are not detected by IE signals. If the ratio is greater than 0.83, then the reinforcing steel dominates the IE response (Sansalone and Streett 1997, pp. 167-179). IE testing was primarily developed for testing of plate-like structures and standard ASTM C1383 defines plate-like structures as having lateral dimensions of greater than six times the depth (ASTM 2015c).
Impulse Response	Single-sided	Has been used for testing of containment structure at Crystal River	IR testing was also developed for testing of plate-like structures (ASTM 2010). In this case, the definition of plate-like structures in ASTM C1383 is used, which defines plate-like structures as having lateral dimensions of greater than six times the depth (ASTM 2015c).
Ultrasonic Surface Waves Spectral Analysis of Surface Waves	Single-sided	SASW is inherently a full thickness technique as the source must generate signals with wavelengths that exceed the specimen thickness. USW is a partial thickness technique. The depth of sampling is approximately equal to the longest wavelength in the excitation signal.	SASW testing of thick members requires greater spacing between receivers. Thus, testing of thick structural members requires access to large surface areas (Naus 2009a, pp. 37-45). Reflections can cause fluctuations to appear in the dispersion curves. To minimize the influence of reflections from edges, Sheu et al. (1988) recommend placement of the source between the boundary edge and receivers when the transducer array is oriented perpendicular to the edge. When the edge is oriented parallel to the transducer array, it is recommended to position the array very close to the boundary so that reflected waves are in phase with the source waves, or positioning the array as far from the reflecting boundary as possible so that reflected waves experience more attenuation and are of low amplitude. The source and receiving transducers are usually spaced such that the distance from the source to nearest receiver is equal to the distance between the receiving transducers. When investigating concrete pavements and structural members, the receivers are located relatively close together with the closest spacing of about 0.15 m (6 in.). The spacing is increased by a factor of two for subsequent tests.

NDE Method	Single or Two-Sided Access Requirement	Sampling Depth Potential	Other Relevant Considerations
Audio Methods	Single-sided	Usually limited to an effective region of penetration not exceeding the concrete cover depth	
Ultrasonic Pulse Velocity – Direct Transmission	Two-sided	Full thickness	Measurement paths intersecting reinforcing steel can overestimate velocity (Naik et al. 2004, pp.8-1–8-15). For most applications, 50 kHz resonant frequency transducers are suitable, whereas low resonant frequency transducers (20 kHz) are used for mass concrete (ASTM 2009b).
Ultrasonic Pulse Velocity – Indirect Transmission	Single-sided	For concrete member with homogeneous properties, UPV is based on sampling materials within a wavelength of the surface. At 50 kHz, the wavelength would be approximately 75 mm (3 in.) assuming a velocity of 4000 m/s. If a damaged surface layer exists on top of sound concrete, the concrete within a wavelength of the surface and within a wavelength of the interface between degraded and sound concrete will be sampled.	Measurement paths intersecting reinforcing steel can overestimate velocity (Naik et al. 2004, pp.8-1–8-15).
Infrared Thermography	Single-sided	Depth of penetration on the order of a few inches	The capability of IRT testing is significantly influenced by the depth of flaws and the thickness of the specimen under test. It becomes less effective in the detection of subsurface flaws as the thickness of the object increases. Field of view is related to standoff distance of the camera.

NDE Method	Single or Two-Sided Access Requirement	Sampling Depth Potential	Other Relevant Considerations
Acoustic Emission	Single-sided	Full thickness	The reviewed literature indicates that active loads are required to stimulate a sufficient AE response from a concrete structure. Standard ASTM E1932, "Standard Guide for Acoustic Emission Examination of Small Parts," assumes that a controlled or measured stress is applied to the part being monitored (ASTM 2012a). Active loads are not required for monitoring of active corrosion of reinforcing steel. Extensive laboratory testing is required to validate AE testing for field testing.
Ground Penetrating Radar	Single-sided	Depth of penetration limited to cover depth for heavy reinforcement. If reinforcement is not an issue, it may penetrate 0.5–2.0 m of concrete (ACI 2013b, pp. 53-61).	For concrete structures that are heavily reinforced, GPR has limited ability to penetrate beyond the first layer of embedded reinforcing steel (ACI 2013b, pp. 53-61). In one source, it is stated that features below a layer of embedded reinforcing steel cannot be detected when the rebar size is 32 mm (1.26 in.) diameter or greater and the spacing is at 200 mm (8 in.) given a frequency of 1 GHz and a cover depth of 25 to 50 mm (1 to 2 in.) (ACI 2013b, pp. 53-61). Another source states that it is possible to detect below a mesh of reinforcing steel that is 12 mm (0.5 in.) in diameter and spaced at 150 mm (6 in.) at 900 MHz (IAEA 2002, pp. 137-151). GPR testing of concrete can be performed using an air-coupled or ground-coupled antenna. The air-coupled configuration usually consists of a horn antenna mounted approximately 150 to 500 mm (6 to 20 in.) above the test structure (ACI 2013b, pp. 53-61). A bow tie antenna is normally used for the ground-coupled scenario. For this case, the spacing between the antenna and the test structure should be no more than 1/10 of a wavelength to achieve adequate coupling of the signal (IAEA 2002, pp. 137-151).
Radiography	Two-sided	Full thickness (requires linear accelerator source for thicknesses greater than 500 mm (20 in.).)	Gamma radiation exposure precludes the use of detector inside of the HSM with loaded canister. Linear accelerator sources are required for thicknesses greater than 500 mm (20 in.).

NDE Method	Single or Two-Sided Access Requirement	Sampling Depth Potential	Other Relevant Considerations
Nuclear Methods (through-transmission)	Two-sided	Full thickness (front wall thickness may limit implementation with radioisotopic sources)	Reinforcing steel can influence the signal of gamma-ray source devices for density measurements and the measurements should be conducted in a way that ensures that reinforcing steel does not intersect the sampled volume (ASTM 2013c). Heavy reinforcement may limit the effectiveness of testing by gamma radiometry (ASTM 2013c).
Nuclear Methods (backscatter)	Single-sided	Neutron source devices penetrate up to 350 mm (14 in.); gamma source devices penetrate 40 to 100 mm (1.6 to 4 in.)	Reinforcing steel can influence the signal of gamma-ray source devices for density measurements and the measurements should be conducted in a way that ensures that reinforcing steel does not intersect the sampled volume (ASTM 2013c). Heavy reinforcement may limit the effectiveness of testing by gamma radiometry (ASTM 2013c).
Half-cell Potential	Electrical contact is required between the positive terminal of the high impedance voltmeter and the embedded reinforcing steel	Not applicable	Electrical contact is required between the positive terminal of the high impedance voltmeter and the embedded reinforcing steel, which may require drilling a hole into the concrete in order to access it (IAEA 2002, 56-60).
Linear Polarization Resistance	Electrical contact is required between the positive terminal of the high impedance voltmeter and the embedded reinforcing steel	Not applicable	Electrical contact is required between the positive terminal of the high impedance voltmeter and the embedded reinforcing steel which may require drilling a hole into the concrete in order to access it (IAEA 2002, 56-60).
Resistivity Measurements	Single-sided	Depth of penetration is a function of the electrodes spacing (IAEA 2002, pp.76-78).	The effect of reinforcing bars is to indicate a much lower resistivity than actual for the concrete. It may be possible to correct for the effect of reinforcing steel when the size of the bars and locations are known (ACI 2013b, pp. 38-42).

Table 5.2. Summary of Remarks for Implementing NDE Methods on Front Wall, Roof Slab, and End Wall Concrete Structures

NDE Method	Remarks about Implementation on Front Wall and Roof Slab	Remarks about Implementation on End Wall
Ultrasonic Pulse Echo	Possible use for detection of horizontally oriented discontinuities (delaminations and voids) located at depths up to 375 mm (15 in.) from outer surface.	Possible use for detection of horizontally oriented discontinuities (delaminations and voids) located at depths up to 375 mm (15 in.) from surfaces. Access to both surfaces could facilitate full thickness coverage of end wall. The surface adjacent to HSM module is only accessible through the gap between the end wall and the HSM module.
Impact Echo	Assuming cover depth of 38–75 mm (1.5–3 in.), the ratio of bar diameter to cover depth may be between 0.3 and 0.83. In this range, the reinforcing steel may influence the response, but will not dominate it. The front wall and roof slab structures do not meet the specifications of a plate-like structure as defined by ASTM C1383 because the widths of the front wall and roof slab are less than six times the front wall and roof slab thicknesses. Further, the front wall contains a large access port for insertion and removal of canisters. Application to non-plate–like structures may result in modes generated by reflections from nearby boundaries resulting in a more complex frequency response. The detection of flaws requires understanding of the frequency response for the unflawed state (ACI 2013b, pp. 10-14).	Assuming cover depth of 38–75 mm (1.5–3 in.), the ratio of bar diameter to cover depth may be between 0.3 and 0.83. In this range, the reinforcing steel may influence the response, but will not dominate it. The end wall does meet the definition of a plate-like structure as defined by ASTM C1383 because its lateral dimensions are greater than six times its thickness.
Impulse Response	The front wall and roof slab structures do not meet the specifications of a plate-like structure as defined by ASTM C1383 because the widths of the front wall and roof slab are less than six times the front wall and roof slab thicknesses. Further, the front wall contains a large access port for insertion and removal of canisters.	The end wall does meet the definition of a plate-like structure as defined by ASTM C1383 because its lateral dimensions are greater than six times its thickness.
Ultrasonic Surface Waves Spectral Analysis of Surface Waves	USW and SASW can be implemented on outer surfaces of front wall and roof slab. Effects of reflections from boundaries can be minimized by limiting wavelength, which will limit the depth of penetration. If wavelength is limited to less than 0.1 times width of front wall and roof slab structures, then maximum wavelength and depth of penetration will be approx. 300 mm (12 in.).	Effects of reflections from boundaries can be minimized by limiting wavelength, which will limit the depth of penetration. If wavelength is limited to less than 0.1 times minimal lateral dimension of the end wall, then maximum wavelength and depth of penetration will be approx. 450 mm (18 in.).

NDE Method	Remarks about Implementation on Front Wall and Roof Slab	Remarks about Implementation on End Wall
Audio Methods	Chain dragging would not be suitable for the front wall because it is vertical, but may be applicable to the roof slab, which is horizontal. Hammer sounding or electromechanical tapping devices may be appropriate for application to the front wall and roof slab.	Chain dragging would not be suitable for the end wall because it is vertical. Hammer sounding or electromechanical tapping devices may be appropriate. The surface adjacent to HSM module is only accessible through the gap between the end wall and the HSM module.
Ultrasonic Pulse Velocity – Direct Transmission	Implementation requires access to inside surface of HSM.	Implementation requires ability to access end wall surface through the gap between the end wall and the side wall of outer HSM module.
Ultrasonic Pulse Velocity – Indirect Transmission	May be implemented to inspect damage in concrete near outer surfaces of the front wall and roof slab.	May be implemented to inspect damage in concrete near surfaces of the end wall. The surface adjacent to HSM module is only accessible through the gap between the end wall and the HSM module.
Infrared Thermography	May be implemented on outer surfaces of front wall and roof slab. Depth of penetration limited to a few inches.	May be implemented on accessible surface opposite to the HSM module. The gap between the end wall and side wall of the HSM module would restrict IRT to a very limited field of view of the end wall surface adjacent to the HSM module.
Acoustic Emission	May be implemented by mounting sensors on outer surfaces of front wall or roof slab.	May be implemented by mounting sensors on accessible surfaces of the end wall. The surface adjacent to HSM module is only accessible through the gap between end wall and the HSM module.
Ground Penetrating Radar	May be implemented on outer surfaces of front wall and roof slab. Depth of penetration primarily limited to the cover depth. Sampling beyond the cover depth may be possible depending on rebar diameter and spacing.	May be implemented on end wall surface opposite to the HSM module. Depth of penetration primarily limited to the cover depth. Sampling beyond the cover depth may be possible depending on rebar diameter and spacing. The surface adjacent to HSM module is only accessible through the gap between the end wall and the HSM module. If access to this surface is feasible, it would be restricted to ground-coupled antennas.

NDE Method	Remarks about Implementation on Front Wall and Roof Slab	Remarks about Implementation on End Wall
Radiography	Implementation requires access to inside surface of HSM. Requires linear accelerator source.	Implementation requires ability to access end wall surface through the gap between the end wall and the side wall of outer HSM module. Linear accelerator source would be required for end wall thickness.
Nuclear Methods (through-transmission)	Implementation requires access to inside surface of HSM.	Implementation requires ability to access end wall surface through the gap between the end wall and the side wall of outer HSM module.
Nuclear Methods (backscatter)	Backscatter gamma and neutron radiometry devices may be implemented to measure density and moisture content near outer surface of front wall and roof slab.	Backscatter gamma and neutron radiometry devices may be implemented to measure density and moisture concentration near surfaces of the end wall. The surface adjacent to HSM module is only accessible through the gap between the end wall and the HSM module.
Half-cell Potential	Implementation may require drilling a hole into front wall or roof slab.	Implementation may require drilling a hole into the end wall.
Linear Polarization Resistance	Implementation may require drilling a hole into front wall or roof slab.	Implementation may require drilling a hole into the end wall.
Resistivity Measurements	May be implemented to measure resistivity of concrete near the outer surfaces of the front wall and roof slab.	May be implemented to measure resistivity of concrete near the surfaces of the end wall. The surface adjacent to HSM module is only accessible through the gap between the end wall and the HSM module.

Table 5.3. Summary of Remarks for Implementing NDE Methods on Side Wall, Back Wall, Floor Slab, and Base Pad Structures

NDE Method	Remarks about Implementation on Side Walls	Remarks about Implementation on Back Wall and Floor Slab	Remarks about Implementation on Base Pad
Ultrasonic Pulse Echo	Possible use for detection of horizontally oriented discontinuities (delaminations and voids) located at depths up to 375 mm (15 in.) from surfaces. Implementation would require access through the gap between HSM modules.	Possible use for detection of horizontally oriented discontinuities (delaminations and voids) located at depths up to 375 mm (15 in.) from surfaces. Implementation requires access to the inside of the HSM module.	Possible use for detection of horizontally oriented discontinuities (delaminations and voids) located at depths up to 375 mm (15 in.) from surfaces. Implementation limited to regions not covered by HSM modules.

NDE Method	Remarks about Implementation on Side Walls	Remarks about Implementation on Back Wall and Floor Slab	Remarks about Implementation on Base Pad
Impact Echo	Assuming cover depth of 38–75 mm (1.5–3 in.), the ratio of bar diameter to cover depth may be between 0.3 and 0.83. In this range, the reinforcing steel may influence the response, but will not dominate it. The side wall does meet the definition of a plate-like structure as defined by ASTM C1383 because its lateral dimensions are greater than six times its thickness. Implementation would require access through the gap between HSM modules.	Assuming cover depth of 38–75 mm (1.5–3 in.), the ratio of bar diameter to cover depth may be between 0.3 and 0.83. In this range, the reinforcing steel may influence the response, but will not dominate it. The back wall and floor slab structures do meet the definition of a plate-like structure as defined by ASTM C1383 because its lateral dimensions are greater than six times its thickness. Implementation requires access to the inside of the HSM module.	Implementation limited to regions not covered by HSM modules.
Impulse Response	The side wall does meet the definition of a plate-like structure as defined by ASTM C1383 because its lateral dimensions are greater than six times its thickness. Implementation would require access through the gap between HSM modules.	The back wall and floor slab structures do meet the definition of a plate-like structure as defined by ASTM C1383 because its lateral dimensions are greater than six times its thickness. Implementation requires access to the inside of the HSM module.	Implementation limited to regions not covered by HSM modules.
Ultrasonic Surface Waves Spectral Analysis of Surface Waves	Effects of reflections from boundaries can be minimized by limiting wavelength, which will limit the depth of penetration. If wavelength is limited to less than 0.1 times minimal lateral dimension of the end wall, then maximum wavelength and depth of penetration will be approx. 450 mm (18 in.), which would achieve full thickness penetration. Implementation would require access through the gap between HSM modules.	Effects of reflections from boundaries can be minimized by limiting wavelength, which will limit the depth of penetration. If wavelength is limited to less than 0.1 times minimal lateral dimensions of the back wall and floor slab structures, then maximum wavelength and depth of penetration will be approx. 300 mm (12 in.), which would achieve full thickness penetration. Implementation requires access to the inside of the HSM module.	Implementation limited to regions not covered by HSM modules.

NDE Method	Remarks about Implementation on Side Walls	Remarks about Implementation on Back Wall and Floor Slab	Remarks about Implementation on Base Pad
Audio Methods	Chain dragging would not be suitable for the side wall because it is vertical. Hammer sounding or electromechanical tapping devices may be appropriate. Implementation would require access through the gap between HSM modules.	Chain dragging would not be suitable for the back wall because it is vertical. Hammer sounding or electromechanical tapping devices may be appropriate for back wall and floor slab structures. Implementation requires access to the inside of the HSM module.	Implementation limited to regions not covered by HSM modules.
Ultrasonic Pulse Velocity – Direct Transmission	Implementation requires access to inside surface of HSM.	The back wall and floor slab structures do not have two accessible sides to allow implementation.	Two accessible surfaces are not available for implementation.
Ultrasonic Pulse Velocity – Indirect Transmission	May be implemented to inspect damage in concrete near outside surface of side wall. Implementation would require access through the gap between HSM modules.	May be implemented to inspect damage in concrete near outside surface of back wall and floor slab structures. Implementation requires access to the inside of the HSM module.	Implementation limited to regions not covered by HSM modules.
Infrared Thermography	The gap between the HSM modules would restrict IRT to a very limited field of view of the end wall surface adjacent to the HSM module.	Lack of direct exposure of floor slab and back-wall surfaces to sunlight would limit the usefulness of IRT even if access to the inside of the HSM module is feasible.	Implementation limited to regions not covered by HSM modules.
Acoustic Emission	Implementation would require access through the gap between HSM modules.	Implementation requires access to the inside of the HSM module.	Implementation limited to regions not covered by HSM modules.
Ground Penetrating Radar	The side wall surface is accessible through the gap between the HSM modules. If access is feasible, it would be restricted to ground-coupled antennas. Depth of penetration primarily limited to the cover depth. Sampling beyond the cover depth may be possible depending on rebar diameter and spacing.	Depth of penetration primarily limited to the cover depth. Sampling beyond the cover depth may be possible depending on rebar diameter and spacing. Implementation requires access to the inside of the HSM module.	Implementation limited to regions not covered by HSM modules.
Radiography	Implementation requires access to inside surface of HSM.	The back-wall and floor slab structures do not have two accessible sides to allow implementation.	Two accessible surfaces are not available for implementation.

NDE Method	Remarks about Implementation on Side Walls	Remarks about Implementation on Back Wall and Floor Slab	Remarks about Implementation on Base Pad
Nuclear Methods (through-transmission)	Implementation requires access to inside surface of HSM.	The back-wall and floor slab structures do not have two accessible sides to allow implementation.	Two accessible surfaces are not available for implementation.
Nuclear Methods (backscatter)	Backscatter gamma and neutron radiometry devices may be implemented to measure density and moisture concentration near surfaces of the side wall. Implementation would require access through the gap between HSM modules.	Backscatter gamma and neutron radiometry devices may be implemented to measure density and moisture concentration near surfaces of the floor slab and back wall. Implementation requires access to the inside of the HSM module.	Implementation limited to regions not covered by HSM modules.
Half-cell Potential	Implementation may require drilling a hole into the side wall. Implementation would require access through the gap between HSM modules.	Implementation may require drilling a hole into the back wall or floor slab. Implementation requires access to the inside of the HSM module.	Implementation may require drilling a hole into the base mate.
Linear Polarization Resistance	Implementation may require drilling a hole into the side wall. Implementation would require access through the gap between HSM modules.	Implementation may require drilling a hole into the back wall or floor slab. Implementation requires access to the inside of the HSM module.	Implementation may require drilling a hole into the base mat.
Resistivity Measurements	May be implemented to measure resistivity of concrete near the surface of the sidewall. Implementation would require access through the gap between HSM modules.	May be implemented to measure resistivity of concrete near the surface of the floor slab and back-wall structures. Implementation requires access to the inside of the HSM module.	Implementation limited to regions not covered by HSM modules.

6.0 Summary of the Applicability of NDE Methods and Implementation to NUHOMS Components

This section summarizes information from Sections 3.0 and 5.0 in tables and figures for more convenient visualization. Section 6.1 provides a summary of the applicability of NDE methods for detecting cracking and localized corrosion in DSCs. This information is based on Sections 3.2 and 2.2. Section 6.2 provides a summary of the applicability of NDE methods to aging effects in concrete and an implementation summary for HSM 80/102 components.

6.1 Summary of the Applicability of NDE Methods for DSCs

A summary of the applicability of NDE methods for detecting cracking and localized corrosion in DSCs is provided in Table 6.1. The information in this summary is based on Sections 3.2 and 2.2. The summary is split to categorize those NDE methods that may be applied to obstructed and unobstructed surfaces. An example of an obstructed surface includes areas of the surface of the DSC in contact with support rails. In general, obstructed surfaces include surfaces that cannot be directly accessed with NDE equipment. This table does not make any assumptions regarding the ability to access DSCs with NDE equipment in situ.

Table 6.1. Summary of Applicability of NDE Methods for Detecting Cracking and Localized Corrosion in DSCs

	Cracking	Localized Corrosion
Unobstructed Surfaces	Eddy Current Bulk UT Ultrasonic Testing Guided Ultrasonic Waves	Visual Eddy Current Acoustic Emission
Obstructed Surfaces	Guided Ultrasonic Waves Bulk UT (PAUT)	Acoustic Emission

6.2 Summary of the Applicability of NDE Methods for Aging Effects in Concrete

A summary of the applicability of NDE methods to aging effects in concrete is provided in Table 6.2. Applicability of each NDE method is considered for five aging effects including delaminations or voids, vertical cracks, continuously distributed degradation, corrosion of embedded steel, and dimensional changes. Applicability is categorized as primary or secondary. In this regard, a primary application refers to an intended or dominant application for an NDE method. Designation as secondary application acknowledges a basis for sensitivity of an NDE method to an aging effect; however, usefulness or experience may be limited and other NDE methods with primary designation may be favored.

An implementation summary for NDE methods on HSM components is provided in Table 6.3. This table conveys accessibility restrictions for implementing NDE methods on specific HSM components and is based on information in Section 5.0. In this case, access for NDE methods is classified as “generally accessible,” “requiring access to gap between HSM modules,” “require access to HSM interior,” or “requiring access to HSM interior and to gap between HSM modules.” Further, the depth of penetration or depth to which an NDE method is capable of sampling is also indicated in Table 6.3. In this case, penetration capabilities are categorized as “Full Thickness Access,” “Near Surface Access,” “Partial Depth Access,” and “Embedded Steel Access.” Near surface access refers to the ability to essentially

sample the cover depth region. Partial depth access indicates ability to sample at depths up to approximately 200 to 375 mm (8 to 15 in.). The "NAs" indicate that implementation of an NDE method to an HSM component is not possible. Question marks ("?") are included in the column for the Base Pad because the thickness of the base pad is not known. Therefore, it is not clear if the base pad is too thick to apply certain techniques such as impact-echo or impulse response, or if AE can effectively sample through the full base pad thickness or if it is limited to partial depth access.

Table 6.2. Summary of the Applicability of NDE Methods to Aging Effects in Concrete

	Delaminations or Voids	Vertical Cracking	Continuously Distributed Degradation	Corrosion of Embedded Steel	Changes in Dimension
Ultrasonic Pulse Echo	●				●
Ultrasonic Pulse Velocity (Direct Transmission)	◘		●		●
Ultrasonic Pulse Velocity (Indirect Transmission)		◘	●		
Impact Echo	●	◘			●
Impulse Response	●				
Spectral Analysis of Surface Waves	◘	◘	●		●
Ultrasonic Surface Waves	◘		●		
Audio Methods	●				
Infrared Thermography	●				
Ground Penetrating Radar	●		◘	◘	
Radiography	●				
Gamma Radiometry			●		
Neutron Radiometry			●		
Half-Cell Potential				●	
Linear Polarization Resistance				●	
Resistivity Measurements				●	
Acoustic Emission	●	●		◘	

●Primary Application
◘ Secondary Application

Table 6.3. Implementation Summary for NDE Methods Applied to HSM 80/102 Components

	Front Wall	Roof Slab	End Wall	Side Wall	Floor Slab	Back Wall	Base Pad*
Ultrasonic Pulse Echo	⊙	⊙	⊙	◘	◆	◆	⊙
Ultrasonic Pulse Velocity (Direct Transmission)	◆	NA	■	✚	NA	NA	NA
Ultrasonic Pulse Velocity (Indirect Transmission)	⊙	⊙	⊙	◘	◇	◇	⊙
Impact Echo	●	●	●	■	◆	◆	?
Impulse Response	NA	NA	●	■	◆	◆	?
Spectral Analysis of Surface Waves	NA	⊙	⊙	◘	◇	◇	⊙
Ultrasonic Surface Waves	⊙	⊙	⊙	◘	◇	◇	⊙
Audio Methods	○	○	○	□	◇	◇	○
Infrared Thermography	○	○	○	NA	NA	NA	○
Ground Penetrating Radar	○	○	○	□	◇	◇	○
Radiography	◆	NA	■	✚	NA	NA	NA
Gamma Radiometry (Backscatter)	○	○	○	□	◇	◇	○
Neutron Radiometry (Backscatter)	⊙	⊙	⊙	◘	◆	◆	⊙
Gamma Radiometry (Through Transmission)	◆	NA	■	✚	NA	NA	NA
Half-Cell Potential	⊙	⊙	⊙	▣	◈	◈	⊙
Linear Polarization Resistance	⊙	⊙	⊙	▣	◈	◈	⊙
Resistivity Measurements	⊙	⊙	⊙	◘	◇	◇	⊙
Acoustic Emission	●	●	●	■	◆	◆	?

●○⊙⊙ No Access Restrictions
■□◘▣ Requires Access to Gap between HSM modules
◆◇◇◈ Requires Access to Interior of HSM modules
✚×▲✷ Requires Access to Interior of HSM modules and Gap Between HSM Modules

●■◆✚ Full Thickness Access
○□◇× Near Surface Access (cover depth)
⊙◘◇▲ Partial Depth Access
⊙▣◈✷ Embedded Steel Access

NA = Not Applicable ? = Uncertain
*Thickness of Base Pad is unknown

Information in Table 6.3 is also illustrated in Figures 6.1 through 6.5. Figures 6.1 and 6.2 show side and front cross sections, respectively, of the HSM illustrating generally accessible regions and which NDE methods can access which regions. Figure 6.3 shows a front cross section illustrating regions of the side walls and end wall that may be accessed if the gaps between HSM modules can be accessed by instrumentation. Figures 6.4 and 6.5 show the side and front cross sections of the HSM illustrating regions that are accessible and what NDE methods may be implemented if the interior of the HSM can be accessed. Finally, Figure 6.6 shows what NDE methods can be applied to the side walls if both the interior of the HSM modules and the gaps between HSM modules can be accessed.

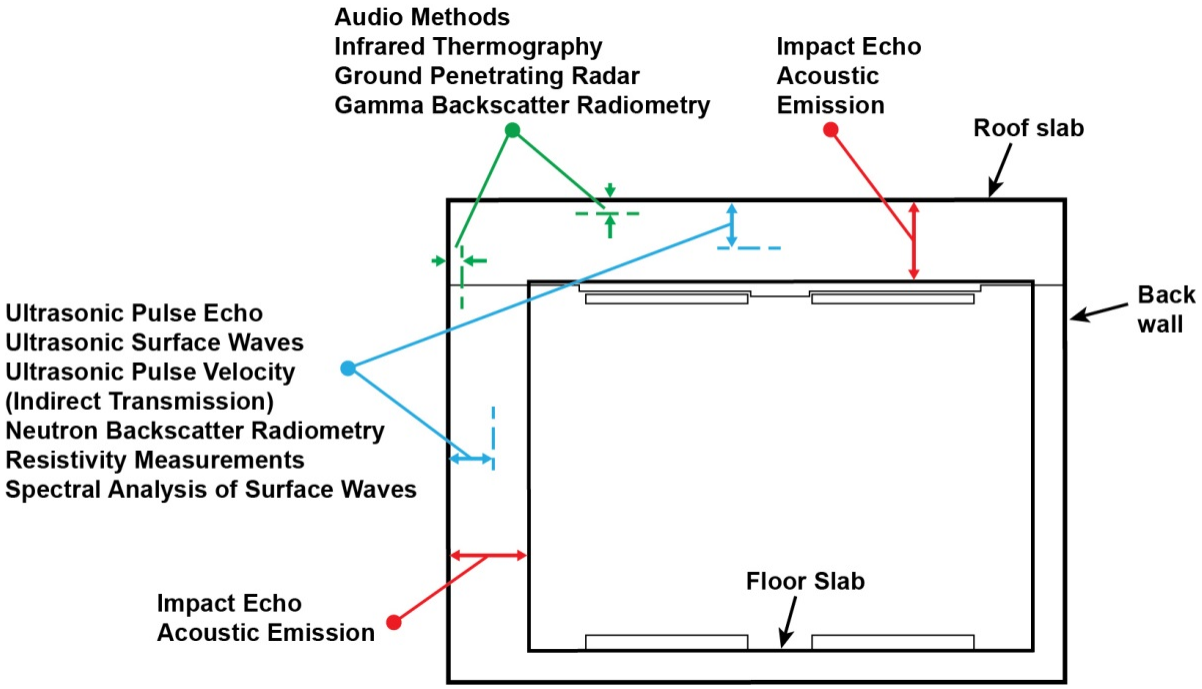

Figure 6.1. Depiction of the Side Cross Section of the HSM 80/102 Module Indicating the General Accessibility of the Front Wall and Roof Slab to NDE Methods and the Approximate Depth into Components They are Capable of Sampling

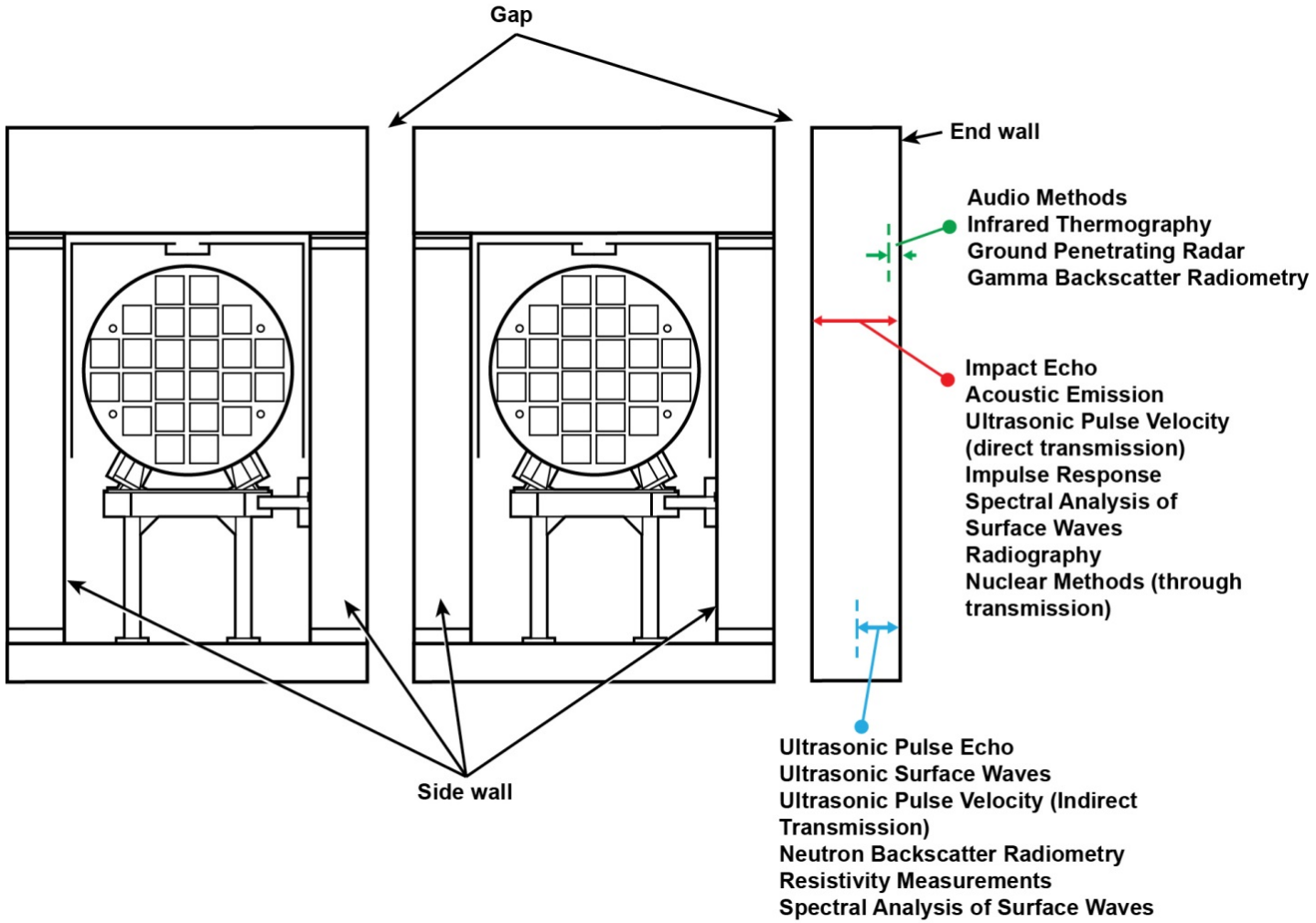

Figure 6.2. Depiction of the Front Cross Section of the HSM 80/102 Module Indicating the General Accessibility of the End Wall to NDE Methods and the Approximate Depth They are Capable of Sampling

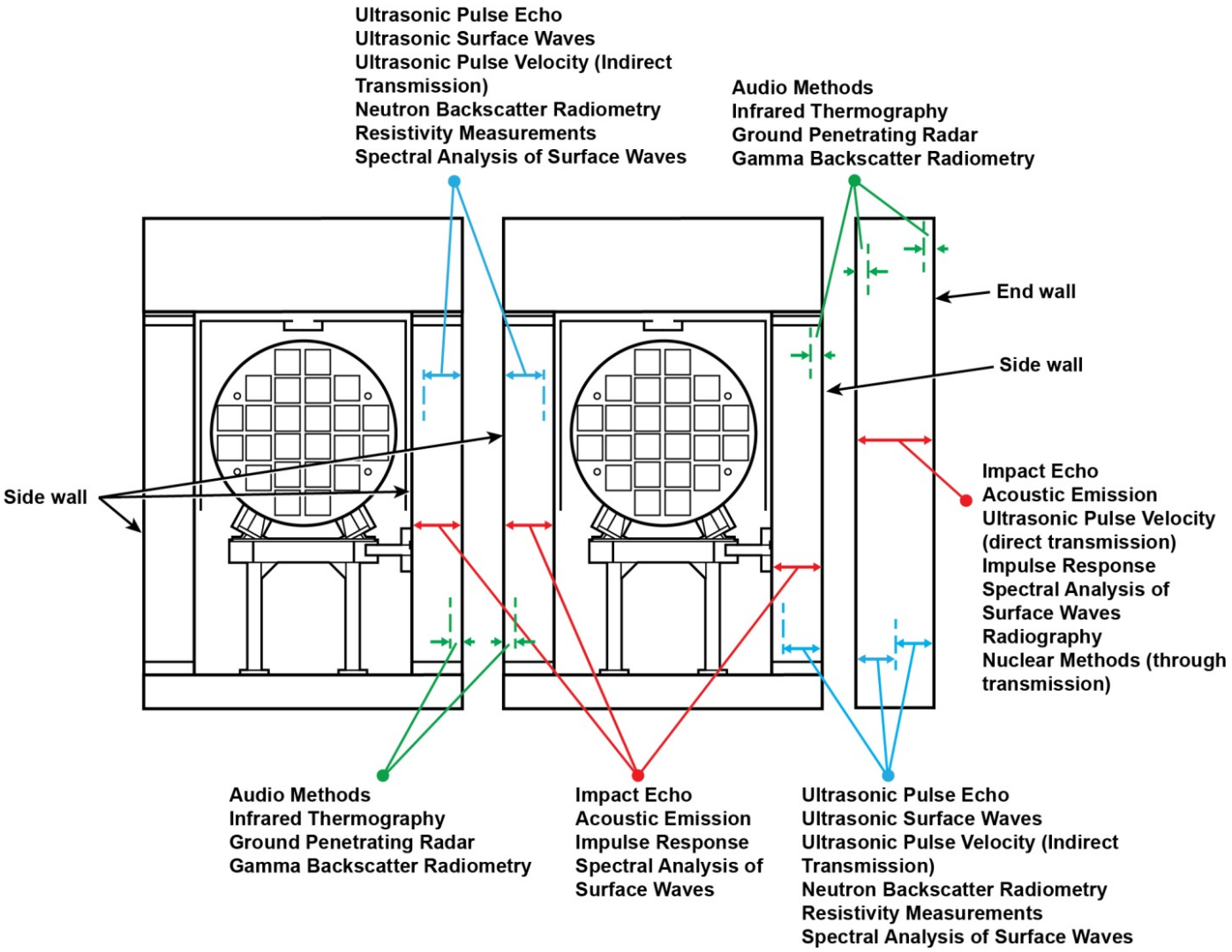

Figure 6.3. Depiction of the Front Cross Section of the HSM 80/102 Module Indicating Regions of the End Wall and Side Walls that are Accessible to NDE Methods Assuming the Gaps between Adjacent HSM Modules and the Gap between the End Wall and HSM Module are/is Accessible. The illustration also indicates approximate depth into components that NDE methods are capable of sampling.

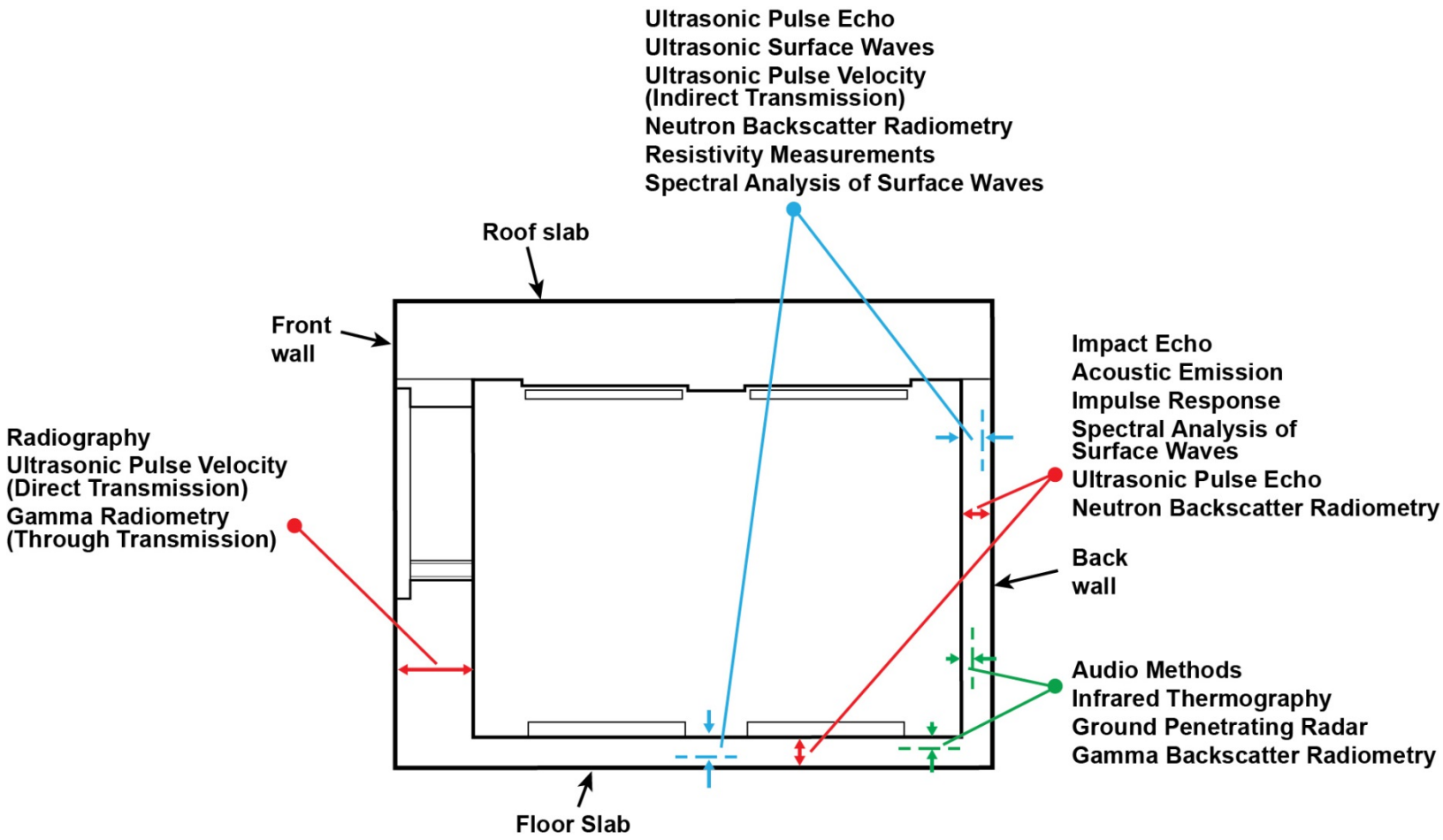

Figure 6.4. Depiction of the Side Cross Section of the HSM 80/102 Module Indicating Regions of the Floor Slab, Back Wall, and Front Wall that became Accessible to NDE Methods Assuming that the Interior of the HSM can be Accessed. The illustration also indicates approximate depth into components that NDE methods are capable of sampling.

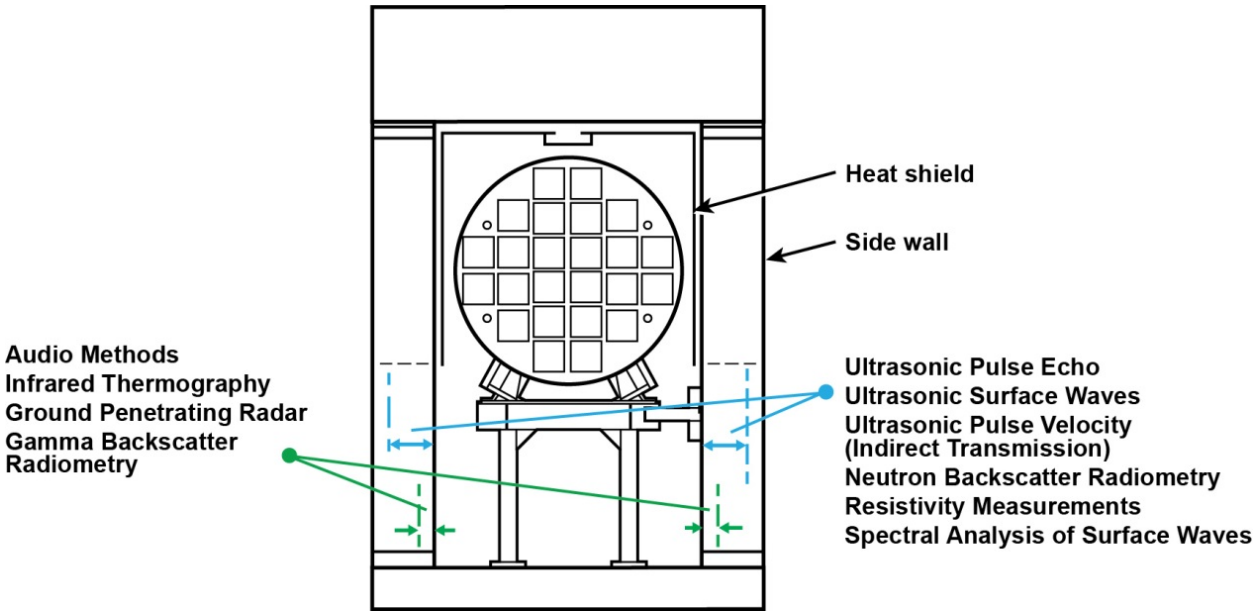

Figure 6.5. Depiction of the Front Cross Section of the HSM 80/102 Module Indicating Regions of the Side Walls that are Accessible to NDE Methods assuming the Interior of HSM Modules are Accessible. The illustration also indicates approximate depth into the Side Walls that NDE methods are capable of sampling.

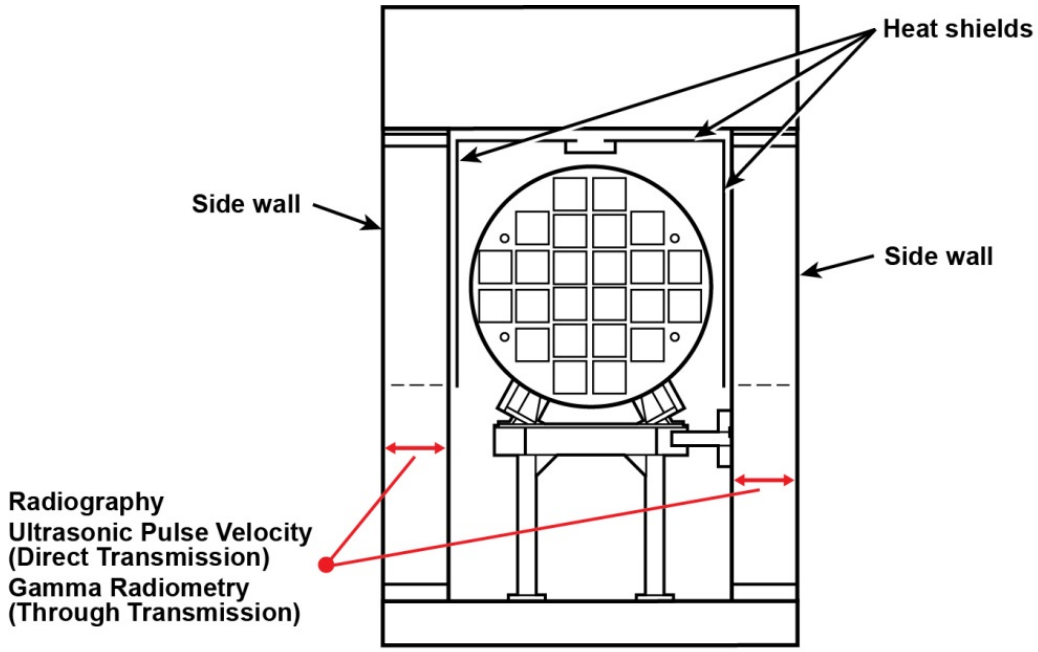

Figure 6.6. Depiction of the Front Cross Section of the HSM 80/102 Module Indicating Regions of the Side Walls that are Accessible to NDE Methods for Full Thickness Sampling Assuming the Interior of HSM Modules and Gaps between HSM Modules are Accessible

7.0 Summary and Conclusions

This report evaluates NDE methods for inspecting concrete and metal canister components of welded canister-type DSSs for spent nuclear fuel by considering applicability to aging effects in concrete and metal materials and compatibility for implementation. The assessment in this report focused on the NUHOMS® HSM 80 and 102 systems. However, the information in Sections 2.0 and 3.0 is not dependent on DSS system design and is applicable to performing similar evaluations for other welded type DSS systems.

Many NDE methods for concrete are considered in this report (see Section 2.1). The NDE methods are based on the propagation of elastic, electromagnetic, or nuclear modalities of energy through concrete specimens. Important considerations include the thickness of structures and the effect of reinforcing steel embedded in concrete structures. Embedded reinforcing steel can adversely impact several of the NDE methods based on all of the energy modalities mentioned above. For GPR testing, heavy reinforcement can limit the ability to sample concrete beyond the cover depth. Several other NDE methods also have limited ability to sample beyond a few inches below the surface such as the audio methods, infrared thermography testing, and backscatter radiometry using gamma rays. The implementation analysis in Section 5.0 and summarized in Section 6.2 indicates that interior HSM concrete surfaces located behind heat shields will be the most difficult to access for inspections, even with the canister removed from the HSM.

Although characteristics of the aggregate (e.g., size, shape, distribution) and other concrete properties, such as density, influence the propagation of energy modalities, the information may not always be known. For relative measurements (i.e., measurements performed over time or at several locations), it is not necessary to know this information because it is only the relative change in concrete properties that is of interest for sampling. Absolute measurements, such as attempts to quantitatively measure strength from a single ultrasonic pulse velocity measurement, require calibration on core samples cut from the test structure, which is undesirable.

The sensitivity of many of the NDE methods for concrete based on the propagation of elastic waves is on the order of one wavelength. For thicker specimens, frequency often must be decreased to counteract the effects of increased signal attenuation. This results in an increase in minimum detectable flaw sizes with increasing specimen thickness or increasing depth of penetration into a concrete specimen.

For the metal canister, the ASME B&PV Code is used primarily as the basis for NDE methods considered, along with currently funded efforts through industry (EPRI) and the DOE to develop inspection technologies for canisters. This limited the scope of NDE methods considered for the metal canister to visual testing, bulk ultrasound testing, guided ultrasonic wave testing, eddy current testing, and acoustic emission testing. The aging effects in metals considered include surface-breaking cracks and localized corrosion. The applicability of NDE methods to cracks in metal is determined on the basis of several studies to assess and document performance of NDE methods for detecting cracks in metallic components in LWRs. In these studies, crack detection was based on direct observation of a crack. Localized corrosion can infer the likelihood of crack formation or may infer that cracking already exists. In this scenario, cracks can be detected indirectly through the observation of localized corrosion. This enhances the potential utility of inspections by visual testing and/or acoustic emission testing for which the performance of crack detection by direct observation may be limited or uncertain relative to eddy current testing or bulk ultrasound testing. To evaluate fitness-for-service, depth sizing must be performed using a volumetric examination technique (e.g., bulk ultrasound testing).

8.0 References

AASHTO. 2012. *AASHTO LRFD Bridge Design Specifications 2012*. American Association of State Highway and Transportation Officials (AASHTO), Washington, D.C.

ACI. 1977. *Guide to Durable Concrete*. American Concrete Institute (ACI), Committee 201, Farmington Hills, Michigan. Available at https://law.resource.org/pub/us/cfr/ibr/001/aci.manual.1.1980.pdf.

ACI. 1980. *Code Requirements for Nuclear Safety Related Concrete Structure and Commentary*. ACI 349-85 and ACI 349R-85, American Concrete Institute (ACI), Detroit, Michigan.

ACI. 1989. *Corrosion of Metals in Concrete*. ACI 222R-89, American Concrete Institute (ACI), Committee 222, Detroit, Michigan.

ACI. 2002. *Evaluation of Existing Nuclear Safety-Related Concrete Structures*. ACI 349.3R-02, American Concrete Institute (ACI), Detroit, Michigan.

ACI. 2006. *ACI Code Requirements for Environmental Engineering*. ACI 350-06, American Concrete Institute (ACI), Farmington Hills, Michigan.

ACI. 2008. *Guide for Conducting a Visual Inspection of Concrete in Service*. ACI 201.1R-08, ACI Committee 201, American Concrete Institute (ACI), Farmington Hills, Michigan.

ACI. 2013a. *ACI Concrete Terminology*. ACI CT-13, American Concrete Institute (ACI), Detroit, Michigan.

ACI. 2013b. *Report on Nondestructive Test Methods for Evaluation of Concrete in Structures*. ACI 228.2R-13, ACI Committee 228, American Concrete Institute (ACI), Farmington Hills, Michigan.

AHEC-IITR. 2013. *Standards/Manuals/Guidelines for Small Hydro Development: 2.2 and 2.3 Civil Works - Hydraulic and Structural Design*. Alternate Hydro Energy Center Indian Institute of Technology Roorkee (AHEC-IITR), with support from Ministry of New and Renewable Energy, Goverment of India, India. Available at http://www.ahec.org.in/publ/standard/standard_pdf/2.2_2.3_Hydraulic_and_structure_design.pdf.

Alleyne DN and P Cawley. 1992. "The Interaction of Lamb Waves with Defects." *IEEE Transactions on Ultrasonics, Ferroelectrics, and Frequency Control* 39:381-397.

Anderson MT, SL Crawford, SE Cumblidge, KM Denslow, AA Diaz and SR Doctor. 2007. *Assessment of Crack Detection in Heavy-Walled Cast Stainless Steel Piping Welds Using Advanced Low-Frequency Ultrasonic Methods*. NUREG/CR-6933, PNNL-16292, U.S. Nuclear Regulatory Commission, Washington, D.C. ADAMS Accession No. ML071020410.

Anderson MT, AA Diaz, AD Cinson, SL Crawford, SE Cumblidge, SR Doctor, KM Denslow and S Ahmed. 2011. *An Assessment of Ultrasonic Techniques for Far-Side Examinations of Austenitic Stainless Steel Piping Welds*. NUREG/CR-7113, PNNL-19353, U.S. Nuclear Regulatory Commission, Washington, D.C.

ASME. 2007a. *2007 ASME Boiler & Pressure Vessel Code, III, Division 2, Code for Concrete Containments: Rules for Construction of Nuclear Facility Components*. American Society of Mechanical Engineers, New York.

ASME. 2007b. "Section XI, Rules for Inservice Inspection of Nuclear Power Plant Components - Division I, Subsection IWG, Reactor Pressure Vessel Internals." In *ASME Boiler and Pressure Vessel Code – An International Code*, American Society of Mechanical Engineers, New York.

ASNT. 2007. *Nondestructive Testing Handbook, Third Edition: Volume 7, Ultrasonic Testing*. PO Moore, D Kishoni and GL Workman, American Society for Nondestructive Testing, Columbus, Ohio.

ASNT. 2010. *Nondestructive Testing Handbook, Third Edition: Volume 9, Visual Testing*. MW Allgaier, RE Cameron and PO Moore, American Society for Nondestructive Testing, Columbus, Ohio.

ASTM. 2009a. *Standard Test Method for Corrosion Potentials of Uncoated Reinforcing Steel in Concrete*. ASTM C876-09, ASTM International, West Conshohocken, Pennsylvania.

ASTM. 2009b. *Standard Test Method for Pulse Velocity Through Concrete*. ASTM C597-09, ASTM International, West Conshohocken, Pennsylvania. ASTM C597-09.

ASTM. 2010. *Standard Practice for Evaluating the Condition of Concrete Plates Using the Impulse-Response Method*. ASTM C1740-10, ASTM International, West Conshohocken, Pennsylvania.

ASTM. 2012a. *Standard Guide for Acoustic Emission of Small Parts*. ASTM E1932-12, ASTM International, West Conshohocken, Pennsylvania.

ASTM. 2012b. *Standard Guide for Mounting Piezoelectric Acoustic Emission Sensors*. ASTM E650/E650M-12, ASTM International, West Conshohocken, Pennsylvania.

ASTM. 2012c. *Standard Practice for Measuring Delaminations in Concrete Bridge Decks by Sounding*. ASTM D4580/D4580M-12, ASTM International, West Conshohocken, Pennsylvania.

ASTM. 2013a. *Standard Guide for Examination and Evaluation of Pitting Corrosion*. ASTM G46, ASTM International, West Conshohocken, Pennsylvania.

ASTM. 2013b. *Standard Test Method for Detecting Delaminations in Bridge Decks Using Infrared Thermography*. ASTM D4788-03 (Reapproved 2013), ASTM International, West Conshohocken, Pennsylvania.

ASTM. 2013c. *Standard Test Methods for In-Place Density of Unhardened and Hardened Concrete, Including Roller Compacted Concrete, By Nuclear Methods*. ASTM C1040/C1040M-08 (Reapproved 2013), ASTM International, West Conshohocken, Pennsylvania.

ASTM. 2015a. *Standard Test Method for Determining the Thickness of Bound Pavement Layers Using Short-Pulse Radar*. ASTM D4748-10 (Reapproved 2015), ASTM International, West Conshohocken, Pennsylvania.

ASTM. 2015b. *Standard Test Method for Evaluating Asphalt-Covered Concrete Bridge Decks Using Ground Penetrating Radar*. ASTM D6087-08 (Reapproved 2015), ASTM International, West Conshohocken, Pennsylvania.

ASTM. 2015c. *Standard Test Method for Measuring the P-Wave Speed and the Thickness of Concrete Plates Using the Impact-Echo Method*. ASTM C1383-15, ASTM International, West Conshohocken, Pennsylvania.

Bentley PG. 1981. "A Review of Acoustic Emission for Pressurised Water Reactor Applications." *NDT International* 14(6):329-335.

Caltrans. 2015. "Chapter 10, Concrete Decks." In *Bridge Design Practice*, California Department of Transportation (Caltrans), Sacramento, California. Available at http://www.dot.ca.gov/hq/esc/techpubs/manual/bridgemanuals/bridge-design-practice/pdf/bdp_10.pdf.

Carino NJ. 2001. "The Impact-Echo Method: An Overview." In *Proceedings of the 2001 Structures Congress and Exposition*, pp. 1-18. May 21-23, 2001, Washington, D.C. DOI 10.1061/40558(2001)15. American Society of Civil Engineers, Reston, Virginia.

Carino NJ. 2004. "Methods to Evaluate Corrosion of Reinforcement." In *Handbook on Non-destructive Testing of Concrete*, eds: VM Malhotra and NJ Carino. CRC Press, Boca Raton, Florida.

Caseres L and TS Mintz. 2010. *Atmospheric Stress Corrosion Cracking Susceptibility of Welded and Unwelded 304, 304L, and 316L Austenitic Stainless Steels Commonly Used for Dry Cask Storage Containers Exposed to Marine Environments*. NUREG/CR-7030, U.S. Nuclear Regulatory Commission, Washington, D.C.

Chavel B. 2012. *Steel Bridge Design Handbook: Bridge Deck Design*. FHWA-IF-12-052--Vol. 17, U.S. Department of Transportation Federal Highway Administration, Washington, D.C.

Cheeke JDN. 2002. *Fundamentals and Applications of Ultrasonic Waves*. CRC Press, Boca Raton. ISBN 0849301300.

Choi KY and SS Kim. 2005. "Morphological Analysis and Classification of Types of Surface Corrosion Damage by Digital Image Processing." *Corrosion Science* 47(1):1-15. http://dx.doi.org/10.1016/j.corsci.2004.05.007.

Clark MR, DM McCann and MC Forde. 2003. "Application of Infrared Thermography to the Non-destructive Testing of Concrete and Masonry Bridges." *NDT & E International* 36(4):265-275.

Clayton D, AP Albright and JH Santos-Villalobos. 2014. *Initial Investigation of Improved Volumetric Imaging of Concrete Using Advanced Processing Techniques*. ORNL/TM-2014/362, Oak Ridge National Laboratory, Oak Ridge, Tennessee.

Clayton D, C Smith, CC Ferraro, J Nelson, L Khazanovich, K Hoegh, S Chintakunta, J Popovics, H Choi and S Ham. 2013. *Evaluation of Ultrasonic Techniques on Concrete Structures*. ORNL/TM-2013/430, Oak Ridge National Laboratory, Oak Ridge, Tennessee.

Codaro EN, RZ Nakazato, AL Horovistiz, LMF Ribeiro, RB Ribeiro and LRO Hein. 2002. "An Image Processing Method for Morphology Characterization and Pitting Corrosion Evaluation." *Materials Science and Engineering: A* 334(1–2):298-306.

Cumblidge SE, MT Anderson and SR Doctor. 2004. *An Assessment of Visual Testing*. NUREG/CR-6860, PNNL-14635, U.S. Nuclear Regulatory Commission, Washington, D.C. ADAMS Accession No. ML043630040.

Cumblidge SE, MT Anderson, SR Doctor, FA Simonen and AJ Elliot. 2007. *A Study of Remote Visual Methods to Detect Cracking in Reactor Components*. NUREG/CR-6943, PNNL-16472, U.S. Nuclear Regulatory Commission, Washington, D.C. ADAMS Accession No. ML073110060.

Cumblidge SE, SR Doctor, PG Heasler and TT Taylor. 2010. *Results of the Program for the Inspection of Nickel Alloy Components*. NUREG/CR-7019; PNNL-18713, Rev. 1, U.S. Nuclear Regulatory Commission, Washington, D.C.

Davis JM. 1998. "Advanced Ultrasonic Flaw Sizing Handbook." *NDT.net* 3(11).

Ekstrom P and J Wåle. 1995. *Crack Characterization for In-service Inspection Planning*. SKI Report 95:70, Swedish Nuclear Power Inspectorate, Stockholm, Sweden.

Ensminger D and LJ Bond. 2011. *Ultrasonics: Fundamentals, Technology and Applications, Third Edition (Revised and Expanded)*. CRC Press, Boca Raton, Florida.

EPRI. 2005. *BWR Vessel and Internals Project, Reactor Vessel Pressure Vessel and Internals Examination Guidelines*. TR-105696-R8 (BWRVIP-03 Rev. 8), Electric Power Research Institute (EPRI), Boiling Water Reactor Owners Group's Vessel and Internals Project, Palo Alto, California.

EPRI. 2015a. *Degradation Mechanisms and Inspection Techniques for Concrete Structures in Dry Storage Systems for Spent Nuclear Fuel*. TR-3002005508, Electric Power Research Institute (EPRI), Palo Alto, California.

EPRI. 2015b. *Materials Reliability Program: Pressurized Water Reactor Internals Inspection and Evaluation Guidelines (MRP-227, Revision 1)*. Final Report 3002005349, Electric Power Research Institute (EPRI), Palo Alto, California.

EPRI. 2016. *Dry Canister Storage System Inspection and Robotic Delivery System Development*. Report 3002008234, Electric Power Research Institute (EPRI), Palo Alto, California.

Golaski L, P Gebski and K Ono. 2002. "Diagnostics of Reinforced Concrete Bridges by Acoustic Emission." *Journal of Acoustic Emission* 20:83-98.

Gostautas RS, JC Duke Jr. and T Shiotani. 2005. "Acoustic Emission Testing of Infrastructure." In *Nondestructive Testing Handbook, Volume 6: Acoustic Emission Testing*, eds: RK Miller, EK Hill and PO Moore. American Society for Nondestructive Testing, Columbus, Ohio.

Greene SR, JS Medford and SA Macy. 2013. *Storage and Transport Cask Data For Used Commercial Nuclear Fuel – 2013 U.S. Edition*. ATI-TR-13047, Advanced Technology Insights, LLC, Knoxville, Tennessee.

Hagemaier DJ. 1990. *Fundamentals of Eddy Current Testing*. American Society for Nondestructive Testing, Columbus, Ohio.

He X, T Mintz, R Pabalan, L Miller and G Oberson. 2014. *Assessment of Stress Corrosion Cracking Susceptibility for Austenitic Stainless Steels Exposed to Atmospheric Chloride and Non-Chloride Salts*. NUREG/CR-7170, U.S. Nuclear Regulatory Commission, Washington, D.C.

Heasler PG and SR Doctor. 1996. *Piping Inspection Round Robin*. NUREG/CR-5068, PNL-10475, U.S. Nuclear Regulatory Commission, Washington, D.C.

Heasler PG and SR Doctor. 2003. *A Comparison of Three Round Robin Studies on ISI Reliability of Wrought Stainless Steel Piping*. NUREG/CR-6795, PNNL-13873, U.S. Nuclear Regulatory Commission, Washington, D.C.

Heasler PG, TT Taylor, JC Spanner, SR Doctor and JD Deffenbaugh. 1990. *Ultrasonic Inspection Reliability for Intergranular Stress Corrosion Cracks: A Round Robin Study of the Effects of Personnel, Procedures, Equipment and Crack Characteristics*. NUREG/CR-4908, PNL-6196, U.S. Nuclear Regulatory Commission, Washington, D.C.

Helmerich R, M Krause, F Mielentz, E Niederleithinger, A Taffe and G Wilsch. 2013. *Non-destructive Testing of Nuclear Power Plant Concrete Structures State of the Art Report*. Bundesanstalt fur Materialforschung und -prufung (BAM), Berlin, Germany.

Hoegh K, L Khazanovich and H Yu. 2011. "Ultrasonic Tomography for Evaluation of Concrete Pavements." *Transportation Research Record: Journal of the Transportation Research Board* 2232:85-94.

Hutton PH, MA Friesel and JF Dawson. 1993. *Continuous AE Crack Monitoring of a Dissimilar Metal Weldment at Limerick Unit 1*. NUREG/CR-5963, PNL-8844, U.S. Nuclear Regulatory Commission, Washington, D.C.

IAEA. 2002. *Guidebook on Non-destructive Testing of Concrete Structures*. Training Course Series No. 17, International Atomic Energy Agency, Vienna, Austria.

IAEA. 2004. *Design of Reactor Containment Systems for Nuclear Power Plants*. Safety Guide No. NS-G-1.10, International Atomic Energy Agency, Vienna, Austria.

Kemppainen M and I Virkkunen. 2011. "Crack Characteristics and Their Importance to NDE." *Journal of Nondestructive Evaluation* 30:143-157.

Kim DS, HW Kim, WS Seo, KC Choi and SK Woo. 2002. "Feasibility Study of the IE-SASW Method for Nondestructive Evaluation of Containment Building Structures in Nuclear Power Plants." *Nuclear Engineering and Design* 219(2):97-110.

Kim DS, WS Seo and KM Lee. 2006. "IE–SASW Method for Nondestructive Evaluation of Concrete Structure." *NDT & E International* 39(2):143-154.

Kittel C. 1949. "Physical Theory of Ferromagnetic Domains." *Review of Modern Physics* 21(4):541-583.

Lareau JP. 2014. "Operating Experience with Chloride Induced Stress Corrosion Cracking (CISCC)." Presented at December 3, 2014, 2014 EPRI Extended Storage Collaboration Program Meeting, Charlotte, North Carolina. PNNL-SA-106950.

Lowe MJS and P Cawley. 2006. *Long Range Guided Wave Inspection Usage - Current Commercial Capabilities and Research Directions*. Imperial College, London.

Macleod ID, R Rowley, MJ Beesley and P Olley. 1991. "Acoustic Monitoring Techniques for Structural Integrity." *Nuclear Engineering and Design* 129:191-200.

MDT. 2002. "Chapter 15, Bridge Decks." In *Montana Structures Manual, Vol. II - Structural Design*, Montana Department of Transportation (MDT), Helena, Montana. Available at http://www.mdt.mt.gov/other/bridge/external/structures-manual/part_II/chp-15-final.pdf.

Meyer R, A Pardini, J Cuta, H Adkins, A Casella, A Qiao, MR Larche, A Diaz and SR Doctor. 2013a. *NDE to Manage Atmospheric SCC in Canisters for Dry Storage of Spent Fuel: An Assessment*. PNNL-22495, Pacific Northwest National Laboratory, Richland, Washington. ADAMS Accession No. ML13276A196.

Meyer R, A Pardini, B Hanson and K Sorenson. 2013b. *Review of NDE Methods for Detection and Monitoring of Atmospheric SCC in Welded Canisters for the Storage of Used Nuclear Fuel*. FCRD-UFD-2013-000085, PNNL-22158, Pacific Northwest National Laboratory, Richland, Washington.

Meyer RM, P Ramuhalli, TL Moran, CA Nove and AF Pardini. 2012. "Understanding the Challenges in the Transition from Film to Digital Radiography in the Nuclear Power Industry." In *9th International Conference on Nondestructive Evaluation in Relation to Structural Integrity for Nuclear and Pressurized Components*, pp. 478-487. May 22-24, 2012, Seattle, Washington. Joint Research Centre, European Commission, Brussels, Belgium.

Miller CG. 2010. Letter to JA Franke. "Crystal River Nuclear Plant - Special Inspection Report 05000302/2009007." October 12, 2010, U.S. Nuclear Regulatory Commission, Region II, Atlanta, Georgia. ADAMS Accession No. ML102861026.

Mindess S. 2004. "Acoustic Emission Methods." In *Handbook on Non-destructive Testing of Concrete*, eds: VM Malhotra and NJ Carino. CRC Press, Boca Raton, Florida.

Mitchell TM. 2004. "Radioactive/Nuclear Methods." In *Handbook on Non-destructive Testing of Concrete*, eds: VM Malhotra and NJ Carino. CRC Press, Boca Raton, Florida.

Moran TL, MS Prowant, CA Nove, AF Pardini, SL Crawford, AD Cinson and MT Anderson. 2015. *Applying Ultrasonic Testing in Lieu of Radiography for Volumetric Examination of Carbon Steel Piping*. NUREG/CR-7204, PNNL-24232, U.S. Nuclear Regulatory Commission, Washington, D.C. ADAMS Accession No. ML1525A674.

Moran TL, P Ramuhalli, AF Pardini, MT Anderson and SR Doctor. 2010. *Replacement of Radiography with Ultrasonics for the Nondestructive Inspection of Welds - Evaluation of Technical Gaps - An Interim Report*. PNNL-19086, Pacific Northwest National Laboratory, Richland, Washington. NRC ADAMS #ML101031254.

Naik TR, VM Malhotra and JS Popovics. 2004. "The Ultrasonic Pulse Velocity Method." In *Handbook on Non-destructive Testing of Concrete*, eds: VM Malhotra and NJ Carino. CRC Press, Boca Raton, Florida.

Nair A and CS Cai. 2010. "Acoustic Emission Monitoring of Bridges: Review and Case Studies." *Engineering Structures* 32(6):1704-1714.

Naus DJ. 2009a. *Inspection of Nuclear Power Plant Structures - Overview of Methods and Related Applications*. ORNL/TM-2007/191, Oak Ridge National Laboratory, Oak Ridge, Tennessee.

Naus DJ. 2009b. "The Management of Aging in Nuclear Power Plant Concrete Structures." *Journal of the Minerals, Metals and Materials Society* 61(7):35-41.

Nazarian S, KH Stokoe II and WR Hudson. 1983. "Use of Spectral Analysis of Surface Waves Method for Determination of Moduli and Thicknesses of Pavement Systems." *Transportation Research Record* 930:38-45.

Nazarian S, D Yuan and MR Baker. 1995. *Rapid Determination of Pavement Moduli with Spectral-Analysis-of-Surface-Waves Method*. Research Report 1243-1, The Center for Geotechnical and Highway Materials Research, The University of Texas at El Paso, El Paso, Texas.

Nielsen J and DF Griffin. 1977. "Acoustic Emission of Plain Concrete." *Journal of Testing and Evaluation* 5(6):476-483.

NRC. 2012. *Potential Chloride-Induced Stress Corrosion Cracking of Austenitic Stainless Steel and Maintenance of Dry Cask Storage System Canisters*. NRC Information Notice 2012-20, U.S. Nuclear Regulatory Commission (NRC), Washington, D.C. ADAMS Accession No. ML12319A440.

NRC. 2016. *Standard Review Plan for Renewal of Specific Licenses and Certificates of Compliance for Dry Storage of Spent Nuclear Fuel*. NUREG-1927, Rev. 1, U.S. Nuclear Regulatory Commission, Washington, D.C. ADAMS Accession No. ML16179A148.

Ohtsu M, T Isoda and Y Tomoda. 2007. "Acoustic Emission Techniques Standardized for Concrete Structures." *Journal of Acoustic Emission* 25:21-32.

PAC. 2005. *DiSP with AEwin, User's Manual, Rev. 3*. PAC Part #: 6320-1001, Physical Acoustics Corporation (PAC), Princeton Junction, New Jersey.

Pidaparti RM, B Hinderliter and D Maskey. 2013. "Evaluation of Corrosion Growth on SS304 Based on Textural and Color Features from Image Analysis." *ISRN Corrosion* 2013. Article ID 376823. http://dx.doi.org/10.1155/2013/376823.

Rao DSP. 2008. "Infrared Thermography and Its Applications in Civil Engineering." *The Indian Concrete Journal* May:41-50.

Renshaw J. 2014. "NDE for Dry Canister Storage System Inspection." Presented at *EPRI Extended Storage Collaboration Program December 2014 Meeting*, December 2-4, 2014, Charlotte, North Carolina.

Renshaw JB, M Guimaraes and DB Scott. 2014. "Thermographic Inspection of Massive Structures." In *Proceedings of the 40th Annual Review of Progress in Quantitative Nondestructive Evaluation*, pp. 978-984. July 21-26, 2013, Baltimore, Maryland. DOI 10.1063/1.4864927. American Institute of Physics, Melville, New York.

Rose JL. 1999. *Ultrasonic Waves in Solid Media*. Cambridge University Press, Cambridge, United Kingdom.

Runow P. 1985. "Use of Acoustic Emission Methods as Aids to the Structural Integrity Assessment of Nuclear Power Plants." *International Journal of Pressure Vessels and Piping* 21(3):157-207.

Sack DA and LD Olson. 2006. "Concrete Spillway and Dam Inspection Using Nondestructive Techniques." In *HydroVision 2006*. July 31-August 4, 2006, Portland, Oregon. HCI Publications, Kansas City, Missouri. CD ROM. Available at http://www.olsoninstruments.com/pdf_downloads/Concrete%20Spillway%20and%20Dam%20Inspection_usingNDT.pdf.

Sansalone M and WB Streett. 1997. *Impact-Echo: Non-Destructive Evaluation of Concrete and Masonry*. Bullbrier Press, Jersey Shore, Pennsylvania. ISBN 0-9612610-6-4.

Scruby CB. 1987. "An Introduction to Acoustic Emission." *Journal of Physics E: Scientific Instruments* 20(8):946-953.

Shah VN and CJ Hookham. 1998. "Long-term Aging of Light Water Reactor Concrete Containments." *Nuclear Engineering and Design* 185:51-81.

Sheu JC, KH Stokoe and JM Roesset. 1988. "Effect of Reflected Waves in SASW Testing of Pavements." *Transportation Research Record* 1196:51-61.

TRB. 2013. *Nondestructive Testing to Identify Concrete Bridge Deck Deterioration*. SHRP2 Report S2-R06A-RR-1, Transportation Research Board (TRB), Washington, D.C. Strategic Highway Research Program (SHRP2) Renewal Research. Available at http://onlinepubs.trb.org/onlinepubs/shrp2/SHRP2_S2-R06A-RR-1.pdf.

USBR. 1987. *Design of Small Dams (The Third Edition)*. United States Department of the Interior, Bureau of Reclamation (USBR), Washington, D.C. Available at http://www.usbr.gov/pmts/hydraulics_lab/pubs/manuals/SmallDams.pdf.

Van Velsor JK, MS Lindsey and OM Malinowski. 2014. "Short-Range Guided Wave Testing of DCSS with Low-Profile EMATs - Feasibility for Inspection of Dry Canister Storage Systems." Presented at *EPRI Extended Storage Collaboration Program December 2014 Meeting*, December 2-4, 2014, Charlotte, North Carolina.

Wåle J. 2006. *Crack Characterisation for In-service Inspection Planning - An Update*. SKI Report 2006:24, Swedish Nuclear Power Inspectorate, Stockholm, Sweden.

Weritz F, R Arndt, M Röllig, C Maierhofer and H Wiggenhauser. 2005. "Investigation of Concrete Structures with Pulse Phase Thermography." *Materials and Structures* 38(9):843-849.

Yuyama S. 1986. "Fundamental Aspects of Acoustic Emission Applications to the Problems Caused by Corrosion." In *Corrosion Monitoring in Industrial Plants Using Nondestructive Testing and Electrochemical Methods*, pp. 43-74. eds: GC Moran and P Labine. ASTM, Philadelphia, Pennsylvania.

Yuyama S, K Yokoyama, K Niitani, M Ohtsu and T Uomoto. 2007. "Detection and Evaluation of Failures in High-Strength Tendon of Prestressed Concrete Bridges by Acoustic Emission." *Construction and Building Materials* 21(3):491-500.

Appendix A

Descriptions of Other Concrete Structural Members

Appendix A

Descriptions of Other Concrete Structural Members

This section provides brief descriptions of other concrete structural members including bridge decks, dams, and reactor containments. The purpose of this section is to enable comparison of features of these concrete structural members to concrete components of HSMs. In addition, information regarding NDE methods employed to the inspection of these components is included to highlight techniques that may be applicable to similar concrete components in HSMs.

A.1 Bridge Design – Concrete Decks

Bridge decks are integral part of a bridge structure, which supports the vertical loads from motor vehicles and directly transfers these loads to the major load-carrying structure. A bridge deck is typically continuous along the span of the bridge and across the width of the span. Concrete decks of a bridge structure can be constructed with cast-in-place or precast methods, and both methods typically include steel reinforcement in the longitudinal and transverse directions (Caltrans 2015).

Designers need to consider required deck thickness. The American Association of State Highway and Transportation Officials (AASHTO 2012) common requires that minimum thickness of concrete deck should not be less than 175 mm (7 in.), excluding any provision for grinding, grooving, and sacrificial surfaces. The typical deck slab thickness varies from 175 to 266 mm (7 to 10-3/8 in.) depending on the girder type and spacing (Caltrans 2015). It is important to check the main longitudinal reinforcement spacing and cover to ensure reinforcing steel can fit within the slab thickness (Chavel 2012). Bridge decks also need to consider corrosion problems. On bridges, salt applied in ice control operations are absorbed by the concrete decks, curbs, railings. In such locations, a minimum cover of 50 mm (2 in.) is recommended (ACI 1977). Figure A.1 is a schematic of a reinforced concrete bridge deck provided in accordance with the AASHTO LRFD Bridge Design Specifications (AASHTO 2012).

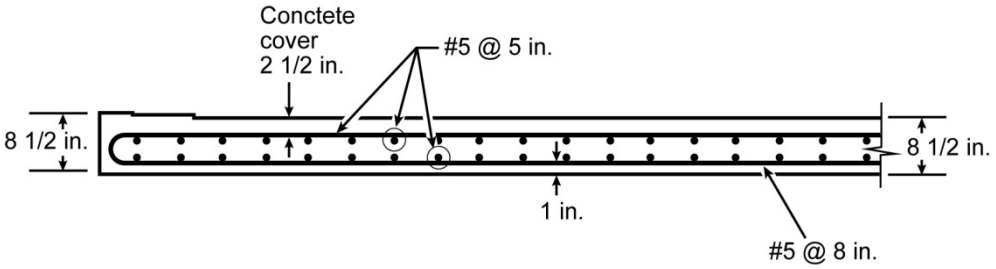

Figure A.1. Typical Concrete Deck (Bridge) Reinforcement (AASHTO 2012)

The most common bridge maintenance problem is the deterioration of concrete bridge decks (MDT 2002). Evaluation methods of identifying bridge deck conditions are for the following deterioration types: 1) delamination, 2) corrosion, 3) cracking, and 4) concrete degradation. Current inspection techniques include nondestructive testing (NDT) and partially destructive testing (PDT). Conventional NDT methods, such as normal chain dragging, hammer sounding, and visual methods, rely on the experience of the inspectors. PDT methods, such as material samples, Windsor probe, and chloride ion testing, are costly and typically cause some damage to the bridge deck. The information collected by most NDT/PDT methods is typically raw data and the information must be analyzed by a specialist to avoid false data under certain conditions. All inspections should be conducted in accordance with applicable American

Society for Nondestructive Testing (ASNT) procedures, American Society for Testing and Materials (ASTM) standards, and AASHTO specifications.

Other NDT techniques, such as impact-echo, ultrasonic pulse echo, ultrasonic surface waves, impulse response, ground penetrating radar (GPR), infrared thermography, microwave moisture technique, eddy current, half-cell potential, galvanostatic pulse measurement, and electrical resistivity have been developed for inspecting concrete bridge decks. These NDT techniques can provide detailed and accurate information about under-the-surface conditions of bridge decks. In order to offer an independent evaluation of the capabilities and limitations of the most common NDT techniques to detect and characterize typical deterioration mechanisms in concrete bridge deck, The Second Strategic Highway Research Program (SHRP 2) (TRB 2013) conducted a series of experiments to evaluate various NDT equipment from different manufacturers. The products from the manufacturers were evaluated on the basis of the same tests, the same environment factors, and the same performance metrics. SHRP 2 evaluated the NDT technologies from the perspective of speed, accuracy, precision, and ease-of-use. The information gathered from the tested technologies was summarized and ranked based on their performance, as shown in Table A.1.

Table A.1. Overview of NDT Technologies for Bridge Deck Deterioration Detection (TRB 2013)

Deterioration Type	Delamination	Corrosion	Vertical Cracks	Concrete Degradation
Impact echo	x		x	x
Ultrasonic surface waves	x		x	x
Ground penetrating radar	x	x		
Half-cell potential		x		
Galvanostatic pulse measurement		x		
Electrical resistivity		x		
Infrared thermography	x			
Chain dragging/hammer sounding	x			

NA = not applicable.

A.2 Concrete Dams

A dam is a hydraulic structure that impounds water. It is usually built across the river to create a reservoir on its upstream side for various purposes, which include irrigation, human consumption, industrial use, aquaculture, and navigability. Hydropower is often used in conjunction with dams to generate electricity. According to *Design of Small Dams* (USBR 1987), the classification usually recognizes the basic type constructed today; namely, earthfill dams, rockfill dams, concrete arch dams, and concrete gravity dams. The construction of earthfill and rockfill dams involves locally available natural materials. A concrete gravity dam is designed to use its own weight to resist the external forces. A concrete arch dam is curved or convex upstream in plan. The force of the water squeezes the arch, compressing and strengthening its structure, and pushing it into its foundation or abutments. Figures A.2 and A.3 are typical sections of concrete gravity and arc dams, respectively.

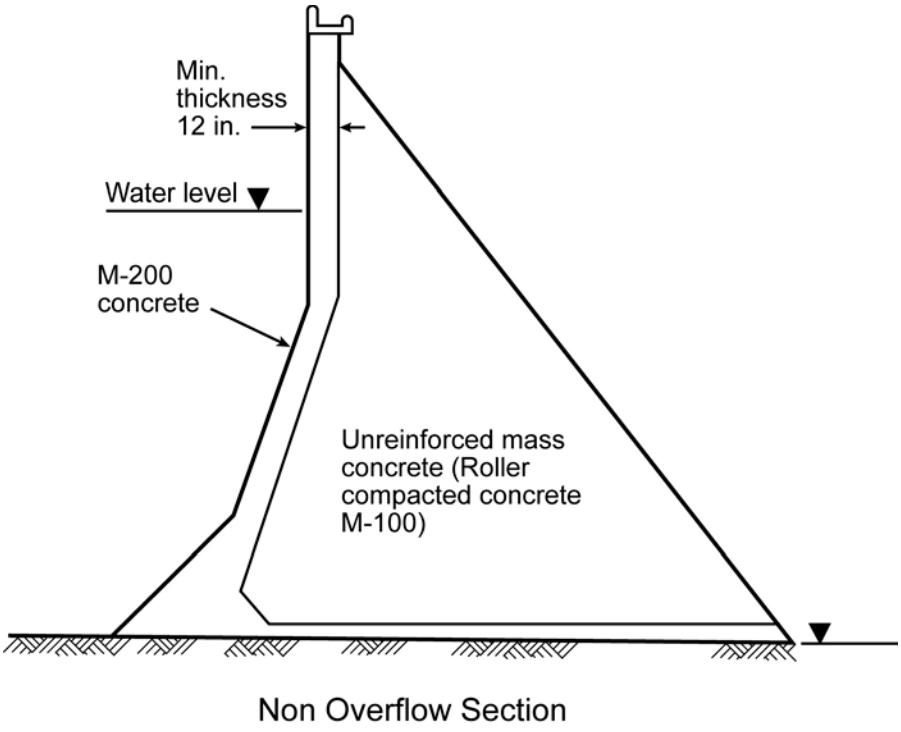

Figure A.2. Schematic of Typical Section of a Concrete Gravity Dam (AHEC-IITR 2013)

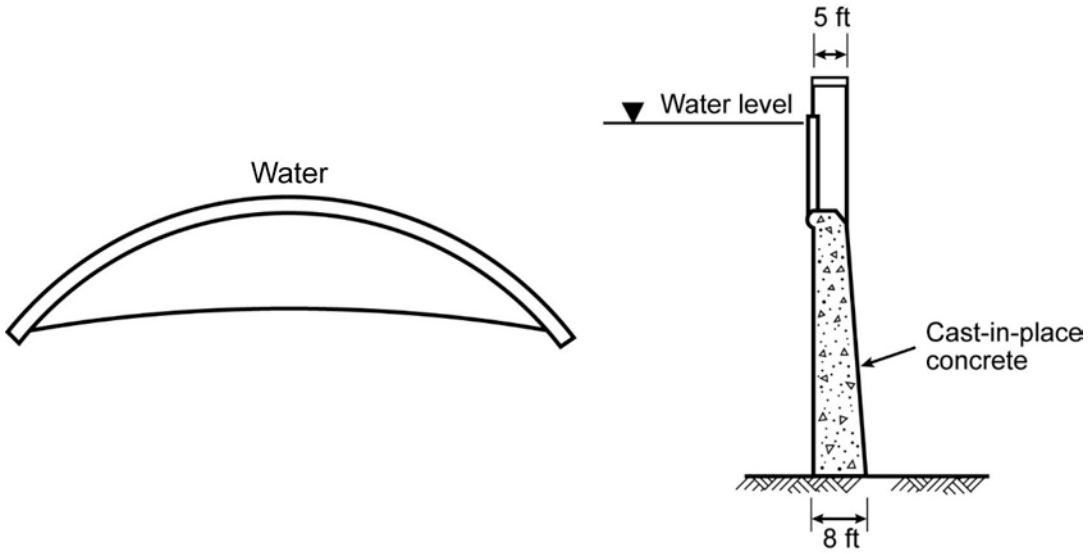

Figure A.3. Schematic of Typical Plan and Section of a Concrete Arch Dam (AHEC-IITR 2013)

For a concrete gravity or arch dam, the whole structure with its ancillary structures (such as spillways) is constructed of concrete. It needs to meet the design criteria for strength, durability, permeability, and other requirements. A spillway is a key feature of a dam, which is a hydraulic structure that passes normal (operational) and/or flood flows in a manner that protects the structural integrity of the dam and/or dikes. It can be controlled or uncontrolled, and can be considered a safety device in a dam, like a safety valve in a boiler.

For most hydraulic structures, ACI 350-06 (ACI 2006) is used to establish minimum reinforced concrete design levels. For significant and high-hazard storage and multipurpose dams and their appurtenant structures (such as spillways), a risk-based evaluation, analysis, and/or design is typically needed, resulting in designs meeting or exceeding the criteria in applicable ACI building codes.

The size of reinforcing bars should be chosen recognizing that cracking can be better controlled by using a larger number of small-diameter bars rather than fewer large-diameter bars. The size of reinforcing bars should not exceed #11. The minimum rebar size is a #4 bar for temperature and shrinkage reinforcement requirements. Spacing of reinforcing bars should be limited to a maximum of 300 mm (12 in.). Concrete cover should be at least 50 mm (2 in.). The minimum thickness of any minor member is 150 mm (6 in.), and when 50 mm (2 in.) cover is required, then it is at least 200 mm (8 in.). Concrete base minimum cover is required 75 mm (3 in.) (ACI 2006).

Below is a table from ACI 350 for concrete covers.

Table A.2. Concrete Minimum Cover Requirements (ACI 2006)

Cover Condition	Minimum Cover, mm (in.)
(a) Concrete cast against and permanently exposed to earth	75 (3)
(b) Concrete exposed to earth or weather, or cast against a concrete work mat:	
Slab and joist	50 (2)
Beams and columns	50 (2)
Walls	50 (2)
Footings and base slabs	50 (2)

Inspections of concrete dams should include close observations for detecting abnormal settlements, heaving, deflections, or lateral movement between structures (USBR 1987). For the close observations, the inspections should involve visual inspection of the dam, which can provide a regular and basic way to make an assessment of the dam's condition. There are a number of NDT methods that can be used to investigate the condition of concrete dam structures as well. The NDT methods, such as sonic/ultrasonic impact echo, spectral analysis of surface waves, slab impulse response, GPR, and cross-dam tomography, are relatively inexpensive ways to determine the extent of damage of concrete dams. The NDT methods are applicable to a variety of concrete elements found on many types of dams. These elements include spillway concrete evaluation, spillway subgrade evaluation, dam wall concrete evaluation, and thin-arch dam interior evaluation (Sack and Olson 2006). Sonic/ultrasonic impact echo and GPR are used to identify voided areas under spillways. Sonic/ultrasonic pulse velocity and impact-echo measurements are also used to determine the condition and integrity of dam and spillway concrete. Many dams and spillways have a shotcrete coating that hides internal deteriorated, weakened concrete from view; in these cases, NDT can use sonic/ultrasonic tomographic data to contour the interior of the structure to locate internal weakness.

A.3 Reactor Containment Structure

Concrete structural elements in nuclear reactor containment structures serve an important role in creating a barrier against environmental degradation and in supporting the functional apparatus that keeps the reactor running. Although concrete structures fall into many different categories in light water reactors (LWRs), those involved in primary containment are described here. Primary containment, in most cases,

surrounds all components that support the primary coolant loop (IAEA 2004) and is made out of either prestressed or reinforced concrete (Naus 2009b). These structures are used in both PWRs and BWRs and are heavily reinforced with mild carbon steel.

Reactor containment is composed of a cylindrical wall, a dome, and a base or basemat, with a 6.3 mm (0.25 in.) carbon steel liner attached on the inside to form a leak-tight barrier (Shah and Hookham 1998). Primary containment systems come in a variety of permutations, but they all share at least these three features in common. The general appearance of this configuration is shown in Figure A.4. As this figure shows, a large portion of the containment structure is below grade, which has significant implications regarding the environmental exposure expected for each portion. The total size of these containers can be 40 to 50 m (131 to 164 ft.) in diameter and 60 to 70 m (197 to 230 ft.) high with dome thicknesses from 0.9 to 1.4 m (3 to 4.6 ft.) and basemat thicknesses from 2.7 to 4.1 m (8.9 to 13.5 ft.) (Naus 2009b). Cylindrical wall thickness, as illustrated in Figure A.5, is approximately 1.4 m (4.5 ft.) thick.

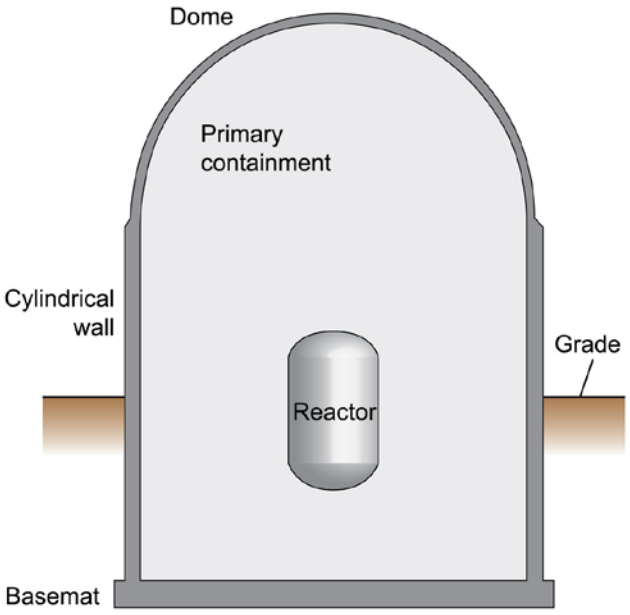

Figure A.4. Schematic Illustration of LWR Primary Containment Showing Key Sections

The concrete is typically composed of Portland cement and is reinforced heavily with steel bars that run both horizontally and vertically in both the side walls and the dome. Concrete primary containments in U.S. nuclear reactors are either reinforced concrete or of prestressed concrete structures. Prestressed concrete structures are not considered here because they are not relevant to HSMs.

Over the outermost layer of structural rebar is a layer of "cover concrete," which is mandated to be at least 19–76-mm thick by the relevant design codes: ACI 222R (1989) and ASME Boiler and Pressure Vessel Code, Section III (ASME 2007a).

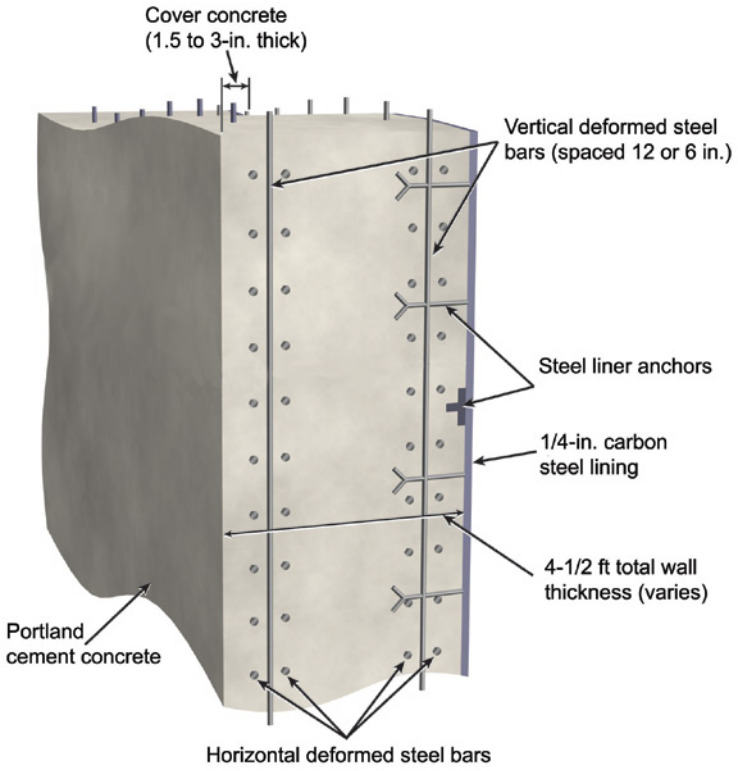

Figure A.5. Schematic of Typical Reinforced Concrete Reactor Containment Wall. Adapted from Shah and Hookham (1998).

Inspection of concrete containment structures in nuclear power plants is performed primarily by visual examination. Requirements for inspection of concrete containments are provided in Subsection IWL of Section XI of the ASME B&PV Code, which specifies general visual examinations and detailed visual examinations for regions of concern identified by the general visual examination. However, many other NDE methods are also applicable and have been reviewed extensively for concrete containment structures in Naus (2009a).

Pacific Northwest
NATIONAL LABORATORY

Proudly Operated by **Battelle** *Since 1965*

902 Battelle Boulevard
P.O. Box 999
Richland, WA 99352
1-888-375-PNNL (7665)

www.pnnl.gov

Prepared for the U.S. Nuclear Regulatory Commission
under a Related Services Agreement with the U.S. Department of Energy
CONTRACT DE-AC05-76RL01830

U.S. DEPARTMENT OF
ENERGY